Instituto Nacional de Matemática Pura e Aplicada

Diffusive effects in Riemann solutions for three phase flow in porous media

Luis Fernando Lozano Guerrero

Rio de Janeiro-RJ
July 2018

Instituto Nacional de Matemática Pura e Aplicada

Diffusive effects in Riemann solutions for three phase flow in porous media

Luis Fernando Lozano Guerrero

. PhD. Thesis presented to the Instituto Nacional de Matemática Pura e Aplicada (IMPA) as a partial requisite for obtaining the PhD. degree in Mathematics.

Advisor: Dr. Dan Marchesin

Rio de Janeiro-RJ
July 2018

Diffusive effects in Riemann solutions for three phase flow in porous media.

Luis Fernando Lozano G.
luisfer@impa.br

Instituto Nacional de Matematica Pura e Aplicada, IMPA
Rio de Janeiro, Brasil
July 2018

Dedicado a
Mi madre Rosa M.
mi amada esposa Yesi
a mis hijos Jahleel y Joezer
y por supuesto Jesucristo a quien le debo todo.

Acknowledgments

Ante todo, quiero agradecer primeramente a Dios por permitirme conseguir este sueño.
Quiero expresar mi más sinceros agradecimientos a mi orientador, el Prof. Dr. Dan Marchesin, por el apoyo continuo en mi investigación, por su paciencia, motivación, entusiasmo, conocimiento y sus buenos consejos.

Agradezco al Prof. Dr. Frederico Furtado, por su inestimable consejo y orientación. Especialmente su colaboración durante la parte final de mi doctorado que fue fundamental para completar mi trabajo.

Quiero agradecer al personal del Laboratorio de Dinámica de Fluidos: a Sergio y Ankie por su colaboración y apoyo logístico. A Ismael y Edson por sus grandes contribuciones en la programación y asistencia de los programas "RPN" y "ELI". Al Prof. B. Plohr por sus contribuciones al algoritmo de sucesión y al desarrollo de "ELI". A todos mis companeros que hicieron mucho mejor mis días en el laboratorio: Guillerme, Ciro, Elvis, Hugo, Jose, Julia y David.

Agradezco a todos mis amigos del grupo "futbol do IMPA". También agradezco al grupo de Colombianos del IMPA, en especial al grupo de Univallunos: Jhovanny, Diana, Haimer, Alexander, Brian, Eric, Plinio, Heber, Yulieth, Alex Zamudio y Viviana quienes hacian sentir el IMPA como CALI.

Agradezco a los Profesores Dr. André Nachbin y Dr. Amaury Alvarez quienes con sus consejos me ayudaron a tomar mejores decisiones.

Agradezco a mis amigos Davi lima, Jamerson y Valdir quienes fueron mis compañeros de casa durante mi primera etapa en Rio de Janeiro. Tambien agradezco a Leo, Marilene y a todo el personal del "castelo" quienes tuvieron muchísima paciencia con mi familia.

Agradezco a mi madre Rosa Guerrero que siempre me dio su amor y apoyo incondicional desde el momento que se entero que viajaria a Rio de Janeiro a cumplir con mi sueño. A mi familia en Colombia que siempre estaban pendientes de nosostros. Agradezco a mi esposa y a mis hijos por ser el soporte emocional durante este periodo. Yesi, sabes que esto no seriá posible sin ti.

Agradezco a los miembros de la banca examinadora por sus correciones y sugerencias para mejorar la elaboración del texto final. Al Prof. Dr Pablo Castañeda por leer el texto con tanto ánimo, espero que esos viajes en el autobús hayan sido entretenidos con mi tesis. Al Prof. Dr. Alexei Mailybaev por todas las sugerencias y referencias de artículos fundamentales para la bibliografía. Al Prof. Dr. Aparecido de Souza por el minucioso trabajo de lectura que ayudó a encontrar muchos errores tipográficos y de notación, muchas gracias.

Quiero expresar mi agradecimiento especial a Guillerme T. G. quien leyó con mucho cuidado mis borradores y me ayudó muchísimo con la redacción y la escritura en inglés. Además de ser un gran amigo y compañero.

Por último, pero no menos importante, me gustaría agradecer a las agencias de financiamiento ANP y CNPq que me dieron el soporte financiero para culminar este trabajo.

Luisfer
IMPA, Rio de Janeiro.

El principio de la sabiduría
es el temor a Jehova.
Sal 111:10

Abstract

We study the physical diffusive effect caused by capillary pressure between phases in three-phase flow in porous media, disregarding gravitational effects. The problem is modeled by a system of two nonlinear conservation laws. We solve a class of Riemann problems for this model where one of the viscosities is higher than the other two. To this end, we first developed a methodology using artificial diffusion and identified the transitional surfaces and associated shocks, which appear as a result of loss of strict hyperbolicity at an isolated point in the space of saturations. We identify the surfaces that characterize solutions which require transitional shocks as part of the solution to Riemann problems. We use the wave curve method to determine the solutions for arbitrary Riemann data (i.e., left and right states), except for a small set of right states that utilize transitional rarefactions for the corresponding solutions. This methodology combines theoretical analysis with numerical experiments to furnish scientific evidence for the existence (and uniqueness) of solutions with continuity under variation of data. Finally, we present the transitional surface for the general case where diffusion arises from capillary effects.

Key words: Flows in porous media, Riemann problem, capillary pressure effects, viscous profiles; conservation laws.

Resumo

Estudamos o efeito difusivo causado por pressão capilar entre fases em escoamento trifásico em meios porosos, desconsiderando efeitos gravitacionais. O problema é modelado por um sistema de duas leis de conservação não lineares. Resolvemos uma classe de problemas de Riemann em que a viscosidade do óleo é maior que aquelas da água e do gás. Para isso, desenvolvemos uma metodologia utilizando, inicialmente, difusão artificial e identificamos as superfícies de choques trasicionais associados, que aparecem como resultado da perda de hiperbolicidade estrita em um ponto isolado do espaç de saturações. Identifcamos as superficies que caracterizam as soluções que requerem choques transicionais como parte da solução do problema de Riemann. Usamos o metodo da curva de onda para determinar as soluçoes para dados de Riemann (i.e., estados a esquerda e a direita) arbitrarios, exceto para um pequeno conjunto de estados a direita que exigem o uso de rarefações transicionais para as soluções correspondentes. Essa metodologia combina análise teórica e experimentos numéricos para fornecer evidência científica da existência (e unicidade) de soluções com continuidade sob variação dos dados. Finalmente, apresentamos a superfície transicional para o caso real onde a difusão surge de efeitos capilares.

Palavras chave : Escoamentos em meios porosos, Problema de Riemann, efeitos de pressão capilar,

perfis viscosos; leis de conservação

Contents

Chapter 1

Introduction

In the present thesis, we solve a now longstanding unresolved problem in shock wave theory, namely, to characterize the nonlinear wave structure that emerges from discontinuous (Riemann) initial data for the problem of three phase flow in a porous medium. The wave structure is described for most pairs of constant states, and a precise notion of uniqueness and continuous dependence on initial states is formulated and demonstrated to apply.

The equations of three-phase flow in porous media are now a classical system of nonlinear conservations laws. The Riemann problem is interesting from several points of view. It is one of the simplest models that follows entirely from the constraints of conservation in oil-reservoir simulation, and hence plays a fundamental role in that subject. In PDE's, it is an easy to express system of equations describing extreme nonlinear wave motion, and since it is derivable from principles of conservation alone, it has taken on the status of a basic model in shock wave theory.

The simplicity of the equations disguise the extreme nonlinearities present, and these place three phase flow far from the classical setting of gas dynamics. As such, the analysis of these equations has long remained beyond the applicability of current mathematical theories. It has remained a longstanding unsolved problem for decades to characterize the nonlinear wave phenomena encoded in the Riemann problem for three phase flow. The attempt to solve this problem has generated significant research, including warm-up problems whose solutions have isolated new nonlinear wave phenomena in more tractable settings and stimulated new mathematical techniques tailored to their solution, each representing pieces of the full nonlinear problem considered here.

The main obstacle to a characterization of nonlinear waves in three-phase flow is the presence of umbilic points where wave speeds coincide. This leads to the presence of complicated waves that obscure the recognition of stable wave structures from unstable ones. We have given the solution to the Riemann problem for the equations of three-phase flow. This includes formulating and demonstrating a successful entropy condition for choosing the stable family of solutions, and providing strong evidence of the compelling result that such a family exists having the property of continuous dependence on left and right states.

We now describe briefly previous work related to our study. We refer the reader to [29] for a detailed review of the three phase flow theory.

In [19, 21], Isaacson *et. al.* identified transitional waves in the Riemann solution of systems of two conservation laws with general diffusion matrices. Transitional shocks are special in the sense that, unlike classical shocks, the Rankine-Hugoniot constraints linking the shock speed and the states on either side of the shock interface are insufficient to exactly determine the shock speed and the amplitude of waves emerging along outgoing characteristics, when the shock wave is perturbed. It was shown in [22, 27, 28] that the requirement of existence of viscous profiles provides exactly the number of additional equations to resolve this indeterminacy.

In [22, 27, 28], the authors introduce explicitly the additional equations resulting from the viscous profile requirement. They also develop a constructive method for sensitivity analysis, under perturbations of problem parameters, of such shocks in which relations between the states on opposite sides of the shock and the shock speed are derived.

In [8, 9], Azevedo *et. al.* established existence, uniqueness and L^1_{loc}-continuity under change of data of Riemann solutions for green reservoirs, in which a mixture of water, gas ans oil is injected into a reservoir initial saturated with oil. In [3] Andrade *et. al.* exhibited Riemann solutions for right states near to vertex O and left states along of $[G, W]$. Then, in [4] the authors extended the results for right states in a quadrilateral near to vertex O.

In [7] Azevedo, Marchesin, Plohr, and Zumbrun showed that, in the presence of nontrivial diffusion terms, such as those resulting from capillary pressure, it is not the elliptic region that plays the role of an instability region; rather, it is the region defined by Majda-Pego [26], which depends on the diffusion terms too and contains the elliptic region. In [1, 2], Abreu *et. al.*, performed two dimensional numerical simulations of Riemann solutions taking into account diffusive capillary effects and heterogeneities in the porous medium.

We now explain briefly how this work is organized. In Chapter 2, we recall some basic facts of the theory for systems of conservation laws, bifurcation theory of Riemann solutions and the wave curve method, to provide a terse background on these topics. Section 2.7 includes a discussion of the *succession algorithm*, which we employ for the construction of wave curves. This algorithm was developed at the Laboratory of Fluid Dynamics, IMPA, in collaboration with Professor B. Plohr, and implemented in "ELI," our specialized software for the solution of Riemann problems.

In Chapter 3, we derive the system of conservation laws that models three-phase flow in porous media, under a few physical simplifications. We also introduce the Corey model with quadratic permeabilities for the fluid phases which is adopted in this work. We conclude this chapter by presenting relevant properties of capillarity induced diffusive effects and find the physically correct form of the associated viscosity matrix.

In Chapter 4, we describe the main bifurcation manifolds associated to the Corey quadratic permeability model. These manifolds play a crucial role in the investigation of the structural stability of Riemann solutions and their L^1_{loc}-continuity.

We study in Chapter 5 the reduction of the three-phase flow system (3.36) to the scalar Buckley-Leverett conservation law for two-phase flow in porous media. This reduction occurs along certain *invariant lines* in state space, which play a prominent role in the construction of Riemann solutions. We then present properties of a few exceptional points at the intersection of some of the bifurcation manifolds with the invariant lines. We also present a subdivision of the saturation triangle in terms of the location of the umbilic point. Finally, we define and compute the *transitional map* along the invariant lines.

In Chapter 6, we discuss the procedure for the construction of backward fast wave curves and the so-called $\mathscr{R}$-regions associated with them. We also study the behavior of these regions under variation of the fluid viscosities μ_w, μ_o and μ_g.

We construct the surface of transitional shocks in Chapter 7, for a viscosity matrix which is a multiple of the identity matrix. We introduce and use the *three dimensional phase space* in saturations and speeds to investigate the speed compatibility between transitional waves and the fast wave groups constructed in Chapter 6. We also describe the dependence of the transitional surface on the fluid viscosities. This dependence was first studied by Marchesin and Mailybaev in [28] for a general system of n equations and for more general sets of dual-family shocks which include transitional shocks.

In Chapter 8, we determine the $\mathscr{L}$-regions associated to each $\mathscr{R}$-region described in Chapter 6. With this procedure, we detail the solutions of Riemann problems defined by any left state L and right state R belonging to the regions previously defined.

We construct the surface of transitional shocks for a physically correct viscosity matrix in Chapter 9. Surprisingly, this surface displays, essentially, the same topological structure found in the case of an identity viscosity matrix.

The numerical experiments conducted in this work used the specialized softwares "RPN" and "ELI," developed in close collaboration with Professor Bradley Plohr by the Laboratory of Fluid Dynamics, headed by Professor Dan Marchesin. These software packages allowed us to obtain and explore: integral curves, Hugoniot curves, the main bifurcation loci and phase portraits of dynamical systems and wave curves, which are all fundamental for the construction of Riemann solutions. Numerical calculations in MATLAB were also performed.

Chapter 2

Preliminaries

This chapter contains a brief introduction to the theory of Riemann solutions. We refer the reader to [11, 15, 16, 38, 40] for a detailed account on the general theory of conservation laws and Riemann problems.

2.1 Riemann solutions for a system of conservation laws

Consider a system of conservation laws of the form

$$\partial_t U + \partial_x F(U) = 0, \quad x \in \mathbb{R}, \quad t \in \mathbb{R}^+, \tag{2.1}$$

which governs the evolution of a 2-dimensional state vector varying in one spacial dimensional and time

$$U(x,t) = (u(x,t), v(x,t))^T .$$

The function $F : \Omega \subseteq \mathbb{R}^2 \to \mathbb{R}^2$, $F = F(u,v) = (F_1(u,v), F_2(u,v))^T$ is called the flux function and is usually considered of class $C^2(\Omega)$. The characteristic speeds for (2.1) (*i.e.*, the eigenvalues λ^-, λ^+ of the Jacobian matrix $DF(U)$) are given by the formulae

$$\lambda^{\pm}(U) = (1/2)\left(\mathrm{tr}(DF(U)) \pm \sqrt{[\mathrm{tr}(DF(U))]^2 - 4\ \det(DF(U))}\right). \tag{2.2}$$

Definition 2.1.1. System (2.1) is called *hyperbolic* if $\lambda^{\pm}(U) \in \mathbb{R}$, $\forall U \in \Omega \subset \mathbb{R}^2$. In the region of hyperbolicity (where the characteristic speeds are real), we have the natural ordering

$$\lambda^-(U) \leqslant \lambda^+(U). \tag{2.3}$$

We call $\lambda_s = \lambda^-$ the slow-family characteristic speed and $\lambda_f = \lambda^+$ the fast-family characteristic speed. We say that the system is *strictly hyperbolic* if $\lambda_s \neq \lambda_f$, $\forall U \in \Omega$. The non-linearity of F implies that the characteristic speeds depends on U, which in general leads to focusing of waves and the formation of discontinuous solutions. Therefore, (2.1) must be interpreted in the sense of distributions.

Definition 2.1.2. A *Riemann problem* for the conservation law (2.1) is a special Cauchy problem with initial data

$$U(x,0) = \begin{cases} U_L, & \text{if } x < 0 \\ U_R, & \text{if } x > 0 \end{cases}, \tag{2.4}$$

where U_L and U_R are constant.

The general solutions of (2.1) consists of weak solutions that respect the invariance of equation (2.1) under the scaling transformation $(x,t) \to (cx,ct)$ with $c > 0$. Such scale-invariant solutions satisfy the initial conditions of the Riemann problem as well as the PDE (2.1). Conversely, solutions of a Riemann problem are expected to be scale-invariant, *i.e.*, they depend on t and x only through the combination $\xi = x/t$. Although Riemann problems are only special initial value problem may be viewed as a nonlinear superposition of scale invariants solutions [18].

A scale-invariant solution can be partitioned into several groups of waves; the waves in each group move together as a single entity. More precisely, we define a wave group to be a scale-invariant solution that contains no intermediate constant states. Thus a solution of a Riemann problem comprises a sequence of a wave groups moving apart from each other. Waves groups consist of two kinds of fundamental solutions: (almost everywhere smooth) rarefactions and (discontinuous) shocks (see Figure 2.1).

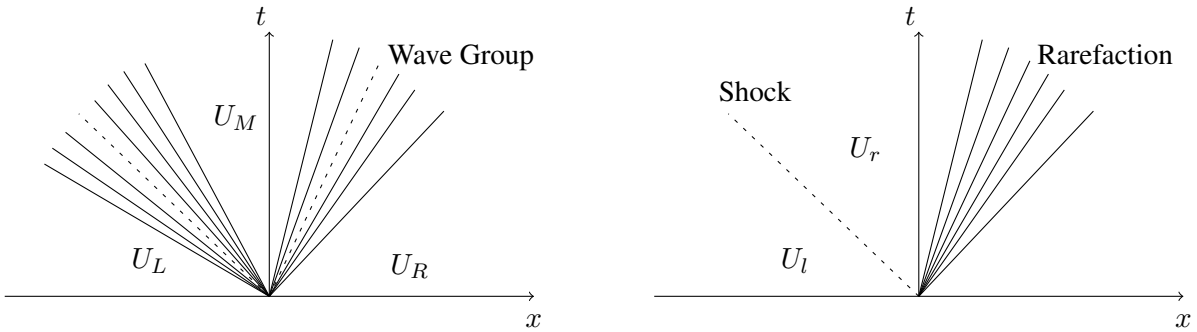

Figure 2.1: Scale-invariant solutions (a) Example of solution for a Riemann problem, comprising a sequence of two wave groups. (b) A centered rarefaction wave and centered discontinuous wave .

2.1.1 Rarefactions waves, rarefaction curves and inflection locus

Assuming U to be a differentiable function of $\xi = x/t$, system (2.1) becomes

$$(DF(U(\xi)) - \xi I)U'(\xi) = 0, \tag{2.5}$$

where I is the identity matrix. As $U'(\xi) \neq 0$, there is a (right) eigenvector of $DF(U))$ associated to each eigenvalue $\xi = \lambda_i(U)$ for $i = s$ or f. Therefore, smooth solutions of system (2.1) lie on an integral

curves of a (right) characteristic field of $DF(U)$ in state space Ω. That is, they satisfy the system of ordinary differential equations,

$$U'(\xi) = r_i(U), \quad i = s, f, \tag{2.6}$$

where r_i is a right eigenvector of $DF(U)$ corresponding to $\lambda_i(U)$ in (2.2).

Definition 2.1.3. For $i = s, f$, the i-inflection locus $\mathcal{I}_i$ is the subset of the strictly hyperbolic region formed by all points U such that $\nabla\lambda_i(U) \cdot r_i(U) = 0$ and the inflection locus is $\mathcal{I} = \mathcal{I}_s \cup \mathcal{I}_f$. The i-inflections are subdivided into $\mathcal{I}_i^+$ and $\mathcal{I}_i^-$ according to whether λ_i is a maximum or a minimum along the integral curves of r_i.

Throughout this work, we loosely use the same notation for $\mathcal{I}_i$ and its closure; it turns out that the closure of $\mathcal{I}_i$ contains the umbilic point.

Remark 2.1.4. In the strictly hyperbolic region, consider integral curves of the eigendirection fields r_s and r_f and the respective eigenvalues along them. Any closed part of s-integral curve (or f-integral curve) where the s-eigenvalue (or f-eigenvalue) is monotonic forms a s-rarefaction curve (or f-rarefaction curve). The rarefaction curves are extended to include umbilic points, preserving the monotonicity of the eigenvalue.

Generically, an integral curve crosses $\mathcal{I}$ transversely and the corresponding eigenvalue on the integral curve reaches an extremum at $\mathcal{I}$. Therefore, rarefaction curves usually end (or start) on $\mathcal{I}$. However, if an integral curve is tangent to $\mathcal{I}$, generically, the eigenvalue is still monotonic, so the corresponding rarefaction curve does not end at $\mathcal{I}$, see [6].

Since an eigenvalue is monotonic on a rarefaction curve, the latter is parametrized by the eigenvalue, *i.e.*, any i-rarefaction curve is the image of a map $\gamma : J \subseteq \mathbb{R} \longrightarrow \Omega, \lambda_i \longmapsto \gamma(\lambda_i)$ where J is a closed interval. Renaming $\xi = \lambda_i$ and $\gamma(\xi) = U(\xi)$, we have $\gamma : J \subseteq \mathbb{R} \longrightarrow \Omega, \xi \longmapsto U(\xi)$.

Definition 2.1.5. Let the map $\gamma : J \subseteq \mathbb{R} \longrightarrow \Omega, \xi \longmapsto U(\xi)$, in a closed interval J, be an i-rarefaction curve. The function $U(\xi),\ \xi = x/t$, is a solution of (2.5) out side the inflection locus (where $U'(\xi)$ is unbounded) and umbilic points (where usually $U'(\xi)$ is not defined). This solution is called i-rarefaction wave and is denoted by R_s or R_f, depending on the family of the vector field used.

A solution of Riemann problem (2.1),(2.4) for an i-rarefaction wave is given by

$$U(x,t) = \begin{cases} U_L, & \text{if } x \leq \lambda_i(U_L)t, \\ \lambda_i^{-1}(x/t), & \text{if } \lambda_i(U_L)t \leq x \leq \lambda_i(U_R)t, \\ U_R, & \text{if } x \geq \lambda_i(U_R)t. \end{cases} \tag{2.7}$$

Definition 2.1.6. The i-th characteristic field of $DF(U)$ is said to be genuinely nonlinear in a subset $\Omega' \subset \Omega$ if $\nabla\lambda_i(U) \cdot r_i(U) \neq 0, \forall U \in \Omega'$. In other words, if the i-th characteristic velocity is a strictly monotonous function on the integral curve of the associated line field in subset Ω'. On the other hand, if $\nabla\lambda_i(U) \cdot r_i(U) \equiv 0$, it is said that the field is linearly degenerate.

2.1.2 Shock waves, Rankine-Hugoniot condition/locus and shock curves

Consider a function $U(\xi)$, $\xi = x/t$, with a jump discontinuity from left state U_l to right state U_r propagating with speed σ, *i.e.*, $\lim_{\xi \nearrow \sigma} U(\xi) = U_l$, $\lim_{\xi \searrow \sigma} U(\xi) = U_r$. Such a function is a discontinuous (shock wave) or weak solution of the initial problem (2.1),(2.4) if and only if *Rankine-Hugoniot condition* holds (see [40]):

$$F(U_r) - F(U_l) - \sigma\,(U_r - U_l) = 0. \tag{2.8}$$

These solutions have the form

$$U(x,t) = \begin{cases} U_l, & \text{if } x < \sigma t, \\ U_r, & \text{if } x > \sigma t. \end{cases} \tag{2.9}$$

The speed σ in (2.8) may be written as $\sigma(U_l; U_r)$. By convention, U_l is on the left side of the discontinuity and U_r is on the right side. In general, these states are different from the states U_L and U_R of the Riemann problem initial data. For a fixed U_l, the set of states U such that the pair $(U_l; U)$ satisfies the Rankine-Hugoniot condition (2.8) for some σ are called the *Hugoniot locus* for the state U_l and is denoted by $\mathcal{H}(U_l)$. In order to construct the Hugoniot locus for a state U_l, we need to solve the follow system

$$H_{U_l}(U, \sigma) \equiv F(U_r) - F(U_l) - \sigma\,(U_r - U_l) = 0, \tag{2.10}$$

where $H_{U_l} : \mathbb{R}^2 \times \mathbb{R} \longrightarrow \mathbb{R}^2$, is called the Hugoniot function. The projection of the zero-set $H_{U_l}(U, \sigma) = 0$ onto state space gives $\mathcal{H}(U_l)$, which is typically one dimensional; we often call it a curve despite having self-intersections and singularities [17, 21]. Notice that $\mathcal{H}(U_r)$ can be defined similarly by fixing U_r instead of U_l in (2.10).

2.2 Entropy condition

Discontinuous waves give rise to no unique solutions of the Riemann problem. Therefore, the relation (2.8) must be supplemented by additional criteria that aim at identifying the unique and physically relevant solutions. These criteria are known as admissibility criteria or entropy criteria, referring to gas dynamics. For conservation laws that are genuinely nonlinear and strictly hyperbolic, Lax [23] introduced an eligibility criterion that associates centered discontinuous waves with family characteristics, so that the characteristic of a family affect both sides of the discontinuity, while features other families cross the discontinuity experiencing a deviation. For more general conservation laws, characteristics can afford to be tangent to the discontinuity, so we have the following definitions for admissibility.

Definition 2.2.1. [**Slow-family and fast-family shock wave**] We define a centered discontinuous wave to be a *Lax discontinuity of the slow-family* (also called a Lax slow-shock or Lax s-shock) provided that the characteristic speeds are related to the propagation speeds as follows:

$$\lambda_s(U_r) < \sigma < \lambda_s(U_l) \quad \text{and} \quad \sigma < \lambda_f(U_r). \tag{2.11}$$

Similarly, we defined a centered discontinuous wave to be a *Lax discontinuity of the fast-family* (Lax fast-shock or Lax f-shock) provided that the characteristic speeds are related to the propagation speed as follows:

$$\lambda_f(U_r) < \sigma < \lambda_f(U_l) \quad \text{and} \quad \lambda_s(U_l) < \sigma. \tag{2.12}$$

Lax used the nomenclature 1- and 2-shock for slow and fast shocks while we adopt the more representative s- and f-shocks or notation. In certain cases we allow some equalities in (2.11) or (2.12), giving way to a generalized Lax criterion, which will be discussed latter in grater detail.

However, both the original and generalized Lax criteria can restrict the analysis too much or not enough, and we might be left with no solutions or too many. We are led to impose that discontinuous waves possess viscous profiles, as described in more detail in Section 2.2.1. This is the viscosity admissibility criterion. In general, it is distinct from the characteristic criterion, since there exist Lax discontinuities that do not have viscous profiles, while some discontinuities with viscous profiles are not of Lax type, see [41]. The viscous criterion, too, can fail to guarantee existence and uniqueness of solutions of Riemann problems. In this work we construct solutions that have viscous profile and can also satisfy Lax criterion.

Definition 2.2.2 (Under-compressive and over-compressive shock waves). We define a centered discontinuous wave to be a *crossing* (also called *transitional*) *discontinuity* provided that the characteristic speeds are related to the propagation speeds as follows:

$$\lambda_s(U_l) < \sigma < \lambda_f(U_l) \quad \text{and} \quad \lambda_s(U_r) < \sigma < \lambda_f(U_r). \tag{2.13}$$

Similarly we defined a centered discontinuous wave to be a *compressive* (also called *over-compressive*) *discontinuity* provided that the characteristic speeds are related to the propagation speed as follows:

$$\lambda_f(U_r) < \sigma < \lambda_s(U_l). \tag{2.14}$$

If the crossing discontinuity is admissible by viscous profile we call it a *transitional shock* (or t-shock). Similarly, an over-compressive discontinuity that has viscous profile is called and over-compressive shock (or o-shock).

2.2.1 Viscosity admissibility criterion

We consider system (2.1) with parabolic regularization by adding a viscous term , *i.e.*

$$\partial_t U + \partial_x F(U) = \varepsilon \partial_x \left(\mathcal{B}(U) \partial_x U \right), \quad \varepsilon > 0. \tag{2.15}$$

Typically, system (2.1) is an approximation to equation (2.15) in the limit of $\varepsilon \to 0^+$. Here $\mathcal{B}(U)$ is a 2×2 viscosity matrix determined by small scale physical effects. This matrix is assumed to be positive definite. Considering the *travelling wave* solution

$$U(x,t) = U(\eta) \quad \text{with} \quad \eta = \frac{x - \sigma t}{\varepsilon},$$

we find that $U(\eta) = (u(\eta), v(\eta))^T$ should satisfy the system of ordinary differential equations

$$-\sigma U(\eta)' + (F(U(\eta)))' = \left(\mathcal{B}(U(\eta)) U(\eta)' \right)'. \tag{2.16}$$

Here prime, denotes differentiation with respect to η. Integrating (2.16) with respect to η we obtain

$$\mathcal{B}(U(\eta)) U(\eta)' = F(U(\eta)) - \sigma U(\eta) + C, \tag{2.17}$$

where C is the constant of integration. We are interested in finding solutions to the Riemann problem (2.1), (2.4) of the form (2.9), where σ satisfies the Rankine-Hugoniot condition (2.8) and $U(\eta)$ satisfies the following boundary condition

$$\lim_{\eta\to-\infty} U(\eta) = U_L \quad \text{and} \quad \lim_{\eta\to+\infty} U(\eta) = U_R. \tag{2.18}$$

From (2.18), U_L is a singularity of (2.17) and

$$C = \sigma U_L - F(U_L). \tag{2.19}$$

From (2.17) and (2.19) we obtain the associated ODE system

$$\mathcal{B}(U(\eta))\, U'(\eta) = -\sigma\,(U(\eta) - U_L) + F(U(\eta)) - F(U_L). \tag{2.20}$$

If we multiply both sides of (2.20) by the *adjugate matrix* $\text{Adj}(\mathcal{B}(U))$ we obtain

$$\det(\mathcal{B}(U(\eta)))\, U' = \text{Adj}(\mathcal{B}(U(\eta)))\,[F(U(\eta)) - F(U_L) - \sigma\,(U(\eta) - U_L)]\,. \tag{2.21}$$

Now we introduce a new rescaled variable ζ , defined by

$$\frac{\partial\eta}{\partial\zeta} = \det(\mathcal{B}(U)). \tag{2.22}$$

Using (2.22) in (2.21) we obtain the ODE system:

$$\dot{U} = \text{Adj}(\mathcal{B}(U))\,[F(U) - F(U_L) - \sigma\,(U - U_L)]\,, \tag{2.23}$$

where the dot represents the derivative with respect to ζ. Now let $X_\sigma(U, U_L)$ be the vector field defined by

$$X_\sigma(U, U_L) = \text{Adj}(\mathcal{B}(U))\,[F(U) - F(U_L) - \sigma\,(U - U_L)]\,. \tag{2.24}$$

Notice that U_L and U_R are singularities of this vector field and that all singularities of X_σ lie on the Hugoniot locus. The singularities of X_σ depend on σ (as well as on U_L and U_R). We recall the following definition.

Definition 2.2.3. Let γ be the orbit of a C^2 vector field X on the plane that passes through a point p. The ω-limit of p is the set

$$\omega(p) = \left\{q \in \mathbb{R}^2 \colon \exists\, \tau \longrightarrow \infty \text{ with } \gamma(\tau) \longrightarrow q\right\}. \tag{2.25}$$

We note that $\omega(p) = \omega(\widetilde{p})$ if $\widetilde{p}$ belongs to the orbit of p. We define the ω-limit set of an orbit as the set of $\omega(p)$ for any $p \in \gamma$. Similarly, we define the $\alpha-$limit set for $\tau \longrightarrow -\infty$. Therefore, for the existence of a shock wave solution of $U_t + (F(U))_x = 0$, which is a limit of traveling wave solutions of the associated parabolic equation (2.15), there must be an orbit γ of the vector field $X_\sigma(U, U_L)$ satisfying

$$\alpha(\gamma) = U_L \quad \text{and} \quad \omega(\gamma) = U_R. \tag{2.26}$$

Definition 2.2.4. We say that the shock (2.9) is *admissible* or that it has a *viscous profile* if there exists an orbit of the vector field $X_\sigma(U, U_L)$ connecting U_L to U_R.

We stress the importance of studying the critical points of the ODE system (2.24) for understanding traveling wave solutions of (2.15). For (2.24), a critical point is a state U_c that satisfies the Rankine-Hugoniot condition for given state U_L and the shock speed σ. The behavior of solutions in the neighborhood of a critical point U_c is reflected in the qualitative features of solutions of the linearization of (2.20) about U_c:

$$\mathcal{B}(U_c)\, U' = [-\sigma + DF(U_c)]\,(U - U_c). \tag{2.27}$$

Such solutions are determined by the eigenvalues μ and corresponding eigenvectors $\hat{U}_\mu$ that satisfy

$$\mu \mathcal{B}(U_c)\, \hat{U}_\mu = [-\sigma + DF(U_c)]\, \hat{U}_\mu. \tag{2.28}$$

For example, $U = U_c + \sum_\mu c_\mu \exp(\mu\eta)\hat{U}_\mu$ when the eigenvalues are distinct. Therefore, the character of the critical point can be determined by the eigenvalues μ.

Definition 2.2.5. Let p be a critical point of a vector field X. We say that p is *hyperbolic* if the linearized field dX has two eigenvalues with nonzero real part at p.

Following [37], we classify discontinuities in terms of the nature of the equilibrium points U_L and U_R of the system of ODEs (2.20). In [37], the following types of equilibria were studied: repeller, repeller-saddle, saddle, saddle-attractor and attractor.

Definition 2.2.6. We have the following combinations between the type of orbit connecting U_L and U_R and the type of these equilibria:

- Lax s-shock, S_s , U_L is a repeller and U_R is a saddle.
- Lax f-shock, S_f , U_L is a saddle and U_R is a attractor.
- Transitional shock, S_T , U_L and U_R are saddles.
- Over-compressive shock, S_O , U_L is a repeller and U_R is a attractor.

Remark 2.2.7. If we consider $\mathcal{B}(U) = I_{2\times 2}$, the eigenvalues of dX_σ are $\mu_k = -\sigma + \lambda_k(U)$, $k = s, f$. Thus the singularities of X_σ fail to be hyperbolic (in sense of Definition 2.2.5) when $\mu_k = 0$, *i.e.*, $\sigma = \lambda_k(U)$, $k = s, f$. Then the sign of μ_k determines the character of the critical point U.

Remark 2.2.8. In the general case where $\mathcal{B}(U)$ is not a multiple of the identity matrix, the signs of $\lambda_i(U) - \sigma$ do not always determine the character of a critical point U. Indeed, a critical point that is a repeller when $\mathcal{B}(U) = I_{2\times 2}$ can become a focus when $\mathcal{B}(U)$ is changed. However, saddles are preserved provided that the determinant of $\mathcal{B}(U)$ is positive; this can be demonstrated as follows. Because μ_f and μ_s are the eigenvalues of $\mathcal{B}(U)^{-1}[-\sigma + DF(U)]$, their product $\mu_f\mu_s$ has the same sign as that of $(\lambda_f - \sigma) \times (\lambda_s - \sigma)$, which is negative. Therefore μ_f and μ_s must be real and have opposite sign.

	Name	Relations
$'S_s$	Left-char. s-shock	$\lambda_s(U_r) < \sigma = \lambda_s(U_l)$ and $\sigma < \lambda_f(U_r)$
S'_s	Right-char. s-shock	$\lambda_s(U_r) = \sigma < \lambda_s(U_l)$ and $\sigma < \lambda_f(U_r)$
$'S'_s$	Doubly-char. s-shock	$\lambda_s(U_r) = \sigma = \lambda_s(U_l)$ and $\sigma < \lambda_f(U_r)$
$'S_f$	Left-char. f-shock	$\lambda_f(U_r) < \sigma = \lambda_f(U_l)$ and $\lambda_s(U_l) < \sigma$
S'_f	Right-char. f-shock	$\lambda_f(U_r) = \sigma < \lambda_f(U_l)$ and $\lambda_s(U_l) < \sigma$
$'S'_f$	Doubly-char. f-shock	$\lambda_f(U_r) < \sigma = \lambda_f(U_l)$ and $\lambda_s(U_l) < \sigma$
$'S_o$	Left-char. over-compressive	$\lambda_f(U_r) < \sigma = \lambda_s(U_l)$
S'_o	Right-char. over-compressive	$\lambda_f(U_r) = \sigma < \lambda_s(U_l)$
$'S'_o$	Doubly-char. over-compressive	$\lambda_s(U_l) < \sigma = \lambda_f(U_l), \lambda_s(U_r) < \sigma < \lambda_f(U_r)$
$'S_T$	Left-char. transitional	$\lambda_s(U_l) < \sigma = \lambda_f(U_l), \lambda_s(U_r) < \sigma < \lambda_f(U_r)$
S'_T	Right-char. transitional	$\lambda_s(U_l) < \sigma < \lambda_f(U_l), \lambda_s(U_r) = \sigma < \lambda_f(U_r)$
$'S'_T$	Doubly-char. transitional	$\lambda_s(U_l) < \sigma = \lambda_f(U_l), \lambda_s(U_r) = \sigma < \lambda_f(U_r)$

Table 2.1: Nomenclature of characteristic and doubly characteristic discontinuities

2.3 Nomenclature for discontinuities

In order to describe the Riemann solution we will use the notation found in [31]. Discontinuities with or without viscous profiles are classified in Definition 2.2.1 and 2.2.2.

Definition 2.3.1. There are eight characteristic discontinuities (*i.e.*, with propagation velocity equal to a characteristic speed):

- Left-characteristic discontinuities:
  1. for slow Lax discontinuities and over-compressive discontinuities with $\lambda_s(U_l) = \sigma$;
  2. for fast Lax discontinuities and transitional discontinuities with $\lambda_f(U_l) = \sigma$.
- Right-characteristic discontinuities:
  1. for slow Lax discontinuities and transitional discontinuities with $\lambda_s(U_r) = \sigma$;
  2. for fast Lax discontinuities and over-compressive discontinuities with $\lambda_f(U_r) = \sigma$.

Table 2.1 presents the inequalities for each characteristic or doubly characteristic discontinuity. Now, we extended the characterization of critical point U_L and U_R of the ODE's (2.20) for characteristic shocks following [37].

Definition 2.3.2. Characteristic shocks are limit cases of i-shock $i \in \{s, f\}$, when the nodes become saddle-nodes.

1. Left-char. s-shock (or slow *sonic* shocks): U_L is a repeller-saddle and U_R is a saddle;

2. Right-char. f-shock (or fast *sonic* shocks): U_L is a saddle and U_R is a saddle-attractor.

A shock of type $X \in \{s, f, O, T\}$ from states A to B is written as $A \xrightarrow{S_X} B$. A prime on the left or on the right of S indicates left- or right-characteristic shocks, respectively. For instance, $A \xrightarrow{S'_s} B$ means that there exists a s-shock from A to B with speed equal to $\lambda_s(B)$, while $C \xrightarrow{'S_O} D$ means that there exists an over-compressive shock from C to D with speed equal to $\lambda_s(C)$.

2.4 Bifurcation manifolds

Away from certain bifurcation points (primary and secondary bifurcation points), a Hugoniot locus is a curve and it may be parametrized by a single variable. By taking a fixed left state L and varying right state U along $\mathcal{H}(L)$, we may consider the speed $\sigma(L;U)$ as a function on $\mathcal{H}(L)$. The following theorem gives an analytic description of the qualitative behavior of shock speed σ.

Theorem 2.4.1 (Bethe-Wendroff, see [42])**.** *Consider the Hugoniot locus through a state L. Let U_0 be a point on $\mathcal{H}(L)$ such that $l_i(U_0)(U_0 - L) \neq 0$, where $l_i(U)$ is the left eigenvector of DF associated to $\lambda_i(U)$. Then, the speed $\sigma(L;U)$, regarded as a function along $\mathcal{H}(L)$, is critical at the state U_0 if and only if $\sigma(L;U_0) = \lambda_i(U_0)$, $i \in \{s, f\}$.*

The Bethe-Wendroff theorem states that the speed on the Hugoniot curve is monotonic if the shock speed is never characteristic. Hence, the speed monotonicity on shock curves.

Now we define certain 1-dimensional manifolds which play a fundamental role in the wave curve construction in our problems of two unknowns. They are not genuine manifolds since they may have self intersections or other singularities.

The secondary bifurcation manifold is composed by the states which do not satisfy the hypothesis of the implicit function theorem; generically the Hugoniot locus changes topology at this locus. In general, we know that through each state U_L there exist locally two Hugoniot branches (each branch transversal to the other), so each U_L is a primary bifurcation.

Definition 2.4.1. A state U belongs to the *secondary bifurcation manifold* for the family i if there exists a state $U' \neq U$ such that

$$U' \in \mathcal{H}(U) \text{ with } \lambda_i(U') = \sigma(U;U') \text{ and } l_i(U')(U' - U) = 0, \tag{2.29}$$

where $l_i(U')$ is the left eigenvector of the Jacobian matrix $DF(U')$ associated to $\lambda_i(U')$.

From Definition 2.4.1 and Theorem 2.4.1, we have the following statement :

Lemma 2.4.2. *Consider the Hugoniot locus through a state U_0 to be tangent at U' to an integral curve of family i. Suppose that U_0 does not belong to the secondary bifurcation manifold. Then $\sigma(U_0, U') = \lambda_i(U')$ and $\sigma' = 0$.*

Definition 2.4.2. A state U lies on the *Hysteresis manifold* for the family i if there is a state $U' \neq U$ such that

$$U \in \mathcal{H}(U') \text{ with } \lambda_i(U') = \sigma(U;U') \text{ and } \nabla\lambda_i(U')\cdot r_i(U') = 0, \tag{2.30}$$

where $r_i(U')$ is a right eigenvector of the Jacobian matrix $DF(U')$.

Remark 2.4.3. Notice that a state U' describe in the definition of the Hysteresis must belong to the inflection manifold.

Definition 2.4.4. A state U belongs to the $(i,j)-$*Double Contact manifold* if there is a state U' such that

$$U' \in \mathcal{H}(U) \text{ with } \lambda_i(U) = \sigma(U;U') = \lambda_j(U'), \tag{2.31}$$

where the families i and j may be the same or different.

Remark 2.4.5. States on the Double Contact manifold can be junctions of composite and rarefaction segments in waves curves. This is analogous to the scalar case, where a shock is embedded between two rarefaction waves, see Oleĭnik [33].

Definition 2.4.6. Let C be a set in state space. For $i \in \{s, f\}$, we define the sets:

$$E_i^-\{C\} = \{U_+ \in \Omega : \exists U_- \in C \text{ such that } U_+ \in \mathcal{H}(U_-), \text{ and } \sigma(U_-;U_+) = \lambda_i(U_-)\}; \tag{2.32}$$

$$E_i^+\{C\} = \{U_+ \in \Omega : \exists U_- \in C \text{ such that } U_+ \in \mathcal{H}(U_-), \text{ and } \sigma(U_-;U_+) = \lambda_i(U_+)\}. \tag{2.33}$$

$E_i^-\{C\}$ is the i-left-extension and $E_i^+\{C\}$ is the i-right-extension of set C.

Definition 2.4.7. The state U belongs to the *boundary contact manifold* for the family i (or the *boundary extension*), if there exists a state U' such that

$$U \in \mathcal{H}(U') \text{ with } U' \text{ on the boundary and } \lambda^i(U) = \sigma(U;U'). \tag{2.34}$$

Notice that it can be defined as $E_i^{\pm}(\partial\Omega)$.

Remark 2.4.8. A boundary contact wave occurs when a junction between wave segments coincides with the boundary.

Remark 2.4.9. Notice that the hysteresis manifold is the (suitable) extension of the inflection manifold.

We conclude this section with the statement of a theorem that is very useful in this work:

Theorem 2.4.3 (The Triple Shock Rule, see [14])**.** *Consider three states U, V, $W \in \Omega$. We have:*

1. *If $V, W \in \mathcal{H}(U)$ and $\sigma(U;V) = \sigma(U;W)$, then $W \in \mathcal{H}(V)$ and $\sigma(U;W) = \sigma(V;W)$;*
2. *If U, V, W are not collinear, $V \in \mathcal{H}(U)$ and $W \in \mathcal{H}(U) \cup \mathcal{H}(V)$, then $\sigma(U;V) = \sigma(V;W) = \sigma(U,W)$.*

2.5 Wave groups

Usually solutions are constructed from the left state to the right state; thus, the speed of the waves must increase in the construction from left to right.

Definition 2.5.1 (Speed compatibility criterion)**.** A sequence of two waves is *compatible* if the head of the first wave is not faster than the take of the second. (Otherwise, the sequence is *incompatible*.)

Our models are not strictly hyperbolic and allow the following wave.

Definition 2.5.2. A *transitional rarefaction wave* is a s-rarefaction which follows a f-rarefaction without any regions with an intermediate constant state between them.

Shocks, rarefactions and sequences of shocks and rarefaction waves without any intermediate constant states form wave groups. In the following definitions, we use the convention from [37], where the terms in parentheses are optional (i.e., they may be absent); recall Definitions 2.1.5 and 2.2.6:

- A s-wave group is either a single S_s or a sequence containing (at least) an R_s:

$$S_s \text{ or } (S_s') \; R_s \; (\prime S_s' \; R_s) \; ... \; (\prime S_s' \; R_s)(\prime S_s). \tag{2.35}$$

- A f-wave group is either a single S_f or a sequence containing (at least) an R_f:

$$S_f \text{ or } (S_f') \; (R_f \; \prime S_f') \; ... \; (R_f \; \prime S_f') \; R_f(\prime S_f). \tag{2.36}$$

- A transitional wave group is (i) either a single S_T or a sequence containing an $R_f \; \prime S_T$,

$$S_T \text{ or } (S_f')(R_f \; \prime S_f')...(R_f \; \prime S_f')R_f \; \prime S_T; \tag{2.37}$$

  or (ii) a sequence containing a $S_T' R_s$,

$$S_T' R_s \; (\prime S_s' \; R_s) \; ... \; (\prime S_s' R_s)(\prime S_s); \tag{2.38}$$

  or (iii) containing even a transitional rarefaction, $R_f R_s$,

$$R_f R_s \; (\prime S_s' R_s) \; ... \; (\prime S_s' \; R_s)(\prime S_s). \tag{2.39}$$

- An over-compressive wave-group is (i) either a single S_O or a sequence containing an $R_s \; \prime S_O$,

$$S_O \text{ or } (S_s')(R_s \; \prime S_s') \; ... \; (R_s \; \prime S_s') \; R_s \; \prime S_O. \tag{2.40}$$

  or (ii) a sequence containing a $S_O' \; R_f$,

$$S_O' \; R_f \; (\prime S_f \; R_f) \; ... \; (\prime S_f' \; R_f)(\prime S_f). \tag{2.41}$$

- A doubly sonic (or doubly characteristic) transitional wave is a single shock

$$'S'_T. \tag{2.42}$$

The *wave structure* of a structurally stable solution for a strictly hyperbolic Riemann problem is necessarily formed by sequences of wave groups as stated in Theorem 2.3 of [37]. Since doubly sonic transitional waves $'S'_T$ (2.42) do nor appear in our examples, we adopt the version of theorem Theorem 2.3 of [37], presented in [31] for wave structures.

Theorem 2.5.1 ([31, 37])**.** *For strictly hyperbolic Riemann problems whose solutions do not contain $'S'_T$ waves (2.42), structurally stable solutions consist of a s-wave group (2.35) followed by an arbitrary number of transitional wave groups (2.37) or (2.38) (in any order), followed by a f-wave group (2.36).*

Given that in our work we have an umbilic point inside of our domain, we can have loss of strict hiperbolicity. Then, the Theorem 2.5.1 motivates the existence of new structures and transitional rarefactions R_2 R_1. In this work we have two wave structures: (i) the standard case of a s-wave group (2.35), followed by a f-wave group; (ii) a s-wave group (2.35) followed by a transitional wave group (2.37) or (2.39), followed by a f-wave group (2.36).

Remark 2.5.3. In our work, there are neither S'_T waves (2.38) nor $'S'_T$ (2.42).

A solution is represented by state names separated by arrows with the name of wave group involved above them, *e.g.,* the Riemann solution for left state L and right state R consisting of a s-rarefaction joining a left-characteristic s-shock $R_s\,'S_s$ followed by a f-shock S_2 is represented as:

$$L \overset{R_s}{\longmapsto} M_1 \overset{'S_s}{\longrightarrow} M_2 \overset{S_f}{\longmapsto} R, \tag{2.43}$$

where constant states occupying regions of physical space are followed by $\mapsto$ while states that occur at a single point are followed by $\rightarrow$. Note that in (2.43) M_1 does not represent a constant state, whereas M_2 does. L and R are always constant states in any Riemann solution .

We define below the composite wave curves, which are fundamental to the construction of Riemann solutions.

Definition 2.5.4. A composite wave of type rarefaction/shock (or shock/rarefaction) is a solution of the Riemann problem (2.1), (2.4) consisting of a sequence of a rarefaction (or shock) wave followed by a shock wave (or rarefaction), with no segment of constant states separating them. We have an i-composite when the two waves are associated with the same ith-family; otherwise, we have a transitional composite.

Definition 2.5.5. A composite curve by a state L of type rarefaction/shock (or shock/rarefaction) is the set of states $U \in \Omega$ which can be connected to L by a composite wave of that type.

It follows from Definition 2.5.5 and the definitions of wave groups given by (2.35)-(2.42), we consider four composite curves, which parametrized successions of waves pairs $R_i\,'S_j$, where $(i,j) \in \{(s,s),(s,O),(f,f),(f,T)\}$.

2.6 Wave Curves

A backward wave curve of the family i, starting at the state R is a parametrization of the states U in state space that can be connected to R, on the left, by an i-wave group. Since the states U are connected to R on the left, we name it the *backward i-wave curve*, $\mathcal{W}_i^-(R)$, associated to state R. In a similar way , we name the *forward i-wave curve*, $\mathcal{W}_i^+(L)$ starting at the state L, the parametrization of states U in the phase space that can be connected on the right to the state L.

Wave curves in this type of problems, where strict hyperbolicity and genuine nonlinearity fail, use three types of elementary waves: shocks, rarefactions and composite waves, unlike classic wave curves which comprise only shock and rarefaction segment. Since Hugoniot curves typically posses nonlocal (*i.e.,* detached) branches, wave curves also have complicated geometry, *e.g.,* the may have disconnected branches.

Now, we define a graphical representation of shock, rarefaction and composite curves, which are the *fundamental wave curves*, that form the wave curves that we consider:

- The s/f-shock curves are represented by blue/red dashed curves.
- The s/f-rarefaction curves are represented by blue/red solid curves. There is an arrow indicating increasing speed direction.
- The s/f-composite curves are represented by blue/red crossed curves.
- When a fundamental wave curve is not admissible it is represented by a black curve.

2.7 Construction of wave curves: Succession Algorithm

In this section, we describe the *succession algorithm* for construction of wave curves. The theoretical basis for this algorithm is the list of compatible wave groups presented in Section 2.5, as restricted by the viscous profile admissibility criterion. The central feature of this algorithm is that it finds *all* wave groups satisfying the admissibility criterion.

Implementation of the succession algorithm presupposes the ability to calculate (1) the Hugoniot locus of a state, (2) the integral curve through a state, and (3) the sonic extension of an integral curve. Calculations (1) and (3) can be performed by a contour plotter (specifically, a method for solving $n-1$ equations in n unknowns for $n = 2$ and 3, respectively), whereas calculation (2) amounts to solving an ODE. Additionally, the implementation requires verifying whether a shock wave has a viscous profile, which likewise entails solving an ODE.

A wave curve is determined by its initial state, family, and its sense (forward or backward). To be concrete, we focus attention on the case of a backward f-wave curve with initial state R. For simplicity, we assume that R is a point of strict hyperbolicity and genuine nonlinearity. (The succession algorithm is easily extended to apply when these simplifying assumptions fail to hold.)

In the following, we first explain how to find all admissible wave groups, and then we describe a constructive algorithm based on this explanation.

2.7.1 Shock wave groups

The simplest admissible wave group consists of a single shock wave, S_f, that has a viscous profile. As the state $U_r = R$ on the right side of the shock wave is known, such a solution is determined by the state $U_l = U$ on the left side along with the shock speed σ, which together satisfy the Rankine-Hugoniot condition (2.8). Therefore the complete set of such wave groups can be obtained by first solving the Rankine-Hugoniot condition for U and σ and second eliminating the shock waves that fail to be admissible. (By eliminating σ between the two components of the Rankine-Hugoniot condition, the first step can be reduced to solving one equation in two unknowns, viz., the two components of U.)

Generically, this solution set, which is called the *shock segment* for R, consists of several connected curves, one (the *local component*) having R as an endpoint, and the others being called *detached components*. By the Bethe-Wendroff theorem, we may orient these components so that the shock speed is nondecreasing along them. (For a forward wave curve, we orient the components so that the speed decreases.) A shock component can end at a state U^e in four ways: (i) the shock speed attains a maximum because $\lambda_f(U^e) = \sigma(U^e; R)$ (i.e., the shock wave (U^e, R) is left-sonic in the fast family); (ii) the speed attains a maximum because $\lambda_s(U^e) = \sigma(U^e; R)$ (i.e., the shock wave (U^e, R) is left-sonic in the slow family); (iii) the shock wave (U^e, R) is not admissible, or all shock waves (U, R) for U on the Hugoniot locus of R beyond and in a small neighborhood of U^e are not admissible; or (iv) U^e lies on the boundary of Ω.

2.7.2 Rarefaction wave groups

The next simplest wave group consists of a single rarefaction wave, R_f. Again because the state on the right edge of this wave is known to be R, such a rarefaction wave is defined by a portion of the fast-family integral curve through R that connects the left edge state U to R; along this portion, the fast-family characteristic speed must be nonincreasing from R to U. Therefore the complete set of such wave groups is parametrized by the maximal portion of the integral curve along which the speed is non-decreasing, which is called the *rarefaction segment* through R. (Thus a rarefaction segment consists of a single connected component.) This component can end at a state U^e for two reasons: (i) the characteristic speed attains a minimum because U^e lies on the fast-family inflection locus; or (ii) U^e lies on the boundary of Ω.

2.7.3 Composite components

Now consider a wave group that is a composite wave of the form $S'_f\ R_f$. Such a wave group involves a fast-family shock wave (U, U') that is adjoined on the right by a rarefaction wave from U' to R; crucially, the sonic condition $\sigma(U; U') = \lambda_f(U')$ must hold. In other words, the shock wave (U, U') is right-sonic in the fast family. For a specific wave group, U lies on the Hugoniot locus of U' and satisfies the sonic condition. For a given U', the U is generically one of several isolated points. The complete set of such wave groups is obtained by allowing U' to vary over the rarefaction component through R and finding corresponding states U. This set, the *composite segment* for the rarefaction component through R, is the *sonic extension* of this rarefaction component. Generically, it consists of several connected curves called

composite components. We orient the composite components so that the shock speed is nondecreasing along them, like for shock components (and opposite to rarefaction components).

A composite component can end at a state U^e, with correspond state $(U^e)'$, in five ways: (i) the shock speed attains a maximum because $\lambda_f(U^e) = \sigma(U^e; (U^e)')$ (so that $(U^e, (U^e)')$ is a fast/fast double contact shock wave); (ii) the speed attains a maximum because $\lambda_s(U^e) = \sigma(U^e; (U^e)')$ (so that $(U^e, (U^e)')$ is a slow/fast double contact shock wave); (iii) the shock wave $(U^e, (U^e)')$ is not admissible, or all shock waves (U, U') for U on the Hugoniot locus of U' beyond and in a small neighborhood of U^e are not admissible; (iv) U^e reaches R; or (v) U^e lies on the boundary of Ω.

2.7.4 General wave groups

A wave group of the form $R_f\ 'S_f$ is similar to a one with a single rarefaction wave. Indeed, such a wave group involves a fast-family shock wave (R', R), satisfying the sonic condition $\lambda_f(R') = \sigma(R'; R)$, that is adjoined on the left by a rarefaction wave with left edge state U and right edge state R'. Thus R' is an ending point of type (i) of a shock component, and U lies on the rarefaction component starting at R' (instead of at R); this component likewise can end for two reasons, reaching the fast-family inflection locus or the boundary.

A wave group of the form $R_f\ 'S'_f\ R_f\ ('S_f)$ is also similar to a single rarefaction wave, this time with a rarefaction component starting at the ending point of type (i) (a fast/fast double contact wave) of a composite component. By induction, the more general case $R_f\ 'S'_f\ R_f\ \ldots\ 'S'_f\ R_f\ ('S_f)$ is also similar.

A wave group of the form $S'_f\ R_f\ 'S_f$ is similar to a wave group with a single composite wave $S'_f\ R_f$, except that the right edge state of the rarefaction wave is the left side of a shock wave that is left-sonic in the fast family. Finally, a wave group of the form $S'_f\ R_f\ 'S'_f\ R_f\ ('S_f)$ or $S'_f\ R_f\ 'S'_f\ R_f\ \ldots\ 'S'_f\ R_f\ ('S_f)$ is also similar to a wave group with a single composite wave $S'_f\ R_f$,

2.7.5 Succession algorithm

The foregoing analysis leads to the following *succession algorithm* that finds the complete set of admissible wave groups with right state R.

For convenience, we regard the initial state R as an *initial-state segment* comprising a single *initial-state component*. Also, we employ a *queue* of components, i.e., a first-in/first-out (FIFO) ordered list, which implements two operations: placing a component onto the back of the queue and removing the component at the front of the queue.

We initialize the algorithm by placing the initial-state component onto the back of the queue. Then we repeat the following steps indefinitely.

(I) Remove the component at the front of the queue.

- (a) If this component is the initial-state component, then construct the shock and rarefaction segments through R and place all of their components onto the back of the queue.
- (b) If this component is a shock or composite component with ending point that is a shock wave that is left-sonic in the fast family, then construct the rarefaction segment starting at this ending point and place its components onto the back of the queue.

(c) If this component is a rarefaction component, then construct the composite segment based on it and place all of the composite components onto the back of the queue.

(II) If the queue is empty, terminate the algorithm. Otherwise, go to step (I).

2.7.6 Completeness

As we now argue, algorithm finds all admissible wave groups for the right state R. The argument is based on induction on the *length* ℓ of the wave group (i.e., the number of non-trivial rarefaction and shock waves in it, with the initial-state wave group assigned length zero). Notice that because the component queue used in the succession algorithm is first-in/first-out, wave groups of length ℓ are constructed only after all wave groups of shorter length are constructed.

First consider the case $\ell = 1$. If a wave group consists of a single rarefaction or shock wave, it is constructed in step I(a) prior to constructing any wave groups with $\ell > 1$.

Next consider a wave group with length $\ell > 1$ and assume, as the induction hypothesis, that any wave group with shorter length has previously been constructed by the succession algorithm.

Suppose that the left-most wave is a rarefaction wave. The left edge state of this wave group lies on a certain rarefaction component. Because $\ell > 1$, the starting point of this component must be the left state of the left-most shock wave in the wave group, which is necessarily left-sonic in the fast family. Consider the shorter wave group obtained by omitting the left-most wave (the rarefaction wave). By the induction assumption, this shorter wave group has previously been constructed by the succession algorithm. Therefore the rarefaction component, and hence the full wave group, is constructed in step I(b).

Otherwise, the left-most wave is a shock wave, and because $\ell > 1$, it is right-sonic in the fast family and adjoined on the right by a rarefaction wave. In other words, The left side of this shock wave lies on the composite component associated with a rarefaction component. Again consider the wave group obtained by omitting the left-most wave (the shock wave). By the induction assumption, this shorter wave group has previously been constructed by the succession algorithm. Therefore the composite component, and hence the full wave group, is constructed in step I(c).

Remark 2.7.1. In the literature, usually the algorithm used to construct wave curves is the *continuation algorithm*, which was developed in [25], as a generalization of the Oleĭnik construction for the Riemann solution of scalar equations, [33]. We have performed exhaustive comparisons between the continuation and succession algorithm and we have not found differences when the viscosity matrix identity.

Definition 2.7.2. Consider a state $R \in \Omega$. We say that a segment C of discontinuities is a *local shock* for R if for any $M \in C$ the state M lies on the i-family primary branch of $\mathcal{H}(R)$ and the shock speed varies monotonically along the segment C.

Notice that this definition coincides with Liu's admissibility criterion [24], originating from Oleĭnik's envelope construction [33]. Then, we establish the follow criterion for admissibility.

Claim 2.7.1. *Local shocks for slow and fast families are admissible.*

Based on the triple shock rule and exhaustive numerical experiments, we present the following result about the admissibility of discontinuities

Claim 2.7.2. *Let R be a state in Ω and M be a state in $\mathcal{H}(R)$. If the discontinuity between R and M is admissible then R and M are in the same region of the saturation triangle with respect to an appropriate secondary bifurcation line (Identity Case).*

Chapter 3

The model

In this chapter, we describe the mathematical model for one dimensional three-phase flow in a porous medium [34], under the physical assumptions listed in Section 3.1. In Section 3.2, we obtain the corresponding dimensionless equations. In Section 3.3, we introduce the Corey model with quadratic permeabilities, define the triangle where the fluid saturations are defined and exhibit proprieties of the flux functions. In the last section , we discuss properties of the diffusion terms appearing in the equations

3.1 Derivation of the system of conservations laws

We will study a simplified model for flow in a porous medium of three phases that do not mix assuming the follows facts:

F1. The fluids fill the entire pore rock space.

F2. The *porosity* ϕ is constant.

F3. The *permeability* of the rock K is constant.

F4. The temperature is constant and there is no mass interchange between phases.

F5. The compressibility effects of the phases and the rock are negligible.

F6. There are neither sources nor sinks.

Let consider the conservation of mass for each phase

$$\phi \frac{\partial s_i}{\partial t} + \frac{\partial u_i}{\partial x} = 0, \quad i = w, o, g, \tag{3.1}$$

where s_i denote saturation and u_i is the seepage velocity of each phase that it is defined as the volume of a phase i, Q_i which traverses a straight cross section of rock, of area, per unit of time, i.e., $u_i = Q_i/t$. We assume that Darcy's Law [10, 34] satisfied for each phase i:

$$u_i = -K\lambda_i \left(\frac{\partial}{\partial x} p_i - \rho_i \mathbf{g} \right), \quad i = w, o, g, \tag{3.2}$$

$\lambda_i \geq 0$ is the mobility of phase i, ρ_i is the volumetric density of each phase i and p_i is the pressure of phase i. The mobility is usually expressed as $\lambda_i = k_i/\mu_i$, the ratio of the relative permeability k_i and the viscosity μ_i of phase i. The facts F4, F5 mean that ρ_w, ρ_o and ρ_g are constants, the fact F4 means that μ_w, μ_o and μ_g are constants and the fact F1 means $s_w + s_o + s_g = 1$. Now we define

$$f_i \equiv \frac{\lambda_i}{\lambda_T}, \quad i = w, o, g, \quad \lambda_T \equiv \lambda_w + \lambda_o + \lambda_g. \tag{3.3}$$

$$p_{ij} \equiv p_i - p_j, \quad i, j = w, o, g, \quad \text{and} \quad i \neq j. \tag{3.4}$$

$$u_T \equiv u_w + u_o + u_g. \tag{3.5}$$

The function f_i is the *fractional flow function* corresponding to each phase i, λ_T is the *total mobility* and u_T is the *total seepage velocity*. The difference of pressures between phases, defined in (3.4), is called the *capillary pressure*. We can assume that capillary pressure between the phases is a know function depending of the saturations. Notice that $p_{ij} = -p_{ji}$, $p_{ik} = p_{ij} + p_{jk}$ and only two of the possible six capillary pressure differences are independent. From (3.3)(a) and (3.4), $f_w + f_o + f_g = 1$. Using the definition of u_T (3.5), Darcy's Law (3.2) and using algebraic manipulation, we can write

$$u_T\, f_i = -K\lambda_i \sum_j f_j \left(\frac{\partial p_j}{\partial x} - \rho_j \mathbf{g} \right), \quad i = w, o, g. \tag{3.6}$$

Subtracting u_i in (3.6) and noting that $\left(\frac{\partial}{\partial x} p_i - \rho_i \mathbf{g}\right) = \left(\sum_j f_j\right) \left(\frac{\partial}{\partial x} p_i - \rho_i \mathbf{g}\right)$ we see that

$$u_T\, f_i - u_i \;= -K\lambda_i \textstyle\sum_j f_j \left(\frac{\partial p_j}{\partial x} - \rho_j \mathbf{g} \right) - K\lambda_i \left(\frac{\partial p_i}{\partial x} - \rho_i \mathbf{g} \right), \tag{3.7}$$

$$= -K\lambda_i \sum_{j \neq i} f_j \left(\frac{\partial p_{ji}}{\partial x} - \rho_{ji} \mathbf{g} \right), \tag{3.8}$$

where

$$\rho_{ij} = \rho_i - \rho_j, \quad \rho_{ji} = -\rho_{ij}, \quad i = w, o, g. \tag{3.9}$$

From (3.8) we obtain

$$u_i = u_T f_i + K f_i \sum_{j \neq i} \lambda_j \left(\rho_{ij} \mathbf{g} - \frac{\partial p_{ij}}{\partial x} \right), \quad i = w, o, g. \tag{3.10}$$

Substituting (3.10) into the system (3.1), we obtain

$$\phi \frac{\partial s_i}{\partial t} + \frac{\partial F_i}{\partial x} = D_i, \quad i = w, o, g, \tag{3.11}$$

where

$$F_i = u_T f_i + G_i, \quad \text{with} \quad G_i = K f_i \sum_{j \neq i} \lambda_j \rho_{ij} \mathbf{g}, \quad i = w, o, g. \tag{3.12}$$

and the diffusion terms in (3.11) are expressed in

$$D_i = \frac{\partial}{\partial x}\left(K f_i \sum_{j \neq i} \lambda_j \frac{\partial p_{ij}}{\partial x} \right), \quad i = w, o, g. \tag{3.13}$$

Using again that $\sum_j f_j = 1$ and that $\sum_j G_j = 0$, we obtain, on the one hand

$$F_o + F_w + F_g = u_T(f_o + f_w + f_g) + (G_o + G_w + G_g) = u_T, \tag{3.14}$$

and on the other hand, adding the three equations in (3.13),

$$f_w\left(\lambda_o \frac{\partial p_{wo}}{\partial x} + \lambda_g \frac{\partial p_{wg}}{\partial x}\right) + f_o\left(\lambda_w \frac{\partial p_{ow}}{\partial x} + \lambda_g \frac{\partial p_{og}}{\partial x}\right) + f_g\left(\lambda_w \frac{\partial p_{gw}}{\partial x} + \lambda_o \frac{\partial p_{go}}{\partial x}\right) = 0. \tag{3.15}$$

Then by adding the equations of the system (3.11) we obtain

$$\phi \frac{\partial}{\partial t}(s_o + s_w + s_g) + \frac{\partial}{\partial x}(F_o + F_w + F_g) = 0. \tag{3.16}$$

$$\frac{\partial}{\partial x} u_T = 0. \tag{3.17}$$

The equation (3.17) reflects the incompressibility of the fluids. We conclude that the total velocity u_T is not a function of the space variable, thus we shall assume that the total velocity u_T is constant. Taking into account the incompressibility property of the fluids and the fact F1 the system (3.11) has a redundant equation, $i.e.$, any of these equations can be derived from the other two.

3.2 Equations in dimensionless form

It is convenient to express the system (3.11) in dimensionless form, in order to identify the most important non-dimensional parameter groups for the evolution problem. To this end, we define the following changes variables:

$$\widetilde{x} = \frac{x}{L}, \qquad \widetilde{t} = \frac{t\, u_{T ref}}{L\, \phi}, \qquad \widetilde{u_T} = \frac{u_T}{u_{T ref}}, \qquad \widetilde{K} = \frac{K}{K_{ref}}, \tag{3.18}$$

$$\widetilde{\lambda_i} = \lambda_i \mu_{ref}, \qquad \widetilde{\mu_i} = \frac{\mu_i}{\mu_{ref}}, \qquad \widetilde{\rho_i} = \frac{\rho_i}{\rho_{ref}}, \qquad \widetilde{p_i} = \frac{p_i}{p_{ref}}, \qquad i = w, o, g. \tag{3.19}$$

We denote $L[\mathrm{m}]$ the reference length of the system, $\rho_{ref}[\mathrm{kg/m^3}]$ the reference density, $u_{T ref}[\mathrm{m/s}]$ the reference velocity of the problem, $K_{ref}[\mathrm{m^2}]$ the reference absolute permeability, $p_{ref}[\mathrm{kg/m/s^2}]$ the reference pressure and $\mu_{ref}[\mathrm{kg/m/s}]$ the reference viscosity. Substituting the dimensionless variables into the system (3.11), we obtain

$$\frac{\partial s_i}{\partial \widetilde{t}} + \frac{\partial}{\partial \widetilde{x}}\left(\widetilde{u_T} \widetilde{f_i} + C_g \widetilde{G_i}\right) = C_v \widetilde{D_i}, \quad i = w, o, g, \tag{3.20}$$

where $\widetilde{f}_i = \frac{\widetilde{\lambda}_i}{\widetilde{\lambda_T}}$, $C_g = \frac{K_{ref}\ \mathbf{g}\ \rho_{ref}}{u_{T\,ref}\ \mu_{ref}}$, $C_v = \frac{K_{ref} p_{ref}}{u_{T\,ref}\ L\ \mu_{ref}}$ and

$$\widetilde{G_i} = \widetilde{K}\widetilde{f}_i \sum_{j \neq i} \widetilde{\lambda}_j \widetilde{\rho_{ij}}, \qquad i = w, o, g, \tag{3.21}$$

and the diffusion terms

$$\widetilde{D_i} = \frac{\partial}{\partial x}\left(\widetilde{K}\widetilde{f}_i \sum_{j \neq i} \widetilde{\lambda}_j \frac{\partial \widetilde{p_{ij}}}{\partial x} \right), \qquad i = w, o, g. \tag{3.22}$$

The constants C_g and C_v are the dimensionless parameters reflecting the gravitational and capillary effects. As we are interested to study the gravity effects maintaining the first term of the flux we choose u_{Tref} such that $\widetilde{u_T} = 1$ and defined

$$\vartheta = \widetilde{K} C_g \text{ and } \epsilon = \widetilde{K} C_v. \tag{3.23}$$

Omitting the 'tilde' and defining the dimensionless gravitational vector $G = (G_w, G_o, G_g)^T$ and the dimensionless diffusion vector $D = (D_w, D_o, D_g)^T$, we obtain the system

$$\frac{\partial s_i}{\partial t} + \frac{\partial}{\partial x}\left(f_i(s_w, s_o, s_g) + \vartheta\, G_i(s_w, s_o, s_g) \right) = \epsilon D_i(s_w, s_o, s_g), \qquad i = w, o, g. \tag{3.24}$$

By recalling that one of these equations is redundant, we notice that for any choices of the two saturations, the system (3.24) reduces to a 2×2 parabolic system of form

$$\frac{\partial U}{\partial t} + \frac{\partial F(U)}{\partial x} = \epsilon \frac{\partial}{\partial x}\left(\mathcal{B}(U) \frac{\partial U}{\partial x} \right), \tag{3.25}$$

where U, $F(U)$ and the matrix $\mathcal{B}(U)$ are given in terms of two saturations and the two selected corresponding flow functions. Although it requires only two saturations to represent a state, often going to use the three components to represent it, so it is clear the values of the three saturations in this state.

3.3 The Corey model

In Petroleum Engineering a frequently used relative permeability model is due to Corey, [28]. In such model the mobilities $\lambda_i(s_i)$ are non-decreasing continuous functions of their own saturations s_i exclusively, $i = w, o, g$. For simplicity in our analysis we neglect the effect of residual saturations.

Based on experimental data, the Corey model consider the following relationships of dependency for relative permeabilities: $k_w = s_w^\alpha$, $k_o = s_o^\beta$ and $k_g = s_g^\gamma$, where α, β and γ are called the Corey exponents. To take advantage of previous work, see [39], we will consider a quadratic model $i.e.$, $\alpha = \beta = \gamma = 2$, which we refer as Corey Quad model. Therefore the mobility and the fractional flow functions for each phase $i = w, o, g$, defined in (3.3) and (3.4) become

$$\lambda_i(s_i) = \frac{s_i^2}{\mu_i}, \qquad i = w, o, g; \qquad \lambda_T = \frac{s_w^2}{\mu_w} + \frac{s_o^2}{\mu_o} + \frac{s_g^2}{\mu_g}; \tag{3.26}$$

$$\text{and} \quad f_i = \frac{s_i^2/\mu_i}{\lambda_T}, \qquad i = w, o, g. \tag{3.27}$$

From (3.26) and (3.27) we obtain the flux functions (3.12) for the *Corey Quad model* as

$$F_i = \frac{s_i^2}{\mu_i}\left[1 + \vartheta \sum_{j \neq i} \rho_{ij} \frac{s_j^2}{\mu_j}\right] / \lambda_T, \qquad i = w, o, g, \tag{3.28}$$

and the diffusion terms

$$D_i = \frac{\partial}{\partial x}\left(\frac{s_i^2}{\mu_i}\left[\sum_{i \neq j} \frac{s_j^2}{\mu_j}\frac{\partial p_{ij}}{\partial x}\right] / \lambda_T\right). \tag{3.29}$$

We will find it convenient later to be flexible in our choice of the two saturations entering in the system of two equations. If we use $(s_w, s_o)^T$ the other saturation s_g is replaced by $1 - s_w - s_o$. Also it is useful to replace p_{wo} by $p_{wg} + p_{go}$. Thus we obtain the following system of two equations, for three-phase flow

$$\frac{\partial}{\partial t}\begin{pmatrix} s_w \\ s_o \end{pmatrix} + \frac{\partial}{\partial x}\begin{pmatrix} F_w(s_w, s_o) \\ F_o(s_w, s_o) \end{pmatrix} = \frac{\partial}{\partial x}\begin{pmatrix} \lambda_w[-f_o \dfrac{\partial p_{og}}{\partial x} + (1 - f_w)\dfrac{\partial p_{wg}}{\partial x}] \\ \lambda_o[-f_w \dfrac{\partial p_{wg}}{\partial x} + (1 - f_o)\dfrac{\partial p_{og}}{\partial x}] \end{pmatrix}, \tag{3.30}$$

where

$$F_w(s_w, s_o) = \frac{s_w^2}{\mu_w}\left[1 + \vartheta\left(\rho_{wo}\frac{s_o^2}{\mu_o} + \rho_{wg}\frac{(1 - s_o - s_w)^2}{\mu_g}\right)\right] / \lambda_T(s_w, s_o), \tag{3.31}$$

$$F_o(s_w, s_o) = \frac{s_o^2}{\mu_o}\left[1 + \vartheta\left(\rho_{ow}\frac{s_w^2}{\mu_w} + \rho_{og}\frac{(1 - s_o - s_w)^2}{\mu_g}\right)\right] / \lambda_T(s_w, s_o), \tag{3.32}$$

with

$$\lambda_T(s_w, s_o) = \frac{s_w^2}{\mu_w} + \frac{s_o^2}{\mu_o} + \frac{(1 - s_o - s_w)^2}{\mu_g}. \tag{3.33}$$

The system (3.30) can be written in form of a system of Conservation Laws (3.25) defining $U = (s_w, s_o)^T$, $F(U) = (F_w(s_w, s_o), F_o(s_w, s_o))^T$ and $\mathcal{B}(U) = Q(U)P'(U)$ where

$$Q(U) = \begin{pmatrix} \lambda_w(1 - f_w) & -\lambda_w f_o \\ -\lambda_o f_w & \lambda_o(1 - f_o) \end{pmatrix} \quad \text{and} \quad P'(U) = \begin{pmatrix} \frac{\partial p_{wg}}{\partial s_w} & \frac{\partial p_{wg}}{\partial s_o} \\ \frac{\partial p_{og}}{\partial s_w} & \frac{\partial p_{og}}{\partial s_o} \end{pmatrix}. \tag{3.34}$$

We refer to $Q(U)$ and $P'(U)$ as *balance matrix* and *capillary pressure Jacobian*, [7].

Remark 3.3.1. Note that the matrix $\mathcal{B}(U)$ does not depend on the gravity term.

To conclude this section we will rewrite the flux functions F_w, F_o given by (3.31)-(3.32) defining the vectors $\mathcal{F}(U) = (f_w(s_w, s_o), f_o(s_w, s_o))^T$ and $\mathcal{G}(U) = (G_w(s_w, s_o), G_o(s_w, s_o))^T$ such that

$$F(U) = \mathcal{F}(U) + \vartheta\, \mathcal{G}(U), \tag{3.35}$$

where $\mathcal{F}(U)$ is given by the fractional flow functions in two saturations (3.27)

$$\mathcal{F}(U) = \begin{pmatrix} f_w(s_w, s_o) \\ f_o(s_w, s_o) \end{pmatrix} = \begin{pmatrix} \dfrac{s_w^2/\mu_w}{\lambda_T(s_w, s_o)} \\ \dfrac{s_o^2/\mu_o}{\lambda_T(s_w, s_o)} \end{pmatrix}, \tag{3.36}$$

and $\mathcal{G}(U)$ is the gravitational vector given by

$$\mathcal{G}(U) = \begin{pmatrix} G_w(s_w, s_o) \\ G_o(s_w, s_o) \end{pmatrix} = \begin{pmatrix} \dfrac{s_w^2}{\mu_w}\left(\rho_{wo}\dfrac{s_o^2}{\mu_o} + \rho_{wg}\dfrac{(1-s_o-s_w)^2}{\mu_g}\right)/\lambda_T(s_w, s_o) \\ \dfrac{s_o^2}{\mu_o}\left(\rho_{ow}\dfrac{s_w^2}{\mu_w} + \rho_{og}\dfrac{(1-s_o-s_w)^2}{\mu_g}\right)/\lambda_T(s_w, s_o) \end{pmatrix}. \tag{3.37}$$

In (3.36) and (3.37) $\lambda_T(s_w, s_o)$ is given by (3.33). Then the system (3.30) can be written in its final form:

$$\frac{\partial}{\partial t}U + \frac{\partial}{\partial x}(\mathcal{F}(U) + \vartheta\,\mathcal{G}(U)) = \frac{\partial}{\partial x}\left(Q(U)P'(U)\frac{\partial}{\partial x}U\right). \tag{3.38}$$

Remark 3.3.2. In this work we do not consider gravity effects, *i.e.,* only consider the case $\vartheta = 0$.

3.3.1 The Saturation Triangle

In order to study the Riemann problem for the three-phase flow without gravity ($\vartheta = 0$), we need to perform all the calculations in the space of saturations. We define the saturation triangle as follow

$$T = \Big\{(s_w, s_o) \in \mathbb{R}^2 \,:\, 0 \le s_w \le 1,\, 0 \le s_o \le 1,\, s_w + s_o \le 1\Big\}; \tag{3.39}$$

and useful alternative definition would be

$$T = \Big\{(s_w, s_o, s_g) \in \mathbb{R}^3 \,:\, 0 \le s_i \le 1,\, i = w, o, g.\; s_g = 1 - s_w - s_o\Big\}, \tag{3.40}$$

as well as the interior of the saturation triangle

$$\widetilde{T} = \Big\{(s_w, s_o) \in \mathbb{R}^2 \,:\, 0 < s_w < 1,\, 0 < s_o < 1,\, s_w + s_o < 1\Big\}. \tag{3.41}$$

A natural choice for the state space for our model is the saturation triangle T (3.39) in barycentric coordinates such that the vertices represent the states with maximum saturation ($s_i = 1$,$i = w, o, g.$) with coordinates $W = (1, 0, 0)^T$, $O = (0, 1, 0)^T$ and $G = (0, 0, 1)^T$, representing total water, oil and gas, respectively, see Figure 3.1(a).

Remark 3.3.3. In [36] was proven that there are four umbilic points for the Corey Quad model: the three vertices G, W, O and $\mathcal{U}$, which is inside saturation triangle. Moreover, the state $\mathcal{U}$ is the intersection of the three secondary bifurcation lines (see Figure 3.1). The coordinates of the umbilic point are

$$\mathcal{U} = \left(\frac{\mu_w}{\mu_w + \mu_o + \mu_g}, \frac{\mu_o}{\mu_w + \mu_o + \mu_g}, \frac{\mu_g}{\mu_w + \mu_o + \mu_g}\right). \tag{3.42}$$

We have three relevant points in the boundary of saturation triangle, as we will see in Chapter 5 the straight lines for these points represent invariant lines for our model and are determined by the viscosity of each phase. The coordinates are

$$B = \left(\frac{\mu_w}{\mu_w+\mu_g}, 0, \frac{\mu_g}{\mu_w+\mu_g}\right),\ D = \left(\frac{\mu_w}{\mu_w+\mu_o}, \frac{\mu_o}{\mu_w+\mu_o}, 0\right),\ E = \left(0, \frac{\mu_o}{\mu_o+\mu_g}, \frac{\mu_g}{\mu_o+\mu_g}\right). \tag{3.43}$$

Remark 3.3.4. The examples and figures of this work use the values $\mu_w = 1, \mu_g = 0.75$ and $\mu_o = 2$, which are from hereon implied unless other values are explicitly stated.

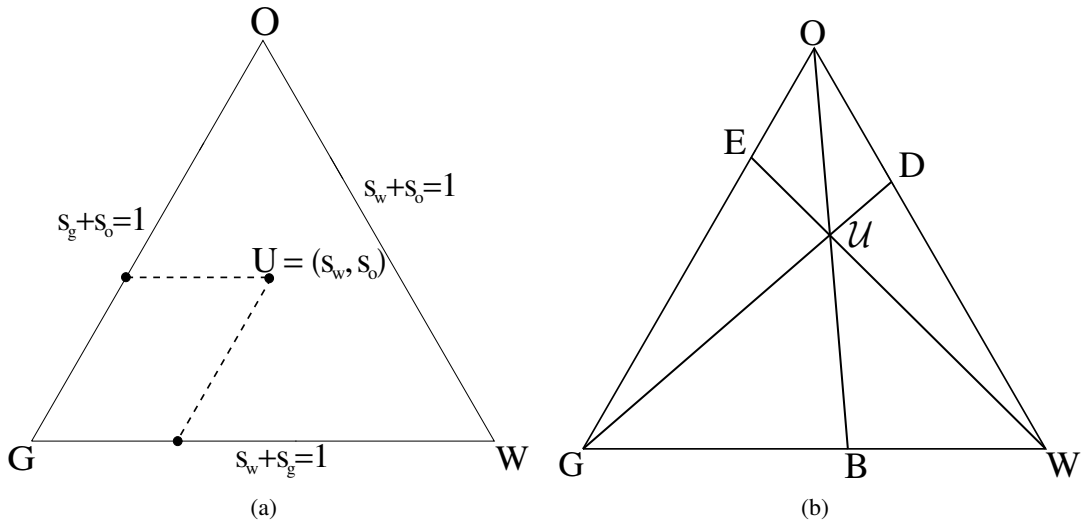

Figure 3.1: (a) In barycentric coordinates a state $U = (s_w, s_o, s_g) \in T$. (b) Points over the boundary B,D and E

.

Remark 3.3.5. Consider the straight line segments $[G, D]$ $[O, B]$ and $[E, W]$ shown in Figure 3.1. These lines satisfy the following equations:

$$[O, B] = \{(s_w, s_o, s_g) \in T \mid s_w/\mu_w = s_g/\mu_g\ ,\ \ s_o = 1 - s_w - s_g\}; \tag{3.44}$$

$$[E, W] = \{(s_w, s_o, s_g) \in T \mid s_g/\mu_g = s_o/\mu_o\ ,\ \ s_w = 1 - s_o - s_g\}; \tag{3.45}$$

$$[G, D] = \{(s_w, s_o, s_g) \in T \mid s_o/\mu_o = s_w/\mu_w\ ,\ \ s_g = 1 - s_w - s_o\}; \tag{3.46}$$

We recall the classification of the umbilic point given in [36], as type I or II. In [5] and [30], the position of the umbilic point was characterized for a general family of models, of which the Corey Quad model is a particular case.

Definition 3.3.6. For the Corey Quad model, we define the triangle $\mathcal{T}_{\mathcal{U}}$ with vertices $(0, 1/2, 1/2)$, $(1/2, 0, 1/2)$, and $(1/2, 1/2, 0)$, see shaded triangle in Figure 3.2(a).

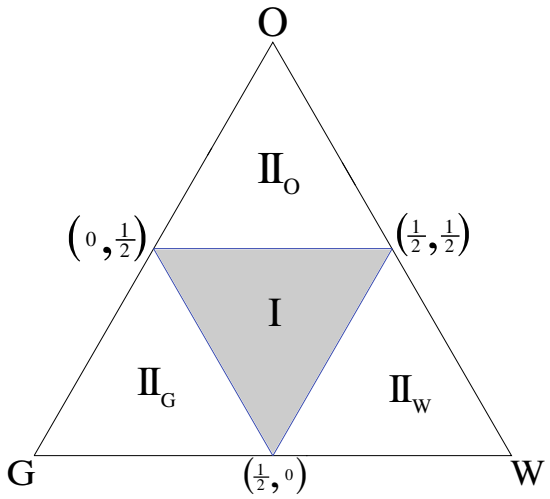

Figure 3.2: Regions where $\mathcal{U}$ is type I and II.

Theorem 3.3.1 ([30, 36]). *For the Corey Quad model the umbilic point is classified as:*

1. *type I if $\mathcal{U}$ lies inside $\mathcal{T}_{\mathcal{U}}$;*
2. *type II if $\mathcal{U}$ lies outside $\mathcal{T}_{\mathcal{U}}$;*
3. *border-type I/II if $\mathcal{U}$ lies on the edges of $\mathcal{T}_{\mathcal{U}}$.*

Definition 3.3.7. Taking into account Theorem 3.3.1, we subdivide the saturation triangle in four regions as follows: the inner triangle $\mathcal{T}_{\mathcal{U}}$ given in Definition 3.3.6 and the outer triangles II_W, II_O and II_G that are characterized as containing one of the vertices of the saturation triangle (see Figure 3.2(a)). We say that the umbilic point is type II if it is in any outer triangle.

3.3.2 Properties of fractional flow functions in Corey Quad model

In this section we use the formulation (3.38) with $\vartheta = 0$, *i.e.,* $F(U) = \mathcal{F}(U)$ given by (3.36), in the space of saturations $(s_w, s_o)^T$. We have according to (3.26) and (3.27) that

$$\frac{\partial f_i}{\partial s_j} = \frac{1}{\lambda_T}\frac{\partial \lambda_i}{\partial s_j} - \frac{\lambda_i}{\lambda_T^2}\frac{\partial \lambda_T}{\partial s_j}. \tag{3.47}$$

Now we follow [7] for study the fractional flow functions properties.

Lemma 3.3.2. *The Corey Quad model satisfies the following assumptions:*

i) *f_w and f_o are continuously differentiable functions on the closed saturation triangle.*

ii) *$f_o \geq 0$ in T with $f_o = 0$ if and only if $s_o = 0$.*

iii) $\frac{\partial f_w}{\partial s_w} > \frac{\partial f_o}{\partial s_o} = 0$ *on the open edge* $\{(s_w, s_o) : s_o = 0, 0 < s_w < 1\}$.

iv) $\frac{\partial f_w}{\partial s_o} > 0$ *and* $\frac{\partial f_o}{\partial s_w} > 0$ *in* $\widetilde{T}$ *near the corner* $s_w = 0$, $s_o = 0$.

Proof. i) and ii) follow from the definitions (3.26) and (3.27).

iii) Since

$$\frac{\partial \lambda_w}{\partial s_w} = \frac{2s_w}{\mu_w}, \quad \frac{\partial \lambda_w}{\partial s_o} = \frac{\partial \lambda_o}{\partial s_w} = 0, \quad \frac{\partial \lambda_o}{\partial s_o} = \frac{2s_o}{\mu_o}, \tag{3.48}$$

$$\frac{\partial \lambda_T}{\partial s_w} = \frac{\partial \lambda_w}{\partial s_w} - \frac{2(1 - s_w - s_o)}{\mu_g}, \quad \frac{\partial \lambda_T}{\partial s_o} = \frac{\partial \lambda_o}{\partial s_o} - \frac{2(1 - s_w - s_o)}{\mu_g}. \tag{3.49}$$

From (3.47) we have on the one hand

$$\frac{\partial f_w}{\partial s_w} = \frac{1}{\lambda_T}\frac{\partial \lambda_w}{\partial s_w} - \frac{\lambda_w}{\lambda_T^2}\frac{\partial \lambda_T}{\partial s_w} = \frac{1}{\lambda_T}\frac{2s_w}{\mu_w} - \frac{\lambda_w}{\lambda_T^2}\left(\frac{2s_w}{\mu_w} - \frac{2\,(1 - s_w - s_o)}{\mu_g}\right), \tag{3.50}$$

then

$$\lambda_T^2 \frac{\partial f_w}{\partial s_w} = \frac{2s_w}{\mu_w}\left(\frac{{s_o}^2}{\mu_o} + \frac{(1 - s_w - s_o)^2}{\mu_g}\right) + \frac{2{s_w}^2}{\mu_w}\left(\frac{1 - s_w - s_o}{\mu_g}\right). \tag{3.51}$$

is nonnegative everywhere and reduces to

$$\lambda_T^2 \frac{\partial f_w}{\partial s_w}\bigg|_{s_o=0} = \frac{2s_w(1 - s_w)}{\mu_w \mu_g}. \tag{3.52}$$

On the other hand

$$\lambda_T^2 \frac{\partial f_o}{\partial s_o} = \frac{2s_o}{\mu_o}\left(\frac{{s_w}^2}{\mu_w} + \frac{(1 - s_w - s_o)^2}{\mu_g}\right) + \frac{2{s_o}^2}{\mu_o}\left(\frac{1 - s_w - s_o}{\mu_g}\right), \tag{3.53}$$

and

$$\lambda_T^2 \frac{\partial f_o}{\partial s_o}\bigg|_{s_o=0} = 0. \tag{3.54}$$

In particular $\frac{\partial f_w}{\partial s_w} = 0$ at the corner $s_w = 0, s_o = 0$. Moreover $\frac{\partial f_w}{\partial s_w} > \frac{\partial f_o}{\partial s_o}$ on the open edge and $s_o = 0,\ \ 0 < s_w < 1$.

iv) From (3.47) and (3.48) we have

$$\frac{\partial f_o}{\partial s_w} = -\frac{\lambda_o}{\lambda_T^2}\left(\frac{2s_w}{\mu_w} - \frac{2\,(1 - s_w - s_o)}{\mu_g}\right), \tag{3.55}$$

and

$$\frac{\partial f_w}{\partial s_o} = -\frac{\lambda_w}{\lambda_T^2}\left(\frac{2s_o}{\mu_o} - \frac{2\,(1 - s_w - s_o)}{\mu_g}\right), \tag{3.56}$$

so that $\frac{\partial f_w}{\partial s_o} > 0$ and $\frac{\partial f_o}{\partial s_w} > 0$ in $\widetilde{T}$ a neighborhood of $(0, 0)$.

■

Remark 3.3.8. Notice that from Lemma 3.3.2(ii) and by (3.55), that $\frac{\partial f_o}{\partial s_w} = 0$ on the edge $s_o = 0$, so that the Jacobian DF is upper triangular and its eigenvalues are $\frac{\partial f_w}{\partial s_w}$ and $\frac{\partial f_o}{\partial s_o}$ associated to the eigenvectors

$$(1,0)^T \quad \text{and} \quad \left(\frac{\partial f_w}{\partial s_w}, \frac{\partial f_w}{\partial s_w} - \frac{\partial f_o}{\partial s_o}\right), \tag{3.57}$$

respectively. Hence assumption (iii) of Lemma 3.3.2 states that the eigenvalues are distinct on each open edge, and that the fast eigenvector (3.57)(a) is parallel to the edge.

Remark 3.3.9. Consider the closed edge $\{(s_w, s_o) : s_o = 0, 0 \leq s_w \leq 1\}$. From (ii) this border is invariant for system (3.25). Indeed, system (3.30) reduces to the scalar conservation law

$$\frac{\partial s_w}{\partial x} + \frac{\partial}{\partial x}\left(\frac{s_w^2/\mu_w}{s_w^2/\mu_w + (1-s_w)^2/\mu_g}\right) + \varepsilon \frac{\partial}{\partial x}\left(\lambda_w(1-f_w)\frac{\partial p_{wg}}{\partial x}\right) = 0. \tag{3.58}$$

Notice that a similar reduction occurs on the other edges. Thus three-phase flow reduces to the Buckley-Leverett equation for two-phase flow along each edge, [12]. In particular, $\frac{\partial f_w}{\partial s_w} = 0$ and $\frac{\partial f_o}{\partial s_o} = 0$ at the corner $s_w = 0, s_o = 0$, reflecting the immiscibility of two-phase flow.

Remark 3.3.10. Assumption (iv) of Lemma 3.3.2 implies that the eigenvalues are distinct in the interior of T near each corner. Thus, the model is strictly hyperbolic near the boundary except at the corners where the eigenvalues coincide.

Remark 3.3.11. The Lemma 3.3.2 should be proof is you choose any phase space state for example $(s_w, s_g)^T$ ou $(s_o, s_g)^T$, thus the conclusions of this section can be applied to any combination of flux functions (f_i, f_j) for $(i,j) = \{(w,o),(w,g),(o,g)\}$.

3.4 Properties of the Viscosity Matrix

In principle the capillary pressures are experimentally measured functions of all saturations. In this work we adopt the same model that [7, 29] for the capillary pressure differences that can be taken to have the form $p_{wo} = -P_{ow}(s_w)$ and $p_{go} = -P_{og}(s_g)$, where P_{ow} and P_{og} are monotone decreasing functions defined by:

$$P_{ow} = c_{ow}\left(\frac{1-s_w}{\sqrt{s_w}}\right) \quad \text{and} \quad P_{og} = c_{og}\left(\frac{1-s_g}{\sqrt{s_g}}\right). \tag{3.59}$$

Here c_{ow} and c_{og} are positive constants. From (3.4) we have $p_{wg} = p_{wo} + p_{og}$, then $P'(U)$ defined in (3.34)(b) is

$$P' = \begin{pmatrix} \varsigma + \tau & \tau \\ \tau & \tau \end{pmatrix}, \tag{3.60}$$

where

$$\varsigma = \frac{c_{ow}}{2}\frac{(1+s_w)}{s_w^{3/2}} \quad \text{and} \quad \tau = \frac{c_{og}}{2}\frac{(2-s_w-s_o)}{(1-s_w-s_o)^{3/2}}. \tag{3.61}$$

Now we show some properties of the matrix $B(U)$ follow [7].

Lemma 3.4.1. *From (3.60) we have*

$$P' \text{ is positive definite and diagonally dominant in } T, \tag{3.62}$$

$$\frac{\partial p_{wg}}{\partial s_w} > 0 \text{ on the edge without vertex } G \ \{(s_w, s_o)^T : s_o = 0, 0 < s_w \leq 1\}. \tag{3.63}$$

Proof. From (3.60), $\frac{\partial p_{wg}}{\partial s_w} = \varsigma + \tau > 0, \quad \forall U \in T$. P' is symmetric and we have

$$\det(P'(U)) = \varsigma\tau > 0 \quad \text{and} \quad \operatorname{tr}(P'(U)) = \varsigma + 2\tau > 0. \tag{3.64}$$

■

Lemma 3.4.2. *Under the hypothesis of Lemma 3.3.2, the balance matrix $Q(U)$ is symmetric and positive definite in the interior of the saturation triangle T, and $\det Q(U) = 0$ on ∂T .*

Proof. Notice that from (3.34)(a) that

$$Q(U) = \begin{pmatrix} \lambda_w(1-f_w) & -\lambda_w f_o \\ -\lambda_o f_w & \lambda_o(1-f_o) \end{pmatrix} = \frac{1}{\lambda_T} \begin{pmatrix} \lambda_w(\lambda_o+\lambda_g) & -\lambda_w\lambda_o \\ -\lambda_o\lambda_w & \lambda_o(\lambda_w+\lambda_o) \end{pmatrix}. \tag{3.65}$$

Then

$$\det(Q(U)) = \frac{1}{\lambda_T^2}\left(\lambda_w\lambda_o(\lambda_o+\lambda_g)(\lambda_w+\lambda_g) - \lambda_w^2\lambda_o^2\right) = \frac{\lambda_w\lambda_o\lambda_g}{\lambda_T}. \tag{3.66}$$

Therefore $\det(Q(U)) = 0$, for $U \in \partial T$. Of course from right side of (3.65) Q is symmetric and diagonal dominant. ■

Lemma 3.4.3. *If P' satisfies the hypothesis of Lemma 3.4.1, then the eigenvalues of the viscosity matrix $\mathcal{B}(U)$ have positive part in the interior of T, whereas on the boundary of T , one eigenvalue of $\mathcal{B}(U)$ is zero and the other is positive.*

Proof. The eigenvalues $\mu(U)$ of $\mathcal{B}(U)$ are

$$\mu^{\pm}(U) = (1/2)\left(tr(\mathcal{B}(U)) \pm \sqrt{[tr(\mathcal{B}(U))]^2 - 4\ \det(\mathcal{B}(U))}\right). \tag{3.67}$$

Thus, $\mathcal{B}(U)$ has eigenvalues with positive real part provided that its trace and determinant are positive. From (3.64) and (3.66) the determinants of both Q and P' are nonnegative, so that $\det(\mathcal{B}) = \det(Q)\det(P') \geq 0$ as well, with strict inequality in the interior of T. From (3.60) and (3.65), we find that

$$\operatorname{tr}(\mathcal{B}) = (\tau\lambda_g\lambda_w + \tau\lambda_o^2 + \varsigma\lambda_g\lambda_w + \varsigma\lambda_o\lambda_w)/\lambda_T > 0. \tag{3.68}$$

Then by (3.67) when $U \in \partial T$, $\mu^-(U) = 0$ and $\mu^+(U) = \operatorname{tr}(\mathcal{B}(U))$. ■

Chapter 4

Properties of Corey Quad model

In this chapter, we present basic facts about the system of conservation laws (3.38) ($\vartheta = 0$). In Section 4.1, we describe the integral field defined by each characteristic family. In Section 4.2, we discuss Hugoniot curves, which play a fundamental role in this work. In Section 4.3, we present a method to obtain the secondary bifurcation locus. In Section 4.4, we describe the mixed double contact and the fast double contact loci, when the umbilic point U is of type II. These bifurcation loci are relevant for the identification of regions of states with the same structure of Riemann solutions. In Section 4.5, we describe the inflection locus for each characteristic family, including their dependence on viscosity values μ_w, μ_o and μ_g. Finally, in Section 4.6, we describe the boundary extension locus.

4.1 Rarefaction Foliation

In this section we study the rarefaction foliation for the slow and fast characteristic fields. In Figures 4.1(a) and (b) we depict integral curves of slow- and fast-families for Corey Quad model with $\mathcal{U} \in II_O$. As seen in [9], these curves form two foliations with singularities at the umbilic point and vertices. To study these foliations, Azevedo *et al.* [9] calculate eigenvectors along edges and secondary bifurcation lines of the triangle.

Claim 4.1.1. *Consider the Corey Quad model and fixed, arbitrary values for μ_w, μ_o and μ_g . Then we have:*

1. *Along each edge of the saturation triangle:*
   - *(a) the fast family eigenvector is parallel to the edge;*
   - *(b) the slow-family eigenvector is parallel at each point to a line connecting this point and the vertex opposite to the edge.*
2. *The directions change between slow and fast eigenvector when passing through $\mathcal{U}$, i.e., over any secondary bifurcation line, along the segment between the vertex and the umbilic point $\mathcal{U}$, the slow-family eigenvector is parallel to the edge opposite to the vertex, while the fast-family is*

parallel to the secondary bifurcation line. On the other hand, along the segment between $\mathcal{U}$ and the opposite side of the vertex, the slow-family is parallel to the secondary bifurcation line, while the fast-family is parallel to edge opposite to the vertex.

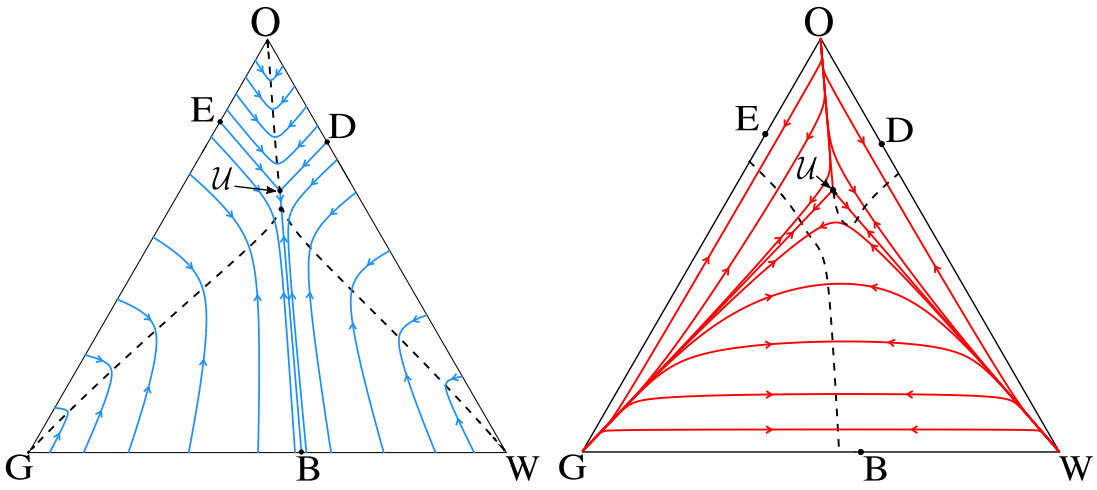

(a) Slow-family integral curves. (b) Fast-family integral curves.

Figure 4.1: Integral curves for (a) slow family and (b) fast family. The arrow indicates the direction on which characteristic speeds increase. The inflection curves for each family are represented by dashed lines. In this figures the umbilic point is of type II_O.

As far as the slow-family rarefaction foliation is concerned, segments $[E,\mathcal{U}]$, $[D,\mathcal{U}]$ and $[B,\mathcal{U}]$ split the saturation triangle in three quadrilaterals in which the rarefaction foliation is invariant and can be regarded as a vector field. Similarly for the fast-family rarefaction foliation, the segments $[O,\mathcal{U}]$, $[W,\mathcal{U}]$ and $[G,\mathcal{U}]$ split the saturation triangle in three sub-triangles in which the rarefaction foliation is invariant and can be regarded as a vector field.

Remark 4.1.1. The description made in Claim 4.1.1 does not take into account the analysis near singularities G, W, O and $\mathcal{U}$. However, a complete analysis and justification can be found in [35] in the context of the wave curve manifold, [20].

4.2 Hugoniot curves

The Hugoniot curve based on a state R consists of two primary branches which intersect at R and possibly a nonlocal branch (detached branch). For R varying along an edge of the saturation triangle, the explicit formula was compute in [9]. It consist of such edge together with a hyperbola. For R varying along any straight line $[G, D]$, $[W, E]$ and $[O, B]$ defined in Remark 3.3.5, was compute in [3]. It consist of such straining line together also with a hyperbola: its attached branch contains the state R. In particular, its

topological structure with two primary (attached) branches and one detached is preserved along invariant lines.

On the other hand, to obtain an expression for the Hugoniot curve for arbitrary states, we consider the system of conservation laws (3.25) with the flow function $F(U) = \mathcal{F}(U)$ given by (3.36) and a constant state $U_l = (s_w^-, s_o^-)^T \in \widetilde{T}$. Then,we want to find solutions $U = (s_w, s_o)^T$ of the system (2.10), *i.e.*,

$$f_w(s_w, s_o) - f_w(s_w^-, s_o^-) = \sigma(s_w - s_w^-), \tag{4.1}$$

$$f_o(s_w, s_o) - f_o(s_w^-, s_o^-) = \sigma(s_o - s_o^-). \tag{4.2}$$

By eliminating σ from (4.1)-(4.2) and using the flux expressions (3.36), we obtain

$$(s_o - s_o^-)\left(\frac{s_w^2/\mu_w}{\lambda_T(s_w, s_o)} - \frac{{s_w^2}^-/\mu_w}{\lambda_T(s_w^-, s_o^-)}\right) - (s_w - s_w^-)\left(\frac{s_o^2/\mu_o}{\lambda_T(s_w, s_o)} - \frac{{s_o^2}^-/\mu_o}{\lambda_T(s_w^-, s_o^-)}\right) = 0. \tag{4.3}$$

In order to solve equation (4.3), we follow the construction introduced by Isaacson, Marchesin, Palmeira and Plohr in [20]. We want to find a function $R : [0, \pi] \to \mathbb{R}$ such that

$$s_w = s_w^- + R(\theta)\cos(\theta), \tag{4.4}$$

$$s_o = s_o^- + R(\theta)\sin(\theta). \tag{4.5}$$

Substituting expressions (4.4),(4.5) in (4.3), we obtain after some simplifications

$$\begin{aligned} R(\theta)\left[B_1\sin^3(\theta) + B_2\cos(\theta)\sin^2(\theta) + B_3\cos^2(\theta)\sin(\theta) + B_4\cos^3(\theta)\right] \\ + B_5\sin^2(\theta) + B_6\cos(\theta)\sin(\theta) + B_7\cos^2(\theta) = 0. \end{aligned} \tag{4.6}$$

Dividing (4.6) by $\cos^3(\theta)$ and solving for $R(\theta)$, we find

$$R(\theta) = -\frac{\sec(\theta)\left(B_5\,\tan^2(\theta) + B_6\,\tan(\theta) + B_7\right)}{B_1\,\tan^3(\theta) + B_2\,\tan^2(\theta) + B_3\,\tan(\theta) + B_4}. \tag{4.7}$$

Here, the coefficients $B_1, B_2, \ldots, B_7$ depend only on constant state $U_l = (s_w^-, s_o^-)^T$ and on the constant values μ_w, μ_o and μ_g. Therefore we conclude that for any point U_l in the interior of the saturation triangle, the Rankine-Hugoniot locus is the set

$$\widetilde{\mathcal{H}}(U_l) = \left\{ (s_w, s_o)^T \in \widetilde{T} \,|\, s_w \text{ and } s_o \text{ are given for (4.4) and (4.5) for } R(\theta) \text{ expressed in (4.7)} \right\}. \tag{4.8}$$

4.3 Secondary Bifurcation

The secondary bifurcation manifold consists of the states which do not satisfy the hypothesis of the implicit function theorem; generically, the Hugoniot locus changes topology at such a locus. We follow the ideas set forth by [13] for the calculation of states belonging to a secondary bifurcation lines and

their corresponding such that Definition 2.4.1 satisfied. Given a steady state $U_l = (s_w^-, s_o^-)^T$, we use the equation (4.3), and define

$$E(s_w, s_o, s_w^-, s_o^-) = \frac{\frac{{s_w}^2}{\lambda_T(s_w,s_o)} - \frac{{s_w^-}^2}{\lambda_T(s_w^-,s_o^-)}}{\mu_w(s_w - s_w^-)} - \frac{\frac{{s_o}^2}{\lambda_T(s_w,s_o)} - \frac{{s_o^-}^2}{\lambda_T(s_w^-,s_o^-)}}{\mu_o(s_o - s_o^-)}. \tag{4.9}$$

We want to find all the points $U_r = (s_w, s_o)^T$ such that the following system is solvable:

$$\begin{aligned} E\left(s_w, s_o, s_w^-, s_o^-\right) &= 0, \\ \frac{\partial E}{\partial s_w}\left(s_w, s_o, s_w^-, s_o^-\right) &= 0, \\ \frac{\partial E}{\partial s_o}\left(s_w, s_o, s_w^-, s_o^-\right) &= 0. \end{aligned} \tag{4.10}$$

Now observe that the initial state U_l that we give to solve system (4.10) must belong to Rankine-Hugoniot locus. We want to study the states of corresponding secondary bifurcation that are on the straights lines $[G, D]$, $[E, W]$ and $[O, B]$. Without loss of generality we consider the states that are on the line $[G, D]$ as the others are obtained by the symmetry of the problem by making a change of variables. To begin, we will use a parametrization of the line $[G, D]$. First we define the function

$$p(\alpha, \beta, t) = \frac{\alpha\, t}{\alpha + \beta}. \tag{4.11}$$

where $\alpha, \beta \in \{\mu_w, \mu_o, \mu_g\}$ $\alpha \neq \beta$ and $t \in [0, 1]$. Then any state over $[G, D]$ can be written the form

$$(s_w, s_o)^T = (p(\mu_w, \mu_o, t), p(\mu_o, \mu_w, t))^T \quad t \in [0, 1]. \tag{4.12}$$

Remember that by definition $s_g = 1 - s_w - s_o = 1 - p(\mu_w, \mu_o, t) - p(\mu_o, \mu_w, t) = 1 - t$. Now taking initial state U_l as (4.12), we solve the system

$$\begin{aligned} E\left(s_w, s_o, p(\mu_w, \mu_o, t), p(\mu_o, \mu_w, t)\right) &= 0, \\ \frac{\partial E}{\partial s_w}\left(s_w, s_o, p(\mu_w, \mu_o, t), p(\mu_o, \mu_w, t)\right) &= 0, \\ \frac{\partial E}{\partial s_o}\left(s_w, s_o, p(\mu_w, \mu_o, t), p(\mu_o, \mu_w, t)\right) &= 0. \end{aligned} \tag{4.13}$$

If we defined the function

$$\mathcal{K}(\alpha, \beta, \gamma, t) = \frac{\alpha\, t}{2(\alpha + \beta + \gamma)t^2 - 2(\alpha + \beta)t + \alpha + \beta}, \tag{4.14}$$

where $\alpha, \beta, \gamma \in \{\mu_w, \mu_o, \mu_g\}$ and $t \in [0, 1]$, the solution of the system (4.13) is

$$s_w = \mathcal{K}(\mu_w, \mu_o, \mu_g, t) \quad \text{and} \quad s_o = \mathcal{K}(\mu_o, \mu_w, \mu_g, t). \tag{4.15}$$

We can to conclude that for any state U_l (primary bifurcation) over $[G, D]$ there is a state U_r of secondary bifurcation corresponding to U_l over $[G, D]$ such that $\forall t \in [0, 1]$,

$$U_l = (p(\mu_w, \mu_o, t), p(\mu_o, \mu_w, t))^T \quad \text{and} \quad U_r = (\mathcal{K}(\mu_w, \mu_o, \mu_g, t), \mathcal{K}(\mu_o, \mu_w, \mu_g, t))^T. \tag{4.16}$$

For the symmetry of the problem we can to find the secondary bifurcation states corresponding to the lines $[O, B]$ and $[W, E]$ from the solution of the before case. Only need to make a change of coordinates as follows

- For any state U_l over $[O, B]$ we obtain for $t \in [0, 1]$,

$$U_l = (p(\mu_w, \mu_g, t), 1 - t)^T, \tag{4.17}$$
$$U_r = (\mathcal{K}(\mu_w, \mu_g, \mu_o, t), 1 - \mathcal{K}(\mu_w, \mu_g, \mu_o, t) - \mathcal{K}(\mu_g, \mu_w, \mu_o, t))^T. \tag{4.18}$$

- For any state U_l over $[W, E]$ we obtain for $t \in [0, 1]$,

$$U_l = (1 - t, p(\mu_o, \mu_g, t))^T, \tag{4.19}$$
$$U_r = (1 - \mathcal{K}(\mu_g, \mu_o, \mu_w, t) - \mathcal{K}(\mu_o, \mu_g, \mu_w, t), \mathcal{K}(\mu_o, \mu_g, \mu_w, t))^T. \tag{4.20}$$

Remark 4.3.1. It is possible that for U_l inside the saturation triangle his corresponding U_r state is outside. We only consider the states U_r that is in the saturation triangle.

Remark 4.3.2. In the Corey Quad models this procedure to find the secondary bifurcation locus is correct, because do not have elliptic and coincident regions. But, for other models this procedure would be obtain solutions that satisfies the system (4.10) but do not satisfies Definition 2.4.1, *e.g.*, curves with cusp points.

4.4 Double contact Locus

In this section we describe the mixed and fast double contact locus. These bifurcation loci were given in Definition 2.4.4 and are represent at by pairs of states that remain inside the saturation triangle, such that there are unique pairs of corresponding states. The existence of these bifurcation curves and their shape depends on the choice of viscosity values; these curves do not exist for some combinations of values. Only certain parts of these manifolds are relevant, namely, those that involve shock waves that admit viscous profiles or those that limits regions where we have bifurcation of some backward fast wave curves. In this work we call *fast double contact* the $(2, 2)$-double contact manifold and *mixed double contact* the $(1, 2)$ (or $(2, 1)$)-double contact manifold.

In this section it is not our intention to make an exhaustive analysis of these manifolds, but it is important to understand their behavior and the admissibility of discontinuities between segments of the corresponding states of these locus to define the wave curves, as well as the $\mathscr{L}$ and $\mathscr{R}$ regions (see Chapter 6). All the analysis in this section was done using specialized software.

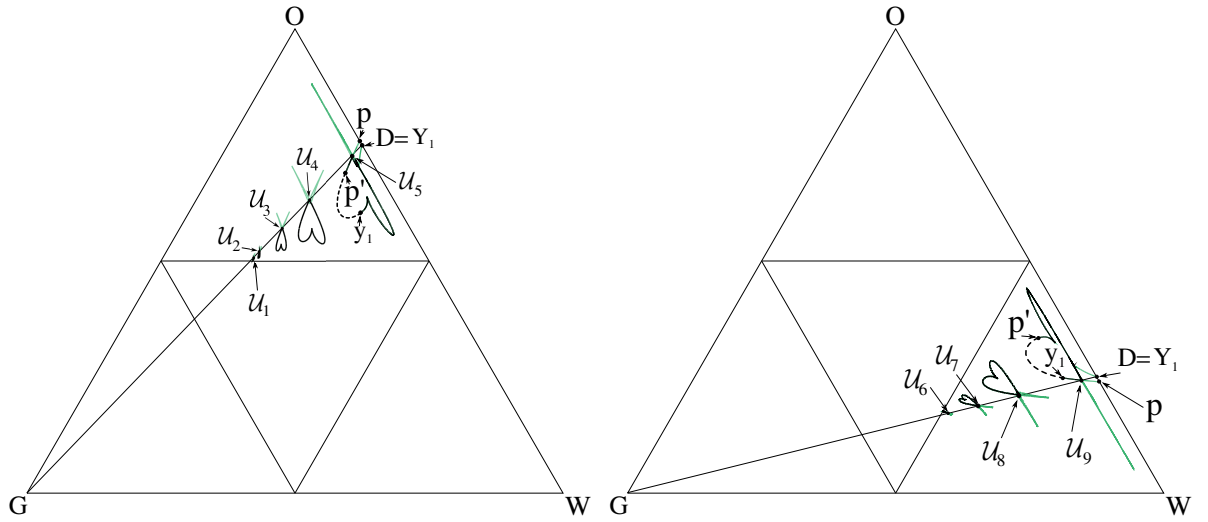

(a) Behavior of mixed contact locus with $\mathcal{U} \in II_O$.

(b) Behavior of mixed contact locus with $\mathcal{U} \in II_W$.

Figure 4.2: Mixed double contact for distinct umbilic points $\mathcal{U}_i$ for $i \in \{1, .., 9\}$ of type II; two viscosities values are fixed and we vary μ_g. In both figure, $\mathcal{Y}_1$ and Y_1 are the corresponding pair of mixed double contact states, where Y_1 intersects $[G, D]$. The corresponds points to dashed curve $(\mathcal{Y}_1, P')$ are outside of the saturation triangle, therefore $(\mathcal{Y}_1, P')$ does not belong to a mixed contact locus.

4.4.1 Mixed double contact

Mixed double contacts are shown in Figure 4.2(a) and (b). We see that this locus does not exist if $\mathcal{U} \in \mathcal{T}_{\mathcal{U}}$. When $\mathcal{U}$ is near to straight line $s_w = 1/2$, $s_o = 1/2$ or $s_w + s_o = 1/2$, the locus is small and it increases as $\mathcal{U}$ approaches the edges of the saturation triangle. The black curves in Figure 4.2 correspond to the states $\mathcal{Y}$ that satisfy $\lambda_s(\mathcal{Y}) = \sigma$, while the green curve corresponds to the states that satisfy $\lambda_f(Y) = \sigma$, where $\sigma = \sigma(\mathcal{Y}; Y)$. Strong numerical evidence indicates that discontinuities of mixed contact are not admissible in our model.

4.4.2 Fast double contact

In this section we describe the behavior of the fast double contact locus when we vary μ_w, μ_o and μ_g. This locus was defined in Definition 2.4.4 as the set of pairs of states in the saturation triangle such that the speed of a shock between them is equal to the fast characteristic speed at each state. This bifurcation is relevant in the construction of fast wave curves (both forward and backward) because when the shock between a pair of states in this set is admissible we automatically have Bethe-Wendroff points and we can concatenate a f- rarefaction curve to these states. Notice that this locus consists of multiple disconnected curves (normally three pair curves) such that there is a unique correspondence between states of different curves.

In [21] was studied the completely symmetric case (see Figure 4.3(a)). In [17], it was studied when one of the viscosities increases by a small amount (see Figure 4.4). In [31], the case of two equal

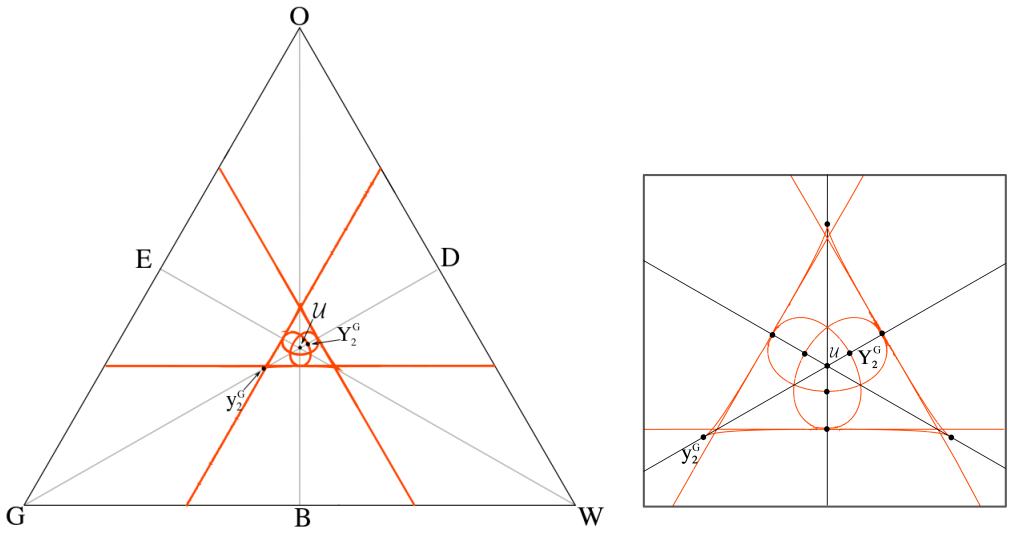

(a) Completely symmetric. (b) Zoom of a neighborhood of $\mathcal{U}$.

Figure 4.3: Fast double contact for the case $\mu_w = \mu_o = \mu_g$. In both figure, $\mathcal{Y}_2^G$ and Y_2^G are the corresponding pair of fast double contact states, where both states intersect $[G, D]$.

viscosities was studied (see Figure 4.5 (b)).

We describe the case in that the umbilic point is of type II_O and the viscosities μ_w and μ_o are different. With out loss of generality assume that $\mu_g \leq \mu_w < \mu_o$. We have two cases:

1. Symmetric case: Refer to Figure 4.5(b). In this case we observe that there are three pair of curves that can be described with respect to the influence of the secondary bifurcation lines. For each pair of curve we have the next correspondence: the curve $[H_1^\Gamma, Y_2^\Gamma, H_4^\Gamma, P]$ corresponds to $[H_1'^\Gamma, \mathcal{Y}_2^\Gamma, H_4'^\Gamma, P]$ with $\Gamma \in \{G, W\}$ and $[P, J_2^W, H_2^G]$ corresponds to $[P, \mathcal{J}_2^G, H_2'^G]$. The state P lies $[O, B]$ and it corresponds to itself. When we consider $\mathcal{B}(U) = I$ only the pair of segments $[Y_2^\Gamma, H_4^\Gamma]$, $[\mathcal{Y}_2^\Gamma, H_4'^\Gamma]$ are admissible by viscous profile for $\Gamma \in \{G, W\}$.

2. $\mu_g < \mu_w$: Refer to Figure 4.5(a). In this case we observe that there are three curves that can be described with respect to the influence of the secondary bifurcation lines. The points of one of the curves correspond to points on the same curve. For each pair of curve we have the next correspondence: the curve $[H_1^G, Y_2^G, \widehat{Y_2^G}, J_2^W, H_2^G]$ corresponds to $[H_1'^G, \mathcal{Y}_2^G, \widehat{y_2^G}, \mathcal{J}_2^G, H_2'^G]$ and $[H_1^W, Y_2^W, H_4^W, P]$ corresponds to $[H_1'^W, \mathcal{Y}_2^W, H_4'^W, P]$. The fast double contact and the fast-inflection locus are tangents at point P. When we consider $\mathcal{B}(U) = I$ only the pair of segments $[Y_2^G, \widehat{Y_2}^G]$ corresponds to $[\mathcal{Y}_2^G, \widehat{y_2}^G]$ and $[Y_2^W, H_4^W]$ corresponds to $[\mathcal{Y}_2^W, H_4'^W]$ are admissible by viscous profile.

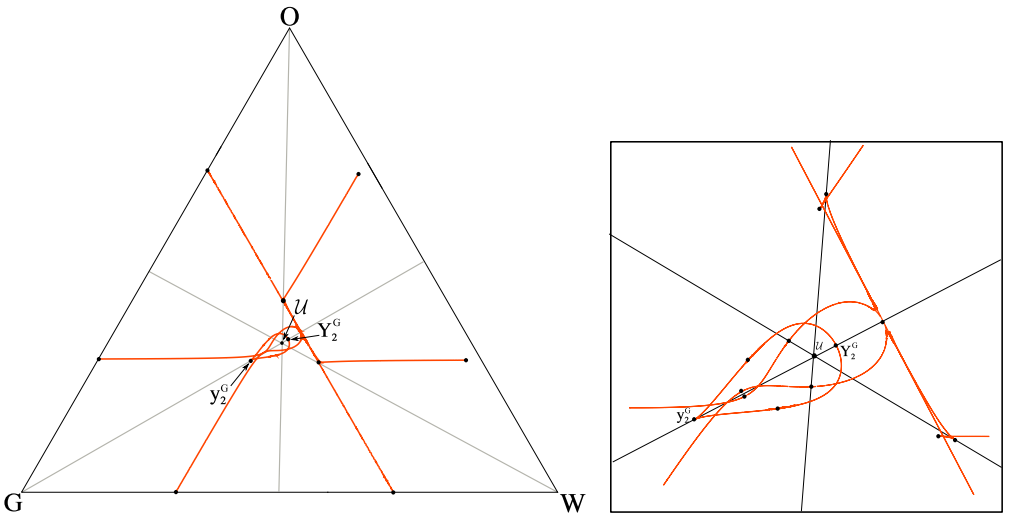

(a) Behavior of double contact locus with $\mathcal{U} \in \mathcal{T}_{\mathcal{U}}$.

(b) Zoom of a neighborhood of $\mathcal{U}$.

Figure 4.4: Fast double contact for the case $\mu_w = \mu_o = \eta$, and $\mu_g > \eta$. In both figure, $\mathcal{Y}_2^G$ and Y_2^G are the corresponding pair of fast double contact states, where both states intersect $[G, D]$.

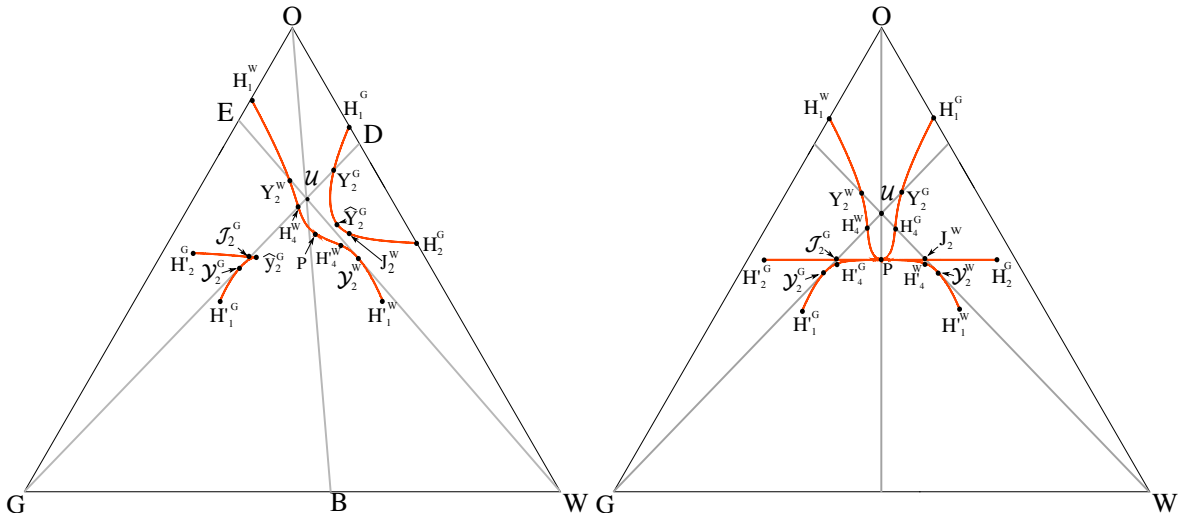

(a) Behavior of fast double contact locus with $\mathcal{U} \in II_O$ with $\mu_g < \mu_w$.

(b) Behavior of fast double contact locus with $\mathcal{U} \in II_O$ simmetric case ($\mu_w = \mu_g$).

Figure 4.5: Fast double contact for the case $\mathcal{U} \in II_O$. In both figure, $\mathcal{Y}_2^G$ and Y_2^G are the corresponding pair of fast double contact states, where both states intersect $[G, D]$.

4.5 Inflection locus

In this section we describe the behavior of the inflection locus when we vary μ_w, μ_o and μ_g. This locus was defined in Definition 2.1.3 as the set of critical points of the characteristic speed for each family. Work [21] studied the completely symmetric case (see Figure 4.6(a)). In [17], it was studied how the inflection locus bifurcates when one of the viscosities increases by a small amount. In [31], the case of two equal viscosities was studied.

Let α, β and γ represent each of phases $\{w, o, g\}$ while $\mathcal{A}, \mathcal{B}$ and Γ stand for any of the vertices $\{G, W, O\}$, such that $(\alpha, \mathcal{A}), (\beta, \mathcal{B}), (\gamma, \Gamma) \in \{(w, W), (g, G), (o, O)\}$. We describe the behavior of inflection locus for any combination of values μ_α, μ_β and μ_γ. The choice of values for μ_α, μ_β and μ_γ depends on choice of vertices $\mathcal{A}, \mathcal{B}$ and Γ. The description of the inflection locus depends on the type of umbilic point and on the family of characteristic speeds studied, so we will make the analysis for each case separately.

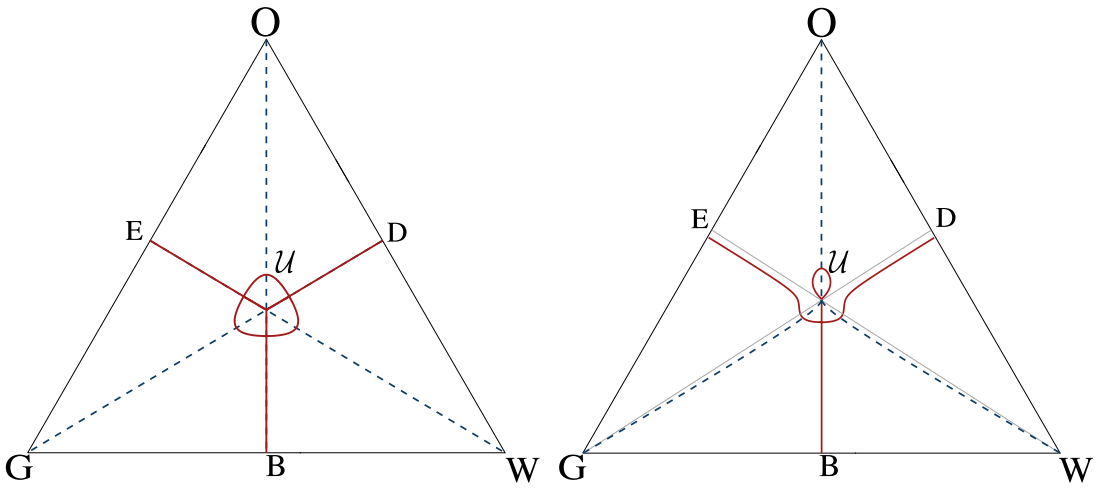

(a) Completely symmetric.

(b) $\mu_w = \mu_g = \eta$ and $\mu_o > \eta$.

Figure 4.6: Slow and fast inflection locus. Dashed curve is the slow inflection and red continuous curve is the fast inflection. (a) Case $\mu_w = \mu_o = \mu_g$. (b) Case 2.a) for $\mathcal{U}$ of type I , with the associations between vertices and viscosities $(\alpha, \mathcal{A}) = (w, W)$, $(\beta, \mathcal{B}) = (o, O)$ and $(\gamma, \Gamma) = (g, G)$. In this case $\mu_w = \mu_g = 1$ and $\mu_o = 1.2$

4.5.1 Slow inflection

We classify the slow inflection (s-inflection) in the following cases, according to the type of the umbilic point and the relationships between viscosities:

4.5.1.1 Umbilic point of type I

Assuming that $\mathcal{U} \in \mathcal{T}_{\mathcal{U}}$, we have the following cases:

1. Three equal viscosities (completely symmetric case, see blue curve Figure 4.6(a)): The s-inflection consists of three line segments that coincide with part of the secondary bifurcation. They come from the umbilic point to each of the vertices $\mathcal{A}, \mathcal{B}$ and Γ.

2. Two equal viscosities: Let $\eta = \mu_\alpha = \mu_\gamma$ be a fixed real value with $\eta \in [0, 1]$. We have two sub cases depending on μ_β:

   a) $\mu_\beta > \eta$ (see Figure 4.6(b), blue curve): The s-inflection consists of one line segment from vertex $\mathcal{B}$ to $\mathcal{U}$ (along symmetry axes) and two curves which begin at the umbilic point and finish in the other two vertices. These curves remains in the triangle $\widehat{\mathcal{A}\,\mathcal{U}\,\Gamma}$.

   b) $\mu_\beta < \eta$ (see Figure 4.7(a), blue curve): This case differs from the previous one in that the curves lie outside the triangle $\widehat{\mathcal{A}\,\mathcal{U}\,\Gamma}$.

3. No equal viscosities (see Figure 4.7(b), blue curve): Assume that $\mu_\beta < \mu_\alpha < \mu_\gamma$. The s-inflection consists of three curves which begin at the umbilic point and finish in each one of the vertices $\mathcal{A}, \mathcal{B}$ and Γ. The curves with vertex Γ and $\mathcal{A}$ lie outside triangle $\widehat{\mathcal{A}\,\mathcal{U}\,\Gamma}$, while the other curve remains inside the triangle $\widehat{\mathcal{B}\,\mathcal{U}\mathcal{A}}$.

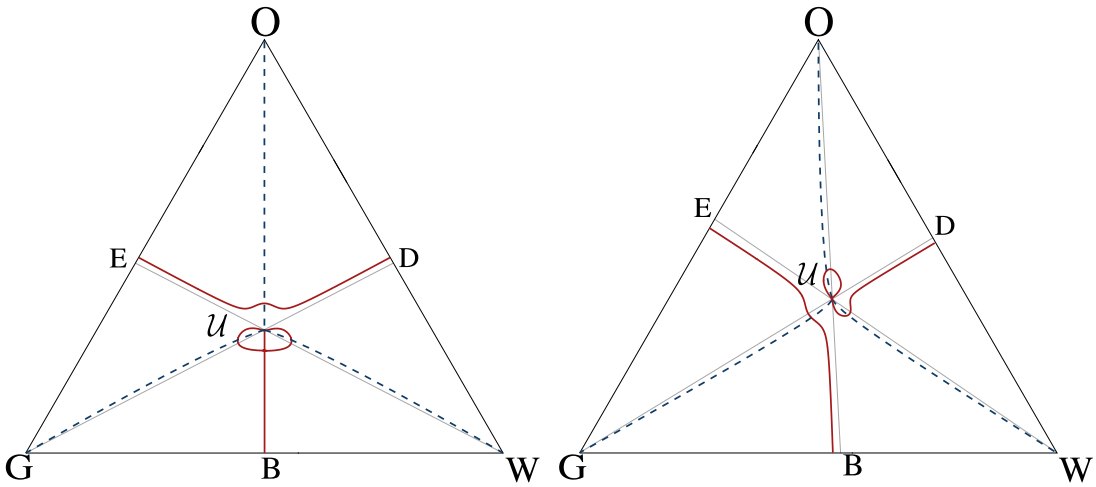

(a) $\mu_w = \mu_g = \eta$ and $\mu_o < \eta$ (b) $\mu_g < \mu_w < \mu_o$.

Figure 4.7: Slow and fast inflection locus. Dashed curve is the slow inflection and red continuous curve is the fast inflection. (a) Consists of the cases 2.b) for $\mathcal{U}$ of type I, with the associations between vertices and viscosities $(\alpha, \mathcal{A}) = (w, W)$, $(\beta, \mathcal{B}) = (o, O)$ and $(\gamma, \Gamma) = (g, G)$. The figure was made with $\mu_w = \mu_g = 1$ and $\mu_o = 0.8$. (b) Consists of the case 3 for $\mathcal{U}$ of type I, with the associations between vertices and viscosities $(\gamma, \Gamma) = (o, O)$, $(\alpha, \mathcal{A}) = (w, W)$, $(\beta, \mathcal{B}) = (g, G)$ and $\mathbb{B} = D$. The figure was made with $\mu_w = 1, \mu_g = 0.9$ and $\mu_o = 1.1$.

4.5.1.2 Umbilic point of type II

Without loss of generality, assume that $\mathcal{U} \in II_{\mathcal{B}}$, the other cases are analogous via a rotation. We have two cases:

1. $\mu_\alpha = \mu_\gamma$: The s-inflection consists of a line segment that connects the umbilic point with the vertex $\mathcal{B}$. It also consists of two curves that begin in vertices $\mathcal{A}$ and Γ and intersect the secondary bifurcation given by $\mathcal{B}$ at state $\mathbb{I}$. This state does not lie in segment $[\mathcal{B},\mathcal{U}]$. These curves remain inside of triangle $\widehat{\mathcal{A}\,\mathbb{I}\,\Gamma}$. Notice that there is a "gap" between the states $\mathcal{U}$ and $\mathbb{I}$ (see Figure 4.8(a), blue curve).

2. $\mu_\alpha > \mu_\gamma$: This case differs from previous one in that we have a curve from vertex $\mathcal{B}$ to the umbilic point. This curve lies inside triangle $\widehat{\mathcal{B}\,\mathcal{U}\,\Gamma}$ (see Figure 4.8(b), blue curve).

4.5.2 Fast inflection

We classify the fast inflection (f-inflection) in the following cases, according to the type of the umbilic point and the relationships between viscosities:

4.5.2.1 Umbilic point of type I

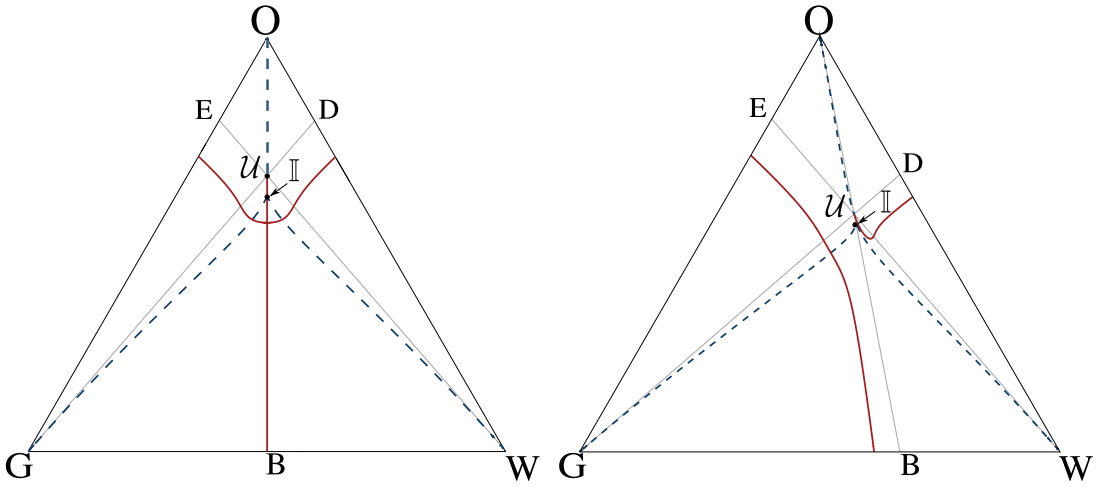

(a) $\mu_w = \mu_g$ and $\mathcal{U} \in II_O$.

(b) $\mu_w > \mu_g$ and $\mathcal{U} \in II_O$.

Figure 4.8: Slow and fast inflection locus. Dashed curve is the slow inflection and red continuous curve is the fast inflection; the state $\mathbb{I}$ is the intersection between the slow inflection and invariant line $[O, B]$. (a) Consists of the case 1. for $\mathcal{U} \in II_O$, with the associations between vertices and viscosities $(\alpha, \mathcal{A}) = (w, W)$, $(\beta, \mathcal{B}) = (o, O)$ and $(\gamma, \Gamma) = (g, G)$. The figure was made with $\mu_w = \mu_g = 0.25$ and $\mu_o = 2$. (b) Consists of the case 2. for $\mathcal{U} \in II_O$, with the associations between vertices and viscosities $(\alpha, \mathcal{A}) = (w, W)$, $(\beta, \mathcal{B}) = (o, O)$, $(\gamma, \Gamma) = (g, G)$ and $\mathbb{G} = D$. The figure was made with $\mu_w = 1$, $\mu_g = 0.5$ and $\mu_o = 2$.

Assuming that $\mathcal{U} \in \mathcal{T}_{\mathcal{U}}$, we have the following cases:

1. Three equal viscosities (completely symmetric case, see Figure 4.6(a) red curve): The f-inflection consists of simply connected closed curve that surrounds $\mathcal{U}$ and three line segments that coincide with part of the secondary bifurcation, coming from $\mathcal{U}$ to the sides of the triangle opposite each of the vertices $\mathcal{A}, \mathcal{B}$ and Γ.

2. Two equal viscosities: Let $\eta = \mu_\alpha = \mu_\gamma$ be a fixed real value with η in $[0, 1]$. We have two sub cases depending of μ_β:

   a) $\mu_\beta > \eta$ (see Figure 4.6(b), red curve): The f-inflection consists of a simply connected closed curve passes through $\mathcal{U}$ and intersects only the segment $[\mathcal{U}, \mathcal{B}]$. It includes a line segment that connects $\mathcal{U}$ and the side opposite of vertex $\mathcal{B}$ and a curve that intersects it, connecting adjacent sides of vertex $\mathcal{B}$.

   b) $\mu_\beta < \eta$ (see Figure 4.7(a), red curve): The f-inflection consists of a non-simply connected curve that closes at $\mathcal{U}$ and intersects another part of the f-inflection, a segment that connects $\mathcal{U}$ and the side opposite of vertex $\mathcal{B}$. It includes a curve that connects the sides adjacent to vertex $\mathcal{B}$ and intersects the segment $[\mathcal{U}, \mathcal{B}]$.

3. No equal viscosities (see Figure 4.7(b), red curve): Assume that $\mu_\beta < \mu_\alpha < \mu_\gamma$. The f-inflection consists of a curve that connects the sides that form vertex $\mathcal{B}$ while intersecting segment $[\mathcal{U}, \mathcal{B}]$. It includes a curve that comes from the side opposite to vertex $\mathcal{B}$ and ends at $\mathcal{U}$. This curve is totally contained in the triangle $\widehat{\mathcal{B}\,\mathbb{B}\,A}$, where $\mathbb{B}$ is the intersection point between the secondary bifurcation that leaves vertex $\mathcal{B}$ with the side opposite to it. We also have a simply connected closed curve that passes through $\mathcal{U}$ and is completely contained in the triangle $\widehat{\mathcal{B}\,\mathbb{B}\,\Gamma}$.

4.5.2.2 Umbilic point of type II

Without loss of generality, assume that $\mathcal{U} \in II_{\mathcal{B}}$. We have two cases:

1. $\mu_\alpha = \mu_\gamma$ (see Figure 4.8(a), red curve): The f-inflection consists of a segment that connects $\mathcal{U}$ and the side opposite to vertex $\mathcal{B}$. It also consists of a curve that joins both sides that form the vertex $\mathcal{B}$ and intersects the secondary bifurcation that leaves the vertex $\mathcal{B}$ in the segment $[\mathcal{U}, \mathbb{B}]$.

2. $\mu_\alpha > \mu_\gamma$ (see Figure 4.8(b), red curve): The f-inflection consists of the curve that joins both sides that form the vertex Γ and intersects the line segment $[\Gamma, \mathcal{U}]$. It also consists of a curve that connects $\mathcal{U}$ and the side opposite to Γ. This curve is completely contained in the triangle $\widehat{\mathcal{A}\Gamma\mathbb{G}}$ where $\mathbb{G}$ is the intersection point between the secondary bifurcation that leaves the vertex Γ and the side opposite to Γ.

4.6 Boundary Extension sets

These sets are extremely relevant in the construction of wave curves, since they are also borders where the wave curves change of structure and are also associated to composites curves. As the name suggests,

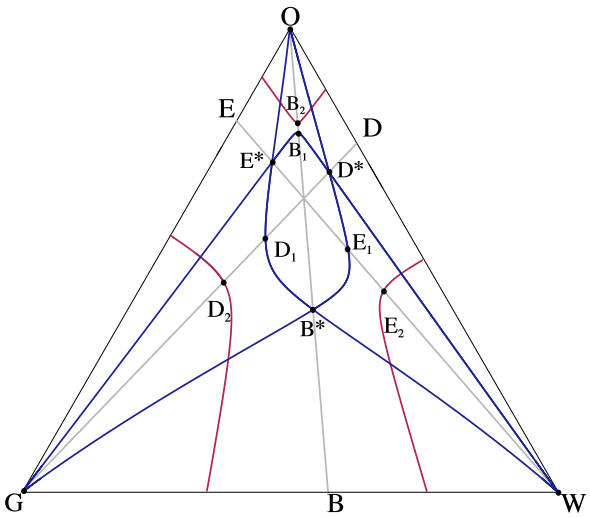

Figure 4.9: Slow and fast boundary extension

a boundary extension set is the set E_i^+ (with $i = s, f$) in phase space that satisfies Definition 2.4.6 for the boundaries $[W, O]$, $[W, G]$ or $[G, O]$ of the saturation triangle. The border extension sets useful to this work are illustrated in Figure 4.9 and were obtained computationally. An analytic expression for these curve may be found in [14] in convex permeabilities Corey models. The blue curve (G, B^*, E_1, D^*, O) represents the s-right-extension boundary of $[G, O]$: for any state M in this curve, there is a state $L \in [G, O]$ such that $\sigma(M; L) = \lambda_s(M)$. The blue curves (G, E^*, B_1, D^*, W) and (W, B^*, D_1, E^*, O) represent the s-right-extension boundaries of $[G, W]$ and $[W, O]$, respectively. In the same way, the red curve that contains state D_2 and intersects the sides that form vertex G represents the f-right-extension boundary of $[W, O]$: for any state M in this curve, there is a state $R \in [W, O]$ such that $\sigma(M; R) = \lambda_f(M)$. The f-right-extension boundaries of $[G, W]$ and $[G, O]$ are the red curves that intersect the sides that form vertices O and W, respectively.

The boundary of saturation triangle can be associated to secondary bifurcation lines such that each edge is corresponding to the straight line that start in the vertex opposite and ends to the side. Hence, the s- and f-right-extension boundaries of edge opposite to vertex Γ and with state $\mathbb{B}$ intersect the straight line $[\Gamma, \mathbb{B}]$ in states $\mathbb{B}_1$ and $\mathbb{B}_2$, respectively. Therefore D_1 and D_2 are the intersection of s- and f-left-extension boundaries of edge $[W, O]$. Similarly E_1 and E_2, and B_1 and B_2 corresponding to s- and f-extension boundaries of edges $[G, O]$ and $[G, W]$, respectively. On the other hand, state $\mathbb{B}^* \in [\Gamma, \mathbb{B}]$ is the intersection of two s-extension boundaries associated to the edges than form the vertex Γ; *i.g.,* $E^* \in [W, E]$ is the intersection between the sides $[W, G]$ and $[W, O]$.

Chapter 5

The role of reduced two-phase flow

In this chapter we study the reduction of our system given in (3.36) to the scalar Buckley-Leverett conservation law for two-phase flow in porous media. As we see in [9] and the Remark 3.3.8, this reduction follows straightforwardly along each of the edges of the saturation triangle. However for Corey Quad model without gravity and $\mathcal{B} = I$, it also occurs along the straight lines $[G, D]$, $[W, E]$ and $[O, B]$ as well, turning them into invariant lines of our PDE (3.38) (with $\vartheta = 0$). Note that these invariant lines coincide with the secondary bifurcation manifolds. According to [17] and [21], for the viscosity matrix equal to identity, the only admissible non-Lax shocks arise in the associated traveling wave ODE (2.23) as heteroclinic orbits lying on the invariant lines. These transitional shocks have an important role in solving the general Riemann problem under the viscous profile criterion. Because of this reason, we are interested in characterizing these invariant lines and studying their properties.

5.1 Parameters and coordinates

Points of the phase space along the line $[G, D]$ (see Figure 3.1) satisfy the identity

$$\frac{s_w}{\mu_w} = \frac{s_o}{\mu_o} = \frac{s_w + s_o}{\mu_w + \mu_o}. \tag{5.1}$$

Let us define along $[G, D]$ the "effective" saturation and "effective" viscosity respectively as

$$s = s_w + s_o, \quad \text{and} \quad \mu_{wo} = \mu_w + \mu_o. \tag{5.2}$$

Then, the line segment $[G, D]$ is parametrized in s as

$$s_w = \frac{\mu_w}{\mu_{wo}} s \quad \text{and} \quad s_o = \frac{\mu_o}{\mu_{wo}} s, \tag{5.3}$$

where $0 \leq s \leq 1$. Now consider the formulation (3.38) with $\vartheta = 0$, *i.e.,* $F(U) = \mathcal{F}(U)$ given by (3.36) in the space of saturations $(s_w, s_o)^T$. The system of PDEs is

$$\frac{\partial}{\partial t} \begin{pmatrix} s_w \\ s_o \end{pmatrix} + \frac{\partial}{\partial x} \begin{pmatrix} F_w(s_w, s_o) \\ F_o(s_w, s_o) \end{pmatrix} = \frac{\partial^2}{\partial x^2} \begin{pmatrix} s_w \\ s_o \end{pmatrix}. \tag{5.4}$$

We define $D(s) = \frac{s^2}{\mu_{wo}} + \frac{(1-s)^2}{\mu_g}$. Substituting (5.3) in (5.4) we obtain

$$\frac{\partial}{\partial t}\left(\frac{\mu_w}{\mu_{wo}}s\right) + \frac{\partial}{\partial x}\left(\frac{\mu_w s^2}{\mu_{wo}^2 D(s)}\right) = \frac{\partial^2}{\partial x^2}\left(\frac{\mu_w}{\mu_{wo}}s\right), \tag{5.5}$$

$$\frac{\partial}{\partial t}\left(\frac{\mu_o}{\mu_{wo}}s\right) + \frac{\partial}{\partial x}\left(\frac{\mu_o s^2}{\mu_{wo}^2 D(s)}\right) = \frac{\partial^2}{\partial x^2}\left(\frac{\mu_o}{\mu_{wo}}s\right), \tag{5.6}$$

which are two copies of the equation

$$\frac{\partial s}{\partial t} + \frac{\partial}{\partial x}\left(\frac{s^2}{s^2 + \nu(1-s)^2}\right) = \frac{\partial^2 s}{\partial x^2}. \tag{5.7}$$

Thus, we see that system (5.4) reduces to the scalar Buckley-Leverett equation

$$\frac{\partial s}{\partial t} + \frac{\partial}{\partial x} f(s,\nu) = \frac{\partial^2 s}{\partial x^2}, \tag{5.8}$$

where the flux function f and the viscosity ratio ν are

$$f(s,\nu) = \frac{s^2}{s^2 + \nu(1-s)^2}, \quad \nu = \frac{\mu_w + \mu_o}{\mu_g}. \tag{5.9}$$

The Rankine-Hugoniot condition (2.8) for a shock with speed σ between M and N reduces to

$$-\sigma(s_N - s_M) - f(s_N,\nu) - f(s_M,\nu) = 0. \tag{5.10}$$

Remark 5.1.1. The relationships (5.8), (5.9) are valid over any invariant line $[G,D]$, $[O,B]$ and $[W,E]$, which are identified by the vertex where it begins, $\Gamma \in \{G,W,O\}$. Sometimes it is useful to express the final point of the invariant line, $\mathbb{B} \in \{D,E,B\}$. The choice of vertex specifies a relation between phase saturations: $\gamma \in \{g,w,o\}$ corresponds to the phase at the vertex Γ and α, β represent the two interchangeable phases. Then, the quantity s, the viscosity ratio and the effective viscosity are respectively

$$s = s_\alpha + s_\beta, \quad \nu_\Gamma = \mu_{\alpha\beta}/\mu_\gamma, \quad \text{with} \quad \mu_{\alpha\beta} = \mu_\alpha + \mu_\beta. \tag{5.11}$$

Notice that with this parametrization the vertices G, W and O have always value s equal to zero and states D, E and B on the opposite edge have value s equal to one.

Remark 5.1.2. We introduce further notation for states over any invariant line in "effective" quantity. For example, let $A = (A_w, A_o)$ be a state in the saturation triangle belonging to $[G,D]$. Then, we write $s_A \in (0,1)$ to indicate that the state is specified by one effective saturation parameter.

Finally, we provide an identity for effective shocks. Given a speed and a left (or right) state in an invariant line, it returns the right (or left) state of an admissible shock. Let M and N be two states on an invariant line. Then substituting (5.9) into (5.10) we obtain

$$\frac{\sigma}{\nu}\left[s_M^2 + \nu(1-s_M)^2\right]\left[s_N^2 + \nu(1-s_N)^2\right] = s_N + s_M - 2\,s_N s_M. \tag{5.12}$$

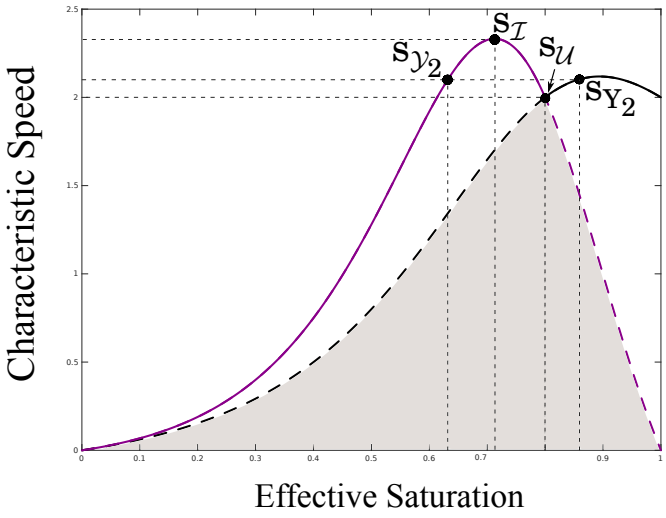

Figure 5.1: Graphs for expressions λ_a (black curve) and λ_b (purple curve) above the white region. The dashed (resp. solid) line above the shaded region is the slow (resp. fast) characteristic speed λ_s (resp. λ_f) defined in (5.14). The horizontal axis corresponds to a parametrization of an invariant line in terms of effective saturation s, and the vertical axis is characteristic speed. The states $s_{\mathcal{U}}$, $s_{\mathcal{Y}_2}$ and s_{Y_2} are given in (5.15), 5.21(a) and (b). The definition of $s_{\mathcal{I}}$ is given in Remark 5.3.1.

5.2 Analytic expressions for certain states over invariant lines

Taking into account the fact that over the invariant lines the flux function reduces to (5.8), we derive a few expressions for states over these lines that turn out to help in characterizing the Riemann solutions for states in the saturation triangle. First, we fix the parameters μ_w, μ_o and μ_g, choose an invariant line by a specific Γ and compute the value for ν_Γ using (5.11). We write $f(s,\nu) = f(s)$ to represent the effective flux on this line. Then we calculate the characteristic speeds λ_a and λ_b for states over the invariant line. In this model the eigenvalues were obtained using (2.2), but in this context we substitute the quantity (5.11)(a) into (2.2). Hence the expressions:

$$\lambda_a(s) = \frac{2s}{\mu_{\alpha\beta} D(s)}, \qquad \lambda_b(s) = \frac{2s(1-s)}{\mu_{\alpha\beta}\mu_\gamma D(s)^2}, \qquad \text{with } D(s) = \frac{s^2}{\mu_{\alpha\beta}} + \frac{(1-s)^2}{\mu_\gamma}. \tag{5.13}$$

Remark 5.2.1. Of course λ_b can be obtained as $f'(s)$, the derivative of flux function (5.9). Moreover, if the reduced state s lies between the vertex and the umbilic point $\mathcal{U}$, we have $\lambda_a(s) < \lambda_b(s)$. Conversely, if the state s lies between the umbilic point and the edge opposite to vertex, then $\lambda_b(s) < \lambda_a(s)$. We have

$$\lambda_s(s) = \min\{\lambda_a(s), \lambda_b(s)\} \quad \text{and} \quad \lambda_f(s) = \max\{\lambda_a(s), \lambda_b(s)\}, \tag{5.14}$$

the slow and fast characteristic speeds for a state s along any invariant line (Figure 5.1).

From the definition of the umbilic point we have $\lambda_a(s_{\mathcal{U}}) = \lambda_b(s_{\mathcal{U}})$. Then from the expressions (5.13) we obtain $s_{\mathcal{U}}\left((1+\nu)s_{\mathcal{U}} - \nu\right) = 0$. Thus, the reduced saturation of the umbilic point in each invariant line associated to ν_Γ can be calculated as

$$s_{\mathcal{U}} = \frac{\nu_\Gamma}{1+\nu_\Gamma}. \tag{5.15}$$

Remark 5.2.2. Over each invariant line, it is possible to derive the expressions for two distinguished states. These states are denoted by $\mathcal{Y}_2$ and Y_2 and belong to the fast double contact locus (see Definition 2.4.4 and Figure 5.2). We take the assumption when the umbilic point lies between $\mathcal{Y}_2$ and Y_2 ($s_{\mathcal{Y}_2} \in (0, s_{\mathcal{U}})$, $s_{Y_2} \in (s_{\mathcal{U}}, 1)$), such that satisfy

$$Y_2 \in \mathcal{H}(\mathcal{Y}_2) \;\text{ and }\; \sigma(\mathcal{Y}_2; Y_2) = \lambda_f(\mathcal{Y}_2) = \lambda_f(Y_2), \tag{5.16}$$

the value $\sigma(\mathcal{Y}_2; Y_2)$ is the speed of the shock between $\mathcal{Y}_2$ and Y_2. From the expressions (5.13) and definitions (5.14) and (5.16) we have

$$\lambda_b(s_{\mathcal{Y}_2}) = \sigma(s_{\mathcal{Y}_2}; s_{Y_2}) = \lambda_a(s_{Y_2}). \tag{5.17}$$

Substituting (5.17) into (5.12) we obtain the equations related to the first and second equalities in:

$$\frac{2s_{\mathcal{Y}_2}(1-s_{\mathcal{Y}_2})(s_{Y_2}^2 + \nu(1-s_{Y_2})^2)}{s_{\mathcal{Y}_2}^2 + (1-s_{\mathcal{Y}_2})^2} = s_{\mathcal{Y}_2} + s_{Y_2} - 2s_{\mathcal{Y}_2}s_{Y_2} = \frac{2s_{Y_2}\left(s_{\mathcal{Y}_2}^2 + \nu(1-s_{\mathcal{Y}_2})^2\right)}{\nu}. \tag{5.18}$$

Equating the second and the last expression of (5.18) we obtain

$$s_{Y_2} = \frac{s_{\mathcal{Y}_2}\nu}{2s_{\mathcal{Y}_2}^2(\nu+1) - 2\nu s_{\mathcal{Y}_2} + \nu}. \tag{5.19}$$

Notice that $2s_{\mathcal{Y}_2}^2(\nu+1) - 2s_{\mathcal{Y}_2}\nu + \nu \neq 0$, then substituting (5.19) in the first and second equation of (5.18) and equating the results we obtain

$$2\left(s_{\mathcal{Y}_2}(\nu+1) - \nu\right)\left(2s_{\mathcal{Y}_2}^2(\nu+1) - \nu\right)s_{\mathcal{Y}_2}^2 = 0. \tag{5.20}$$

Because we seek a solution different from umbilic point, we arrive at the expressions in increasing order

$$s_{\mathcal{Y}_2} = \frac{1}{2}\sqrt{\frac{2\nu}{\nu+1}}, \qquad s_{Y_2} = -\frac{1}{2}\frac{\sqrt{2\nu(\nu+1)}}{\sqrt{2\nu(\nu+1)} - 2(\nu+1)} = \frac{1}{2}\frac{\nu + \sqrt{2\nu(\nu+1)}}{\nu+2}. \tag{5.21}$$

Now, consider the intersection point between the invariant line and the triangle edge transversal to that line. The value of s in this state is one (see Remark 5.1.1). Let us compute $\mathbb{B}_1$ and $\mathbb{B}_2$, the slow and fast left-extensions of this intersection point, respectively that were given in Definition 2.4.6. These states lie on the invariant line $[\Gamma, \mathcal{U}]$ with $\Gamma \in \{G, W, O\}$ and satisfy

$$\lambda_s(s_{\mathbb{B}_1}) = \sigma(s_{\mathbb{B}_1}; 1), \tag{5.22}$$

$$\lambda_f(s_{\mathbb{B}_2}) = \sigma(s_{\mathbb{B}_2}; 1). \tag{5.23}$$

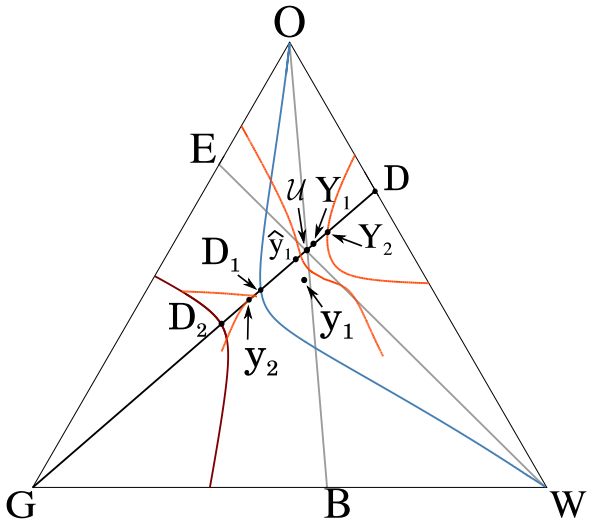

Figure 5.2: Bifurcation curves in phase space that contain the states $D_2 = \mathbb{B}_2$ and $D_1 = \mathbb{B}_1$ defined respectively in (5.25)(a) and (b) for $[G, D]$; the states $\mathcal{Y}_2$ and Y_2 defined respectively in (5.21) (a) and (b); and the states $\mathcal{Y}_2$ and Y_2 defined respectively in (5.21) (a) and (b); and the pair of states of mixed double contact $\mathcal{Y}_1$ and Y_1 with $Y_1 \in [G, D]$ (see Section 4.4). The blue (resp. red) curve is the left slow (fast) boundary extension of edge $[O, W]$ (see Definition 2.4.6). The orange curves are the double fast contact and the gray ones are the invariant lines $[G, D]$, $[O, B]$ and $[W, E]$.

Substituting equations (5.22) and (5.23) in (5.12), we obtain respectively

$$\frac{2s_{\mathbb{B}_1}}{\nu} + s_{\mathbb{B}_1} - 1 = 0 \qquad \text{and} \qquad (\nu+1)s_{\mathbb{B}_2}^2 - 2(\nu+1)s_{\mathbb{B}_2} + \nu = 0. \tag{5.24}$$

Thus we have the expressions in increasing order

$$s_{\mathbb{B}_2} = \frac{\sqrt{\nu+1}-1}{\sqrt{\nu+1}}, \qquad s_{\mathbb{B}_1} = \frac{\nu}{2+\nu}. \tag{5.25}$$

Finally, we define the extension for the umbilic point, *i.e.*, the state $\mathbb{B}_0$ on the invariant line $[\Gamma, \mathbb{B}]$such that

$$\lambda_s(s_{\mathcal{U}}) = \lambda_f(s_{\mathcal{U}}) = \sigma(s_{\mathbb{B}_0}; s_{\mathcal{U}}). \tag{5.26}$$

Substituting (5.15) into (5.13) we obtain $\lambda_s(s_{\mathcal{U}}) = \lambda_f(s_{\mathcal{U}}) = 2$. Then using (5.12) and (5.26) we have

$$(2s_{\mathbb{B}_0} - 1)(s_{\mathbb{B}_0}\nu + s_{\mathbb{B}_0} - \nu) = 0, \qquad \text{therefore} \qquad s_{\mathbb{B}_0} = 1/2. \tag{5.27}$$

Remark 5.2.3. We denoted E_0 and B_0 to the extensions of the umbilic point, that satisfy (5.26) along the invariant lines $[W, E]$ and $[O, B]$ respectively. As in case of s_{D_0}, $s_{E_0} = 1/2$ and $s_{B_0} = 1/2$.

Remark 5.2.4. The analysis in this section can be done for any invariant line, by changing only the value of ν according to the chosen line following Remark 5.1.1.

5.3 Dependence of distinguished two-phase states on fluid viscosities

In this section we study the location of certain important points, such as the umbilic point, the fast double and mixed contact points, when we vary the parameters μ_w, μ_o and μ_g. Moreover, it is possible to characterize the position of contact points in terms of the position of the umbilic point in the saturation triangle. All of these states lie on an invariant line, so it suffices to explain the variation of these states along a single invariant line, the other cases are similar.

The following result characterizes the viscosity ratios in terms of the location of the umbilic point and it follows from Theorem 3.3.1.

Corollary 5.3.1. *For the Corey Quad model, if the umbilic point $\mathcal{U}$ is type II then two of the ratios ν_O, ν_G and ν_W are greater than one while the other is less than one. Conversely, if the umbilic point $\mathcal{U}$ is type I, all ratios ν_O, ν_G and ν_W defined in 5.11)(b), are greater than one. To be more precise:*

1. $\mathcal{U} \in II_O \;\Leftrightarrow\; \nu_O < 1$, $\nu_G > 1$ *and* $\nu_W > 1$;
2. $\mathcal{U} \in II_W \;\Leftrightarrow\; \nu_W < 1$, $\nu_G > 1$ *and* $\nu_O > 1$;
3. $\mathcal{U} \in II_G \;\Leftrightarrow\; \nu_G < 1$, $\nu_O > 1$ *and* $\nu_W > 1$;
4. $\mathcal{U} \in \mathcal{T}_U \;\Leftrightarrow\; \nu_O$, ν_G *and* ν_W *are greater than one.*

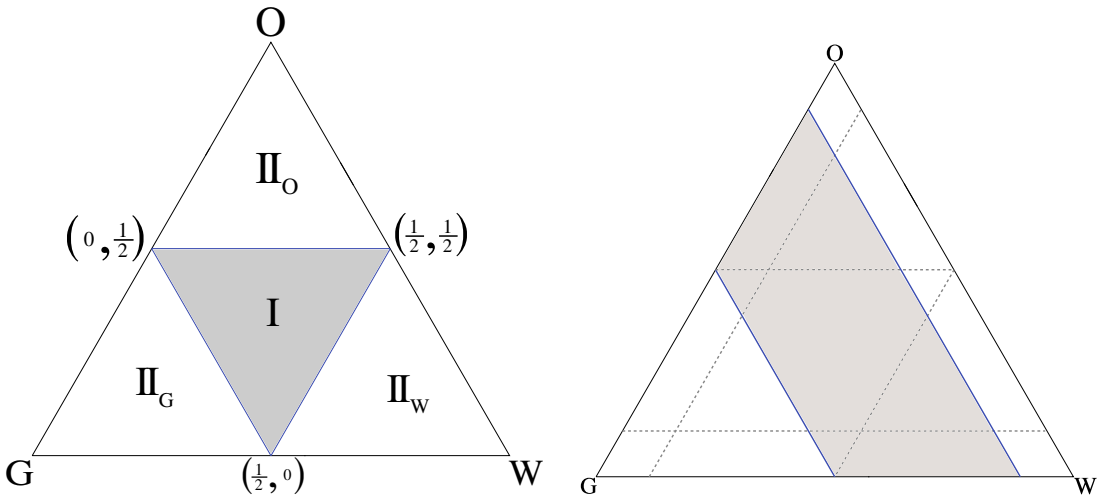

(a) Regions where $\mathcal{U}$ is type I and II.

(b) Region for $\mathcal{U}$ such that made Y_2 relevant for the invariant lines associated to vertex G.

Figure 5.3: Position of the umbilic point $\mathcal{U}$. (a) Classification of $\mathcal{U}$ as type I or II given in Corollary 5.3.1. (b) Region associated to vertex G where the location of $\mathcal{U}$ imply the existence of the reduced states $s_{\mathcal{Y}_2}$ and s_{Y_2}.

Proof. Consider the umbilic point $\mathcal{U} = (\mathcal{U}_w, \mathcal{U}_o)^T$ inside the Region II_O. This means that $0 < \mathcal{U}_w < 1/2$ and $1/2 < \mathcal{U}_o < 1$, by (3.42) we have

$$\frac{1}{2} < \frac{\mu_o}{\mu_w + \mu_o + \mu_g} < 1, \quad \text{and} \quad 0 < \frac{\mu_w}{\mu_w + \mu_o + \mu_g} < \frac{1}{2}; \tag{5.28}$$

if and only if,

$$\mu_o > \mu_w + \mu_g, \quad \mu_o + \mu_g > \mu_w, \quad \text{and} \quad \mu_w + \mu_o > \mu_g. \tag{5.29}$$

Thus from (5.11) and (5.29) we obtain the condition 1 of this corollary. Similar inequalities are obtained for $\mathcal{U} \in II_W$. On the other hand, let us consider the umbilic point satisfying $\mathcal{U}_w < 1/2$ and $\mathcal{U}_o < 1/2$, *i.e.*,

$$\frac{\mu_w}{\mu_w + \mu_o + \mu_g} < \frac{1}{2} \quad \text{and} \quad \frac{\mu_o}{\mu_w + \mu_o + \mu_g} < \frac{1}{2}. \tag{5.30}$$

We have two possibilities: (i) $\mathcal{U} \in II_G$ or (ii) $\mathcal{U} \in \mathcal{T}_U$.

(i) If $\mathcal{U} \in II_G$, from Theorem 3.3.1 we have $\mathcal{U}_w + \mathcal{U}_o = \dfrac{\mu_w + \mu_o}{\mu_w + \mu_o + \mu_g} < \dfrac{1}{2}$. Thus

$$\mu_w < \mu_o + \mu_g \ , \mu_o < \mu_w + \mu_g \ \text{ and } \ \mu_g > \mu_w + \mu_o. \tag{5.31}$$

(ii) If $\mathcal{U} \in \mathcal{T}_U$, from Theorem 3.3.1 we have $\mathcal{U}_w + \mathcal{U}_o = \dfrac{\mu_w + \mu_o}{\mu_w + \mu_o + \mu_g} > \dfrac{1}{2}$. Thus

$$\mu_w < \mu_o + \mu_g \ , \mu_o < \mu_w + \mu_g \ \text{ and } \ \mu_g < \mu_w + \mu_o. \tag{5.32}$$

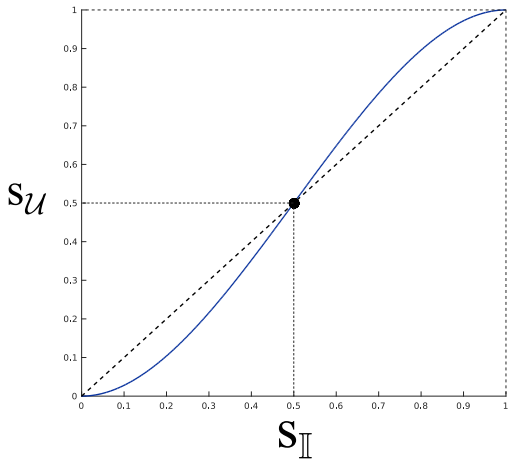

Figure 5.4: Plot of the relation between $\mathcal{U}$ and the fast inflection point $s_{\mathbb{I}}$ along any of the invariant lines, see (5.34) and (5.35)

Therefore, from (5.11), (5.31) and (5.32) we obtain the other conditions. ∎

Remark 5.3.1. Notice that the derivative of the effective flux function (5.9) with $\nu = \nu_G$ along $[G, D]$ is continuous and has a maximum at $s_{\mathbb{I}}$ (see Section 4.5). This state represents the inflection point of the effective flux function. The meaning of $s_{\mathbb{I}}$ over any invariant line depends on its position with respect to the umbilic point. If $s_{\mathbb{I}}$ is to the left of $s_{\mathcal{U}}$, it is a fast inflection point, otherwise it is a slow inflection point (see equations (5.13) and Figure 5.1). Let us study the inflection point $s_{\mathbb{I}}$. If we differentiate $f(s)$ twice and we equate the result to zero, we obtain

$$2{s_{\mathbb{I}}}^3 - 3{s_{\mathbb{I}}}^2 + \frac{\nu_G}{\nu_G + 1} = 2{s_{\mathbb{I}}}^3 - 3{s_{\mathbb{I}}}^2 + s_{\mathcal{U}} = 0. \tag{5.33}$$

Therefore, the discriminant of the cubic equation (5.33) is $108 s_{\mathcal{U}}(1 - s_{\mathcal{U}})$. Then $\triangle \geq 0$ if and only if $0 \leq s_{\mathcal{U}} \leq 1$. Therefore, when $s_{\mathcal{U}} = 0$ or $s_{\mathcal{U}} = 1$ there is only the trivial solution $s_{\mathbb{I}} = s_{\mathcal{U}}$ for $s_{\mathbb{I}} \in [0, 1]$. Now, let $P_{s_{\mathcal{U}}}(s_{\mathbb{I}}) = 2{s_{\mathbb{I}}}^3 - 3{s_{\mathbb{I}}}^2 + s_{\mathcal{U}}$ be the function associated to (5.33). Notice that $P_{s_{\mathcal{U}}}(0) = s_{\mathcal{U}} \geq 0$ and $P_{s_{\mathcal{U}}}(1) = s_{\mathcal{U}} - 1 \leq 0$ for all $s_{\mathcal{U}} \in [0, 1]$. Additionally $P'_{s_{\mathcal{U}}}(s_{\mathbb{I}}) = 6 s_{\mathbb{I}}(s_{\mathbb{I}} - 1) \leq 0$ for all $s_{\mathbb{I}} \in [0, 1]$ and $s_{\mathcal{U}} \in [0, 1]$. Therefore, there is only one solution of (5.33) in $[0, 1]$ for all $s_{\mathcal{U}} \in [0, 1]$. In Figure 5.4, we plot the implicit relation between $s_{\mathcal{U}}$ and $s_{\mathbb{I}}$ given by (5.33). From Figure 5.4 we see that

$$\text{if} \quad \nu_G \leq 1 \quad \Leftrightarrow \quad s_{\mathcal{U}} = \tfrac{\nu_G}{\nu_G + 1} \leq \tfrac{1}{2} \quad \Leftrightarrow \quad s_{\mathcal{U}} \leq s_{\mathbb{I}} \leq \tfrac{1}{2}; \tag{5.34}$$

$$\text{if} \quad \nu_G > 1 \quad \Leftrightarrow \quad s_{\mathcal{U}} = \tfrac{\nu_G}{\nu_G + 1} > \tfrac{1}{2} \quad \Leftrightarrow \quad \tfrac{1}{2} < s_{\mathbb{I}} < s_{\mathcal{U}}. \tag{5.35}$$

The following result, which was stated in [4], shows the relationship between the viscosity ratio ν_Γ and the existence of states $\mathcal{Y}_2$ and Y_2 along $[G, D]$ of fast double contact.

Lemma 5.3.2. *Consider the invariant line $[G, D]$. There are two states of fast double contact over $[G, D]$ if and only if $1 < \nu_G \leq 8$.*

Remark 5.3.2. Notice that in terms of position of the umbilic point in the saturation triangle, the two states of fast double contact over $[G, D]$ exist and are relevant if and only if the umbilic point, $\mathcal{U} = (\mathcal{U}_w, \mathcal{U}_o)$ is in the region bounded by the straight lines $\mathcal{U}_w + \mathcal{U}_o = 1/2$ and $\mathcal{U}_w + \mathcal{U}_o = 8/9$. (See shaded region in Figure 5.3 (b)).

Proof of Lemma 5.3.2. First, we rewrite s_{Y_2} as

$$s_{Y2} = -\frac{1}{2}\frac{\sqrt{2\nu_G(\nu_G+1)}}{\sqrt{2\nu_G(\nu_G+1)} - 2(\nu_G+1)} = -\frac{1}{2}\frac{A}{A-2}, \tag{5.36}$$

where $A = \sqrt{\frac{2\nu_G}{\nu_G+1}}$. Then, for $\nu_G > 0$ we have $A > 0$ and

$$A\,(A-1)^2 > 0 \quad \Leftrightarrow A^3 - 2A^2 + A \;>\; 0, \tag{5.37}$$

$$\Leftrightarrow A \;>\; 2A^2 - A^3 \;=\; A^2\,(2-A)\,. \tag{5.38}$$

As $2 - A > 0$, from (5.38) we obtain $s_{Y_2} = \frac{1}{2}\frac{A}{2-A} > s_{\mathcal{U}}$. Notice that when $\nu_G = 1$ we have $s_{\mathcal{Y}_2} = s_{Y_2} = s_{\mathcal{U}} = 1/2$ by (5.21). Otherwise, $\frac{2\nu_G}{\nu_G+1} > 1 \Leftrightarrow \nu_G > 1$. Thus

$$\nu_G > 1 \Leftrightarrow \frac{\nu_G}{\nu_G+1} \;>\; \frac{1}{2}\sqrt{\frac{2\nu_G}{\nu_G+1}}. \tag{5.39}$$

Therefore, we have that $s_{\mathcal{U}} > s_{\mathcal{Y}_2}$, if $\nu_G > 1$. On the other hand, consider the case in which $\nu_G < 1$. It implies that $\frac{2\nu_G}{\nu_G+1} < 1$. Thus $\frac{\nu_G}{\nu_G+1} > \frac{1}{2}\sqrt{\frac{2\nu_G}{\nu_G+1}}$. Therefore $s_{\mathcal{U}} < s_{\mathcal{Y}_2}$. This contradicts our assumption given in Remark 5.2.2 that the umbilic point lies between $s_{\mathcal{Y}_2}$ and s_{Y_2}. Thus we conclude that when $\nu_G < 1$, the expressions given in (5.25) for $s_{\mathcal{Y}_2}$ and s_{Y_2} do not represent a pair of states of fast double contact along the invariant line $[G, D]$.

Let us prove that over any invariant line, there cannot be states of fast double contact on the same side of the umbilic point. Assume that there are two states s_M, s_N in $(s_{\mathcal{U}}, 1]$, $s_M \neq s_N$, such that $\sigma(s_M; s_N) = \lambda_f(s_M) = \lambda_f(s_N)$. Substituting the expressions (5.17) in (5.12) we obtain

$$\frac{2s_M({s_N}^2 + \nu_G(1-s_N)^2)}{\nu_G} = s_M + s_N - 2s_M s_N = \frac{2s_N\left({s_M}^2 + \nu_G(1-s_M)^2\right)}{\nu_G}. \tag{5.40}$$

Equating the left and right expressions of (5.40) we have

$$(s_M - s_N)(s_M s_N(\nu_G+1) - \nu_G) = 0 \;\;\Leftrightarrow\;\; s_M = \frac{\nu_G}{s_N(\nu_G+1)}. \tag{5.41}$$

Substituting (5.41)(b) in the equality between the left and center expressions of (5.40) we obtain

$$s_N^2\nu_G + s_N^2 - 2s_N\nu_G + \nu_G = 0. \tag{5.42}$$

The discriminant of (5.42) is $4\nu_G^2 - 4(1+\nu_G)\nu_G = -4\nu_G < 0$. Therefore we have a contradiction. When considering the case s_M, s_N in $(0, s_{\mathcal{U}})$ we obtain another contradiction. Thus we conclude that $\nu_G > 0$ implies $s_{\mathcal{U}} < s_{Y_2}$.

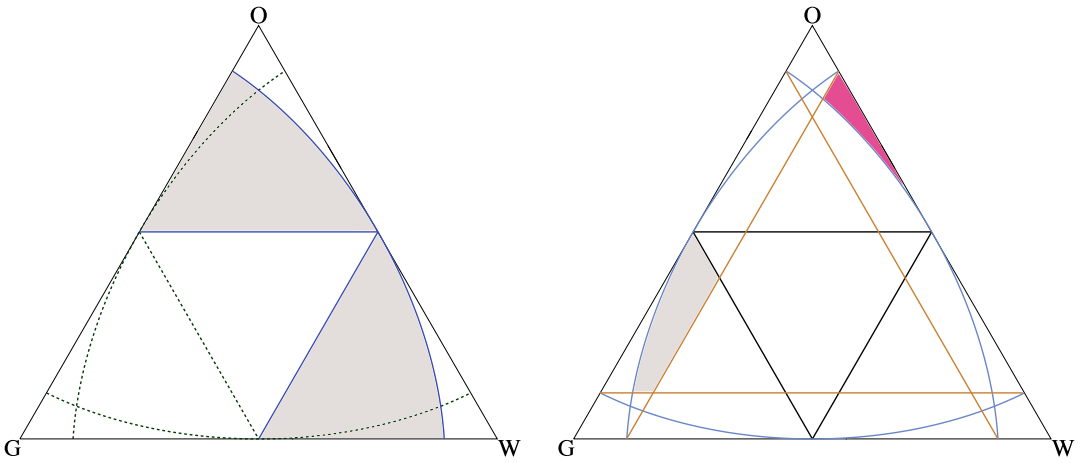

(a) Region for $\mathcal{U}$ in which Y_1 is relevant for the invariant line associated to vertex G.

(b) Example of two of the 32 regions for $\mathcal{U}$.

Figure 5.5: Diagrams for the position of the umbilic point $\mathcal{U}$. (a) Region associated to vertex G where the location of $\mathcal{U}$ implies the existence of the reduced state s_{Y_1}. (b) All 32 regions for $\mathcal{U}$ determined by different conditions on ν_W, ν_O and ν_G.

Let us assume that Y_2 coincides with D (E or B depending on which invariant line). Then $s_{Y_2} = s_D = 1$. Substituting in expression (5.21) we obtain

$$-\frac{1}{2}\frac{\sqrt{2\nu_G(\nu_G+1)}}{\sqrt{2\nu_G(\nu_G+1)}-2(\nu_G+1)} = 1 \quad \Leftrightarrow \quad -7\nu_G^2+48\nu_G+64=0. \tag{5.43}$$

As $\nu_G \geq 0$, then $\nu_G = 8$. Now assume that the umbilic point lies inside the shaded region of Figure 3.2(b). This means that

$$\frac{1}{2} < \mathcal{U}_w + \mathcal{U}_o \leq \frac{8}{9} \;\Leftrightarrow \frac{1}{2} < \frac{\mu_w+\mu_o}{\mu_w+\mu_o+\mu_g} \leq \frac{8}{9} \;\Leftrightarrow\; \frac{1}{2} < \frac{\nu_G}{\nu_G+1} \leq \frac{8}{9}. \tag{5.44}$$

Then, the last expression of (5.44) implies $1 < \nu_G \leq 8$. ∎

Remark 5.3.3. Assume that $\nu_G > 1$. Then from (5.35) we have $\frac{1}{2} < s_{\mathbb{I}} < s_{\mathcal{U}}$. Following Remark 5.3.1, notice that by (5.33) and (5.21)(a) $P_{s_{\mathcal{U}}}(s_{\mathcal{Y}_2}) = 2s_{\mathcal{Y}_2}^3 - 3s_{\mathcal{Y}_2}^2 + s_{\mathcal{U}} = s_{\mathcal{U}}/2\left(\sqrt{2\,s_{\mathcal{U}}}-1\right) > 0$. Therefore we have

$$\nu_G > 1 \;\Leftrightarrow\; s_{\mathcal{U}} = \frac{\nu_G}{\nu_G+1} > \frac{1}{2} \;\Leftrightarrow\; s_{\mathcal{Y}_2} < s_{\mathbb{I}} < s_{\mathcal{U}}. \tag{5.45}$$

Let us discuss the mixed double contact points above. We are interested in the state Y_1 that is the intersection between the mixed double contact locus and the invariant line $[G, D]$, see Section 4.4. Unlike fast double contact states $\mathcal{Y}_2$ and Y_2, the state $\mathcal{Y}_1$ and its correspondent state Y_1 are not in the same invariant line $[G, D]$ (see Fig 5.2). Moreover, $\mathcal{Y}_1$ is not part of any invariant line. Because of this reason,

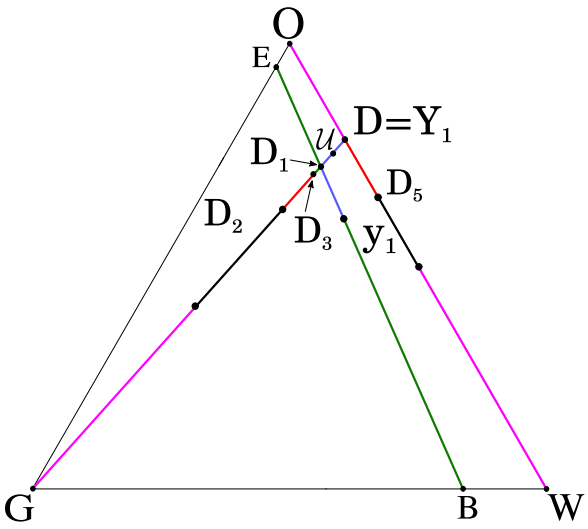

Figure 5.6: Typical example of a Hugoniot locus from $U_l = D$. In this case μ_w, μ_o and μ_g satisfies $\frac{(\mu_w-\mu_o)^2}{\mu_g(\mu_w+\mu_o)} = 8$. The states D_2 and D_1 were defined in (5.25)(a) and (b), respectively; the state D_3 satisfy $\sigma(Y_1; D_3) = \sigma(Y_1, \mathcal{Y}_1)$, where Y_1 and $\mathcal{Y}_1$ are states of mixed double contact.

we cannot characterize them using the reduced saturation parameter (additionally, the shock between $\mathcal{Y}_1$ and Y_1 is not admissible). But the location of Y_1, like that of Y_2, has an important role in our analysis as they define regions where certain wave curves bifurcate (see chapter 6).

Strong numerical evidence shows that the mixed double contact locus exists only when the umbilic point lies in one of the regions of type II (see Section 4.4). Even so, from the knowledge that Y_1 is in $[G, D]$ (for example when Y_1 lies on the boundary of the saturation triangle) we can extract important information about conditions for Y_1 to lie inside of saturation triangle (See Figure 5.6).

Now, we present a result that shows the relationship between the viscosity ratio ν_Γ and the existence of mixed double contact state Y_1 along the invariant segment $[G, D]$. This result was first shown in [4].

Definition 5.3.4. Following Remark 5.1.1 we define

$$\nu_\Gamma^- = \mu_{\alpha\beta}^-/\mu_\gamma, \quad \text{with} \quad \mu_{\alpha\beta}^- = \mu_\alpha - \mu_\beta. \tag{5.46}$$

Lemma 5.3.3. *Consider the invariant line $[G, D]$ and the umbilic point in region II_O or II_W. Then the state Y_1 of mixed double contact over $[G, D]$ lies inside the saturation triangle if and only if $\frac{\nu_G^{-2}}{\nu_G} \leq 8$.*

Remark 5.3.5. Notice that in terms of position of the umbilic point in the saturation triangle, the state Y_1 is inside the saturation triangle if and only if the umbilic point $\mathcal{U} = (\mathcal{U}_w, \mathcal{U}_o)$ is in the region bounded by the straight lines $\mathcal{U}_w + \mathcal{U}_o = 1/2, \mathcal{U}_o = 1/2$ and the ellipse $9\mathcal{U}_w^2 + 14\mathcal{U}_w\mathcal{U}_o + 9\mathcal{U}_o^2 - 8\mathcal{U}_w - 8\mathcal{U}_o = 0$ (see shaded region in Figure 5.5 (a)).

Proof. Assume that $\mathcal{U}$ is in region II_O or II_W and Y_1 coincide with D. Then we have that

$$Y_1 = D = (D_w, D_o)^T = \left(\frac{\mu_w}{\mu_w + \mu_o}, \frac{\mu_o}{\mu_w + \mu_o}\right)^T \quad \text{and} \quad s_D = 1 = s_{Y_1}. \tag{5.47}$$

Using (5.21) we have that $2 = \lambda_f(s_D) = \lambda_f(s_{Y_1})$. Consider the Hugoniot curve for D. From Lemma 4.8 of [9] the $\mathcal{H}(D)$ consisting the three straight lines $[O, W]$, $[G, D]$ and $[E, B]$, see Figure 5.6. Since for all states M over the branch $[O, W]$, the slow characteristic speed is zero, the state $\mathcal{Y}_1$ corresponding to Y_1 is not in this branch. In Figure 5.7 the branches $[E, B]$ and $[G, D]$ are is plotted. Let $\mathcal{Y}_1 = (\mathcal{Y}_{1w}, \mathcal{Y}_{1o})^T$ be the corresponding state to Y_1; from Definition 2.4.4 we have

$$\sigma(\mathcal{Y}_1; Y_1) = \lambda_s(\mathcal{Y}_1) = \lambda_f(Y_1) = 2. \tag{5.48}$$

From the Rankine-Hugoniot condition (2.8) we have

$$F_w(\mathcal{Y}_{1w}, \mathcal{Y}_{1o}) - F_w(D_w, D_o) = 2\left(\mathcal{Y}_{1w} - D_w\right), \tag{5.49}$$

$$F_o(\mathcal{Y}_{1w}, \mathcal{Y}_{1o}) - F_o(D_w, D_o) = 2\left(\mathcal{Y}_{1o} - D_o\right). \tag{5.50}$$

From (3.36) we have

$$F_w(D_w, D_o) = \frac{\mu_w}{\mu_w + \mu_o} \quad \text{and} \quad F_o(D_w, D_o) = \frac{\mu_o}{\mu_w + \mu_o}. \tag{5.51}$$

Hence, substituting (5.51) into (5.49) and (5.50) we obtain

$$\frac{\mathcal{Y}_{1w}^2/\mu_w}{\mathcal{Y}_{1w}^2/\mu_w + \mathcal{Y}_{1o}^2/\mu_o + (1 - \mathcal{Y}_{1w} - \mathcal{Y}_{1o})^2/\mu_g} = 2\mathcal{Y}_{1w} - \tfrac{\mu_w}{\mu_w + \mu_o}, \tag{5.52}$$

$$\frac{\mathcal{Y}_{1o}^2/\mu_o}{\mathcal{Y}_{1w}^2/\mu_w + \mathcal{Y}_{1o}^2/\mu_o + (1 - \mathcal{Y}_{1w} - \mathcal{Y}_{1o})^2/\mu_g} = 2\mathcal{Y}_{1o} - \tfrac{\mu_o}{\mu_w + \mu_o}. \tag{5.53}$$

Therefore, dividing (5.52) by (5.53) and simplifying we obtain

$$\frac{\mathcal{Y}_{1w}^2}{\mu_w}\left(2\mathcal{Y}_{1o} - \frac{\mu_o}{\mu_w + \mu_o}\right) - \frac{\mathcal{Y}_{1o}^2}{\mu_o}\left(2\mathcal{Y}_{1w} - \frac{\mu_w}{\mu_w + \mu_o}\right) = 0. \tag{5.54}$$

On the other hand, taking into account Lemma 4.8 of [9] where the analytic expression of the Rankine-Hugoniot locus is displayed, the nonlocal branch of $\mathcal{H}(D)$ that joins the states E and O is given by the equation in variables $\mathcal{Y}_{1w}$, $\mathcal{Y}_{1o}$

$$\left(1 + \frac{\mu_g}{\mu_w}\right)\mathcal{Y}_{1w} + \left(1 + \frac{\mu_g}{\mu_o}\right)\mathcal{Y}_{1o} - 1 = 0. \tag{5.55}$$

Since (5.55) is a straight line we can parametrize it by

$$\mathcal{Y}_{1o} = (1 - M)\frac{\mu_o}{\mu_o + \mu_g}, \qquad M \in [0, 1]. \tag{5.56}$$

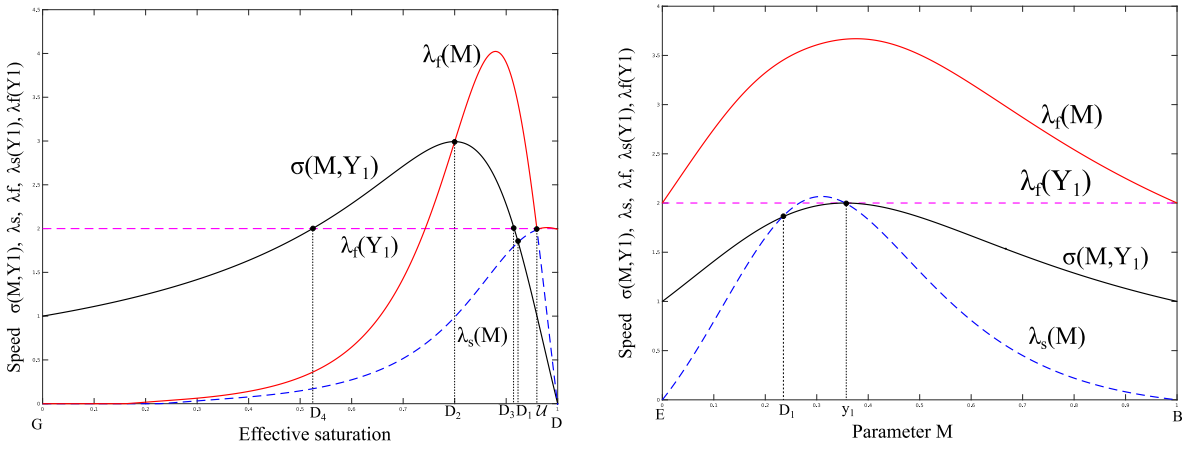

(a) Speed diagram : branch $[G, D]$ of $\mathcal{H}(D)$.

(b) Speed diagram : branch $[E, B]$ of $\mathcal{H}(D)$.

Figure 5.7: Speed diagram for $\mathcal{H}(D)$ in Figure 5.6. $\lambda_s(M)$ (resp. $\lambda_f(M)$) is the blue curve (resp. red curve) and $\sigma(M; Y_1)$ is the black curve with (a) varying the reduced saturation and (b) varying M defined in (5.55). The pink curve is $\lambda_f(Y_1)$ in both diagrams.

Substituting (5.56) into (5.55) we obtain

$$\mathcal{Y}_{1w} = M\frac{\mu_w}{\mu_w + \mu_g}, \qquad M \in [0, 1]. \tag{5.57}$$

Therefore, substituting (5.56), (5.57) into (5.54) we obtain

$$\mu_w\mu_o\left[(2\mu_g + \mu_o + \mu_w)M - \mu_g - \mu_w\right]\left[2(\mu_w + \mu_o)M^2 - (3\mu_w + \mu_o)M + \mu_w + \mu_g\right] = 0. \tag{5.58}$$

Then

$$(2\mu_g + \mu_o + \mu_w)M - \mu_g - \mu_w = 0 \quad \text{or} \tag{5.59}$$

$$2(\mu_w + \mu_o)M^2 - (3\mu_w + \mu_o)M + \mu_w + \mu_g = 0. \tag{5.60}$$

Notice that if (5.59) is true, then $\mathcal{Y}_{1w} = \mu_w/(2\,\mu_g + \mu_o + \mu_w)$ and $\mathcal{Y}_{1o} = \mu_o/(2\,\mu_g + \mu_o + \mu_w)$. Notice that $\mathcal{Y}_{1w}/\mu_w = \mathcal{Y}_{1o}/\mu_o$; thus the state $\mathcal{Y}_1$ would be on invariant line $[G, D]$. Then $s_{\mathcal{Y}_1} = (\mu_w+\mu_o)/(2\,\mu_g+\mu_o+\mu_w) = \nu_G/(2+\nu_G)$. But $\sigma(s_{\mathcal{Y}_1}; s_{Y_1}) = 2(2+\nu_G)/(\nu_G+4) \neq 2,\ \forall\ \nu_G \in (0, 1)$. This contradicts (5.48). Therefore (5.60) holds. Let us analyzed the discriminant of (5.60). Notice that

$$\triangle = (3\mu_w + \mu_o)^2 - 8(\mu_w + \mu_o)(\mu_w + \mu_g) = (\mu_w - \mu_o)^2 - 8\mu_g(\mu_w + \mu_o). \tag{5.61}$$

Given that we seek a unique solution of (5.60), we need that $\triangle = 0$. Therefore $Y_1 = D$ if and only if

$$\frac{(\mu_w - \mu_o)^2}{\mu_g(\mu_w + \mu_o)} = \frac{(\nu_G^-)^2}{\nu_G} = 8. \tag{5.62}$$

■

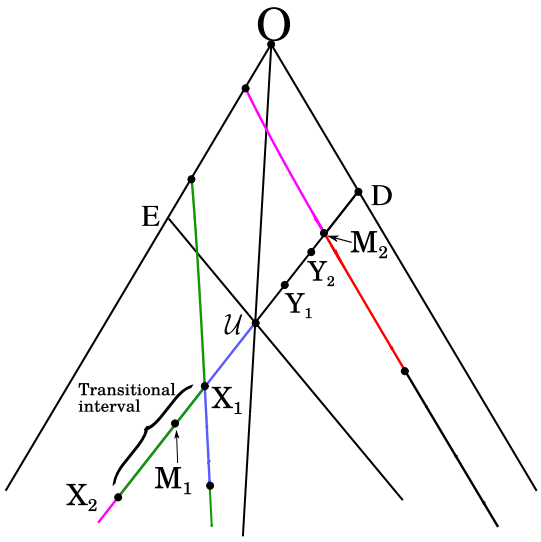

Figure 5.8: Transitional interval $[X_2(M_2), X_1(M_2)]$ of all states M_1 that has a transitional shock with M_2

In Figure 5.5(b) it is shown two regions for $\mathcal{U}$ where the choice of the distinguish invariant line imply that it satisfies different properties. For example in the shaded region we have that $\mathcal{U}$ is type II_G, $\nu_W > 8,\ \nu_G < 1, 1 < \nu_O < 8,\ \frac{(\nu_W^-)^2}{\nu_W} < 8$ and $\frac{(\nu_O^-)^2}{\nu_O} < 8$. But in the pink region we have that $\mathcal{U}$ is type $II_O, \nu_G > 8,\ \nu_O < 1, 1 < \nu_W < 8,\ \frac{(\nu_G^-)^2}{\nu_G} > 8$ and $\frac{(\nu_W^-)^2}{\nu_W} < 8$.

Remark 5.3.6. Lemmas 5.3.2 and 5.3.3 still hold if we replace the invariant line $[G, D]$ by $[W, E]$ or $[O, B]$ using (5.11). Over all there are 32 different regions where the umbilic point could be; they are shown in Figure 5.5(b).

5.4 Transitional shocks in reduced two-phase flow model

Transitional waves were introduced in [19, 21] to solve Riemann problems for non-strictly hyperbolic systems of conservation laws. Transitional shock waves for generic flux functions are characterized by a *transitional map* $T : \mathbb{R}^3 \to \mathbb{R}^3$ defined on an open set $A \in \mathbb{R}^3$, the *transitional region*. The transitional map carries each point (U, σ) in A to a unique point (U', σ) in A' with $U' = T(U)$, $A' = T(A)$ and such that U and U' are connected by an admissible crossing discontinuity with shock speed $\sigma = \sigma(U; U')$. For viscous matrix $\mathcal{B} = I$, transitional shocks arise only along the invariant lines and, regions A and A' are projected over the phase space as line segments on both sides of $\mathcal{U}$. These regions lie over suitable planes perpendicular to phase space and cross them along the invariant lines, as described in more detail in chapter 7.

Taking advantage of the formulation of the reduced model, we can study the transitional map between states along the same invariant line in an explicit way. That is, for each state M_2 on the segment $[\mathcal{U}, \mathbb{B}]$,

$\mathbb{B} \in \{E, D, B\}$, there are states X_1, X_2 along the segment $[\Gamma, \mathcal{U}]$ with $\Gamma \in \{G, W, O\}$ such that any state M_1 between $[X_2, X_1]$ has an admissible transitional shock to M_2. This map can be characterized by means of the reduced saturation on the invariant line studied in previous sections. In order to facilitate the explanation, we use the inverse transitional map $T^{-1}(M_2)$ with respect to the direction of orbits along points in these invariant lines. This procedure is analogous to choosing a state M_1 along $[\Gamma, \mathcal{U}]$ and calculating the forward transitional map $T(M_1)$ and the interval defined by X_1 and X_2 along $[\mathcal{U}, \mathbb{B}]$.

Notice that for $M_2 = \mathbb{B}$ we have a straightforward limit for transitional shocks given by the reduced states $s_{\mathbb{B}_2}$ and $s_{\mathbb{B}_1}$ calculated in (5.25), such that all points between $\mathbb{B}_1$ and $\mathbb{B}_2$ satisfy Definition 2.4.6.

The limits of transitional shocks are clear extrema of the transitional map T, *i.e.*, these states are characteristic shocks of the suitable families. For this reason, we use expressions (5.12) and (5.13) (a)-(b) for reduced states to find explicitly the map that determines the extrema of the transitional interval associated with M_2.

Theorem 5.4.1. *Let M_2 be a state along the secondary bifurcation line associated to the vertex $\Gamma \in \{G, W, O\}$ on the invariant segment $(\mathcal{U}, \mathbb{B}]$, $\mathbb{B} \in \{D, E, B\}$ with $1 < \nu_\Gamma \leq 8$. Then, there are two states X_1, X_2 along the segment $[\Gamma, \mathcal{U})$ such that for any state M_1, with $s_{M_1} \in (s_{X_2}, s_{X_1})$, we have a transitional shock between M_1 and M_2 with transitional speed $\sigma_T(M_1; M_2)$. The state X_1 satisfy*

$$\sigma(X_1; M_2) = \lambda_s(X_1). \tag{5.63}$$

For the state X_2 we have two cases depending on Y_2 (Remark 5.2.2):

a. If $s_{M_2} \in (s_{\mathcal{U}}, s_{Y_2}]$

$$\sigma(X_2; M_2) = \lambda_f(M_2). \tag{5.64}$$

b. If $s_{M_2} \in (s_{Y_2}, 1]$

$$\sigma(X_2; M_2) = \lambda_f(X_2). \tag{5.65}$$

Proof. We first compute X_1. Substituting (5.63) in (5.14)(a) and using (5.12) we obtain

$$s_{X_1} = \frac{\nu_\Gamma s_{M_2}}{2(1+\nu_\Gamma)s_{M_2}^2 + \nu_\Gamma(1 - 2s_{M_2})}. \tag{5.66}$$

Notice that the denominator of (5.66) is nonzero and for M_2 in the edge opposite to the vertex Γ ($s_{X_1} = \nu_\Gamma/(2+\nu_\Gamma) = s_{\mathbb{B}_1}$ and $s_{M_2} = 1$), coinciding with (5.25)(b). Given that $\nu_\Gamma \geq 1$ then $s_{M_2} > s_{\mathcal{U}} \geq 1/2$ then $1 - 2s_{M_2} < 0$. Thus

$$s_{M_2}(1 - 2s_{M_2}) < s_{\mathcal{U}}(1 - 2s_{M_2}) \quad \Leftrightarrow s_{M_2} < 2s_{M_2}^2 + s_{\mathcal{U}}(1 - 2s_{M_2}), \tag{5.67}$$

$$\Leftrightarrow \frac{s_{M_2} s_{\mathcal{U}}}{2s_{M_2}^2 + s_{\mathcal{U}}(1 - 2s_{M_2})} < s_{\mathcal{U}}. \tag{5.68}$$

Hence, substituting (5.15) in (5.68) we obtain $s_{X_1} = \dfrac{s_{M_2}\nu_\Gamma}{2(1+\nu_\Gamma)s_{M_2}^2 + \nu_\Gamma(1-2s_{M_2})} < s_{\mathcal{U}}$. Therefore, we conclude that for $s_{M_2} \in (s_{\mathcal{U}}, 1]$, $s_{D_1} \leq s_{X_1} < s_{\mathcal{U}}$. Now, from Lemma 5.3.2 there are $\mathcal{Y}_2$ and Y_2 along the invariant line defined by vertex Γ, with $s_{\mathcal{Y}_2} \in (0, s_{\mathcal{U}}]$ and $s_{Y_2} \in [s_{\mathcal{U}}, 1]$. Notice that these points naturally define a bifurcation over their corresponds segments, because they are the only points along the invariant line that satisfy (5.16). Next, we study the cases for X_2:

a. Case $s_{M_2} \in (s_{\mathcal{U}}, s_{Y_2}]$. We seek a state X_2 that satisfies (5.64). Then from (5.12) and (5.14)(b) we obtain the quadratic equation

$$As_{X_2}^2 + Bs_{X_2} + C = 0, \tag{5.69}$$

where

$$A = 2s_{M_2}(1+\nu_\Gamma), \quad B = -(2s_{M_2}+1)\nu_\Gamma, \quad \text{and} \quad C = \nu_\Gamma s_{M_2}. \tag{5.70}$$

Notice that the discriminant of quadratic equation (5.69) is

$$B^2 - 4AC = -r\left[(4\nu_\Gamma + 8)s_{M_2}^2 - 4\nu_\Gamma s_{M_2} - \nu_\Gamma\right], \tag{5.71}$$

the sign of which is nonnegative if and only if

$$(4\nu_\Gamma + 8)s_{M_2}^2 - 4\nu_\Gamma s_{M_2} - \nu_\Gamma \leq 0. \tag{5.72}$$

$$B^2 - 4AC \geq 0 \Leftrightarrow \frac{1}{2}\frac{\nu_\Gamma - \sqrt{2\nu_\Gamma(\nu_\Gamma+1)}}{\nu_\Gamma+2} < \frac{\nu_\Gamma}{\nu_\Gamma+1} < s_{M_2} \leq \frac{1}{2}\frac{\nu_\Gamma + \sqrt{2\nu_\Gamma(\nu_\Gamma+1)}}{\nu_\Gamma+2} = s_{Y_2}. \tag{5.73}$$

Moreover, when $M_2 = Y_2$, we have $B^2 - 4AC = 0$. Then,

$$s_{X_2} = \frac{-(s_{Y_2}+1)\nu_\Gamma}{4s_{Y_2}(1+\nu_\Gamma)} = \frac{1}{2}\sqrt{\frac{2\nu_\Gamma}{\nu_\Gamma+1}} = s_{\mathcal{Y}_2}. \tag{5.74}$$

Therefore, s_{X_2} is in $[s_{\mathcal{Y}_2}, s_{\mathcal{U}})$. Otherwise, since that $s_{M_2} < s_{Y_2}$, then s_{X_2} is chosen such that the biggest root of quadratic equation (5.69), because the other one implies that $s_{X_2} < s_{\mathcal{Y}_2}$ which contradicts the given assumptions.

b. Case $s_{M_2} \in (s_{Y_2}, 1]$. We seek a state X_2 that satisfies (5.65). From (5.12) and (5.14)(b), we obtain the quadratic equation

$$As_{X_2}^2 + Bs_{X_2} + C = 0, \tag{5.75}$$

where

$$A = (2s_{M_2} - 1)(\nu_\Gamma + 1), \quad B = -2s_{M_2}(\nu_\Gamma+1) \quad \text{and} \quad C = \nu_\Gamma. \tag{5.76}$$

Notice that the discriminant of equation (5.75) is

$$B^2 - 4AC = (\nu_\Gamma+1)\left[(\nu_\Gamma+1)s_{M_2}^2 - 2\nu_\Gamma s_{M_2} + \nu_\Gamma\right], \tag{5.77}$$

which is positive for all $s_{M_2} \in (s_{Y_2}, 1]$. Additionally, if we consider $s_{M_2} = 1$, we obtain $s_{X_2} = \frac{\sqrt{\nu_\Gamma+1}\pm 1}{\sqrt{\nu_\Gamma+1}}$. Notice that the largest of these two values for s_{X_2} is greater than one, which is not valid. Then for $s_{M_2} = 1$, we obtain $s_{X_2} = \frac{\sqrt{\nu_\Gamma+1}-1}{\sqrt{\nu_\Gamma+1}}$ which coincides with s_{D_2}, see equation (5.25)(a). On the other hand, as the pair of states s_{Y_2} and $s_{\mathcal{Y}_2}$ also satisfies (5.65), the solution of quadratic equation (5.75) for $s_{M_2} = s_{Y_2}$ is $s_{X_2} = s_{\mathcal{Y}_2}$, hence $s_{X_2} \in [s_{\mathbb{B}_2}, s_{\mathcal{Y}_2})$. We conclude that s_{X_2} is the lowest solution of the quadratic equation defined by the coefficients (5.76), because if we choose the other one $s_{X_2} > 1$ which contradicts the given assumptions.

■

Corollary 5.4.2. *For $\nu_\Gamma > 8$ (or $(\nu_\Gamma^-)^2/\nu_\Gamma > 8$) in the context of Theorem 5.4.1, the state X_1 satisfies (5.63). The case a) holds for X_2 with $s_{M_2} \in (s_{\mathcal{U}}, 1]$ and $s_{X_2} \in [s_{\widehat{\mathbb{B}_2}}, s_{\mathcal{U}})$, where $\widehat{\mathbb{B}_2}$ satisfy $\sigma(\widehat{\mathbb{B}_2}; \mathbb{B}) = \lambda_f(\mathbb{B})$, for $\mathbb{B} \in \{D, E, B\}$.*

Proof. As seen in Lemma 5.3.2 (or Lemma 5.3.3), when $\nu_\Gamma > 8$ (or $(\nu_\Gamma^-)^2/\nu_\Gamma > 8$)

$$s_{Y_2} = \frac{1}{2}\frac{\nu_\Gamma + \sqrt{2\nu_\Gamma(\nu_\Gamma+1)}}{\nu_\Gamma + 2} > 1. \tag{5.78}$$

Then, state Y_2 is not inside of the saturation triangle and M_2 must be chosen in $(\mathcal{U}, \mathbb{B}]$ (*i.e.,* $s_{M_2} \in (s_{\mathcal{U}}, 1]$). State X_1, which is the lower extreme of transitional segment, is calculate as in (5.66) and satisfies $s_{X_1} \in [s_{\mathbb{B}_1}, s_{\mathcal{U}})$. The upper extreme X_2 is found as in the proof of Theorem 5.4.1 with s_{M_2} satisfying quadratic equation (5.69) with coefficients (5.70). Notice that for $s_{M_2} = 1$, we obtain from the equation (5.69)

$$s_{X_2} = \frac{1}{4}\frac{3\nu_\Gamma \pm \sqrt{\nu_\Gamma(\nu_\Gamma - 8)}}{\nu_\Gamma + 1} < \frac{\nu_\Gamma}{\nu_\Gamma + 1} = s_{\mathcal{U}}. \tag{5.79}$$

We name $\widehat{\mathbb{B}_2} \in [G, \mathcal{U}]$ the state associate to $\mathbb{B}$, with $\mathbb{B} \in \{D, E, B\}$ such that $\sigma(\mathbb{B}, \widehat{\mathbb{B}_2}) = \lambda_f(\mathbb{B})$ and $s_{\widehat{\mathbb{B}_2}} = \frac{1}{4}\frac{3\nu_\Gamma + \sqrt{\nu_\Gamma(\nu_\Gamma-8)}}{\nu_\Gamma+1}$. Now, consider $s_{M_2} \in (s_{\mathcal{U}}, 1)$. Dividing the coefficients (5.70) by $\nu_\Gamma + 1$, the solutions of (5.68) are

$$s_{X_2} = \frac{s_{\mathcal{U}}(2s_{M_2}+1) \pm \sqrt{s_{\mathcal{U}}^2(2s_{M_2}+1)^2 - 8s_{M_2}^2 s_{\mathcal{U}}}}{4s_{M_2}}, \tag{5.80}$$

among which we consider the largest value of s_{X_2} that satisfy $s_{\widehat{\mathbb{B}_2}} < s_{X_2} < s_{\mathcal{U}}$. ■

Theorem 5.4.3. *For $\nu_\Gamma \leq 1$ in the setting of Theorem 5.4.1, but $M_2 \in [\mathbb{B}_0, 1]$, with $\mathbb{B}_0$ defined in (5.26). Then X_1 satisfies (5.63) and case b) holds for X_2.*

Proof. Notice that the state $\mathbb{B}_0$ defined in (5.27), $\mathbb{B}_0$ and $\mathcal{U}$ satisfies both equations (5.63) and (5.65). Furthermore $s_{\mathcal{U}} \leq 1/2 = s_{\mathbb{B}_0}$. We have two options for the choice of M_2: (i) $M_2 \in [\mathbb{B}_0, \mathbb{B}]$ *i.e.,* $1/2 \leq s_{M_2} \leq 1$; or (ii) $M_2 \in (\mathcal{U}, \mathbb{B}_0)$, *i.e.,* $s_{\mathcal{U}} < s_{M_2} < 1/2$.

In the first possibility, the equation (5.66) for s_{X_1} is computed as in proof of Theorem 5.4.1 and satisfies $s_{X_1} \in [s_{\mathbb{B}_1}, s_{\mathcal{U}}]$. For the upper extreme X_2, we have the part b) of Theorem 5.4.1 with s_{X_2} satisfying the quadratic equation 5.75 with coefficients (5.76) and $s_{M_2} \in [1/2, 1]$. Notice that when $s_{M_2} = 1/2$ we obtain $s_{X_2} = s_{\mathcal{U}}$ while when $s_{M_2} = 1$, $s_{X_2} = s_{\mathbb{B}_2}$. Then, we have that for $s_{M_2} \in (s_{\mathbb{B}_0}, 1]$ the upper extreme X_2 satisfy $s_{\mathbb{B}_2} < s_{X_2} \leq s_{\mathcal{U}}$.

In the second possibility, the equation (5.66) for s_{X_1} is also computed as in proof of Theorem 5.4.1 and satisfies $s_{X_1} \in [s_{\mathcal{U}}, 1/2]$, *i.e.,* in this case both states M_2 and X_1 lie in the same side of $\mathcal{U}$, which contradicts our assumption of the transitional interval must be lie in $[\Gamma, \mathcal{U}]$. Therefore, there are transitional shocks joining states $M_2 \in [\mathbb{B}_0, \mathbb{B}]$ and $M_1 \in [X_2, X_1] \subset [\Gamma, \mathcal{U}]$. ■

Remark 5.4.1. Notice that for $\nu_\Gamma \geq 1$ the Theorem 5.4.1 and Corollary 5.4.2 guarantee that any state $s_{M_2} \in [s_{\mathcal{U}}, 1]$ has an inverse transitional map. In Theorem 5.4.3 when $\nu_\Gamma < 1$ we have that the inverse transitional map only exists for $s_{M_2} \in [s_{\mathbb{B}_0}, 1]$. If $s_{\mathcal{U}} < s_{M_2} < 1/2$ then by (5.67) and (5.68) $s_{X_1} > s_{\mathcal{U}}$, therefore we do not have an inverse transitional map for these states.

5.5 Transitional Rarefaction waves

Transitional rarefactions were described in [19] for models of two conservation laws. Such waves arise when an integral curve of the fast family is followed by an integral curve of the slow family (in the direction of increasing characteristic speed). It is necessary that the two characteristic speeds coincide at the point where these curves join. In our model, these waves arise when the umbilic point is type II_Γ with $\Gamma \in \{G, W, O\}$, and when considering solutions of Riemann problems that involve states along the invariant line with viscosity ratio $\nu_\Gamma < 1$. As seen in Remark 5.3.1, when $\nu_\Gamma < 1$, the parameter $s_{\mathbb{I}}$ represents the intersection between the slow inflection locus and the invariant line defined by vertex Γ and satisfy $s_{\mathcal{U}} < s_{\mathbb{I}} < s_{\mathbb{B}_0} = 1/2$. We follow the same procedure presented for transitional shocks in the previous section. We consider a state M_2 along $[s_{\mathcal{U}}, s_{\mathbb{B}_0}]$ and show how to build transitional rarefaction waves.

Theorem 5.5.1. *Consider $\nu_\Gamma < 1$ in the setting of Theorem 5.4.1, but for $s_{M_2} \in [s_{\mathcal{U}}, s_{\mathbb{B}_0}]$ with $\mathbb{B}_0$ defined in (5.26). Let M_1 be a state along $[0, s_{\mathcal{U}}]$, then there is a transitional rarefaction wave between M_1 and M_2 with transition state between the fast and slow rarefaction at the umbilic point. We have two cases for this transitional rarefaction :*

a. If $s_{M_2} \in (s_{\mathcal{U}}, s_{\mathbb{I}}]$, then the transitional rarefaction consists of the follows sequence of waves

$$M_1 \xrightarrow{R_2} \mathcal{U} \xrightarrow{R_1} M_2. \tag{5.81}$$

b. If $s_{M_2} \in (s_{\mathbb{I}}, s_{\mathbb{B}_0}]$, then there is a state M_3, $s_{M_3} \in [s_{\mathcal{U}}, s_{\mathbb{I}})$ with $\sigma(M_3; M_2) = \lambda_s(M_3)$, such that the transitional rarefaction consists of the follows sequence of waves

$$M_1 \xrightarrow{R_2} \mathcal{U} \xrightarrow{R_1} M_3 \xrightarrow{'S_1} M_2. \tag{5.82}$$

Proof. As we see in Remark 5.2.1 $\lambda_b(s) = f'(s)$ and satisfy $\lambda_b(s) = \lambda_f(s)$ for $s \in [0, s_{\mathcal{U}}]$ and $\lambda_b(s) = \lambda_s(s)$ for $s \in [s_{\mathcal{U}}, 1]$. Moreover

$$\lambda_b'(s) = \frac{2\nu_G[2(\nu_G+1)s^3 - 3(\nu_G+1)s^2 + \nu_G]}{((\nu_G+1)s^2 - 2\nu_G s + \nu_G)^3} = \frac{2s_{\mathcal{U}}(2s^3 - 3s^2 + s_{\mathcal{U}})}{(\nu_G+1)(s^2 - 2s_{\mathcal{U}}s + s_{\mathcal{U}})^3}. \tag{5.83}$$

From Remark 5.3.1 $\lambda_b'(s_{\mathbb{I}}) = 0$ and $s_{\mathcal{U}} < s_{\mathbb{I}} < 1/2$. By (5.83) we see that $\lambda_b(s)$ is an increasing function in $(0, s_{\mathbb{I}})$. Then, we can put in $s_{\mathcal{U}}$ a slow rarefaction preceded by a fast rarefaction satisfying the speed compatibility criteria. Therefore, if $s_{M_2} \in (s_{\mathcal{U}}, s_{\mathbb{I}}]$ we have the sequence given in (5.81) for

any state $s_{M_1} \in [0, s_{\mathcal{U}})$. Now, consider $s_{M_2} \in (s_{\mathbb{I}}, 1/2]$ and we seek a state M_3, $s_{M_3} \in [s_{\mathcal{U}}, s_{\mathbb{I}})$ such that satisfy $\sigma(M_3; M_2) = \lambda_s(M_3)$. Therefore from (5.12) and (5.14)(a) we obtain the quadratic equation

$$As_{M_3}^2 + Bs_{M_3} + C = 0, \tag{5.84}$$

where

$$A = (2s_{M_2} - 1)(\nu_\Gamma + 1), \quad B = -2s_{M_2}(\nu_\Gamma + 1) \quad \text{and} \quad C = \nu_\Gamma. \tag{5.85}$$

Notice that the discriminant of (5.84) is positive for all s_{M_2} with $s_{M_2} < 1/2$. Thus, one solution of the quadratic equation is negative and the other one is positive. If M_2 is equal to $\mathbb{B}_0$, A is null in (5.85) then we have a linear equation $-(\nu_\Gamma + 1)s_{M_3} + \nu_\Gamma = 0$. Hence $s_{M_3} = s_{\mathcal{U}}$. Moreover, notice that

$$s_{\mathcal{U}}(s_{\mathcal{U}} - 1)(2s_{M_2} - 1)^2 \leq 0 \quad \Leftrightarrow (-2s_{M_2}s_{\mathcal{U}} + s_{M_2} + s_{\mathcal{U}})^2 \leq s_{M_2}^2 - 2s_{M_2}s_{\mathcal{U}} + s_{\mathcal{U}} \tag{5.86}$$

$$\Leftrightarrow -2s_{M_2}s_{\mathcal{U}} + s_{M_2} + s_{\mathcal{U}} \leq \sqrt{s_{M_2}^2 - 2s_{M_2}s_{\mathcal{U}} + s_{\mathcal{U}}} \tag{5.87}$$

$$\Leftrightarrow s_{\mathcal{U}} \leq \frac{s_{M_2} - \sqrt{s_{M_2}^2 - 2s_{M_2}s_{\mathcal{U}} + s_{\mathcal{U}}}}{2s_{M_2} - 1} = s_{M_3}. \tag{5.88}$$

We next prove that $s_{M_3} < s_{\mathbb{I}}$. Let $P_{s_{\mathcal{U}}}(s) = 2s^3 - 3s^2 + s_{\mathcal{U}}$ be the function associated to (5.33). From Remark 5.3.1 $P_{s_{\mathcal{U}}}(s_{\mathbb{I}}) = 0$, $P_{s_{\mathcal{U}}}(s) > 0$ for $s \in [0, s_{\mathbb{I}})$ and $P_{s_{\mathcal{U}}}(s) < 0$ for $s \in (s_{\mathbb{I}}, 1]$ for all $0 \leq s_{\mathcal{U}} \leq 1$. On the other hand, dividing the equation (5.85) by $(\nu_\Gamma + 1)$, we obtain

$$(2s_{M_2} - 1){s_{M_3}}^2 - 2s_{M_2}s_{M_3} + s_{\mathcal{U}} = 0. \tag{5.89}$$

From (5.89) we have $s_{\mathcal{U}} = 2s_{M_2}s_{M_3} - (2s_{M_2} - 1)s_{M_3}^2$. Notice that

$$P_{s_{\mathcal{U}}}(s_{M_3}) = 2s_{M_3}^3 - 3s_{M_3}^2 + s_{\mathcal{U}} = \quad 2s_{M_3}^3 - 3s_{M_3}^2 + \left(2s_{M_2}s_{M_3} - (2s_{M_2} - 1)s_{M_3}^2\right) \tag{5.90}$$

$$= \quad 2s_{M_3}(1 - s_{M_3})(s_{M_2} - s_{M_3}) > 0. \tag{5.91}$$

Hence, $s_{\mathcal{U}} \leq s_{M_3} < s_{\mathbb{I}}$. Therefore, if $s_{M_2} \in (s_{\mathbb{I}}, s_{\mathbb{B}_0}]$ there is a state M_3, with $s_{M_3} \in [s_{\mathcal{U}}, s_{\mathbb{I}})$, such that the transitional rarefaction is given by the sequence (5.82) for any state $s_{M_1} \in [0, s_{\mathcal{U}})$.

■

Chapter 6

Wave curves

In this chapter, we characterize the wave curves that appear in the Corey Quad model with $\mathcal{B}(U) = I$. These wave curves are constructed using the succession algorithm defined in Section 2.7. Since we want to use the wave curves to solve the Riemann problem in the whole saturation triangle for $\mathcal{U}$ of type II, we first identify the regions where the wave curves have the same number and types of waves groups. Then, we study how these regions change when μ_w, μ_o and μ_g vary. The results in this chapter provide scientific evidence for the existence of Riemann solutions, based on a combination of analytical an computational techniques

6.1 Division of saturation triangle in $\mathcal{SR}_i$ and $\mathcal{FR}_i$ regions

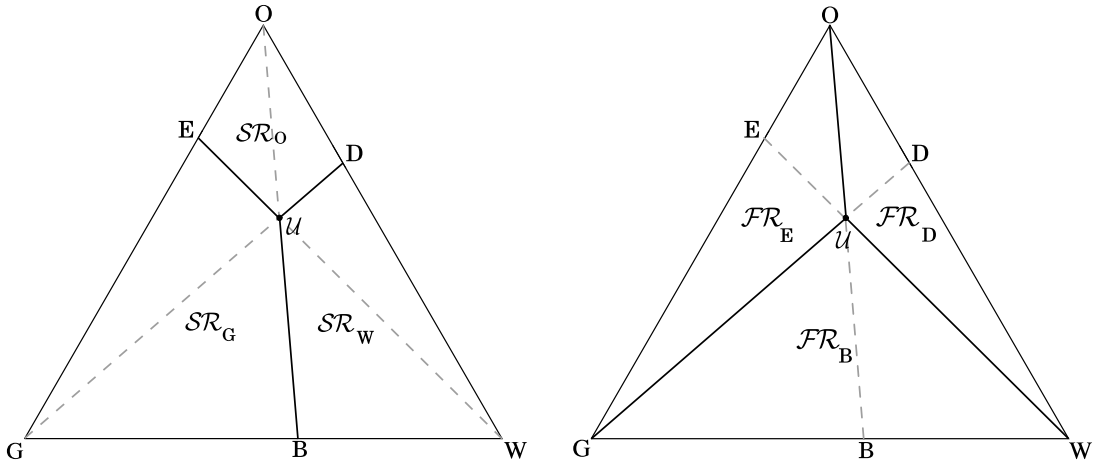

(a) Slow macro regions.

(b) Fast macro regions.

Figure 6.1: Division of saturation triangle in macro regions for slow and fast characteristic families for $\mathcal{U} \in II_O$.

For each characteristic family, we divide the saturation triangle into three macro regions. This divi-

sion is induced by the geometry of the characteristic fields defined in Section 4.1, where we discussed the importance of the features of eigenvectors for both families along the boundaries of the saturation triangle and the secondary bifurcation locus (see Figure 4.1). Actually, that this division is not influenced by the choice of viscosity matrix in the study of admissibility criteria, but it is more straightforward when we adopt $\mathcal{B}_{2\times 2} = I$ because in this case secondary bifurcations are invariant lines and transitional shocks lie along them (see Chapter 5).

Before proceeding, let us introduce some notation. We use the notation (A, B), $[C, D]$ and their combinations to denote segments in the saturation triangle joining A to B (with endpoints excluded), and segments joining C and D including the end points. We write $[A, B, C]$ for a curve between A and C which passes through a relevant point B. The notation $\widehat{ABC}$ represents the triangle with vertices A, B and C.

Definition 6.1.1. Three quadrilateral *slow macro regions* are defined between the triangle's sides and the Y-shaped curve formed by the segments of the secondary bifurcation joining at $\mathcal{U}$ (see Figure 6.1 (a)). We identify each region $\mathcal{SR}_\Gamma$ by the vertex $\Gamma \in \{G, W, O\}$ within it.
Three triangular *fast macro regions* are defined between the $\perp$-shaped curve formed by the segments of secondary bifurcation joining $\mathcal{U}$ with the triangle's vertex (see Figure 6.1 (b)). We identify each region $\mathcal{FR}_\mathbb{B}$ by the intersection point between the invariant line and the boundary of saturation triangle $\mathbb{B} \in \{E, D, B\}$.

Notice that each invariant line passes through a slow quadrilateral region and a fast triangular region. In our description, it is useful to refer to this correspondence, *e.g.*, $\mathcal{SR}_O$ and $\mathcal{FR}_B$ are the regions associated with invariant line $[O, B]$.

Definition 6.1.2. Let T be an open set of states in the saturation triangle. We say that T is a backward (alternatively, a forward) $\mathscr{R}$-region if for every right state $R \in T$, the backward (forward) fast wave curve $\mathcal{W}_f^-(R)$ ($\mathcal{W}_f^+(R)$), has the same structure, *i.e*, it has exactly the same wave sequence. In the same way we define forward (backward) $\mathscr{L}$-regions.

For each macro region, it is convenient to construct the $\mathscr{L}$-regions and $\mathscr{R}$-regions in a particular way: that it is $\mathcal{SR}_\Gamma$ with $\Gamma \in \{G, W, O\}$ is subdivided into forward $\mathscr{L}$-regions and $\mathcal{FR}_\mathbb{B}$ with $\mathbb{B} \in \{D, E, B\}$ is subdivided in backward $\mathscr{R}$-regions. Though in principle $\mathscr{L}$- and $\mathscr{R}$-regions are constructed independently, their relationship is usually studied in order to prove existence (and uniqueness) of solutions to Riemann problems.

Let $\mathscr{R}_i$ be a backward $\mathscr{R}$-region. For each $R \in \mathscr{R}_i$ the saturation triangle is subdivided into several backward $\mathscr{L}$-regions (actually a family of regions depending on R) where the solutions of the Riemann problems have the same structure (not just the same wave curves). That is, let $\mathscr{L}_j(R)$ be an $\mathscr{L}_{\mathscr{R}_i}$-region depending of R, then the solutions that connect the left state $L \in \mathscr{L}_i(R)$ to R have the same structure, *i.e.*, they have exactly the same wave sequences.

The solution of the Riemann problem (2.1),(2.4) is parametrized by a sequence of wave curves, which necessarily go from U_L to U_R. However, in the description of our work we construct the backward $\mathscr{R}$-regions and from these regions we build the associated backward $\mathscr{L}_\mathscr{R}$-regions, see for example [4, 3]. But it is possible to proceed in the opposite direction: first we construct the forward $\mathscr{L}$-regions and later build the associated forward $\mathscr{R}_\mathscr{L}$-regions, see for example [17, 21, 31]

6.2 Subdivision of $\mathcal{SR}_G$ in forward $\mathscr{L}$ -regions

In this section we describe the subdivisions of $\mathcal{SR}_G$ in forward $\mathscr{L}$-regions. Since we adopt the description of Riemann solutions in terms of backward $\mathscr{R}$-regions and $\mathscr{L}_{\mathscr{R}}$-regions, as an illustration we only show the subdivision and the methodology used for their construction. For a detailed description of $\mathscr{L}$-regions and the construction of the slow forward wave curves see [17, 31].

The forward $\mathscr{L}$-regions and their boundaries for slow forward wave curves are shown in Figure 6.2. They are formed by portions of the bifurcation manifold and by backward rarefactions from certain exceptional points computed numerically.

In Figure 6.2(a), we have the following portions of the bifurcation manifolds: the slow inflection $\mathcal{I}_s$; the curves $[B^*, Q_3]$ and $[D_1, E^*]$ which are part of the s-right-extension boundary of edge $[W, O]$; curve $[B^*, G]$ that is part of s-right-extension boundary of edge $[G, O]$ while $[E^*, G]$ that is part of the s-right-extension boundary of edge $[G, W]$; the segment $[D_1, \mathcal{U}]$ that is part of the invariant line $[G, D]$ and curve $[\mathcal{U}^*, Q_3]$ is the s-right-extension of segment $[D_1, \mathcal{U}]$; the Lax s-shock segment $[D_1, Q_3]$ is part of the nonlocal branch of $\mathcal{H}(D)$.

The slow inflection has some relevant points which intersect the follow segments: $\mathcal{I}_s^1$ is in segment $[\mathcal{U}, B]$ and $\mathcal{I}_s^2$ is the intersection with the Lax s-shock segment $[D_1, Q_3]$.

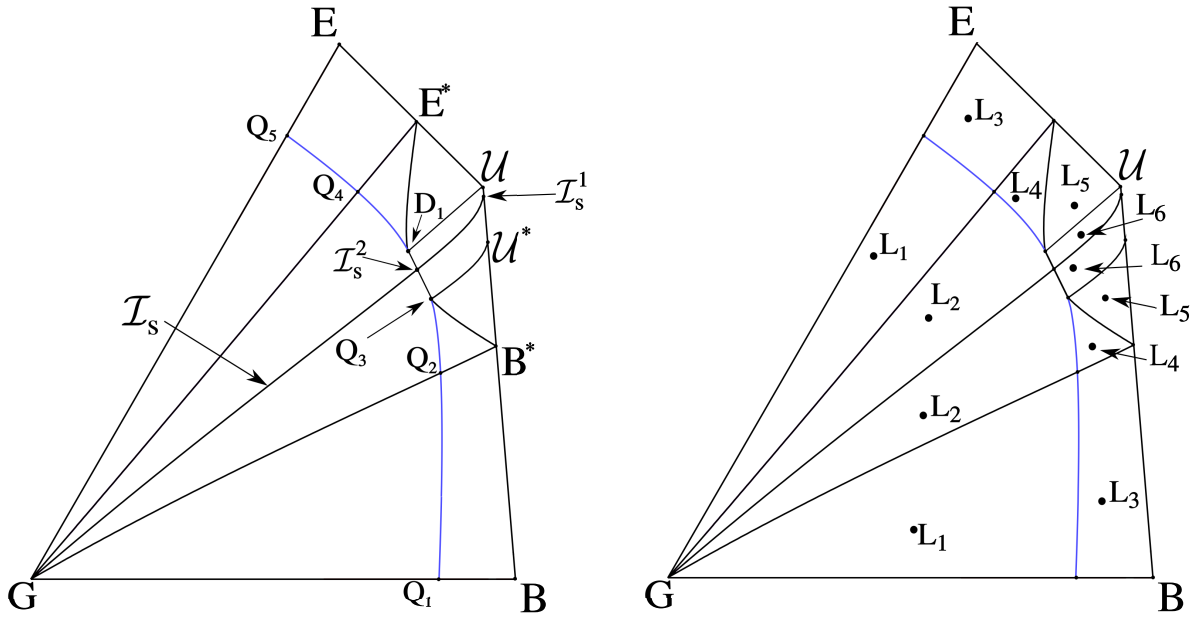

(a) $\mathscr{L}$-Boundaries. (b) Forward $\mathscr{L}$-regions.

Figure 6.2: Subdivision of $\mathcal{SR}_G$ in six distinct forward $\mathscr{L}$-regions.

We can classify the $\mathscr{L}$-regions into two groups, see Figure 6.2(b): those regions where the slow wave curve only has a local branch and those where it also has nonlocal branches. For a state L in regions $\mathscr{L}_1$ or $\mathscr{L}_2$, the slow forward wave curve $\mathcal{W}_s^+(L)$ only has a local branch. For a state L in regions $\mathscr{L}_i$

with $i \in \{3,4,5,6\}$, the slow forward wave curve $\mathcal{W}_s^+(L)$ has a local branch and a nonlocal branch. The local branches of $\mathcal{W}_s^+(L)$ for L in $\mathscr{L}_1$ or $\mathscr{L}_3$ are similar and so are the local branches for L in $\mathscr{L}_i$ with $i \in \{2,4,5,6\}$. The construction of these forward slow wave curves can be found in [21] for the completely symmetric case or in [17] for the case of two equal viscosities. In general, these $\mathscr{L}$-regions do not change greatly when the viscosities vary.

6.3 Compatibility and admissibility boundaries

In this section we define the compatibility and admissibility boundaries. These boundaries are important in the definition of the $\mathscr{R}$ regions that divide the saturation triangle in areas where the same solution properties are preserved. They are also important in the construction of boundaries by the surface of transitional shocks that will be studied in Chapter 7. In the case of the velocity compatibility criterion, for example, the triple shock rule 2.4.3 can be used together with the fact that the speed between different wave groups is increasing to determine the compatibility boundary to be where the speeds of slow and fast waves are the same. The nonlocal admissibility boundary separates regions where the Hugoniot locus has a nonlocal branch from those where it does not.

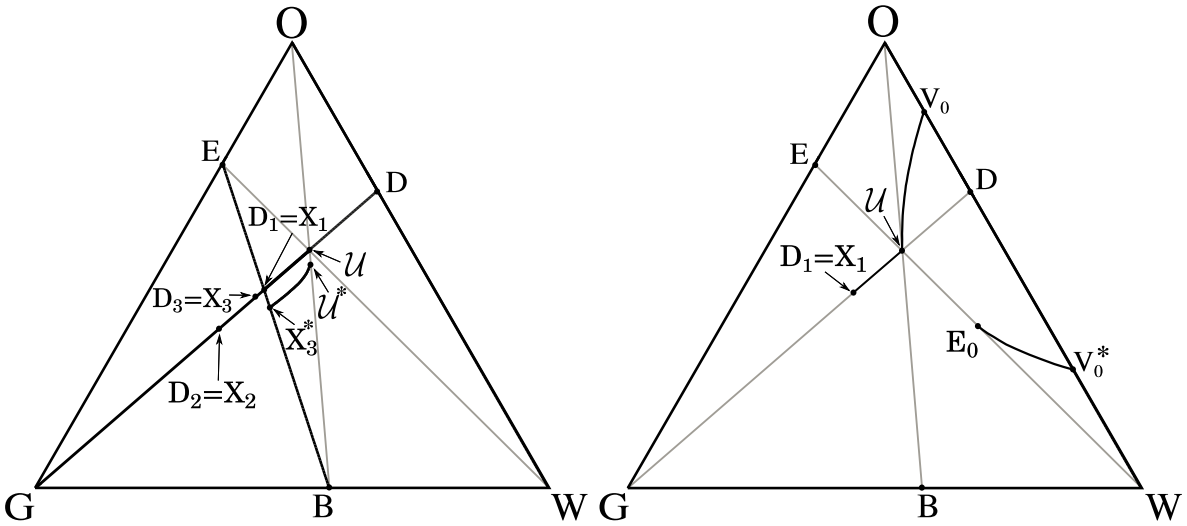

(a) Relevants states associated to Hugoniot curve for D.

(b) Boundaries for loss of compatibility of transitional and fast shocks inside $\mathcal{FR}_D$.

Figure 6.3: (a) States D_1, D_2, D_3 and X_3^* associated to $\mathcal{H}(D)$, they are invoked in Remarks 6.3.1-6.3.3 in order to illustrate the procedure used to build the compatibility and admissibility boundaries. They satisfy: $\sigma(D_1;D) = \lambda_s(D_1)$, $\sigma(D_2;D) = \lambda_f(D_2)$ and $\sigma(D_3;D) = \sigma(X_3;D) = \lambda_s(X_3^*)$. The curve $[X_3^*, \mathcal{U}^*]$ is the right s-extension of segment $[D_3, \mathcal{U}]$. (b) Boundaries of the lower and upper region $\mathscr{R}_1$ which is defined in Section 6.4.1.

Remark 6.3.1. Consider a state M along the invariant line $[G,D]$ (see Figure 6.3(a)). In the case $M = D$, the Hugoniot curve $\mathcal{H}(M)$ is formed by three straight lines: $[O,W]$, $[G,D]$ and $[E,B]$.

From Theorem 5.4.1, it is possible to compute the secondary bifurcation point of $\mathcal{H}(D)$ named X_1 (in this case $X_1 = D_1$) with $\sigma(X_1, D) = \lambda_s(X_1)$, using the reduced parameter s (see Chapter 5). The speed diagram in Figure 6.5 compares the local branches $[O, W]$ and $[G, D]$ of $\mathcal{H}(D)$. We see that there are two states V_0 and V_0^* along $[O, W]$ that satisfy $\sigma(X_1; D) = \sigma(V_0; D) = \sigma(V_0^*; D)$. Notice that for any state $S \in [O, V_0) \cup (V_0^*, W]$, we have $\sigma(S; D) < \sigma(X_1; D)$ and for $S \in [V_0, V_0^*]$ we have $\sigma(S; D) \geq \sigma(X_1; D)$.

Remark 6.3.2. Let us consider the local branch $[G, D]$ of $\mathcal{H}(D)$ (see Figure 6.3(a)). Using Theorem 5.4.1, we compute the state of $X_2 = D_2$ on the secondary bifurcation such that $\sigma(X_2, D) = \lambda_f(X_2)$ using the reduced parameter s (see Chapter 5). In Figure 6.5, the speed diagram compares the local branches $[O, W]$ and $[G, D]$ of $\mathcal{H}(D)$. We see that there are two states V_2 and V_2^* along $[O, W]$ that satisfy $\sigma(X_2; D) = \sigma(V_2; D) = \sigma(V_2^*; D)$. Notice that for any state $S \in [O, V_2) \cup (V_2^*, W]$ we have $\sigma(S; D) < \sigma(X_2; D)$, and for $S \in [V_2, V_2^*]$ we have $\sigma(S; D) \geq \sigma(X_2; D)$.

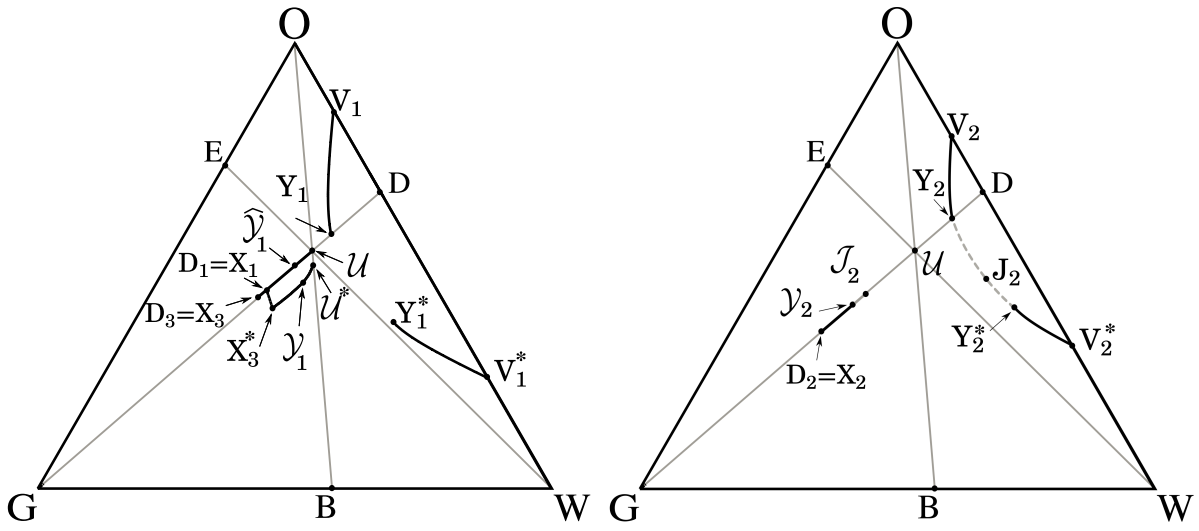

(a) Boundaries for loss of compatibility of sonic shocks. (b) Boundaries for loss of admissibility of nonlocal shocks.

Figure 6.4: (a) States D_1, D_2, D_3 and X_3^* associated to $\mathcal{H}(D)$. Curve $[X_3^*, \mathcal{Y}_1, \mathcal{U}^*]$ is the right s-extension of segment $[X_3, \widehat{\mathcal{Y}_1}, \mathcal{U}]$. The curve $[V_1, Y_1]$ and $[V_1^*, Y_1^*]$ are the double extension of segment $[X_3^*, \widehat{\mathcal{Y}_1}]$, see Remark 6.3.4. (b) The pairs states $(\mathcal{Y}_2, Y_2)$ and $(\mathcal{J}_2, J_2)$ belong to the fast double contact; Boundaries $[V_2, Y_2]$ and $[V_2^*, Y_2^*]$ are the right f-extension of the segment $[D_2, \mathcal{Y}_2]$. The curve (dashed) $[Y_2, Y_2^*]$ is the right f-extension of the segment $[\mathcal{Y}_2, \mathcal{J}_2]$.

Remark 6.3.3. Let us consider the nonlocal branch $[E, B]$ of $\mathcal{H}(D)$ (see Figure 6.3(a)). Since this branch is a straight line that connects E to B, it is possible to compute explicitly the state $X_3^* \in [E, B]$ that satisfies $\sigma(D; X_3^*) = \lambda_s(X_3^*)$. In Figure 6.5, the speed diagram compares the local and nonlocal branches of $\mathcal{H}(D)$, $[O, W]$ and $[E, B]$. We see that there are two states V_1 and V_1^* along $[O, W]$ that satisfy $\sigma(X_3^*; D) = \sigma(V_1; D) = \sigma(V_1^*; D)$. Moreover, there is a state $X_3 = D_3 \in [G, D]$ such that

$\sigma(X_3; D) = \sigma(X_3^*; D)$. Notice that, for any state $S \in (V_0, V_1] \cup (V_1^*, V_0^*]$, we have $\sigma(S; D) > \sigma(X_1; D)$ and $\sigma(S; D) < \sigma(X_3; D)$.

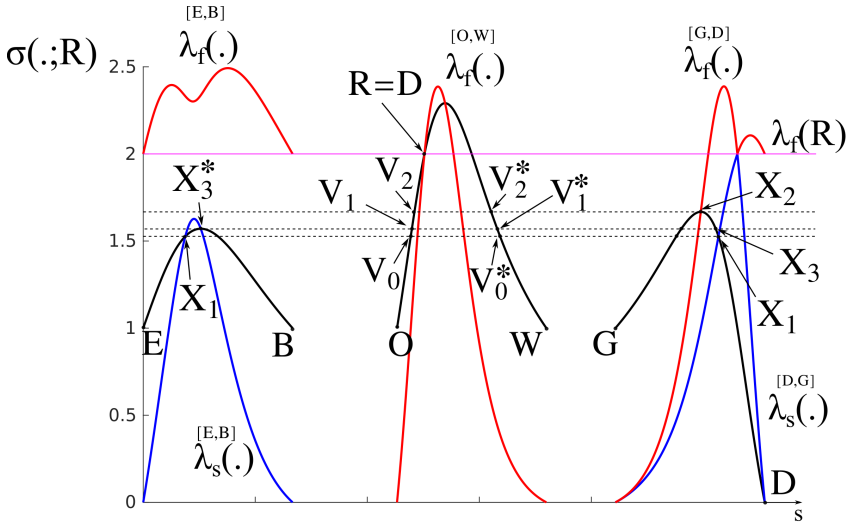

Figure 6.5: Schematic speed diagrams comparing speed along the three branches of $\mathcal{H}(D)$. Black curves are the shock speed $\sigma(M, R)$ with M varying along the Hugoniot branches $[E, B]$, $[O, W]$ and $[G, D]$. States on the same horizontal dashed line satisfy the triple shock rule. The blue curves (red curves) are the slow characteristic speed, λ_s (fast characteristic speed λ_f).

6.3.1 Boundary for loss of compatibility between transitional and fast shocks

Consider a state M_2 along $[\mathcal{U}, D]$ (or $[D_0, D]$, if $\nu_\Gamma < 1$ in the regime of Theorem 5.4.3. See Figure 6.34(a)). As seen in Section 5.4, there is a segment $(X_2, X_1) \subset [G, D]$ such that, for all $M_1 \in (X_2, X_1)$, we have a transitional shock between M_1 and M_2 with shock speed $\sigma_T = \sigma(M_1; M_2)$ satisfying $\sigma(X_2; M_2) > \sigma_T > \sigma(X_1; M_2)$. But in the context of Riemann problems, when a solution involves one of these transitional shocks they must satisfy the criterion of compatible speeds between the slow, transitional and fast wave groups which constitute the solution of the desired Riemann problem. As X_1 and X_2 depend on M_2 we also write $X_1(M_2)$ and $X_2(M_2)$.

Since the speed $\sigma_{X_1} = \sigma(X_1; M_2)$ for all M_2 along $[\mathcal{U}, D]$ (or $[D_0, D]$) is the smallest speed that a transitional shock can have between M_2 and $M_1 \in (X_2, X_1)$, we can use the triple shock rule 2.4.3, the speed σ_{X_1} and the fact that we know the explicit form of the $\mathcal{H}(M_2)$, to find the boundary with shock speeds equal to σ_T, which separates regions that admit transitional shocks from those that do not.

We proceed by constructing the *boundary for loss of compatibility between transitional and fast shocks*. First, consider Remark 6.3.1 where we found the states V_0 and V_0^* associated to D and $X_1 = D_1$ such that $\lambda_s(X_1) = \sigma(X_1; D) = \sigma(V_0; D) = \sigma(V_0^*; D)$. Since $\mathcal{H}(M_2)$, $X_1(M_2)$ and $\sigma(X_1(M_2); M_2)$

are known explicitly for M_2 varying on the segment $(D,\mathcal{U})$, and using that such a variation is continuous, we can build the upper and lower boundaries of all states $V_0(M_2)$ and $V_0^*(M_2)$ such that $\sigma(X_1(M_2);M_2) = \sigma(V_0(M_2);M_2) = \sigma(V_0^*(M_2);M_2)$ (see Figures 6.6(b) and 6.9(a)). Notice that when M_2 approaches $\mathcal{U}$, $X_1(M_2)$ and $V_0(M_2)$ approach $\mathcal{U}$ and $V_0^*(M_2)$ approaches E_0 (see Remark 5.2.3). Therefore, we have two (upper and lower) boundaries for loss of compatibility between transitional and fast shocks inside $\mathcal{FR}_D$, given by the curves $[V_0,\mathcal{U}]$ and $[V_0^*, E_0]$; see Figure 6.3(b).

6.3.2 Boundary for loss of admissibility of nonlocal shocks

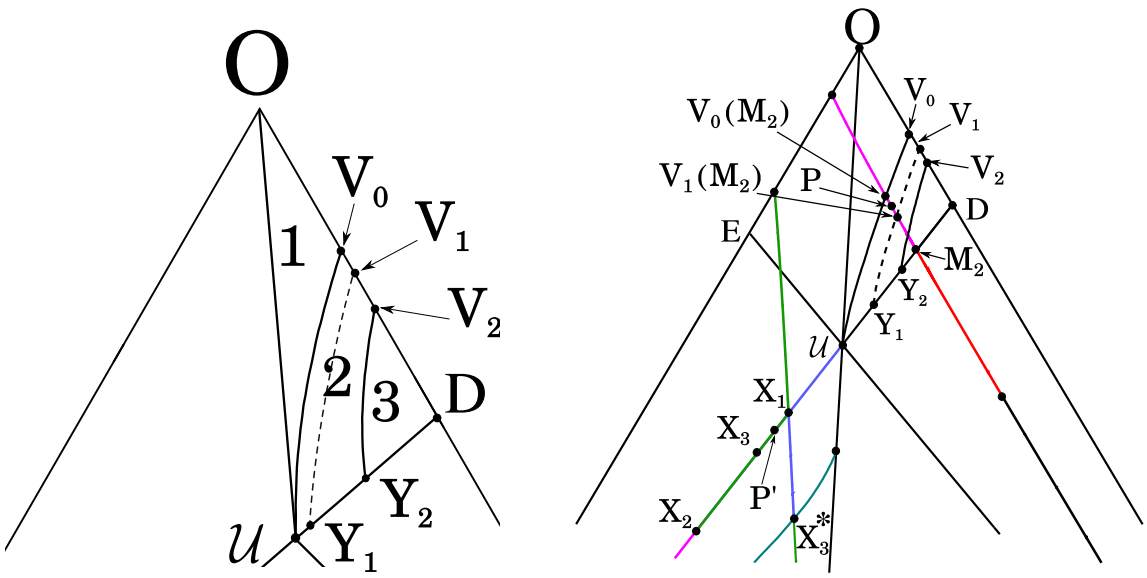

(a) Upper regions $\mathscr{R}_i$, $i \in \{1,2,3\}$ for fast macro region $\mathcal{FR}_D$.

(b) Hugoniot curve for M_2 in $[\mathcal{U}, D]$.

Figure 6.6: Construction of regions $\mathscr{R}_i$ for $i \in \{1,2,3\}$. (a) Dashed line represents the boundary for loss of compatibility of sonic shocks. (b) Hugoniot curve for $M_2 \in [Y_2, D]$ with states $V_0(M_2) \in [V_0,\mathcal{U}]$, $P \in \mathcal{H}(M_2)$ and $V_1(M_2) \in [V_1, Y_1]$. The transitional shocks that reach M_2 from the transitional segment $[P', X_1(M_2)] \subset [G,\mathcal{U}]$ are compatible with the state P, where $\sigma(P';M_2) = \sigma(P;M_2) > \sigma(Q;M_2)$, for any $Q \in [P', X_1(M_2)]$.

From Claim 2.7.2, if a discontinuity between two states is admissible, then these states are on the same side with respect to a suitable invariant line. Using this "geometric" requirement for the characterization of admissible shocks, we can identify when discontinuities in nonlocal branches of a Hugoniot curve need to be used in the construction of Riemann solutions. Let R be a right state in region $\mathcal{FR}_D$ (with $R \notin [\mathcal{U}, D]$) such that there is a state X_2 in a nonlocal branch of $\mathcal{H}(R)$ tangent to $[G,\mathcal{U}]$ and such that the intersection state M_2 between $\mathcal{H}(R)$ and $[\mathcal{U}, D]$ belongs to segment $[Y_2, D]$. From Lemma 2.4.2 and from the triple shock rule 2.4.3, X_2 and M_2 satisfy $\sigma(R;M_2) = \sigma(R;X_2) = \lambda_f(X_2)$. Then, using $\mathcal{H}(M_2)$ instead of $\mathcal{H}(R)$, we can find the states R and X_2 associated to $M_2 \in [Y_2, D]$ such that $\sigma(R;M_2) = \sigma(R;X_2) = \lambda_f(X_2)$ and that the nonlocal branch of $\mathcal{H}(R)$ is tangent to $[G,\mathcal{U}]$ at X_2.

We proceed by constructing a *boundary for loss of admissibility of nonlocal shocks*. First, consider Remark 6.3.2 where we found the states V_2 and V_2^* associated to D and $X_2 = D_2$ such that $\lambda_f(X_2) = \sigma(X_2; D) = \sigma(V_2; D) = \sigma(V_2^*; D)$. Since $\mathcal{H}(M_2)$, $X_2(M_2)$ and $\sigma(X_2(M_2); M_2)$ are known explicitly for M_2 varying on the segment (D, Y_2) and that such a variation is continuous, we can build the upper and lower boundaries of all states $V_2(M_2)$ and $V_2^*(M_2)$ such that $\sigma(X_2(M_2); M_2) = \sigma(V_2(M_2); M_2) = \sigma(V_2^*(M_2); M_2)$ (see Figure 6.4(b)). Notice that, when M_2 approaches Y_2, X_2 approaches $\mathcal{Y}_2$ and the pair M_2, $V_2(M_2)$ contracts to a point $Y_2 = M_2 = V_2(M_2)$ so that the shock between Y_2 and $V_2(M_2)$ has zero strength and the shock speed $\sigma(M_2; V_2(M_2))$ tends to $\lambda_f(Y_2)$. Therefore, when $M_2 = Y_2$ and $X_2 = \mathcal{Y}_2$, the discontinuity joining X_2 to M_2 is a double contact discontinuity. On the other hand, when M_2 approaches Y_2, $V_2^*(M_2)$ approaches Y_2^* with $\sigma(Y_2^*; Y_2)$ approaching $\lambda_f(Y_2)$. Therefore, we have two (upper and lower) boundaries for loss of admissibility of nonlocal shocks inside of $\mathcal{FR}_D$, given by the curves $[V_2, Y_2]$ and $[V_2^*, Y_2^*]$; see Figure 6.4(b).

6.3.3 Boundary for loss of compatibility of sonic shocks

As seen in Section 4.5, when the umbilic point is of type II, the slow inflection does not coincide with the secondary bifurcation. Recall that if we want to use transitional shocks in Riemann solutions we first need to reach a secondary bifurcation line with a forward slow wave curve. Because of this, there is always a region of the saturation triangle from which the appropriate invariant line can only be reached by a slow sonic shock. This observation hints at the existence of a boundary in the saturation triangle which defines a region of right states R for which such slow sonic shocks do not arise in Riemann solutions with transitional waves. The construction of this boundary is based on computation of states $X_3(M_2)$ for M_2 varying along $[\mathcal{U}, D]$.

The procedure is similar to the one used to construct the boundary for loss of admissibility of nonlocal shocks: first, consider Remark 6.3.3 where we found the states V_1 and V_1^* associated to D and $X_3 = D_3$ (actually X_3^*) such that $\lambda_s(X_3^*) = \sigma(X_3^*; D) = \sigma(X_3; D) = \sigma(V_1; D) = \sigma(V_1^*; D)$, see Figure 6.4(a). We build the *boundary for loss of compatibility of sonic shocks* by varying M_2 along $(Y_1, D]$ to obtain all states $V_1(M_2)$ and $V_1^*(M_2)$ such that $\sigma(X_3(M_2); M_2) = \sigma(V_1(M_2); M_2) = \sigma(V_1^*(M_2); M_2)$ (see Figure 6.4(a)). Notice that when M_2 approaches Y_1, X_3 approaches $\widehat{\mathcal{Y}_1}$ and X_3^* approaches $\mathcal{Y}_1$, and that the pair $(M_2, V_1(M_2))$ contracts to a point $Y_1 = M_2 = V_1(M_2)$, so that the shock between Y_1 and $V_1(M_2)$ has zero strength and the shock speed $\sigma(M_2; V_1(M_2))$ tends to $\lambda_f(M_2)$. Then, when $M_2 = Y_1$ and $X_3^* = \mathcal{Y}_1$, the discontinuity joining X_3^* to M_2 is a mixed double contact discontinuity. On the other hand, when M_2 approaches Y_1, $V_1^*(M_2)$ approaches Y_1^* with $\sigma(Y_1^*; Y_1)$ approaching $\lambda_f(Y_1)$. Therefore, we have two (upper and lower) boundaries for loss of compatibility of sonic shocks inside of $\mathcal{FR}_D$, given by the curves $[V_1, Y_1]$ and $[V_1^*, Y_1^*]$; see Figure 6.4(a).

Remark 6.3.4. Notice that in the construction of boundaries of Sections 6.3.1- 6.3.3, given M on a curve in the saturation triangle, we find all discontinuities that have speed equal to one of the characteristic speeds at M. Then, using Definition 2.4.6 we can compute the compatibility and admissibility boundaries as extensions or the double extension of suitable segments of the invariant line $[G, D]$.

- Consider the segment $[D_1, \mathcal{U}]$. The boundary for loss of compatibility between transitional and fast shocks ($[V_0, \mathcal{U}]$ and $[V_0^*, E_0]$ given in Figure 6.3(b)) is calculated as the s-left-extension of

segment $[D_1, \mathcal{U}]$, *i.e.*, $E_s^-([D_1, \mathcal{U}])$.

- Consider the segment $[D_2, \mathcal{Y}_2]$. A boundary for loss of admissibility of nonlocal shocks ($[V_2, Y_2]$ and $[V_2^*, Y_2^*]$ given in Figure 6.4(b)) is calculated as the f-left-extension of segment $[D_2, \mathcal{Y}_2]$, *i.e.*, $E_f^-([D_2, \mathcal{Y}_2])$. If we consider the segment $[\mathcal{Y}_2, \mathcal{J}_2]$ with $\mathcal{J}_2$ corresponding to J_2 being an intersection of the fast double contact with $[G, \mathcal{U}]$, then $[Y_2, Y_2'] = E_f^-([\mathcal{Y}_2, \mathcal{J}_2])$ is part of the boundary for loss of admissibility of nonlocal shocks joining the upper and lower boundaries constructed in Section 6.3.2 (see Figure 6.4(b)).

- Consider the segment $[X_3, \widehat{\mathcal{Y}_1}]$. The boundary for loss of compatibility of sonic shocks ($[V_1, Y_1]$ and $[V_1^*, Y_1^*]$ given in Figure 6.4(a)) is a *double extension curve* of the segment $[X_3, \widehat{\mathcal{Y}_1}]$ in the following sense: first, we compute the segment $[X_3^*, \mathcal{Y}_1] = E_s^+([X_3, \widehat{\mathcal{Y}_1}])$ and then, we compute its s-left-extension (see Figure 6.4).

6.4 Subdivision of $\mathcal{FR}_i$ for $i \in \{D, E, B\}$ in backward $\mathscr{R}$ -regions: umbilic point type II

In this section, we study the subdivision of the macro region $\mathcal{FR}_i$ for $i \in \{D, E, B\}$ into backward $\mathscr{R}$-regions when the umbilic point is of type II. Recall that this subdivision is given by regions where the structure of $\mathcal{W}_f^-$ is the same. The methodology for the construction of the $\mathscr{R}$-regions is as follows: first, we find the bifurcation manifolds studied in Chapter 4 and the boundaries for compatibility and admissibility loss studied in Section 6.3. We also consider the extensions of segments of the invariant line associated the macro region $\mathcal{FR}_i$ for $i \in \{D, E, B\}$. Then, we build the backward fast wave curves in $\mathcal{FR}_i$ using the succession algorithm described in Section 2.7, studying the behavior of each wave group with respect to the bifurcation manifolds and the compatibility boundaries, and verifying numerically if each Lax f-shock (or characteristic shock) has viscous profile.

In order to study the admissibility of these discontinuities, we analyze the behavior of the Hugoniot curve and use speed diagrams to classify shocks and to identify the equilibria associated to the same speed. Whenever possible, we use the explicit formula for the Hugoniot locus to characterize the behavior of discontinuities in some regions.

Without loss of generality, we restrict this presentation to the fast macro region $\mathcal{FR}_D$. We first study the case with umbilic point $\mathcal{U} \in II_O$, where $\nu_W > 1$, $\nu_O < 1$ and $1 < \nu_G \leq 8$, and then the case with umbilic point $\mathcal{U} \in II_G$ where $\nu_W > 1$, $\nu_O > 1$ and $\nu_G < 1$. The other cases can be derived from these two, considering the behavior of some special points that were studied in Section 5.3.

6.4.1 Subregions $\mathscr{R}_1$, $\mathscr{R}_2$ and $\mathscr{R}_3$

Regions $\mathscr{R}_1, \mathscr{R}_2$ and $\mathscr{R}_3$ were studied in [4, 3] for the construction of Riemann solutions in our regime ($\mathcal{U}$ of type II_O) for left states along $[G, W]$ and right states in the quadrilateral of sides $[E, \mathcal{U}]$, $[\mathcal{U}, D]$, $[D, O]$ and $[O, E]$. In [4, 3], Andrade *et al.* defined $\mathscr{R}_1$ as a region close to the vertex O such that, for all right states $R \in \mathscr{R}_1$, the solutions of Riemann problems for L restricted to $[G, W]$ do not use transitional

shocks. Unlike $\mathscr{R}_1$, regions $\mathscr{R}_2$ and $\mathscr{R}_3$ can use transitional shocks to solve Riemann problems for certain left states L and they are characterized as follows:

i) If R belongs to region $\mathscr{R}_2$, the transitional wave is always a single shock.

ii) If R belongs to region $\mathscr{R}_3$, the transitional wave is either a single shock or a composite transitional wave, depending on state L.

We adopt the same characterization of the regions $\mathscr{R}_1$, $\mathscr{R}_2$ and $\mathscr{R}_3$ as in [4, 3], but we do not restrict the left state L to $[G, W]$. This leads to different definitions for the boundaries that separate regions $\mathscr{R}_1$ and $\mathscr{R}_2$. For the bottom boundary of $\mathscr{R}_1$, we consider the curve $[V_0, \mathcal{U}]$ (see Figure 6.6(a)) defined in Section 6.3.1 while in [3] that boundary is the curve $[V_1, Y_1]$.

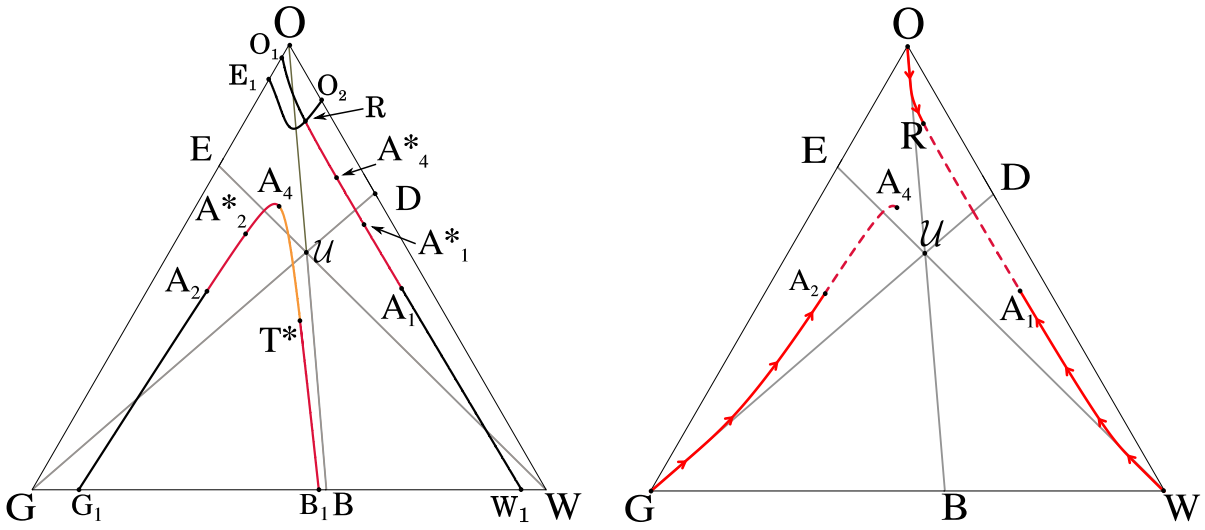

(a) Typical Hugoniot curve for a state R in $\mathscr{R}_1$.

(b) $\mathcal{W}_f^-(R)$, for $R \in \mathscr{R}_1$.

Figure 6.7: Hugoniot curve and backward f-wave curve for a state $R \in \mathscr{R}_1$. (a) The states A_1^*, A_2^*, T^*, A_4 and A_4^* satisfy $\sigma(R; A_1^*) = \sigma(R; T^*) = \sigma(R; A_2^*)$ and $\sigma(R; A_4) = \sigma(R; A_4^*)$. (b) Continuous lines are f-rarefaction segments and dashed lines are Lax f-shock segments.

Consider a Hugoniot curve from a state $M_2 \in [\mathcal{U}, D]$ (see Figure 6.6(b)). We compute the states $X_1(M_2), X_2(M_2)$ and $X_3(M_2)$ on $[G, D]$ associated to M_2 (see Theorem 5.4.1). We also take states $V_0(M_2)$ and $V_1(M_2)$ in boundaries $[V_0, \mathcal{U}]$ and $[V_1, Y_1]$, respectively (see Remarks 6.3.1 and 6.3.3). Let P be a state in $\mathcal{H}(M_2)$ between $V_0(M_2)$ and $V_1(M_2)$ such that $\sigma(P; M_2) = \sigma(P'; M_2)$ with $P' \in (X_3(M_2), X_1(M_2)) \subset \mathcal{H}(M_2)$. Since

$$\sigma(X_2(M_2); M_2) > \sigma(X_3(M_2); M_2) > \sigma(X_1(M_2); M_2),$$

we have $\sigma(X_3(M_2); M_2) > \sigma(P'; M_2) > \sigma(X_1(M_2); M_2)$. Then, for any M_1 in the transitional segment $[P', X_1)$, the transitional shock joining M_1 and M_2 satisfies $\sigma(X_1(M_2); M_2) < \sigma_T(M_1; M_2) \leq$

$\sigma(P'; M_2)$. Moreover, the transitional segment $[P', X_1)$ can be reached using a slow forward wave curve (see Chapter 7). Therefore, the region of $\mathcal{FR}_D$ between the curves $[V_0, \mathcal{U}]$ and $[V_1, Y_1]$ belongs to the region $\mathscr{R}_2$ (see Figure 6.6(b)).

Now, we describe the Hugoniot curves and the backward f-wave curves for regions $\mathscr{R}_1$, $\mathscr{R}_2$ and $\mathscr{R}_3$. The propositions stated bellow are verified in [4, 3].

Claim 6.4.1. *Let R be a state in region $\mathscr{R}_1$. The Hugoniot curve of R possesses segments $[A_2, A_4]$, $[A_4, T^*]$, $[T^*, B_1]$ and $[A_1, R]$ (see Figure 6.7(a)) with the following properties :*

(i) For M in either (A_2, A_4), (B_1, T^*) or (A_1, R), the discontinuity from M to R is a Lax f-shock; for M in (T^*, A_4) it is an over-compressive shock.

(ii) The states A_1, A_2, A_4 and T^* are Bethe-Wendroff points. They satisfy $\sigma(A_j; R) = \lambda_f(A_j)$, for $j = 1, 2$; $\sigma(A_4; R) = \lambda_s(A_4)$; and $\sigma(T^*; R) = \lambda_s(T^*)$.

(iii) For M in either $[A_2, A_4]$, $[A_4, T^*]$ or $[A_1, R)$, the discontinuity from M to R satisfies the viscous profile admissibility criterion; for M in $(T^*, B_1]$ it does not.

(iv) The states $A_1^* \in [R, A_1]$ and $A_2^* \in [A_2, A_4]$ satisfy the triple shock rule 2.4.3, with $\sigma(T^*; A_j^*) = \sigma(A_j^*; R) = \sigma(A_j^*; A_k^*) = \sigma(T^*; R)$, $j \neq k$ assuming values 1 or 2; the state $A_4^* \in [R, A_1]$ satisfies the triple shock rule 2.4.3 with $\sigma(A_4; R) = \sigma(A_4^*; R) = \sigma(A_4; A_4^*)$.

Claim 6.4.2. *The fast backward wave curve for a state $R \in \mathscr{R}_1$ has a local branch with the following wave structure:*

(i) Lax f-shock segment $(R, A_1]$ with $\sigma(R; A_1) = \lambda_f(A_1)$;

(ii) backward f-rarefaction segment $[R, O]$;

(iii) backward f-rarefaction segment $(A_1, W]$.

It also has a nonlocal branch with the following wave structure:

(iv) Lax f-shock segment $[A_4, A_2]$ with $\sigma(R; A_2) = \lambda_f(A_2)$;

(v) backward f-rarefaction segment $(A_2, G]$.

Remark 6.4.1. In [3], the construction of $\mathcal{W}_f^-(R)$ for $R \in \mathscr{R}_1$ was proved only for those parts of $\mathcal{W}_f^-(R)$ that must be reached by an s-wave curve leaving from $L \in [G, W]$. For example, they did not take into account the segments of admissible Lax f-shocks $(R, A_1^*]$ and $[A_2^*, A_4]$ and the backward f-rarefaction $[R, O]$ (here, they were considered in Claim 6.4.1 and Figure 6.7). The proof for these segments follows by straightforward adaptation of the procedure in [3].

Remark 6.4.2. Recall that in Section 6.3.1 we constructed two boundaries $[V_0, \mathcal{U}]$ and $[V_0^*, E_0]$ which separate regions of the same type inside $\mathcal{FR}_D$. Now, we define the lower $\mathscr{R}_1$ region as the region bounded by $[W, E_0]$, $[W, V_0^*]$ and $[V_0^*, E_0]$ for which all right states R belonging to this region satisfy Claims 6.4.1 and 6.4.2 (see Figure 6.9(a)).

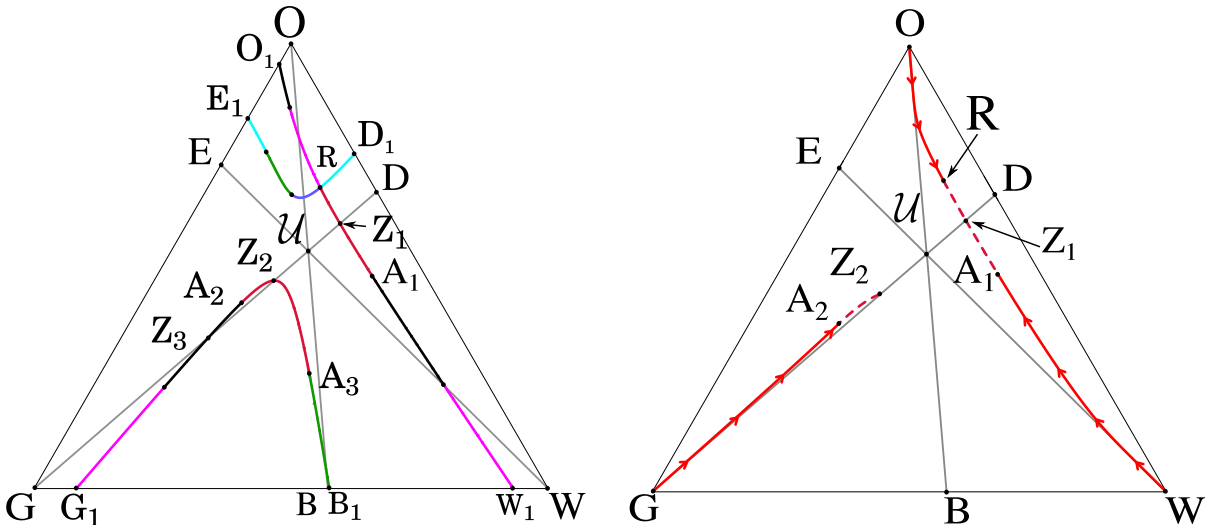

(a) Typical Hugoniot curve for a state R in upper region $\mathscr{R}_2$.

(b) $\mathcal{W}_f^-(R)$, for $R \in \mathscr{R}_2$.

Figure 6.8: Hugoniot curve and backward f-wave curve for a state $R \in \mathscr{R}_2$. (a) The states Z_1, Z_2 and Z_3 satisfy $\sigma(R; Z_1) = \sigma(R; Z_2) = \sigma(R; Z_3)$. (b) Continuous lines are f-rarefaction segments and dashed lines are Lax f-shock segments. For any $R \in \mathscr{R}_2$ the nonlocal branch of $\mathcal{W}_f^-(R)$ begins at state Z_2 on $[G, D]$.

Following the conclusions given at the beginning of this section, the region $\mathscr{R}_2$ has as top boundary the curve $[V_0, \mathcal{U}]$ and as bottom boundary the curve $[V_2, Y_2]$. Although the curve $[V_1, Y_1]$ (see Section 6.3.3) passes through this $\mathscr{R}$-region, the wave curve $\mathcal{W}_f^-(R)$ does not change its structure as the right state R crosses this boundary.

Claim 6.4.3. *Let R be a state in region $\mathscr{R}_2$. In addition to states Z_1, Z_2 and Z_3 on $[G, D]$, the Hugoniot curve $\mathcal{H}(R)$ possesses states A_1, A_2 and A_3 with the following properties:*

(i) States A_1, A_2 and A_3 are Bethe-Wendroff points. They satisfy $\sigma(A_1; R) = \lambda_f(A_1)$, $\sigma(A_2; R) = \lambda_f(A_2)$ and $\sigma(A_3; R) = \lambda_f(R)$.

(ii) If M is a state on one of the branches $[O_1, W_1]$ or $[G_1, B_1]$ of $\mathcal{H}(R)$, the discontinuity joining M to R is a Lax f-shock if M is in (A_1, R) or in (A_2, A_3).

(iii) Moreover, this discontinuity is admissible if M is in $[A_1, R)$ or in $[A_2, Z_2)$; it is inadmissible if M belongs to $[A_3, Z_2)$.

Claim 6.4.4. *The fast backward wave curve for a state $R \in \mathscr{R}_2$ has a local branch with the following wave structure:*

(i) Lax f-shock segment $(R, A_1]$ with $\sigma(R; A_1) = \lambda_f(A_1)$;

(ii) backward f-rarefaction segment $[R, O]$;

(iii) backward f-rarefaction segment $(A_1, W]$.

It also has a nonlocal branch with the following wave structure:

(iv) Lax f-shock segment $(Z_2, A_2]$ with $\sigma(R; A_2) = \lambda_f(A_2)$ and $Z_2 \in [G, \mathcal{U}]$;

(v) backward f-rarefaction segment $(A_2, G]$;

Now we describe the lower $\mathscr{R}_2$ region:

Remark 6.4.3. In Section 6.3.3 we constructed two curves $[V_1, Y_1]$ and $[V_1^*, Y_1^*]$ which separate the same type of region inside of $\mathcal{FR}_D$. Just as for the upper region $\mathscr{R}_2$, the lower region $\mathscr{R}_2$ is not affected by the boundary $[V_1^*, Y_1^*]$ since we do not restrict the left states L to $[G, W]$; actually, it is the s-left-extension of the s-inflection (or slow hysteresis) which causes a bifurcation in the lower $\mathscr{R}_2$ region. More precisely, when R crosses the s-hysteresis, the nonlocal Lax f-shocks segment $[Z_2, A_2]$ (Claim 6.4.4(iv)) splits into two segments of Lax f-shocks separated by a segment of over-compressive shock. But, we do not regard this bifurcation as defining two distinct regions because the type of wave and the location do not change. However, when we build the $\mathscr{L}$-regions associated to the lower region $\mathscr{R}_2$, this bifurcation subdivides the lower $\mathscr{R}_2$ region into two distinct $\mathscr{L}$-regions.

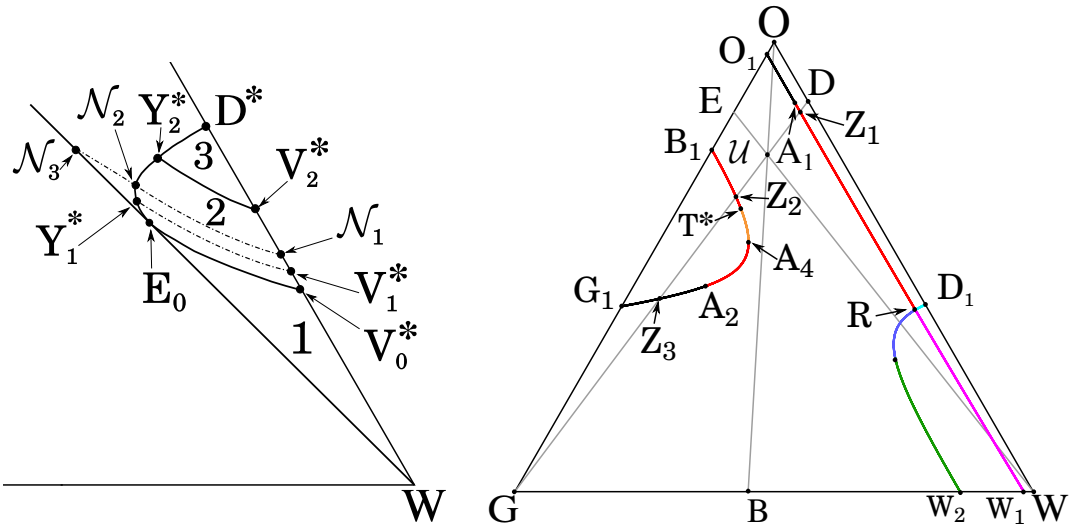

(a) Lower regions $\mathscr{R}_i$, $i \in \{1, 2, 3\}$ for fast macro region $\mathcal{FR}_D$.

(b) Hugoniot curve for R in lower region $\mathscr{R}_2$.

Figure 6.9: (a) Boundaries that define the lower regions $\mathscr{R}_i$, $i \in \{1, 2, 3\}$. Curve $[V_1^*, Y_1^*]$ is the boundary for loss of compatibility of sonic shocks (see Remark 6.3.3) and $[\mathcal{N}_1, \mathcal{N}_2, \mathcal{N}_3]$ is the left s-hysteresis, see Definition 2.4.2. (b) Hugoniot curve for R inside of area bounded by the curves $[E_0, \mathcal{N}_2]$, $[\mathcal{N}_2, \mathcal{N}_1]$, $[\mathcal{N}_1, V_0^*]$ and $[V_0^*, E_0]$; we call this area $\mathscr{R}_2^H \subset \mathscr{R}_2$. The over-compressive admissible shock segment $[T^*, A_4]$ separates two admissible segments of Lax f-shocks, $[Z_2, T^*)$ and $(A_4, A_2]$.

Consider a right state R in the lower region $\mathscr{R}_1$, close to $V_0^* \in [W,O]$, see Figure 6.9(a). From Claim 6.4.1 (i) and (iii), the segment of over-compressive shocks (A_4,T^*) belonging to $\mathcal{H}(R)$ intersects the invariant line $[G,D]$ with T^* in the opposite side as R and A_4 in the same side as R; the segment $(T^*,B_1]$ is not admissible from Claim 2.7.2. When R moves toward to vertex O and crosses the boundary $[V_0^*,E_0]$, T^* crosses $[G,D]$ toward the edge $[G,W]$, such that the segment $[B_1,T^*)$ of Lax f-shocks intersects $[G,D]$ in Z_2, see Figure 6.9(b). Therefore, in the nonlocal branch of $\mathcal{H}(R)$ we have two segments of Lax f-shocks, $[A_2,A_4]$ and $[T^*,Z_2)$, separated by the segment of over-compressive shocks (A_4,T^*) (with every segment of interest in the same side as R), and the segment of Lax f-shocks $[Z_2,B_1]$ in the side opposite to R with respect to $[G,D]$ (see Figure 6.9(b)).

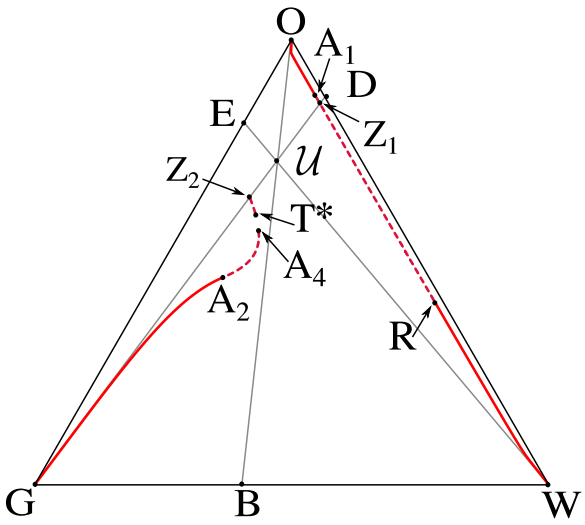

Figure 6.10: Backward f-wave curve for R in $\mathscr{R}_2^H \subset \mathscr{R}_2$. The nonlocal branch of $\mathcal{W}_f^-(R)$ contains two segments of Lax f-shocks, $[Z_2,T^*]$ and $[A_2,A_4]$.

If R continues to move towards vertex O, the size of the over-compressive segment $[T^*,A_4]$ decreases until T^* and A_4 collapse when R reaches the s-hysteresis $[\mathcal{N}_1,\mathcal{N}_3]$, where $\mathcal{N}_1 \in [O,W]$ and $\mathcal{N}_3 \in [W,\mathcal{U}]$, see Figure 6.9(a) . Notice that if R crosses over the curve $[V_2^*,Y_2^*]$ into $\mathscr{R}_3$, the nonlocal branch $[G_1,B_1]$ of $\mathcal{H}(R)$ crosses $[G,D]$, leaving the triangle $\widehat{GWD}$, and causing any nonlocal shock to be inadmissible. On the other hand, there is another boundary for the lower $\mathscr{R}_2$ region (given by curve $[E_0,Y_2^*]$), whose description will be completed when we discuss regions $\mathscr{R}_{4'}$-$\mathscr{R}_{6'}$ in Section 6.4.3; see Figure 6.9(a).

Claim 6.4.5. *If R is in the region limited by $[V_2^*,Y_2^*]$, $[Y_2^*,\mathcal{N}_2]$ and $[\mathcal{N}_1,\mathcal{N}_2]$ in Figure 6.9(a), the backward f-wave curve $\mathcal{W}_f^-(R)$ satisfies Claim 6.4.4. If R is in the region limited by $[V_0^*,E_0]$, $[E_0,\mathcal{N}_2]$ and $[\mathcal{N}_1,\mathcal{N}_2]$ (which we call $\mathscr{R}_2^H$), the local branch of $\mathcal{W}_f^-(R)$ also satisfies Claim 6.4.4, but it is formed by a nonlocal branch that has the following wave groups (refer to Figure 6.10):*

(i) two Lax f-shock segments $(Z_2,T^*]$ and $[A_4,A_2]$, with $\sigma(R;A_2)=\lambda_f(A_2)$ and $Z_2 \in [G,\mathcal{U}]$;

(ii) backward f-rarefaction segment $(A_2, G]$.

Moreover, $\mathcal{H}(R)$ possesses an admissible over-compressive shock segment $[T^*, A^4]$.

Finally, we describe the regions $\mathscr{R}_3$. The upper region $\mathscr{R}_3$ has $[V_2, Y_2]$ as its top boundary, $[V_2, D]$ as its right boundary and the segment $[Y_2, D]$ as its bottom boundary (see Figure 6.6(a)). As seen in the construction of the lower region $\mathscr{R}_2$, when state R crosses the boundary $[V_2^*, Y_2^*]$, the nonlocal branch of $\mathcal{H}(R)$ crosses the invariant line $[G, D]$, making this curve be the bottom boundary of lower region $\mathscr{R}_3$ (see Figure 6.9(a)). The top boundary for lower region $\mathscr{R}_3$ is directly related to right-characteristic f-shocks leaving the secondary bifurcation $[G, D]$. This boundary is given by the curve $[Y_2^*, D^*]$ which separates the lower regions $\mathscr{R}_3$ and $\mathscr{R}_{4'}$ and whose description will be completed when we discuss regions $\mathscr{R}_{4'}$-$\mathscr{R}_{6'}$ in Section 6.4.3; see Figure 6.9(a).

Claim 6.4.6. *Let R be a state in region $\mathscr{R}_3$. The Hugoniot curve for R has only one segment $[R, A_1]$ such that, for all $M \in [R, A_1]$, the discontinuity from M to R is a Lax f-shock and A_1 is a Bethe-Wendroff point that satisfies $\sigma(A_1; R) = \lambda_f(A_1)$. Moreover, this discontinuity is admissible (i.e., has viscous profile). Refer to Figure 6.11(a).*

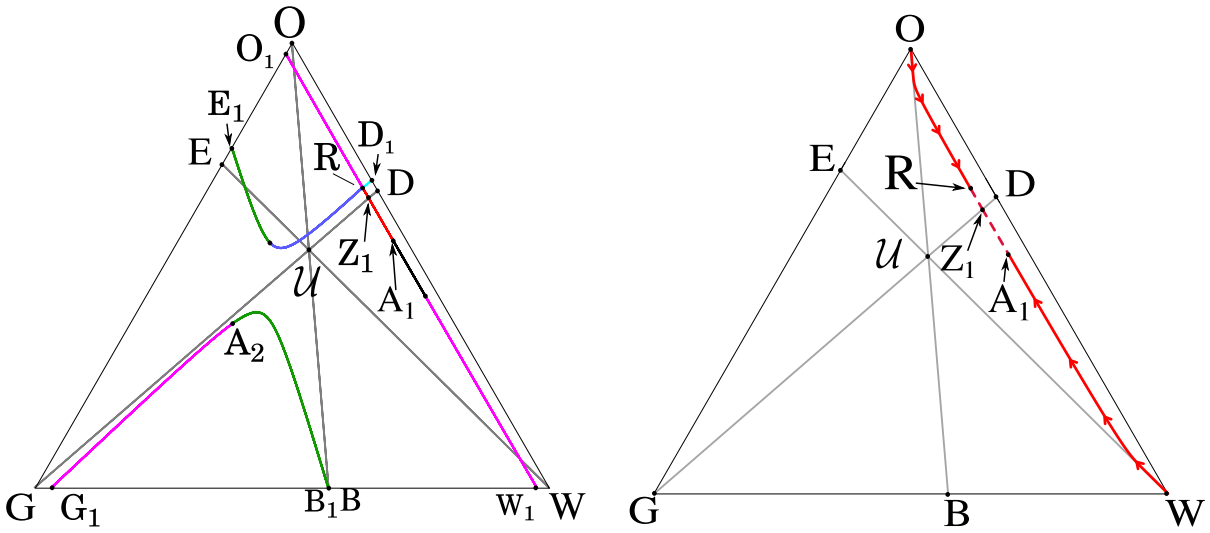

(a) Typical Hugoniot curve for $R \in \mathscr{R}_3$.

(b) $\mathcal{W}_f^-(R)$, for R in upper region $\mathscr{R}_3$.

Figure 6.11: Hugoniot curve and wave curve for a state $R \in \mathscr{R}_3$. Notice that $\mathcal{W}_f^-(R)$ does not have a nonlocal branch.

Claim 6.4.7. *The backward fast-family wave curve of a state $R \in \mathscr{R}_3$ consists of states along the segment $(R, A_1]$ of admissible fast shocks in the Hugoniot curve $\mathcal{H}(R)$, joined by states along the fast rarefaction segments $[O, R]$ and $[W, A_1)$. Refer to Figure 6.11(b).*

Remark 6.4.4. As seen for $R \in \mathscr{R}_1$ (Remark 6.4.1), the construction in [4] of $\mathcal{W}_f^-(R)$ for $R \in \mathscr{R}_2$ or $R \in \mathscr{R}_3$ only considered those parts of $\mathcal{W}_f^-(R)$ that can be reached by s-wave curves leaving from $L \in [G, W]$. The complete proof follows by straightforward adaptation of the procedure given by Andrade *et al.* in [4].

6.4.2 Subregions $\mathscr{R}_4$, $\mathscr{R}_5$ and $\mathscr{R}_6$

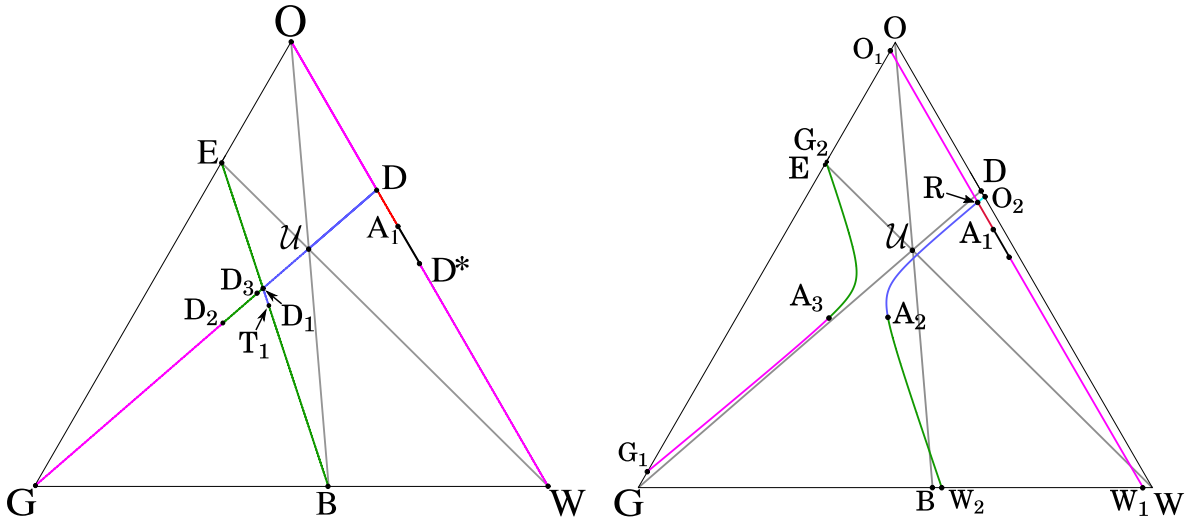

(a) Hugoniot curve for $R = D$.

(b) Typical Hugoniot curve for $R \in \mathscr{R}_4$.

Figure 6.12: Hugoniot curve for states $R = D$ and $R \in \mathscr{R}_4$. (a) Primary branches coincide with the edge $[W, O]$ and the invariant line $[G, D]$. The nonlocal branch is a straight line segment $[E, B]$.

The construction of Riemann solutions for states $R \approx D$ within region $\mathscr{R}_3$ was described in [4] and was summarized in Section 6.4.1. Here, we move the state R across the invariant line $[G, D]$ while staying close to state D inside the saturation triangle. A typical Hugoniot curve for a state R in this region is shown in Figure 6.12(b). It can be considered as a perturbation of the Hugoniot curve for D that was obtained explicitly in [9] (see Figure 6.12(a)). The Hugoniot curve for R possesses two primary branches, $[O_1, W_1]$ and $[O_2, W_2]$ (which intersect at R), and a nonlocal branch $[G_1, G_2]$. Notice that this nonlocal branch lies inside triangle $\widehat{GDO}$, therefore it is inadmissible by Claim 2.7.2.

Claim 6.4.8. *Let $R \approx D$ lie below the secondary bifurcation $[G, D]$. The Hugoniot curve for R has only one segment $[R, A_1]$ such that, for all $M \in [R, A_1]$, the discontinuity from M to R is a Lax f-shock and A_1 is a Bethe-Wendroff point that satisfies $\sigma(A_1; R) = \lambda_f(A_1)$. Moreover, this discontinuity is admissible (i.e., has viscous profile).*

Proof. To justify this claim we refer to Figures 6.12 and 6.13. We compare the characteristic speeds $\lambda_s(R)$, $\lambda_f(R)$, $\lambda_s(M)$ and $\lambda_f(M)$ with the shock speed $\sigma(M, R)$ as M varies along the branches $[O_1, W_1]$, $[O_2, W_2]$ and $[G_1, G_2]$. We identify the (local) segment $[R, A_1]$ as the single segment formed

by Lax f-shocks (see Definition 2.2.1 and rectangular cut of Figure 6.13(a), zoomed in Figure 6.13(b)). Moreover, the black and red curves in Figure 6.13(b) intersect at A_1, meaning that $\sigma(A_1; R) = \lambda_f(A_1)$. The admissibility of this segment is guaranteed by Claim 2.7.1 because $[R, A_1]$ is a local shock segment from R. ■

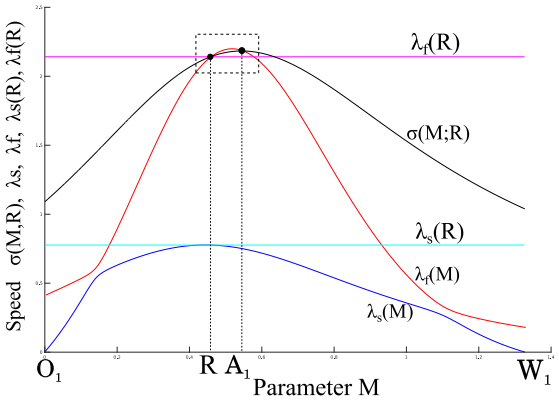

(a) Speed diagram: Primary branch $[O_1, W_1]$, of $\mathcal{H}(R)$ with $R \in \mathscr{R}_4$.

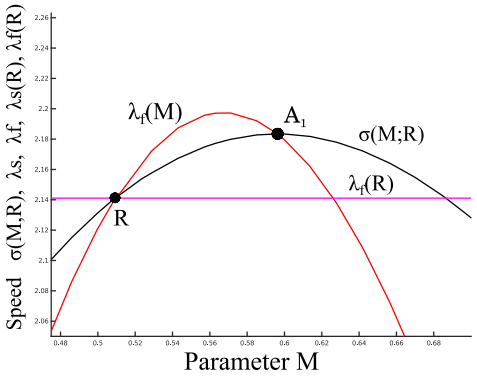

(b) Speed diagram: Zoom of segment $[R, A_1]$, of $\mathcal{H}(R)$ with $R \in \mathscr{R}_4$.

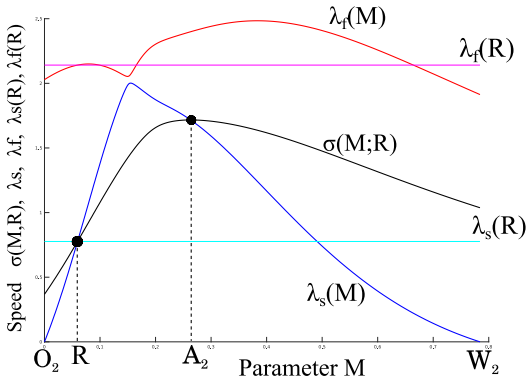

(c) Speed diagram: Primary branch $[O_2, W_2]$, of $\mathcal{H}(R)$ with $R \in \mathscr{R}_4$.

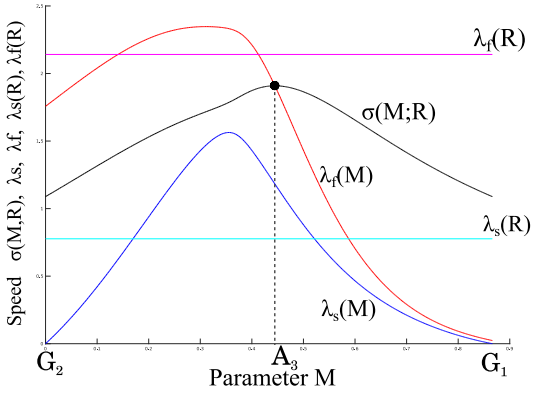

(d) Speed diagram: Nonlocal branch $[G_1, G_2]$, of $\mathcal{H}(R)$ with $R \in \mathscr{R}_4$.

Figure 6.13: Speed diagram for $\mathcal{H}(R)$ in Figure 6.12(b). The horizontal axis corresponds to a parametrization given in terms of arc length, and the vertical axis is speed. The blue (resp. red) line is the characteristic speed λ_s (resp. λ_f) while the black line is the shock speed σ. Horizontal cyan and magenta lines correspond to the constant values $\lambda_s(R)$ and $\lambda_f(R)$, respectively. (a) Segment (A_1, R) of Lax f-shocks in the primary branch $[O_1, W_1]$. (b) Zoomed in picture of squared region in (a). (c) Segment (A_2, R) of Lax s-shocks in the primary branch $[O_2, W_2]$. (d) Segment (G_2, A_3) of transitional shocks in the nonlocal branch $[G_2, G_1]$.

From Claim 6.4.8, we observe that $\mathcal{W}_f^-(R)$ does not have nonlocal f-shocks. Now, we move state

R parallel to edge $[O, W]$ toward of vertex W. By the description given in Section 4.5.2, there is a fast inflection curve $\mathcal{I}_f$ that causes the bifurcation of the f-shock curve $[R, A_1]$; the f-inflection consists of the segment $[\mathcal{I}_f^1, \mathcal{I}_f^2]$, with $\mathcal{I}_f^1 \in [W, \mathcal{U}]$ and $\mathcal{I}_f^2 \in [W, D]$, see Figure 6.32(a). Indeed, as R approaches $\mathcal{I}_f$, $[R, A_1]$ becomes smaller until it contracts to a single state $R \in \mathcal{I}_f$. Hence, the bottom boundary of region $\mathscr{R}_4$ is $\mathcal{I}_f$.

Next, we move state R toward $\mathcal{U}$ parallel to the invariant segment $[\mathcal{U}, D]$ and consider the forward f-rarefaction that begins at $Y_2 \in [\mathcal{U}, D]$, with Y_2 belonging to the fast double contact, see Remark 5.2.2. This rarefaction ends at state $Y_2' \in \mathcal{I}_f$ (see Figure 6.32). The f-rarefaction curve $[Y_2, Y_2']$ represents a bifurcation for the backward fast wave curve because if R belongs to or crosses $[Y_2, Y_2']$, then the backward f-rarefaction in $\mathcal{W}_f^-(R)$ intersects the double fast locus $[Y_2, \widehat{Y_2}]$ producing a nonlocal branch (see Figure 6.32 and Section 4.4.2, Figure 4.5(a)).

Claim 6.4.9. *Region $\mathscr{R}_4$ has the invariant segment $[Y_2, D]$ for its top boundary, $[Y_2', \mathcal{I}_f^2]$ (which is part of $\mathcal{I}_f$) for its bottom boundary and the f-rarefaction segment $[Y_2, Y_2']$ as its left boundary. Moreover, the fast backward wave curve for a state $R \in \mathscr{R}_4$ consists of only a local branch that has the following wave structure (refer to Figure 6.14(a)):*

1. *Lax f-shock segment $(R, A_1]$ with $\sigma(A_1; R) = \lambda_f(A_1)$;*
2. *backward f-rarefaction segment $[R, O]$;*
3. *backward f-rarefaction segment $(A_1, W]$.*

Proof. Refer to Figure 6.14(a). Consider any state in region $\mathscr{R}_4$. From Claim 6.4.8, we have the Lax f-shock curve $[R, A_1]$ where A_1 is a Bethe-Wendroff state. Following the succession algorithm (Section 2.7) for building $\mathcal{W}_f^-(R)$, we concatenate a backward f-rarefaction curve from state R to O and from A_1 to W. In Figure 6.14(a), we see the f-rarefaction curves $[R, O]$ and $[A_1, W]$, which intersect the fast double contact locus at states P_1 and P_3, respectively. Moreover, $[R, O]$ intersects the fast boundary extension of $[G, W]$ at state P_2, and $[A_1, W]$ intersects the fast boundary extension of $[O, G]$ at state P_4. The fast extensions of rarefaction curves $[R, O]$ and $[A_1, W]$ are the curves $[P_1', P_2']$ and $[P_3', P_4']$, respectively, and correspond to segments $[P_1, P_2]$ and $[P_3, P_4]$. Notice that the segments $[P_1, P_2]$ and $[P_1', P_2']$ are in opposite sides of the invariant line $[G, D]$, which means that the f-composite segment $[P_1', P_2']$ is inadmissible due to Claim 2.7.2. The same justification proves the inadmissibility of the f-composite segment $[P_3', P_4']$ (see Figure 6.14(a)). ∎

We now define $\mathscr{R}_5$ by moving the state R across the forward f-rarefaction segment $[Y_2, Y_2']$ (coming from $\mathscr{R}_4$, see Figure 6.32(b)). We have two other natural boundaries: the fast double contact $[Y_2, \widehat{Y_2}]$ as the left boundary and $\mathcal{I}_2$ as the bottom boundary. We call $\mathscr{R}_5$ the region defined by these three boundaries. For some combinations of μ_w, μ_o and μ_g, it is possible for another boundary to appear in this region, as described in Remark 6.4.5.

Moreover, as seen in the Remark 6.3.4, the f-left extension $E_f^-([\mathcal{Y}_2, \mathcal{J}_2])$ given by segment $[Y_2, Y_2^*]$ passes through this region, producing two possibilities for the Hugoniot curve $\mathcal{H}(R)$: the nonlocal branch crosses the invariant line $[G, D]$ (or not, see Figure 6.32(d)), depending on which side of $[Y_2, Y_2^*]$ the

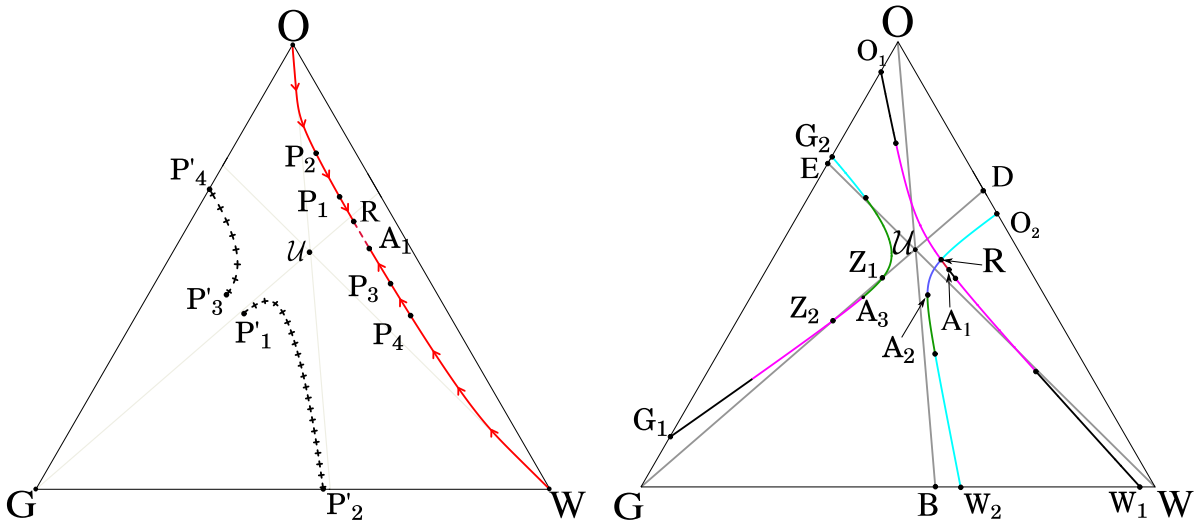

(a) $\mathcal{W}_f^-(R)$ for $R \in \mathscr{R}_4$.

(b) Typical Hugoniot curve for $R \in \mathscr{R}_5$.

Figure 6.14: (a) Backward f-wave curve $\mathcal{W}_f^-(R)$ for $R \in \mathscr{R}_4$. Continuous lines are f-rarefaction segments and dashed lines are Lax f-shock segments. The black crossed curves $[P_1', P_2']$ and $[P_3', P_4']$ are inadmissible f-composite waves corresponding to the f-rarefaction segments $[P_1, P_2]$ and $[P_3, P_4]$, respectively. Notice that $\mathcal{W}_f^-(R)$ does not have a nonlocal branch. (b) Hugoniot curve for $R \in \mathscr{R}_5$. Notice that the segment $[Z_2, A_3, Z_1]$ in the nonlocal branch $[G_1, G_2]$ crosses the invariant segment $[G, D]$.

state R lies. In Figure 6.14(b), a Hugoniot curve is shown for a state R inside $\mathscr{R}_5$ it possesses two primary branches $[O_1, W_1]$ and $[O_2, W_2]$ (which intersect at R), and a nonlocal branch $[G_1, G_2]$. Notice that in this case the nonlocal branch intersects the invariant line $[G, D]$ at states Z_1 and Z_2, so segment $[Z_1, Z_2]$ is on the same side of $[G, D]$ as R.

Claim 6.4.10. *The Hugoniot curve of a state $R \in \mathscr{R}_5$ has only one segment $[R, A_1]$ such that for all states $M \in [R, A_1]$ the discontinuity from M to R is a Lax f-shock and A_1 is a Bethe-Wendroff point that satisfies $\sigma(A_1; R) = \lambda_f(A_1)$. Moreover, this discontinuity is admissible (i.e., has viscous profile).*

Proof. The justification of this claim is similar to the proof of Claim 6.4.8, but it is based on Figures 6.14(b) and 6.15. Notice that segments $[G_2, Z_1]$ and $[G_1, Z_2]$ lie inside triangle $\widehat{GDO}$, so states on this curve are not admissible. From Figure 6.15(d) we see that for $M \in [Z_1, A_3]$, $\lambda_f(M) - \sigma > 0$, which implies that it does not comprise a Lax f-shock. Similarly there is no Lax f-shock for $M \in [A_3, Z_2]$, since $\lambda_f(R) - \sigma > 0$. For the case where the nonlocal branch $[G_1, G_2]$ of $\mathcal{H}(R)$ does not cross $[G, D]$, the segment $[G_1, G_2]$ is discarded by Claim 2.7.2. ∎

Claim 6.4.11. *The fast backward wave curve for a state $R \in \mathscr{R}_5$ possesses a local branch with the following wave structure (refer Figure 6.16):*

(i) Lax f-shock segment $(R, A_1]$ with $\sigma(A_1; R) = \lambda_f(A_1)$;

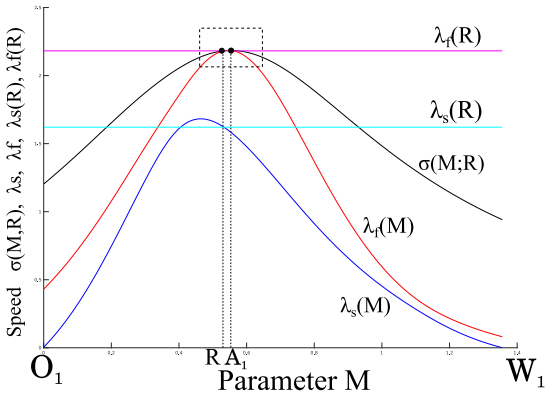

(a) Speed diagram: Primary branch $[O_1, W_1]$ of $\mathcal{H}(R)$ with $R \in \mathscr{R}_5$.

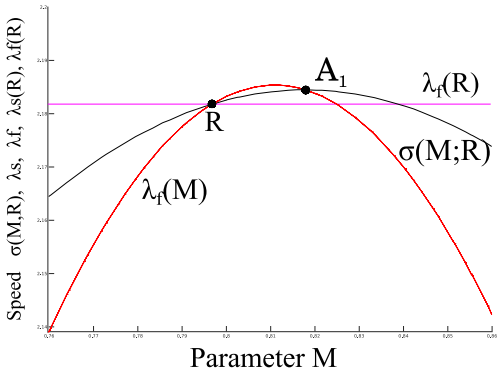

(b) Speed diagram: Zoom of segment $[R, A_1]$ of $\mathcal{H}(R)$ with $R \in \mathscr{R}_5$.

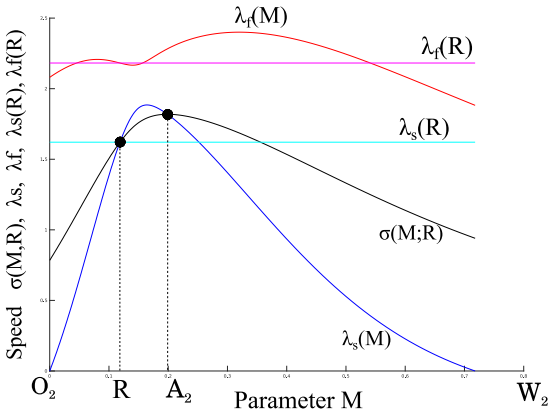

(c) Speed diagram: Primary branch $[O_2, W_2]$, for $\mathcal{H}(R)$ with $R \in \mathscr{R}_5$.

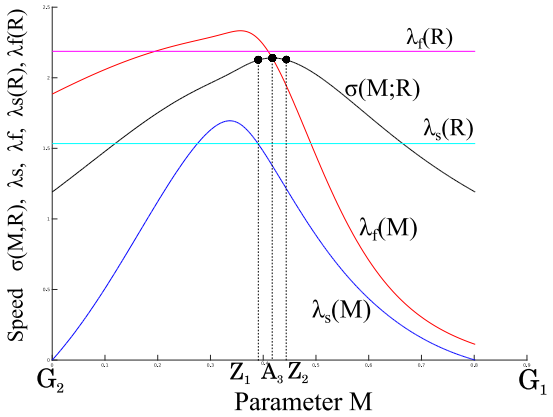

(d) Speed diagram: Nonlocal branch $[G_1, G_2]$, for $\mathcal{H}(R)$ with $R \in \mathscr{R}_5$.

Figure 6.15: Speed diagram for $\mathcal{H}(R)$ in Figure 6.14(b). The horizontal axis corresponds to a parametrization given in terms of arc length, and the vertical axis is speed. The blue (resp. red) line is the characteristic speed λ_s (resp. λ_f) while the black line is the shock speed σ. Horizontal cyan and magenta lines correspond to the constant values $\lambda_s(R)$ and $\lambda_f(R)$, respectively. (a) Segment (A_1, R) of Lax f-shocks in the primary branch $[O_1, W_1]$. (b) Zoomed in picture of squared region in (a). (c) Segment (A_2, R) of Lax s-shocks in the primary branch $[O_2, W_2]$. (d) Segment (Z_1, A_3, Z_2) in the nonlocal branch $[G_2, G_1]$. Notice that for any $M \in [G_2, G_1]$, $\lambda_f(R) - \sigma > 0$.

(ii) backward f-rarefaction segment $[R, O]$;

(iii) backward f-rarefaction segment $(A_1, W]$.

It also possesses a nonlocal branch with the following wave structure:

(iv) backward f-composite segment $[M_2', P_1')$ corresponding to $[M_2, P_1)$;

(v) backward f-rarefaction segment $[P_1', G]$, with $\sigma(P_1; P_1') = \lambda_f(P_1) = \lambda_f(P_1')$.

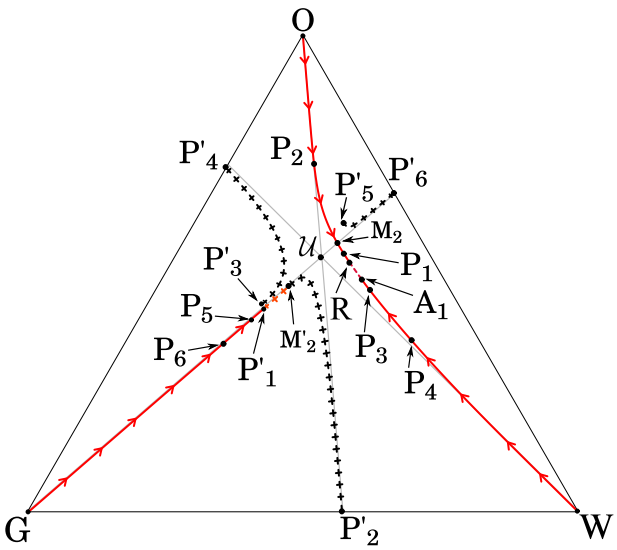

(a) $\mathcal{W}_f^-(R)$ for $R \in \mathscr{R}_5$.

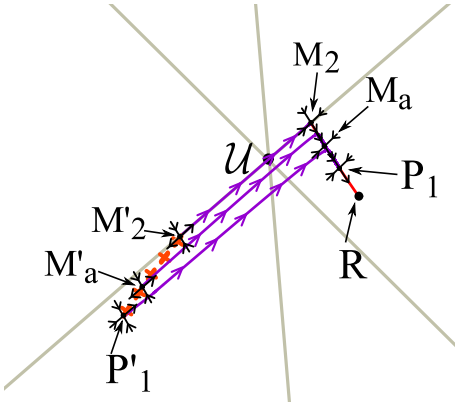

(b) Orbits between states on the f-composite segment $[P_1', M_2']$ and the corresponding states on the backward f-rarefaction segment $[P_1, M_2]$ belonging to $\mathcal{W}_f^-(R)$ for $R \in \mathscr{R}_5$.

Figure 6.16: (a) Backward f-wave curve for $R \in \mathscr{R}_5$, $\mathcal{W}_f^-(R)$. Continuous lines are f-rarefaction segments, dashed lines are Lax f-shock segments and crossed lines are f-composite segments . The black crossed curves $(M_2', P_2']$, $[P_3', P_4']$ and $[P_5', P_6']$ are inadmissible f-composite waves corresponding to f-rarefaction segments $(M_2, P_2]$, $[P_3, P_4]$ and $[P_5, P_6]$ respectively. Notice that the local branch of $\mathcal{W}_f^-(R)$ intersects the invariant line $[G, D]$ with a f-rarefaction wave at state M_2; the nonlocal branch starts in the corresponding state $M_2' \in [G, U]$ with an admissible f-composite wave $[M_2', P_1']$ corresponding to f-rarefaction segment $[M_2, P_1]$, where the pair (P_1, P_1') belongs to the fast double contact. (b) Orbits of the dynamical systems (2.24) for $U_L = M_a' \in [M_2', P_1']$, $U = M_a \in [M_2, P_1]$ and $\sigma = \sigma(M_a, M_a')$. Notice that the equilibria $M_a \in [M_2, P_1]$ are saddle-attractors and $M_a' \in [M_2', P_1')$ are saddles.

Proof. The justification of *(i), (ii) and (iii)* is similar to the one in Claim 6.4.9. Let P_3 and P_4 be the intersection points of the backward f-rarefaction $[A_1, W]$ with the fast double contact and the fast boundary extension of $[G, O]$, respectively (see Figure 6.16(a)). The fast extension $[P_3', P_4']$ of $[P_3, P_4]$ is not admissible by Claim 2.7.2. On the other hand, let P_1, P_2 and M_2 be the intersection points of the backward f-rarefaction $[R, O]$ with the fast double contact, the fast boundary extension of $[G, W]$ and the invariant line $[G, D]$, respectively. The fast extension of $[P_2, M_2]$ is the curve $[P_2', M_2']$ that lies in the triangle $\widehat{GDW}$. This curve is not admissible by Claim 2.7.2.

Now, notice that M_2 lies on $[G, D]$, so we have an explicit Hugoniot curve $\mathcal{H}(M_2)$ and we can find the corresponding state $M_2' \in [G, D]$ using Theorem 5.4.1(a) with $M_2' = X_2$. In Figure 6.17(a) we present the phase portraits of the dynamical system (2.24) for states $U_L = M_2'$ and $U = M_2$ with

$\sigma = \sigma(M_2; M_2')$. We see that there is an orbit from the saddle M_2' to the saddle-attractor M_2. Therefore, the characteristic f-shock between M_2' and M_2 is admissible. Moreover, this connection is structurally stable under small perturbations of M_2, M_2' and σ ([37]). Then, if we consider a state $M_a \approx M_2$ as a perturbation of M_2, in the direction of the eigenvector $\vec{r}_f(M_2)$, we see that: a) the state $M_a' \approx M_2'$ lies on the nonlocal branch of $\mathcal{H}(M_a)$; b) M_a' moves in the same direction as M_a so that both lie in the triangle $\widehat{GDW}$; and c) the connection between the saddle M_a' and the saddle-attractor M_a persists (see Figure 6.17(b)). Therefore, for any $M_a' \in (P_1', M_2']$ there is an orbit joining one of the unstable directions of the saddle M_a' to the saddle-attractor $M_a \in (P_1, M_2)$. Hence, the f-composite curve $(P_1', M_2']$ corresponding to $(P_1, M_2]$ is admissible (see Figure 6.16(b)).

Finally, since P_1' is a Bethe-Wendroff admissible point, the succession algorithm (Section 2.7) allows the concatenation of the backward f-rarefaction segment $[P_1', G]$. Notice in Figure 6.16(a) that this curve intersects the fast double contact and the fast boundary extension in states P_5 and P_6, respectively. Their fast extension is the curve $[P_5', P_6']$, which lies in the opposite side of $[P_5, P_6]$ relative to $[G, D]$; hence by virtue of Claim 2.7.2 this curve is inadmissible. ■

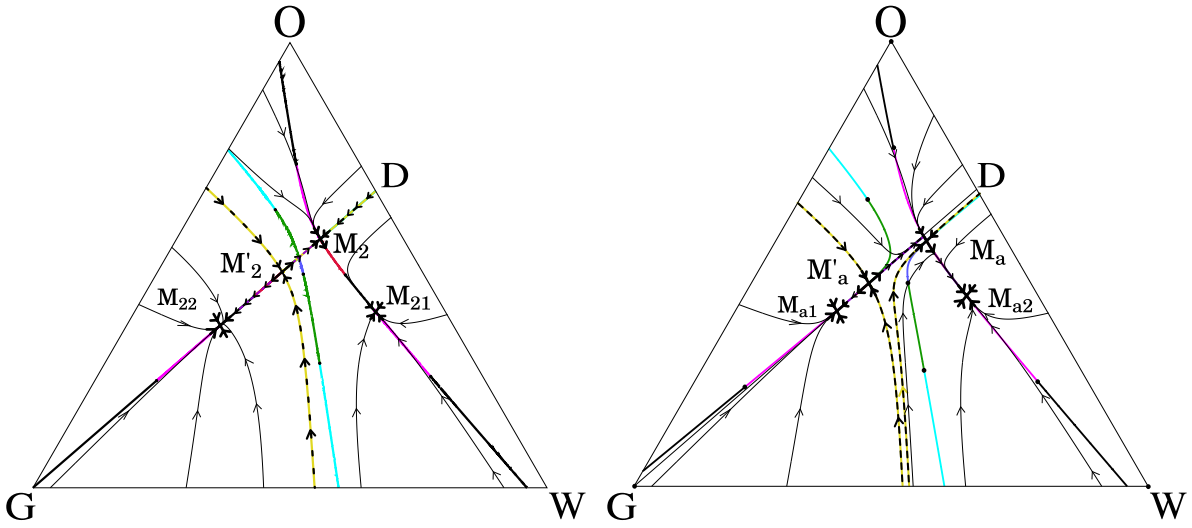

(a) Flow of the dynamical system (2.24) for $U_L = M_2'$, $U = M_2$ and $\sigma = \sigma(M_2; M_2')$. $\mathcal{H}(M_2)$ with $M_2 \in [\mathcal{U}, D]$.

(b) Flow of the dynamical system (2.24) for a perturbation of M_a' and M_a near M_2 where $U_L = M_a'$, $U = M_a$ and $\sigma = \sigma(M_a; M_a')$. $\mathcal{H}(M_a)$ with $M_a \in [P_1, M_2]$ and $M_a' \in [P_1', M_2']$.

Figure 6.17: Numerical analysis of admissibility of the f-composite curve $[M_2', P_1')$ of $\mathcal{W}_f^-(R)$ for $R \in \mathscr{R}_5$. (a) Hugoniot curve for $M_2 \in [G, D]$, with $M_2' = X_2(M_2)$ an extremum of the transitional segment $[X_2(M_2), X_1(M_2)]$ computed from Theorem 5.4.1. The equilibria M_2' and M_{22} are saddles, M_{21} is an attractor and M_2 is a saddle-attractor of the dynamical system (2.24) where $U_L = M_2'$, $U = M_2$ and $\sigma = \sigma(M_2; M_2')$. (b) Hugoniot curve for $M_a \in [M_2, P_1]$, with M_a a perturbation of M_2. The type and number of equilibria is maintained with respect to the case (a), *i.e.,* M_a' and M_{a1} are saddles, M_{a2} is an attractor and M_a is a saddle-attractor of the dynamical system (2.24) where $U_L = M_a'$, $U = M_a$ and $\sigma = \sigma(M_a; M_a')$.

Remark 6.4.5. As seen in Section 4.4.2, the fast double contact has three possible configurations when limited to a fast macro region $\mathcal{FR}_i$ for $i \in \{D, E, B\}$ with umbilic point of type II: if the state Y_2 is inside the saturation triangle, the admissible part of the double contact inside $\mathcal{FR}_i$ starts at Y_2 and ends when it intersects either the fast inflection $\mathcal{I}_2$ or one of the secondary bifurcation segments that are boundaries of $\mathcal{FR}_i$. Conversely, if Y_2 is outside the saturation triangle, the admissible part that we consider in this locus begins at the edge of the saturation triangle boundary and ends at $\mathcal{I}_2$.

In Figures 6.32 (b) and (c), we see two of the three fast double contact configurations for region $\mathscr{R}_5$. In the first one, shown in Figure 6.32 (b), region $\mathscr{R}_5$ has the fast double contact $[Y_2, \widehat{Y_2}]$ as its left boundary, $\mathcal{I}_2$ as its bottom boundary and the fast forward rarefaction $[Y_2, Y_2']$ as its right boundary. In the second configuration (Figure 6.32 (c)), region $\mathscr{R}_5$ has for its top boundary the curve $[Y_2, H_4]$, with H_4 on the invariant line $[W, E]$ (see Figure 4.4), for its left boundary $[H_4, \mathcal{I}_f^1]$ (where $\mathcal{I}_f^1$ is the intersection of $[W, E]$ and the fast inflection locus $\mathcal{I}_f$, and is computed using Remark 5.3.1), and segments $[Y_2, Y_2']$ and $[\mathcal{I}_f^1, Y_2']$ for its right and bottom boundaries, respectively.

Let us define region $\mathscr{R}_6$. We move state R across the fast double contact $[Y_2, \widehat{Y_2}]$ (or $[Y_2, H_4]$, considering Remark 6.4.5) such that for its top boundary we have the segment $(\mathcal{U}, Y_2]$, for its left boundary we have $(\mathcal{U}, \mathcal{I}_f^1]$ (or $[\mathcal{U}, H_4]$ if we are considering Remark 6.4.5), and for its right and bottom boundaries we have, respectively, $[Y_2, \widehat{Y_2}]$ and $[\mathcal{I}_f^1, \widehat{Y_2}]$ (in the regime of Remark 6.4.5 we have $[H_4, Y_2]$), see Figure 6.32(b)-(c).

A typical Hugoniot curve for a state R in $\mathscr{R}_6$ is shown in Figure 6.18(a). Since the top boundary of $\mathscr{R}_6$ is part of the segment $(\mathcal{U}, D)$, the Hugoniot curve $\mathcal{H}(R)$ can be considered as a perturbation of the Hugoniot curve for a generic state along $(\mathcal{U}, Y_2]$ which was obtained explicitly in [3] (see Figure 6.17(a)). The Hugoniot curve $\mathcal{H}(R)$ possesses two primary branches, $[O_1, W_1]$ and $[O_2, W_2]$ (which intersect at R), and a nonlocal branch $[G_1, G_2]$. Notice that this nonlocal branch intersects the invariant line $[G, D]$ at states Z_1 and Z_2 and that segment the $[Z_1, Z_2]$ is on the same side of $[G, D]$ as R, see Figure 6.18(a).

Remark 6.4.6. Observe that region $\mathscr{R}_6$ contains a neighborhood of the umbilic point $\mathcal{U}$. Because of this, it is better to study the expansion of Corey flux functions for states in a neighborhood of $\mathcal{U}$ in terms of homogeneous quadratic polynomials. This was studied by many authors, among others [Dan,matos,brad, etc Azevedo].

Claim 6.4.12. *Let R be a state in region $\mathscr{R}_6$. In addition to states Z_1 and Z_2 on $[G, D]$, the Hugoniot curve $\mathcal{H}(R)$ possesses states A_1 , A_1', A_1^*, A_3 and A_4 with the following properties :*

(i) States A_1, A_3 and A_4 are Bethe-Wendroff points. They satisfy $\sigma(A_1; R) = \lambda_f(A_1)$, $\sigma(A_4; R) = \lambda_f(A_4)$ and $\sigma(A_3; R) = \lambda_f(R)$.

(ii) If M is a state on either of the branches $[O_1, W_1]$ and $[G_1, G_2]$ of $\mathcal{H}(R)$, the discontinuity joining M to R is a Lax f-shock if M is either on $[A_1, R)$ or on $[A_3, A_4]$. Moreover, this discontinuity is admissible.

(iii) States $A_1' \in [A_3, A_4]$ and $A_1^* \in [A_4, Z_2]$ satisfy $\sigma(A_1; A_1') = \sigma(A_1'; R) = \sigma(A_1^*; R)$. Moreover, $\lambda_f(A_1) = \sigma(A_1; A_1')$, but there is no orbit joining A_1 and A_1' for the dynamical system (2.24) with $U_L = A_1'$, $U = A_1$ and $\sigma = \sigma(A_1; A_1')$.

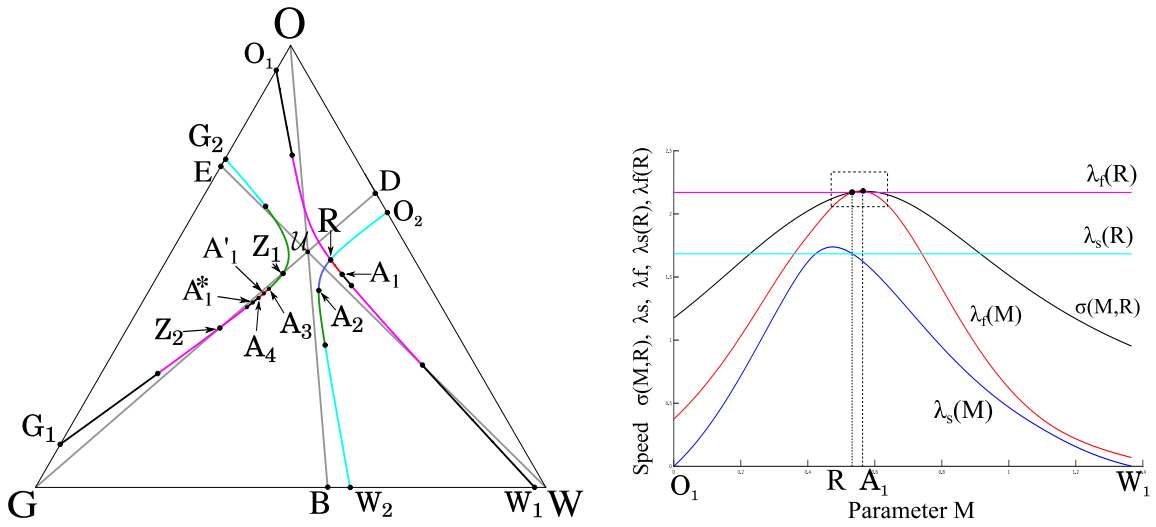

(a) Typical Hugoniot curve for $R \in \mathscr{R}_6$

(b) Speed diagram: Primary branch $[O_1, W_1]$ for $\mathcal{H}(R)$ with $R \in \mathscr{R}_6$

Figure 6.18: (a) Hugoniot curve for $R \in \mathscr{R}_6$. Segments $[R, A_1] \subset [O_1, W_1]$ and $[A_3, A_4] \subset [G_1, G_2]$. The states A_1, A_1' and A_1^* are equilibria of the same dynamical system with $U_L = A_1$, $U = R$ and $\sigma = \sigma(A_1, R)$. (b) Speed diagram for $\mathcal{H}(R)$ in Figure (a). The horizontal axis corresponds to a parametrization is given in terms of arc length, and the vertical axis is speed. The blue (resp. red) line is the characteristic speed λ_s (resp. λ_f) while the black line is the shock speed σ. Horizontal cyan and magenta lines correspond to the constant values $\lambda_s(R)$ and $\lambda_f(R)$, respectively. Segment (A_1, R) of Lax f-shocks in the primary branch $[O_1, W_1]$.

Proof. The justification of this claim is similar to the proof of Claim 6.4.8 but it is based on Figures 6.18-6.21. From Figures 6.19(a),(b) and (c), observe that states M along $[R, A_1]$ or $[A_3, A_4]$ corresponds to Lax f-shocks and states A_1, A_3 and A_4 are Bethe-Wendroff points. This follows by comparing the characteristic speeds $\lambda_s(R)$, $\lambda_f(R)$, $\lambda_s(M)$ and $\lambda_f(M)$ with the shock speed $\sigma(M, R)$ as M varies along the branches $[O_1, W_1]$, $[O_2, W_2]$ and $[G_1, G_2]$. The admissibility of segment $[R, A_1]$ is guaranteed by Claim 2.7.1 since $[R, A_1]$ is a local shock segment from R.

Now we consider the admissibility of segment $[A_3, A_4]$; it was verified numerically in Figures 6.20 and 6.21(a). Figure 6.21(b) depicts a schematic representation of the speed diagram for a given Hugoniot curve $\mathcal{H}(R)$, in order to compare speeds between branches. We begin by defining some auxiliary states, each one of which satisfies the triple shock rule 2.4.3 with respect to the previously defined states A_1 , A_1', A_1^*, A_3, A_4, Z_1 and Z_2 in $\mathcal{H}(R)$.

Let $A_1'$and A_1^* in Figure 6.21(b) be the states on the branch $[G_1, G_2]$ satisfying the triple shock rule with A_1 and R. That is, the discontinuity between A_1' and R or A_1^* and R propagates at the speed of the discontinuity between A_1 and R. In other words, states $A_1'$and A_1^* are equilibria of the ODE system (2.20) for $\sigma = \sigma(A_1; R)$. In a similar way, Z_{22}, Z_{23} and A_{31}, A_{32} on the segments $[A_1, O_1]$ and $[A_1, W_1]$ of $\mathcal{H}(R)$, respectively, are defined in terms of Z_1 and R for the first pair and A_3 and R for the second one. With these auxiliary states in mind, we now describe phase portraits of the ODE system (2.20) with speed $\sigma(M; R)$ as M varies along the Hugoniot branches $[O_1, W_1]$ and $[G_2, G_1]$ in Figures 6.18(b), 6.19

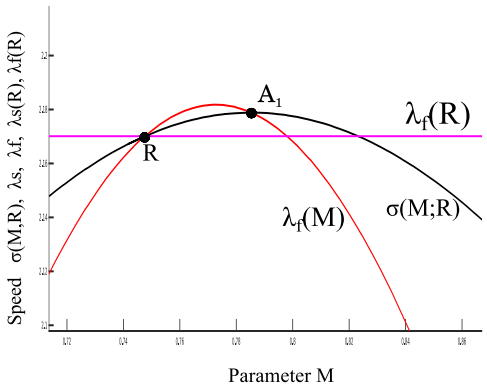

(a) Speed diagram: Zoom of segment $[R, A_1]$ for $\mathcal{H}(R)$ with $R \in \mathscr{R}_6$.

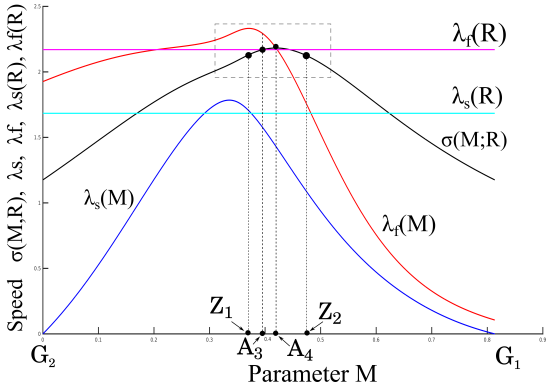

(b) Speed diagram: Nonlocal branch $[G_1, G_2]$, $R \in \mathscr{R}_6$.

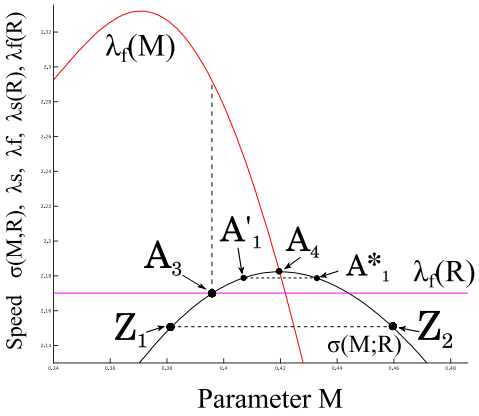

(c) Speed diagram: Zoomed segment $[Z_1.Z_2]$ for $\mathcal{H}(R)$ with $R \in \mathscr{R}_6$.

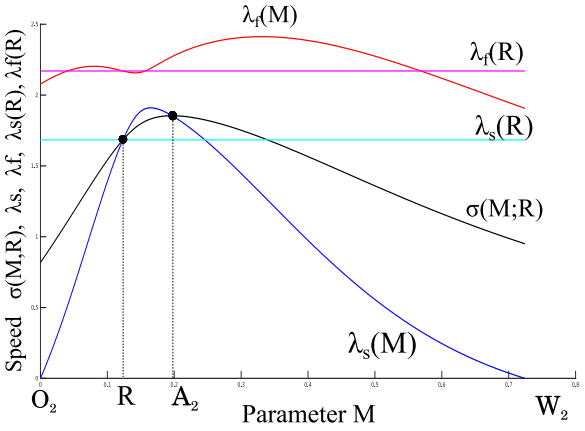

(d) Speed diagram: Primary branch $[O_2, W_2]$ for $\mathcal{H}(R)$ with $R \in \mathscr{R}_6$.

Figure 6.19: Speed diagram for $\mathcal{H}(R)$ in Figure 6.18(a). The horizontal axis corresponds to a parametrization given in terms of arc length, and the vertical axis is speed. The blue (resp. red) line is the characteristic speed λ_s (resp. λ_f) while the black line is the shock speed σ. Horizontal cyan and magenta lines correspond to the constant values $\lambda_s(R)$ and $\lambda_f(R)$, respectively. (a) Zoom of squared region in Figure 6.18(b). (b) Segment (Z_1, A_3, A_4, Z_2) in the nonlocal branch $[G_2, G_1]$. (c) Zoom of squared region in (b). The horizontal dashed lines represent states satisfying the triple shock rule; for instance, A_1' and A_1^* with R or states Z_1 and Z_2 with R. (d) Segment (A_2, R) of Lax s-shocks in the primary branch $[O_2, W_2]$.

and 6.21(b).

For M on $[W_1, A_1)$, the speed diagrams in Figure 6.18(b) and Figure 6.19(a) show that $\lambda_j(M) - \sigma < 0$ for $j = s$ and f, which means that equilibrium M is an attractor. Therefore, there cannot be an orbit connecting M to R; hence the inadmissibility of the discontinuity joining left state M to right state R.

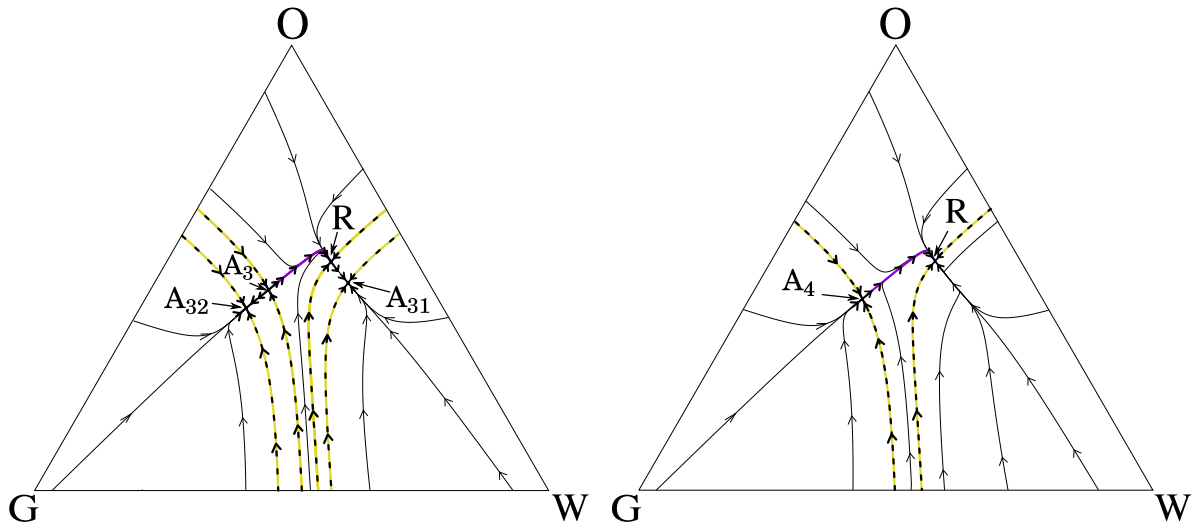

(a) Flow for the dynamical system (2.24) for $U_R = R$, $U = A_3$ and $\sigma = \sigma(R; A_3)$.

(b) Flow for the dynamical system (2.24) for $U_R = R$, $U = A_4$ and $\sigma = \sigma(R; A_4)$.

Figure 6.20: Numerical analysis of admissibility of the Lax f-shock segment $[A_3, A_4] \subset \mathcal{H}(R)$ for $R \in \mathscr{R}_6$. (a) The equilibria A_{31} and A_{32} are attractors, A_3 is a saddle and R is a saddle-attractor of the dynamical system (2.24) (fixing U_R instead U_L) where $U_R = R$, $U = A_3$ and $\sigma = \sigma(R; A_3)$. (b) The equilibrium A_4 is a saddle-node and R is an attractor of the dynamical system (2.24) where $U_R = R$, $U = A_4$ and $\sigma = \sigma(R; A_4)$.

The same argument is used to prove the inadmissibility of $[R, O_1]$.

Consider now M on segment $(A_4, A_1']$ of $\mathcal{H}(R)$, Figure 6.19(c). In this case, there are two equilibrium states on $\mathcal{H}(R)$ besides R: $M \in (A_4, A_1']$ and $M_1 \in (A_4, A_1^*]$. When $M = A_1'$, there is another equilibrium A_1 which is a saddle-node. According to the speed diagrams in Figures 6.19(b) and (c), M is a saddle while M_1 and R are attractors. Moreover, one of the unstable orbits emanating from M connects to the attractor R while the other connects to M_1, see Figure 6.21(a) and (b). Then, there is no orbit joining A_1 and A_1', which together with the previous arguments justifies item (iii) of Claim 6.4.12.

For M on (A_1', A_3) there are five equilibrium states on $\mathcal{H}(R)$: $M, M_1 \in (A_1^*, A_{32})$, $M_2 \in (A_1, A_{31})$, $M_3 \in (A_1, R)$ and R (see Figure 6.21(b)). This is similar to the case $M \in (A_4, A_1']$, where M and M_3 are saddles and M_1, M_2 and R are attractors. Moreover, both M and M_3 have one unstable orbit connecting to the attractor R while the other orbits connect M with M_1 and M_3 with M_2. If $M = A_3$, the saddle M_3 and the attractor R coalesce into a saddle-node equilibrium but the connection between M (*i.e.,* A_3) and R persists by an unstable orbit emanating from M. In conclusion, the discontinuity joining M to R is an admissible shock for all $M \in [A_3, A_4]$, which justifies item *(ii)* (see Figure 6.20(a)).

Finally, when M moves along (A_3, Z_1) toward Z_1 (see Figures, 6.19(a),(c) and 6.21(b)), the equilibria M and R are saddles and $M_1 \in (A_{32}, Z_2)$, $M_2 \in (A_{31}, Z_{23})$ and $M_3 \in (R, Z_{22})$ are attractors. When M reaches Z_1, states M_1, M_2 and M_3 reach Z_2, Z_{23} and Z_{22}, respectively (recall that Z_1, Z_2 and Z_{23} are the intersection points of $\mathcal{H}(R)$ with the invariant line $[G, D]$). For the saddle R, one of its unstable orbits connects to the attractor M_3 (or Z_{22}) and the other connects to attractor M_2 (or Z_{23}). These

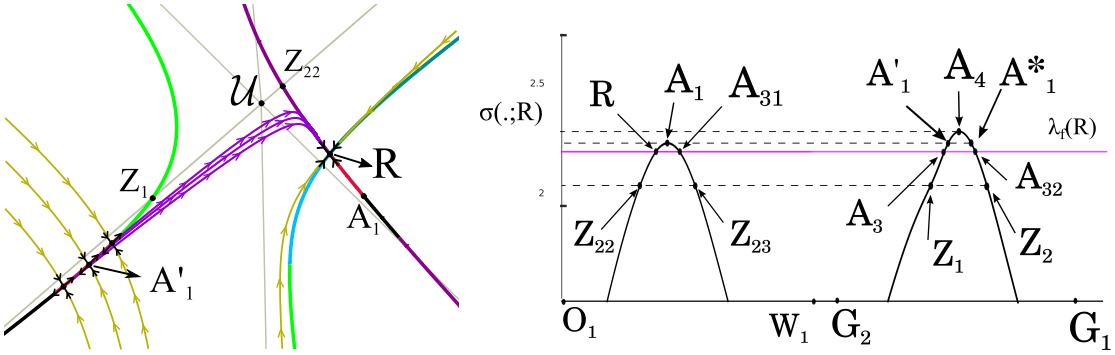

(a) Orbits of ODE's system (2.24) for $U_R = R$ and $U = M$ varying along $[A_3, A_4] \subset \mathcal{H}(R)$ for $R \in \mathscr{R}_6$. Notice that there is no orbit joining A_1' and A_1.

(b) Schematic comparison of speed diagram: Nonlocal branch $[G_1, G_2]$ and primary branch $[O_1, W_1]$ of $\mathcal{H}(R)$, $R \in \mathscr{R}_6$.

Figure 6.21: Numerical analysis of admissibility of the Lax f-shock segment $[A_3, A_4] \subset \mathcal{H}(R)$ for $R \in \mathscr{R}_6$. (a) Orbits of the dynamical systems (2.24) fixing $U_R = R$ and $U = M$, with M varying along $[A_3, A_4]$. When $M \in (A_3, A_4)$, M is a saddle and R is an attractor. (b) Schematic speed diagrams comparing the branches $[O_1, W_1]$ and $[G_2, G_1]$ of $\mathcal{H}(R)$ given in Figure 6.18(a). Black curves are the shock speed $\sigma(M, R)$ with M varying along the Hugoniot branches $[O_1, W_1]$ and $[G_2, G_1]$. States on the same horizontal dashed line satisfy the triple shock rule. The magenta line is the fast characteristic speed, $\lambda_f(R)$.

connections are not admissible because they are incorrectly oriented. For the saddle M (or Z_1), one of the unstable orbits connects to the attractor M_1 (or Z_1) while the other connects to the attractor M_2 (or Z_{23}). Therefore, the segments (A_3, Z_1) and (A_{32}, Z_2) are not admissible. ∎

Claim 6.4.13. *The fast backward wave curve for a state $R \in \mathscr{R}_6$ has a local branch with the following wave structure (refer Figure 6.22(a)):*

(i) Lax f-shock segment $(R, A_1]$ with $\sigma(R; A_1) = \lambda_f(A_1)$;

(ii) backward f-rarefaction segment $[R, O]$;

(iii) backward f-rarefaction segment $(A_1, W]$.

It also has a nonlocal branch with the following wave structure:

(iv) backward f-composite segment $[M_2', A_3)$ corresponding to $[M_2, R]$, with $\sigma(A_3; R) = \lambda_f(R)$;

(v) Lax f-shock segment $[A_3, A_4)$;

(vi) backward f-rarefaction segment $[A_4, G]$, with $\sigma(A_4; R) = \lambda_f(A_4)$.

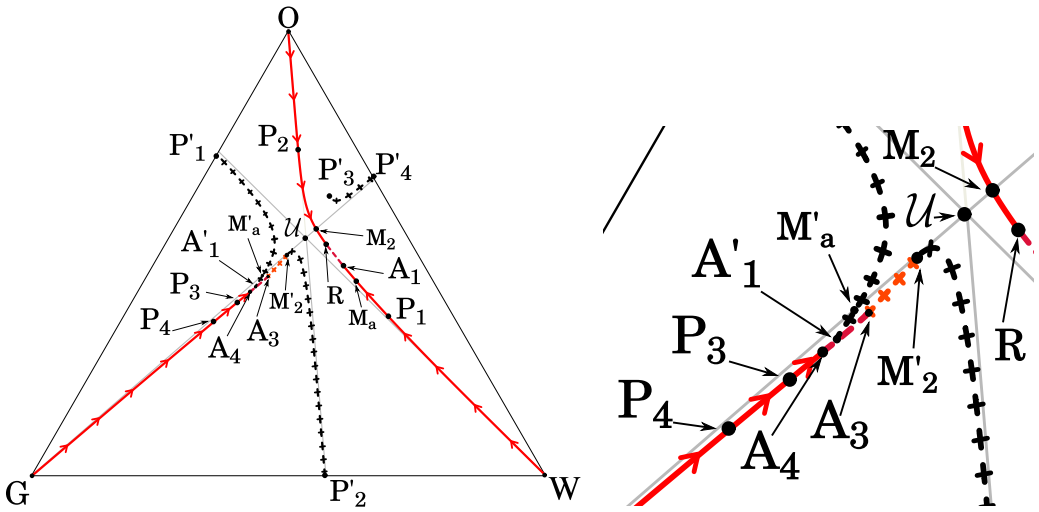

(a) $\mathcal{W}_f^-(R)$ for $R \in R_6$.

(b) Zoom of area close to segment of Lax f-shocks $[A_3, A_4]$.

Figure 6.22: (a) Backward f-wave curve for $R \in \mathscr{R}_6$, $\mathcal{W}_f^-(R)$. Continuous lines are f-rarefaction segments, dashes lines are Lax f-shock segments and crossed lines are f-composite segments. The black crossed curves $(M_2', P_2']$, $[P_1', A_1')$ and $[P_3', P_4']$ are inadmissible f-composite waves corresponding to f-rarefaction segments $[M_2, P_2]$, $[P_1, A_1]$ and $[P_3, P_4]$ respectively. Notice that the local branch of $\mathcal{W}_f^-(R)$ intersects the invariant line $[G, D]$ with a f-rarefaction wave at state M_2; the nonlocal branch starts in the corresponding state $M_2' \in [G,\mathcal{U}]$ with the admissible f-composite segment $[M_2', A_3]$ corresponding to the f-rarefaction segment $[M_2, R]$. Then, the nonlocal branch of $\mathcal{W}_f^-(R)$ has the admissible segment $[A_3, A_4]$ of Lax f-shocks and the backward f-rarefaction segment $[A_4, G]$. (b) Blow-up of region near segment $[A_3, A_4]$ in (a).

Proof. The justification of *(i), (ii) and (iii)* is similar to the proof of Claim 6.4.9. Let P_1 be the intersection point of the backward f-rarefaction $[A_1, W]$ with the fast boundary extension of $[G, O]$ and let M_2 and P_2 be the intersection points of the backward f-rarefaction $[R, O]$ with the invariant line $[G, D]$ and with the fast boundary extension of $[G, W]$, respectively (see Figure 6.22 (a)). The fast extension of the backward f-rarefaction curve $[R, O]$ is the curve $[A_3, P_2']$. This rarefaction and its extension curve can be divided in two parts (see Figure 6.22 (a)): $[P_2', M_2')$ which corresponds to $[P_2, M_2)$ and $[M_2', A_3]$ which corresponds to $[M_2, R)$. The f-composite curve $[P_2', M_2')$ is not admissible by Claim 2.7.2.

An argument similar to the proof that the f-composite $[M_2', P_1')$ is admissible in Claim 6.4.11 is used to prove that the f-composite $[A_3, M_2']$ corresponding to the f-rarefaction $[M_2, R)$ is admissible. Assumption (ii) of Claim 6.4.12 shows that the nonlocal Lax f-shock segment $[A_3, A_4]$ is admissible. This justifies (iv) and (v).

Now, we analyze the fast extension of the f-rarefaction segment $[A_1, W]$. This rarefaction curve and its extension can be divided in two parts: $[P_1', M_a')$ which corresponds to $[P_1, M_a)$ and $[M_a', A_1']$ which corresponds to $[M_a, A_1]$, where M_a' is the intersection of f-composite curve $[P_1', A_1']$ with $[G,\mathcal{U}]$ and $M_a \in [A_1, P1]$ is the corresponding state which satisfies $\sigma(M_a; M_a') = \lambda_f(M_a')$. The f-composite curve $[P_1', M_a')$ is not admissible by Claim 2.7.2 because it is opposite to $[P_1, M_a]$ relative to $[G, D]$

(see Figure 6.22 (a)). From statement (iii) of Claim 6.4.12, there are saddles A_1', A_1 and the attractor R belonging to the same dynamical system; moreover, the unstable orbit of each saddle connects to R. Notice that these connections are structurally stable. Moreover, by the triple shock rule 2.4.3 we conclude that for each $M \in (A_1, M_a]$, there is a corresponding saddle $M' \in [A_1', M_a']$ and an attractor $R' \in \mathcal{H}(M)$, which are part of the same dynamical system, and such that the unstable orbit of the saddle connects to R'. Therefore, there is no connection between $M \in [A_1, M_a]$ and $M' \in [A_1', M_a']$.

Finally, since A_3 is a Bethe-Wendroff admissible point, the succession algorithm (Section 2.7) allows the concatenation of the backward f-rarefaction segment $[A_3, G]$ (see Figure 6.22). This curve intersects the fast double contact and the fast boundary extension of edge $[W, O]$ at states P_3 and P_4, respectively. Their fast extension is the curve $[P_3', P_4']$ which lies opposite to $[P_3, P_4]$ relative to $[G, D]$; hence this curve inadmissible in virtue of Claim 2.7.2. ∎

Remark 6.4.7. Assuming that R lies on the bottom boundary of regions $\mathscr{R}_4$, $\mathscr{R}_5$ and $\mathscr{R}_6$ *i.e.,* $R \in [\mathcal{I}_f^1, \mathcal{I}_f^2]$ (see Figure 6.32(b)), then $\mathcal{W}_f^-(R)$ cannot possess a nonlocal f-shock. Then, we trace the fast integral curve from R to W and O and the local branch of $\mathcal{W}_f^-(R)$ consists only of this fast integral curve. Notice that for R on the bottom boundary for $\mathscr{R}_4$ and $\mathscr{R}_5$, the nonlocal branch of $\mathcal{W}_f^-(R)$ is similar to the one described in Claims 6.4.9 and 6.4.11. For $R \in \mathscr{R}_6$, we see that the nonlocal branch of $\mathcal{W}_f^-(R)$ uses the f-hysteresis curve given in Definition 2.4.2 *i.e.,* the fast composite curve $[M_2', A_3]$ with A_3 on the fast hysteresis for $\mathcal{I}_f^2$, which was obtained in 6.4.13 for R in the interior of $\mathscr{R}_6$.

6.4.3 Subregions $\mathscr{R}_{4'}$, $\mathscr{R}_{5'}$ and $\mathscr{R}_{6'}$

In this section, we study three additional regions that are very similar to the regions $\mathscr{R}_4, \mathscr{R}_5$ and $\mathscr{R}_6$ studied in Section 6.4.2. These new regions appear when we consider states R across the bottom boundary $\mathcal{I}_f$ for the regions $\mathscr{R}_i$ for $i \in \{4, 5, 6\}$. As seen in Remark 6.4.7, this boundary produces a bifurcation in the backward fast wave curves rendering it necessary to define new regions, which we call $\mathscr{R}_{4'}$, $\mathscr{R}_{5'}$ and $\mathscr{R}_{6'}$ in association to the corresponding regions across from $\mathcal{I}_f$. Later on we will see that these new regions only differ from the ones studied in Section 6.4.2 in the description of the local branch of $\mathcal{W}_f^-(R)$. Let us define region $\mathscr{R}_{4'}$. First, we let a state R in $\mathscr{R}_4$ cross the fast inflection close to state $\mathcal{I}_f^2$ (see Figure 6.32). The Hugoniot curve $\mathcal{H}(R)$ in this region is shown in Figure 6.24(a); it can be considered as a perturbation of the Hugoniot curve for a state that lies on $[W, O]$, which was obtained explicitly in [9] (see Figure 6.23). The Hugoniot curve for R possesses two primary branches, $[O_1, W_1]$ and $[O_2, W_2]$ (which intersect at R), and a nonlocal branch $[G_1, G_2]$. Notice that this nonlocal branch lies inside triangle $\widehat{GDO}$, therefore it is inadmissible by Claim 2.7.2.

Unlike the case of state $R \in \mathscr{R}_4$, in this case the segment of fast shock $(R, A_1]$ starts on R and continues toward vertex O until A_1, while the backward f-rarefaction starts at R and ends at vertex W. As $R \in \mathscr{R}_4$, A_1 is a Bethe-Wendroff point and we can concatenate a backward f-rarefaction segment from A_1 to vertex O. This rarefaction intersects the invariant line $[G, D]$ at state M_2. This fact characterizes the regions $\mathscr{R}_i$, with $i \in \{4, 5, 6, 4', 5', 6'\}$.

When R moves toward vertex W, $(R, A_1]$ becomes bigger until state A_1 reaches the invariant segment $[\mathcal{U}, D]$. Therefore, we have a characteristic f-shock with $\sigma(R; A_1) = \lambda_f(A_1)$ with $A_1 \in [G, D]$.

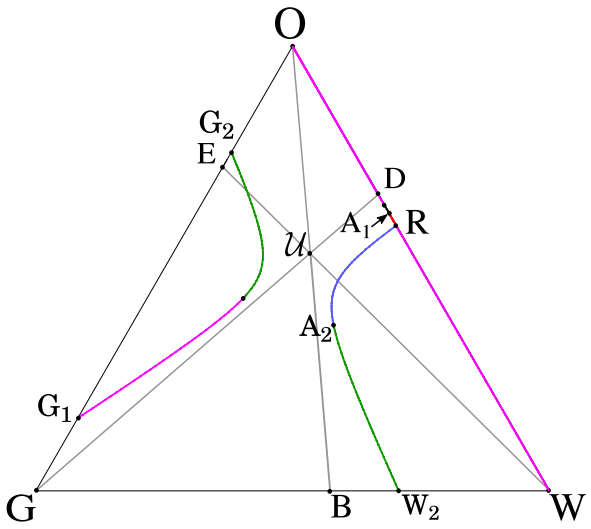

Figure 6.23: Typical Hugoniot curve for $R \in [D, W]$, R close to $\mathcal{I}_f^2$.

Hence, we obtain a bottom boundary for this region because if R moves beyond this position, the intersection M_2 with $[\mathcal{U}, D]$ occurs with a Lax f-shock. The set of all states R that have a characteristic f-shock with a state on $[\mathcal{U}, D]$ is $E_f^-([\mathcal{U}, D])$ (see Definition 2.4.6).

Finally, there is a left boundary for this region formed by the left f-extension of the f-rarefaction segment $[Y_2, Y_2']$. This segment begins at Y_2' and ends at $Y_2^* \in E_f^-([\mathcal{U}, D])$ (see Figure 6.32). The forward f-composite curve $[Y_2', Y_2^*]$ represents a bifurcation for $\mathcal{W}_f^-(R)$ because if R belongs to or crosses $[Y_2', Y_2^*]$, then $\mathcal{W}_f^-(R)$ intersects the double fast locus $[Y_2, \widehat{Y_2}]$ with a fast rarefaction (the state A_1 lies inside region $\mathscr{R}_5$, hence the f-rarefaction from A_1 intersects $[Y_2, \widehat{Y_2}]$ before $[\mathcal{U}, D]$) producing a nonlocal branch (see Figure 6.32 and Section 4.4.2).

Claim 6.4.14. *Region $\mathscr{R}_{4'}$ has the segment $[Y_2', \mathcal{I}_f^2]$ (which is part of $\mathcal{I}_f$) for its top boundary, $[Y_2^*, D^*]$ (which is part of $E_f^-([\mathcal{U}, D])$) for its bottom boundary, the f-composite segment $[Y_2', Y_2^*]$ as its left boundary and the segment $[D^*, \mathcal{I}_f^2]$ as its right boundary (see Figure 6.32(b)). Moreover, the fast backward wave curve for a state $R \in \mathscr{R}_{4'}$ consists of only a local branch with the following wave structure (refer to Figure 6.24(b)):*

1. *Lax f-shock segment $[R, A_1]$ with $\sigma(A_1; R) = \lambda_f(A_1)$;*
2. *backward f-rarefaction segment $[R, W]$;*
3. *backward f-rarefaction segment $[A_1, O]$.*

Proof. Similar to the proof of Claim 6.4.9 (see Figure 6.24). ∎

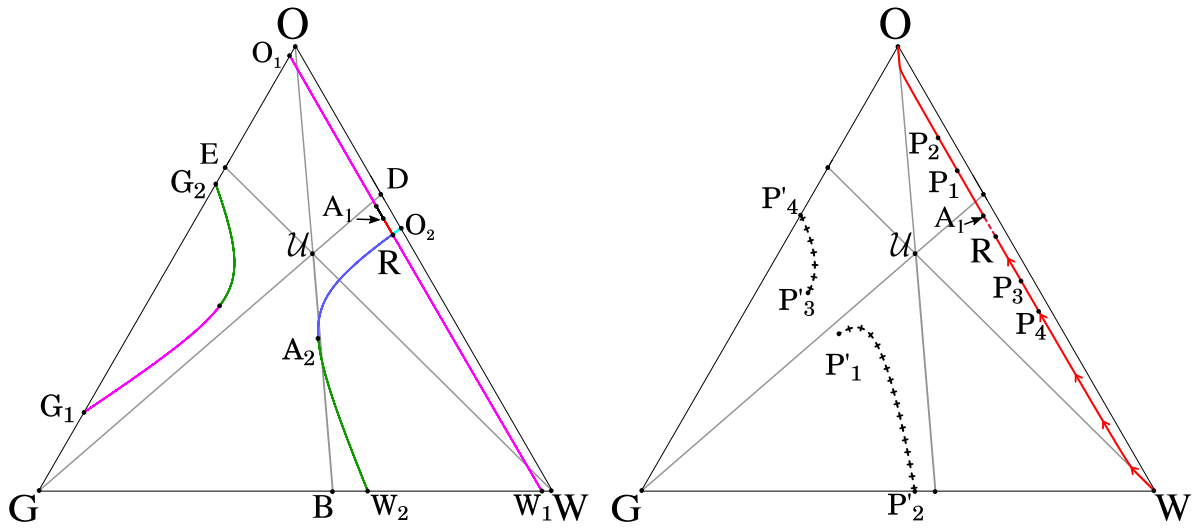

(a) Typical Hugoniot curve for $R \in \mathscr{R}_{4'}$.

(b) $\mathcal{W}_f^-(R)$ for $R \in R_{4'}$.

Figure 6.24: (a) Hugoniot curve for $R \in \mathscr{R}_{4'}$. (b) Backward f-wave curve $\mathcal{W}_f^-(R)$ for $R \in \mathscr{R}_4$. Continuous lines are f-rarefaction segments and dashed lines are Lax f-shock segments. The black crossed curves $[P_1', P_2']$ and $[P_3', P_4']$ are inadmissible f-composite waves corresponding to f-rarefaction segments $[P_1, P_2]$ and $[P_3, P_4]$, respectively. Notice that $\mathcal{W}_f^-(R)$ does not have a nonlocal branch.

Remark 6.4.8. Note that a branch of the fast double contact passes through region $\mathscr{R}_{4'}$. When state R crosses this curve, a new segment $[\widehat{A_3}, \widehat{A_4}]$ of nonlocal Lax f-shocks is generated in the nonlocal branch $[G_1, G_2]$ of $\mathcal{H}(R)$ (see Figure 6.25(a)). This nonlocal f-shock curve is not admissible by Claim 2.7.2, which implies that the region $\mathscr{R}_4'$ is completely determined by Claim 6.4.14 .

We define the region $\mathscr{R}_{5'}$ as the region adjacent to region $\mathscr{R}_{4'}$ and under region $\mathscr{R}_5$. For this, we move the state R across the forward f-composite $[Y_2', Y_2^*]$ (coming from $\mathscr{R}_{4'}$), see Figure 6.32(b). Consider R inside this region, close to state Y_2'. If we move R parallel to boundary $[O, W]$ toward the edge $[G, W]$, the segment $(R, A_1]$ of Lax f-shock becomes bigger until state A_1 coincides with the fast double contact $[Y_2, \widehat{Y_2}]$ (or $[Y_2, H_4]$ if we consider the Remark 6.4.5). If the state A_1 crosses the segment of fast double contact $[Y_2, \widehat{Y_2}]$ (or $[Y_2, H_4]$), R crosses $E_f^-([Y_2, \widehat{Y_2}])$ (or $E_f^-([Y_2, H_4])$).

As in the description of region $\mathscr{R}_5$ in Section 6.4.2, the fact that A_1 crosses $[Y_2, \widehat{Y_2}]$ (or $[Y_2, H_4]$) implies the appearance of a new wave group in $\mathcal{W}_f^-(R)$. Therefore, the left boundary for region $\mathscr{R}_{5'}$ is given by the segment $[\widehat{Y_2}, Y_2^*]$ which is $E_f^-([Y_2, \widehat{Y_2}])$ (or $[H_4^*, Y_2^*]$ as the bottom boundary of $\mathscr{R}_{5'}$ which is $E_f^-([Y_2, H_4])$), see Figure 6.32(b). If we consider Remark 6.4.5, we have segment $[\mathcal{I}_f^1, H_4^*]$ as the left boundary of $\mathscr{R}_5'$.

The Hugoniot curve for $R \in \mathscr{R}_{5'}$ possesses two primary branches, $[O_1, W_1]$ and $[O_2, W_2]$ (which intersect at R), and a nonlocal branch $[G_1, G_2]$ (see Figure 6.25(b)). Notice that the f-left extension $[J_1, Y_2^*]$ and a part of the fast double contact pass through region $\mathscr{R}_{5'}$, see Figure 6.32(d). This subdivides

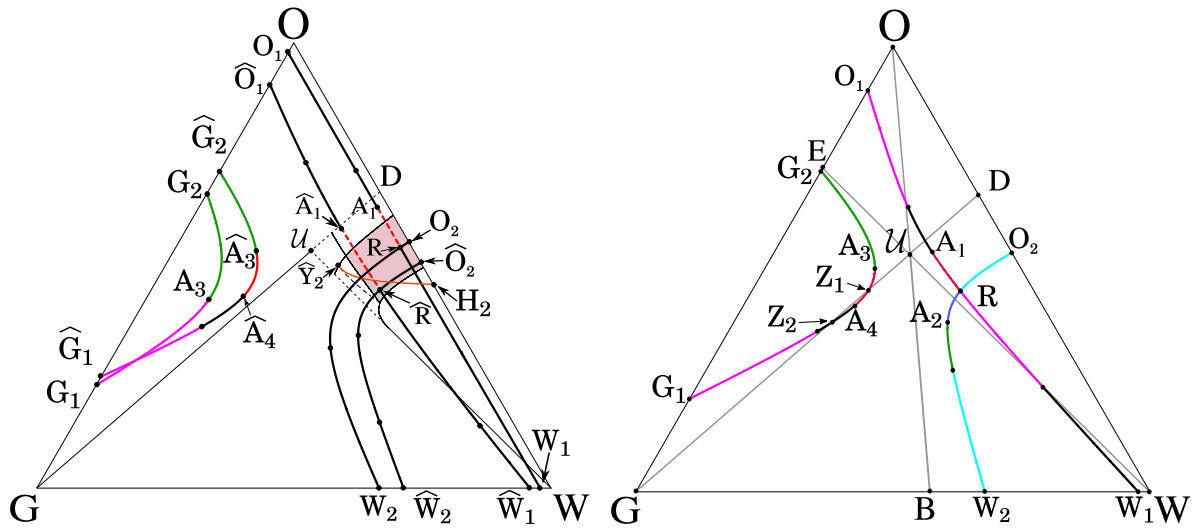

(a) Hugoniot curves for R and $\widehat{R}$ inside regions $\mathscr{R}_{4'}$.

(b) Typical Hugoniot curve for $R \in \mathscr{R}_{5'}$.

Figure 6.25: (a) Hugoniot curves for states R and $\widehat{R}$ in $\mathscr{R}_{4'}$. These two states are in opposite sides of curve $[\widehat{Y_2}, H_2]$ which is a part of the fast double contact locus. The nonlocal branches $[G_1, G_2]$ and $[\widehat{G_1}, \widehat{G_2}]$ do not cross the invariant line $[G, D]$. (b) Hugoniot curve for state R in $\mathscr{R}_4$ case (c) of Figure 6.26.

this region, since the nonlocal branch of Hugoniot curve changes behavior. In Figure 6.32(d), the region A is given by $Y_2' J_1 J_2 J_3$, where J_1 is the intersection point between the segment $[Y_2, Y_2^*]$ and $\mathcal{I}_f$, J_2 is the intersection between the fast double contact with the segment $[Y_2, Y_2^*]$ and J_3 is the intersection of the fast double contact with the f-composite $[Y_2', Y_2^*]$. Regions B, C and D are given by $J_1 \widehat{Y_2} J_2$, $\widehat{Y_2} J_2 Y_2^*$ and $J_2 J_3 Y_2^*$, respectively. When R is in A or D, the nonlocal branch of $\mathcal{H}(R)$ remains opposite to R with respect to $[G, D]$, thus the discontinuities of $[G_1, G_2]$ are not admissible by Claim 2.7.2.

On the other hand if R is in B or C, the non-local branch of $\mathcal{H}(R)$ crosses the invariant line $[G, D]$ intersecting it at Z_1 and Z_2, but R must cross the left f-extension $[J_1, Y_2^*]$ for new segments with discontinuities of Lax type to appear in $\mathcal{H}(R)$. Therefore, if R is inside C, the nonlocal branch of $\mathcal{H}(R)$ has a segment whose discontinuities are Lax f-shocks but, as we will see in the following Claim, they are not admissible, see Figure 6.32(d).

Claim 6.4.15. *Let R be a state in region $\mathscr{R}_{5'}$. The Hugoniot curve $\mathcal{H}(R)$ possesses a segment (A_1, R) of admissible discontinuities of local Lax f-shocks with state A_1 being a Bethe-Wendroff point that satisfies $\sigma(A_1; R) = \lambda_f(A_1)$. Moreover, there are no admissible nonlocal segments of Lax f-shock discontinuities (see Figure 6.25(b)).*

Proof. The justification of the first statement is analogous to the proof of Claim 6.4.8. For the other one, assume R inside C $\subset \mathscr{R}_{5'}$ (see Figure 6.32(d)). As seen in the description of $\mathscr{R}_{5'}$, when R is in the subdivision C, the nonlocal branch $[G_1, G_2]$ of $\mathcal{H}(R)$ crosses the invariant line $[G, D]$ intersecting it at states Z_1 and Z_2, see Figure 6.26. Moreover, $[G_1, G_2]$ has the segment (A_3, A_4) such that for all

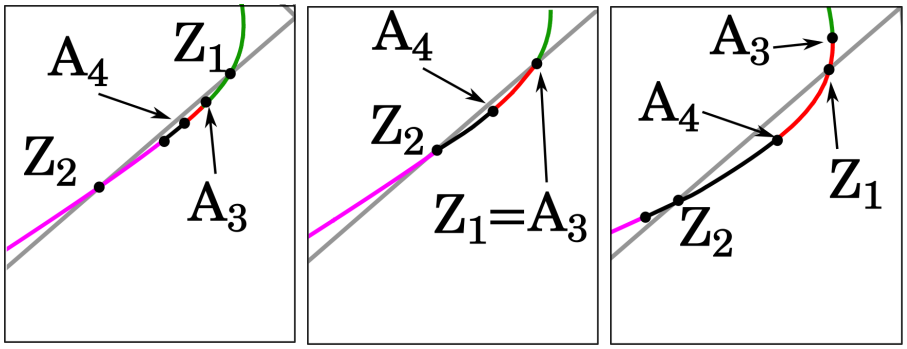

(a) (b) (c)

Figure 6.26: Behavior of the nonlocal branch $[G_1, G_2]$ for R in region $C \subset \mathscr{R}_{5'}$ (see Figure 6.32(d)). (a) R in region C between the f-inflection $\mathcal{I}_f$ and the right f-extension $E_f^+([\mathcal{U}, D])$ given by the segment $[J_4, J_5]$. (b) R in region C at the right f-extension $E_f^+([\mathcal{U}, D])$, *i.e.*, $R \in [J_4, J_5]$. (c) R in region C between the right f-extension $E_f^+([\mathcal{U}, D])$ given by the segment $[J_4, J_5]$ and the curve $[E_0, D^*]$.

$M \in (A_3, A_4)$ the discontinuity between M and R is a Lax f-shock and states A_3 and A_4 are Bethe-Wendroff points satisfying $\sigma(R; A_3) = \lambda_f(R)$ and $\sigma(R; A_4) = \lambda_f(A_4)$ (analogous to proof of Claim 6.4.12). As shown in Figure 6.26, there are three possibilities for the location of $[A_3, A_4]$ on $[G_1, G_2]$ and they depend on the location of R inside of C. Observe in Figure 6.32(d) that the curve $[J_4, J_5]$, which is the right f-extension of $[\mathcal{U}, D]$, divides C in two regions. By the triple shock rule 2.4.3 there is a segment on $[G,\mathcal{U}]$ such that for all $M \in [J_4, J_5]$ there are states $N \in [\mathcal{U}, D]$ and $V \in [D_2,\mathcal{U}]$ that satisfy $N, V \in \mathcal{H}(M)$ and $\sigma(M; N) = \sigma(M; V) = \sigma(V; N)$. Hence, the curve $[J_4, J_5]$ indicates exactly when the state A_3 crosses $[G, D]$ which implies the following cases for the segment $[A_3, A_4]$: (a) if R is between the fast inflection $\mathcal{I}_f$ and $[J_4, J_5]$ the segment $[A_3, A_4]$ is on same side of $[G, D]$ as R (see Figure 6.26(a)); (b) if $R \in [J_4, J_5]$, A_3 coincide with Z_1 and A_4 remains in the triangle $\widehat{GWD}$ (see Figure 6.26(b)); and c) if R crosses $[J_4, J_5]$, the state Z_1 is part of $[A_3, A_4]$ and A_3 is on the opposite side of R with respect to $[G, D]$, see Figure 6.26(c).

First, we study the case (b). Assume that R is on $[J_4, J_5,]$, and let N be on $[\mathcal{U}, Y_2]$ such that $\sigma(N; R) = \lambda_f(R)$. It is clear that $A_3 \in \mathcal{H}(N)$ and by the triple shock rule 2.4.3, $A_3 \in \mathcal{H}(R)$. Moreover, we can compute the state A_3 using Theorem 5.4.1 with $X_2 = A_3$. In Figure 6.27, we compare the speed diagrams of branches $[G_2, G_1]$ and $[O_1, W_1]$ of the Hugoniot curve $\mathcal{H}(R)$. Then, states N, R, Z_2 and $A_3 = Z_1$ are equilibria of the ODE system 2.24 with $U_R = R$ and $\sigma = \sigma(N; R)$. Notice that A_3 is a saddle, N and Z_2 are attractors and R is a saddle-repeller such that one of the unstable orbits emanating from A_3 connect to the attractor N and the other with Z_2, while the unstable orbits emanating from R connect to N. Therefore, the discontinuity between R and A_3 is inadmissible. Next, if we consider a state $M \in (A_3, A_4)$ and increase the speed σ along the shock curve until $M = A_4$, we have five equilibria $M_1 \in (A_4, Z_2)$, $M_2 \in (N, A_{41})$ and $M_3 \in (R, A_{42})$, M and R, such that M and M_3 are saddles and M_1, M_2 and R are attractors (see Figure 6.27). Since $(R, A_{42}) \subset [R, A_1]$ and for $M \in [R, A_1]$ the discontinuity connecting M to R is an admissible Lax f-shock, we conclude that segment $[A_3, A_4]$ is

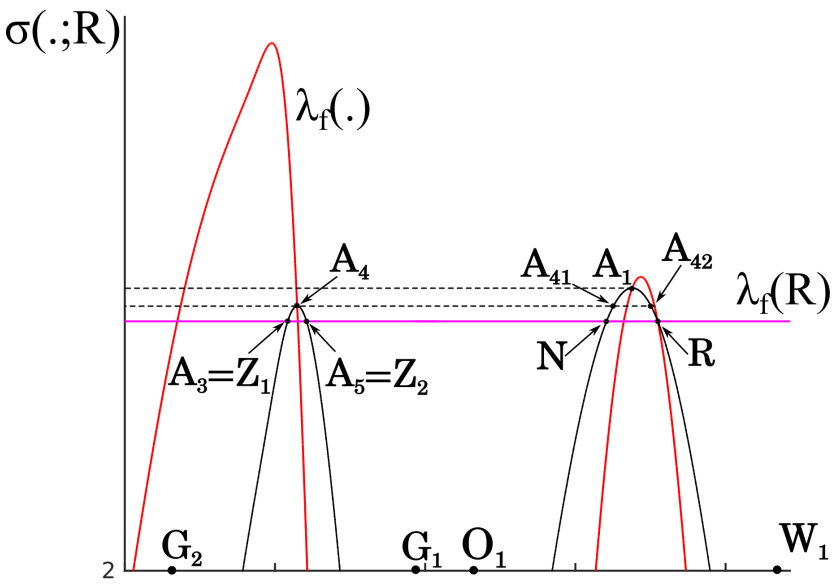

Figure 6.27: Schematic speed diagrams comparing the branches $[O_1, W_1]$ and $[G_2, G_1]$ of $\mathcal{H}(R)$ given in Figure 6.25(b). The state N in the intersection of $[O_1, W_1]$ with $[G, D]$. Black curves are the shock speed $\sigma(M, R)$ with M varying along the Hugoniot branches $[O_1, W_1]$ and $[G_2, G_1]$. States on the same horizontal dashed line satisfy the triple shock rule. The magenta line is the fast characteristic speed, $\lambda_f(R)$. The curve that represent $\lambda_s(.)$ does not appear because its speeds are small.

inadmissible.

Second, we study case (c). It is clear that the segment $[Z_1, A_3]$ is not admissible by Claim 2.7.2 (see Figure 6.26)(c)). On the other hand, the speed diagram comparing the branches $[G_1, G_2]$ and $[O_1, W_1]$ of $\mathcal{H}(R)$ in this case is similar to the one in Figure 6.27 and only differs of case (b) in that Z_1 and Z_2 do not coincide with A_3 and A_5 which implies that the horizontal line that represents their shock speed intersects the black curves above the pink line and under the line that represents the speed of shock between R and A_4, see Figure 6.27. Therefore, we have the same situation of five equilbria as in case (c): $M \in [Z_1, A_4]$, $M_1 \in [A_4, Z_2]$, $M_2 \in [N, A_{41}]$, $M_3 \in [A_{42}, R]$ and R such that the attractor M_2 and the saddle M_3 make it impossible for the discontinuities on $[Z_1, A_4]$ to be admissible. The proof of case (a) is similar to cases (b) and (c). ∎

Claim 6.4.16. *The fast backward wave curve for a state $R \in \mathscr{R}_{5'}$ possesses a local branch with the following wave structure (refer to Figure 6.28):*

(i) Lax f-shock segment $(R, A_1]$ with $\sigma(A_1; R) = \lambda_f(A_1)$;

(ii) backward f-rarefaction segment $[R, W]$;

(iii) backward f-rarefaction segment $(A_1, O]$.

It also possesses a nonlocal branch with the following wave structure:

(iv) backward f-composite segment $[M_2', P_1')$ corresponding to $[M_2, P_1)$;

(v) backward f-rarefaction segment $[P_1', G]$, with $\sigma(P_1; P_1') = \lambda_f(P_1) = \lambda_f(P_1')$.

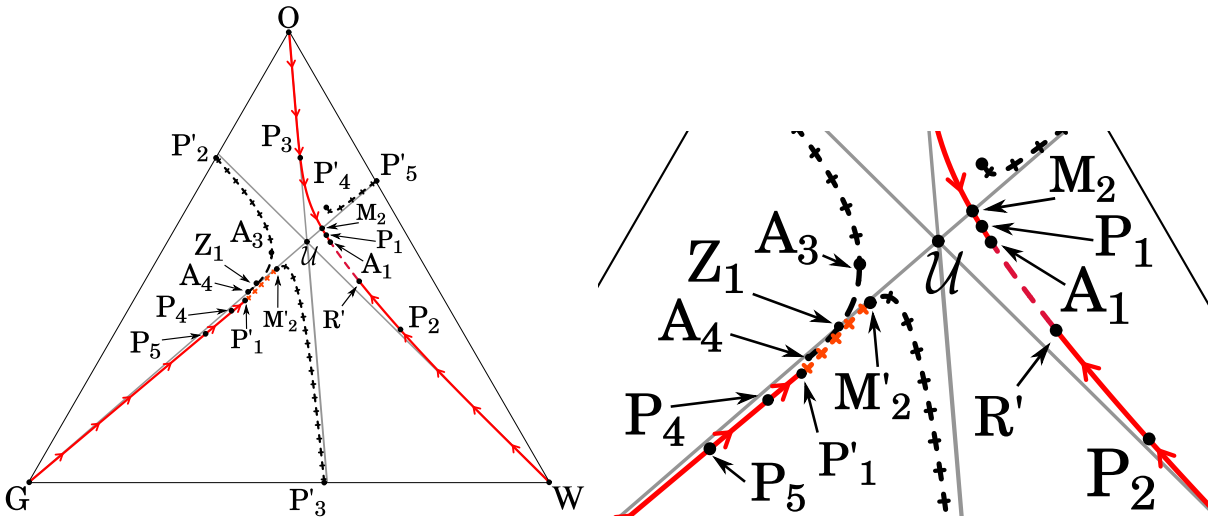

(a) $\mathcal{W}_f^-(R)$ for $R \in R_{5'}$ (b) Zoom of area close to segment of Lax f-shocks $[A_3, A_4]$.

Figure 6.28: (a) Backward f-wave curve $\mathcal{W}_f^-(R)$ for $R \in \mathscr{R}_{5'}$. Continuous lines are f-rarefaction segments, dashed lines are Lax f-shock segments and crossed lines are f-composite segments . The black crossed curves $(M_2', P_3']$, $[P_2', A_3]$ and $[P_4', P_5']$ are inadmissible f-composite waves corresponding to f-rarefaction segments $[M_2, P_3]$, $[P_2, A_1]$ and $[P_4, P_5]$ respectively. The black dashed segment $[A_3, A_4]$ of Lax f-shocks is inadmissible. Notice that the local branch of $\mathcal{W}_f^-(R)$ intersects the invariant line $[G, D]$ with a f-rarefaction wave at state M_2; the nonlocal branch starts at the corresponding state $M_2' \in [G, \mathcal{U}]$ with an admissible f-composite wave $[M_2', P_1']$ corresponding to f-rarefaction segment $[M_2, P_1]$. (b) Zoom of region close to segment $[A_3, A_4]$ in (a).

Proof. Similar to the proof of Claim 6.4.11 (see Figure 6.28). ∎

Let us define the region $\mathscr{R}_{6'}$. We move state R across the f-left extension $[\widehat{Y_2}, Y_2^*]$ of the double contact segment $[Y_2, \widehat{Y_2}]$ (or $[H_4^*, Y_2^*]$, considering Remark 6.4.5) without crossing the fast inflection $\mathcal{I}_f$ (see Figure 6.32(b)). Then, we have a top boundary given by the segment $[\mathcal{I}_f^1, \widehat{Y_2}]$ (considering Remark 6.4.5, the top-right boundary is the segment $[H_4^*, Y_2^*]$), see Figures 6.32(b)-(c). We see that if we move R in the direction of segment $[W, \mathcal{U}]$ following the top boundary (or top-right boundary), then $\mathcal{H}(R)$ does not bifurcate until it reaches the invariant segment $[\mathcal{U}, W]$. Hence, this bifurcation line contains the left boundary of $\mathscr{R}_{6'}$. Notice that the Hugoniot curve $\mathcal{H}(R)$ can be considered as a perturbation of the

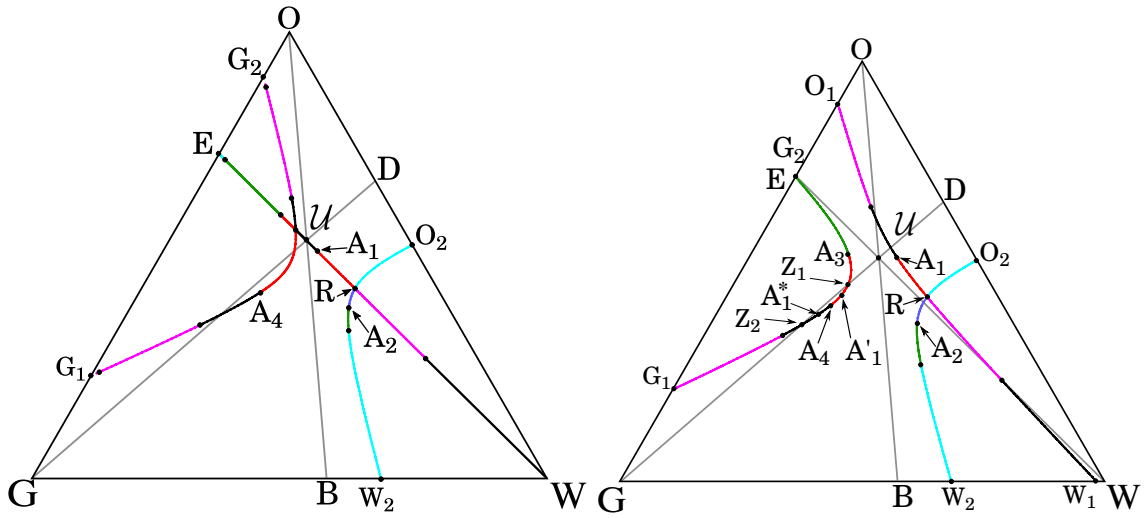

(a) Typical Hugoniot curve for $R \in [E, W]$

(b) Hugoniot curve for $R \in \mathscr{R}_{6'}$

Figure 6.29: (b) Hugoniot curve for R in the region $\mathscr{R}_{6'}$ in area between the right f-extension $E_f^+([\mathcal{U}, D])$ given by the segment $[J_4, J_5]$ and the curve $[E_0, D^*]$, see Figure 6.32(d).

Hugoniot curve for a generic state along the invariant line $[W, E]$ that was obtained explicitly in [3]. It possesses two primary branches, $[O_1, W_1]$ and $[O_2, W_2]$ (which intersect at R), and a nonlocal branch $[G_1, G_2]$ (see Figures 6.29(a)-(b)).

Now, we move R towards vertex W while following the invariant line $[W, E]$. Notice that this nonlocal branch always contains the segment of Lax f-discontinuities $[A_3, A_4]$, and intersects the invariant line $[G, D]$ at states Z_1 and Z_2 such that segment $[Z_1, Z_2]$ is on the same side of $[G, D]$ as R; see Figures 6.29(b) and 6.31(a)-(b). As in the construction of $\mathscr{R}_{4'}$, the bottom boundary of this region is given by segment $[E_0, Y_2^*]$ that is the f-left extension $E_f^-[\mathcal{U}, D]$, with $E_0 \in [W, \mathcal{U}]$ satisfying $\sigma(\mathcal{U}; E_0) = \lambda_f(\mathcal{U})$; see Remark 5.2.3. Therefore, the left boundary of $\mathscr{R}_{6'}$ is the segment $[\mathcal{I}_f^1, E_0]$ (or $[H_4^*, E_0]$, considering Remark 6.4.5) (See Figures 6.32(b)-(c)).

Remark 6.4.9. Observe that before reaching the bottom boundary, we intersect the s-hysteresis $[\mathcal{N}_2, \mathcal{N}_3]$ at which the nonlocal segment of Lax f-discontinuities splits into two segments of f-discontinuities separated by a segment of over-compressive discontinuities. This type of bifurcation was also studied in the construction of the lower $\mathscr{R}_2$ region, see Remark 6.4.3 and Claim 6.4.5. Therefore, we can define a subregion inside of $\mathscr{R}_{6'}$ called $\mathscr{R}_{6'}^H$, limited by the curves $[\mathcal{N}_2, \mathcal{N}_3]$, $[\mathcal{N}_3, E_0]$ and $[E_0, \mathcal{N}_2]$ (see Figure 6.32(b)-(c)).

As seen in the proof of Claim 6.4.15, the right f-extension $[J_4, J_5]$ (see Figure 6.32(d)) of segment $[\mathcal{U}, D]$ crosses the region $\mathscr{R}_{6'}$ producing three possible locations with respect to $[G, D]$ for the nonlocal segment (A_3, A_4) in $[G_1, G_2]$, see Figure 6.26. However, we will see in the next claim that unlike in region $\mathscr{R}_{5'}$, in $\mathscr{R}_{6'}$ a part of (A_3, A_4) is always admissible causing $\mathcal{W}_f^-(R)$ to have a nonlocal Lax f-shock. .

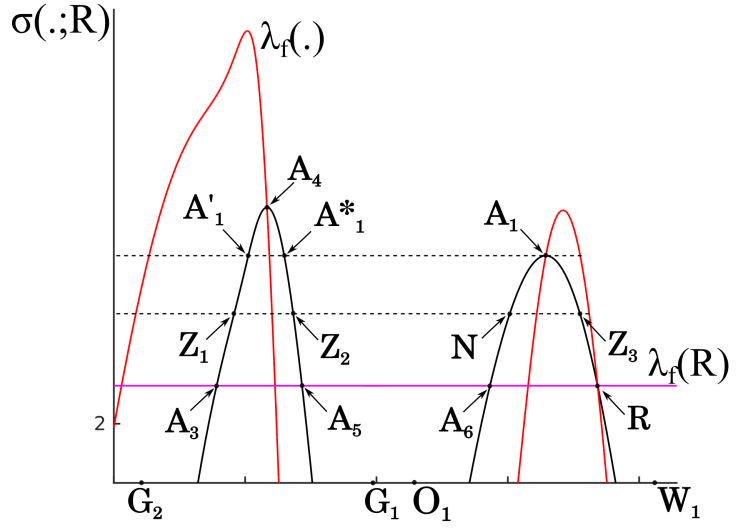

Figure 6.30: Schematic speed diagrams comparing the branches $[O_1, W_1]$ and $[G_2, G_1]$ of $\mathcal{H}(R)$ given in Figure 6.29(b). The state N in the intersection of $[O_1, W_1]$ with $[G, D]$. Black curves are the shock speed $\sigma(M, R)$ with M varying along the Hugoniot branches $[O_1, W_1]$ and $[G_2, G_1]$. States on the same horizontal dashed line satisfy the triple shock rule. The magenta line is the fast characteristic speed, $\lambda_f(R)$. The curve that represent $\lambda_s(.)$ does not appear because its speeds are small.

Claim 6.4.17. *Let R be a state in region $\mathscr{R}_6'$ (see Figure 6.29(b)). In addition to states Z_1 and Z_2 on $[G, D]$, the Hugoniot curve $\mathcal{H}(R)$ possesses states A_1 , A_1', A_1^*, A_3 and A_4 with the following properties:*

(i) States A_1, A_3 and A_4 are Bethe-Wendroff points. They satisfy $\sigma(A_1; R) = \lambda_f(A_1)$, $\sigma(A_4; R) = \lambda_f(A_4)$ and $\sigma(A_3; R) = \lambda_f(R)$.

(ii) If M is a state on either of the branches $[O_1, W_1]$ and $[G_1, G_2]$ of $\mathcal{H}(R)$, the discontinuity joining M to R is a Lax f-shock if M is either on $[A_1, R)$ or on $[A_3, A_4]$. Moreover, this discontinuity is admissible only if $M \in [A_1, R)$ or if $M \in (A_1', A_4]$ with $A_1' \in (A_3, A_4)$.

(iii) States A_1' and $A_1^* \in [A_4, Z_2]$ satisfy $\sigma(A_1; A_1') = \sigma(A_1'; R) = \sigma(A_1^*; R)$. Moreover, $\lambda_f(A_1) = \sigma(A_1; A_1')$ and there is an orbit joining A_1 and A_1'.

Proof. Analogous to the proof of Claims 6.4.12 and 6.4.15 but using Figure 6.30. Notice that for states $M \in (A_1', A_4]$ in Figure 6.30, there are no states M' in the local branch $[O_1, W_1]$ of $\mathcal{H}(R)$ with velocity equal to the shock speed $\sigma(R; A_1)$. As M is a saddle and R is an attractor, for all $M \in (A_1', A_4]$ there is an orbit joining M and R. ∎

Claim 6.4.18. *The fast backward wave curve for a state $R \in \mathscr{R}_{6'}$ possesses a local branch with the following wave structure (refer to Figure 6.31):*

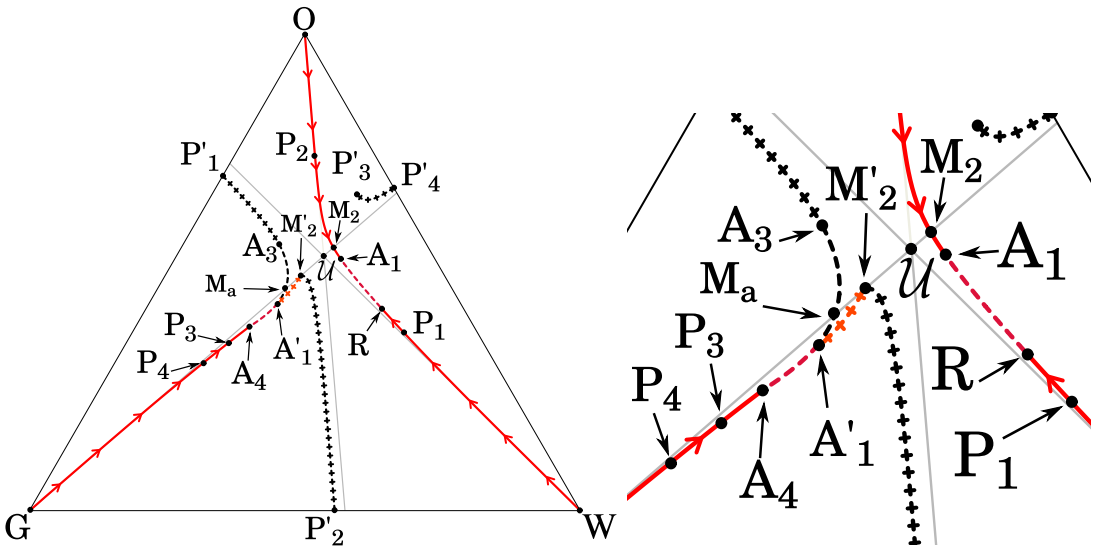

(a) $\mathcal{W}_f^-(R)$ for $R \in R_{6'}$

(b) Zoom of area close to segment of Lax f-shocks $[A_1', A_4]$.

Figure 6.31: (a) Backward f-wave curve $\mathcal{W}_f^-(R)$ for $R \in \mathscr{R}_{6'}$. Continuous lines are f-rarefaction segments, dashed lines are Lax f-shock segments and crossed lines are f-composite segments . The black crossed curves $(M_2', P_2']$, $[P_1', A_3]$ and $[P_3', P_4']$ are not admissible f-composite waves corresponding to f-rarefaction segments $[M_2, P_2]$, $[P_1, R]$ and $[P_3, P_4]$ respectively. The black dashes segment $[A_3, M_a, A_1')$ of Lax f-shock is inadmissible. Notice that the local branch of $\mathcal{W}_f^-(R)$ intersects the invariant line $[G, D]$ with a f-rarefaction wave at state M_2; the nonlocal branch starts in the corresponding state $M_2' \in [G, \mathcal{U}]$ with an admissible f-composite wave $[M_2', P_1']$ corresponding to f-rarefaction segment $[M_2, P_1]$. (b) Zoom of region close to segment $[A_3, A_1', A_4]$ in (a).

(i) Lax f-shock segment $(R, A_1]$ with $\sigma(R; A_1) = \lambda_f(A_1)$;

(ii) backward f-rarefaction segment $[R, W]$;

(iii) backward f-rarefaction segment $(A_1, O]$.

It also has a nonlocal branch with the following wave structure:

(iv) backward f-composite segment $[M_2', A_1']$ corresponding to $[M_2, A_1]$, with $\sigma(A_1; A_1') = \sigma(A_1; R)$;

(v) Lax f-shock segment $(A_1', A_4]$;

(vi) backward f-rarefaction segment $[A_4, G]$, with $\sigma(A_4; R) = \lambda_f(A_4)$.

Proof. Similar to the proof of Claim 6.4.13 (see Figure 6.31(b)). ∎

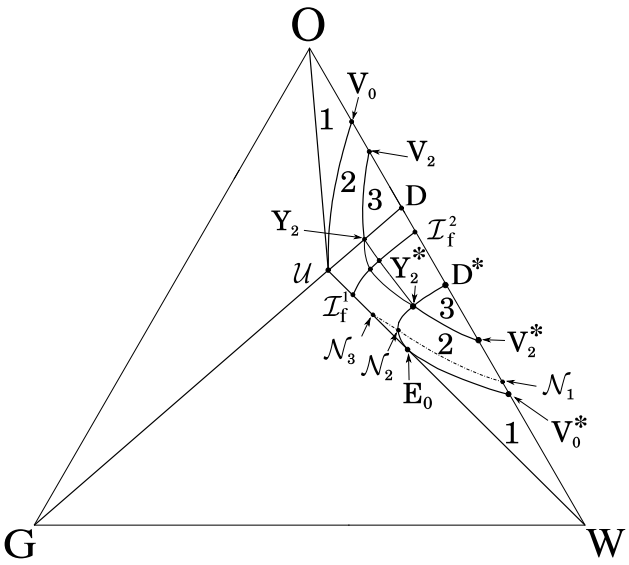

(a) Subdivisions of $\mathcal{FR}_D$ into lower and upper regions $\mathscr{R}_1, \mathscr{R}_2$ and $\mathscr{R}_3$.

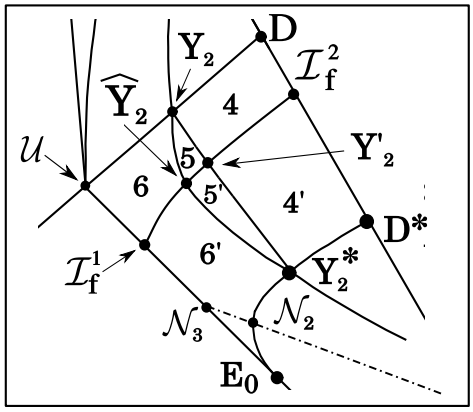

(b) Highlight of regions $\mathscr{R}_i$ for $i \in \{4, 4', 5, 5', 6, 6'\}$.

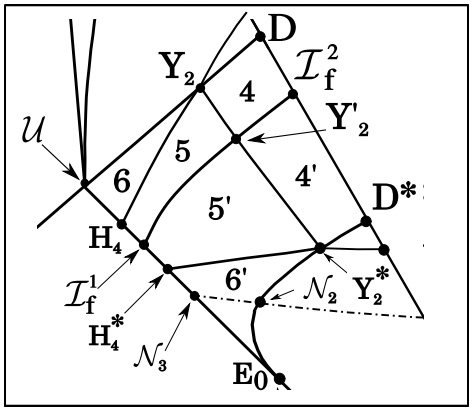

(c) Highlight of regions $\mathscr{R}_i$ for $i \in \{4, 4', 5, 5', 6, 6'\}$ in the case of Remark 6.4.5.

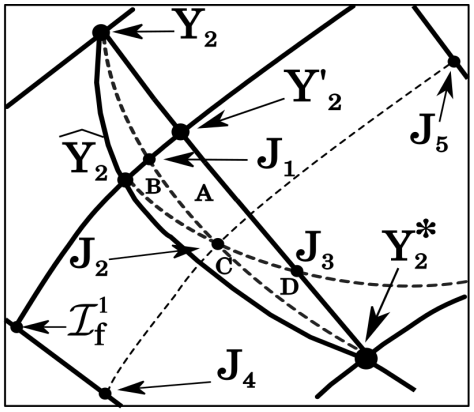

(d) Highlight of regions $\mathscr{R}_i$ for $i \in \{5, 5', 6'\}$ associated to Claim 6.4.15.

Figure 6.32: Subdivisions of $\mathcal{FR}_D$ in $\mathscr{R}$-regions for $1 < \nu_G < 8$ and $\mathcal{U} \in II_O$.

6.4.4 Behavior of subregions $\mathscr{R}$ for $\nu_G > 8$

As seen in Section 5.3, the existence of some points inside the saturation triangle with umbilic point $\mathcal{U}$ of type II depends on the values of ν_Γ. Without loss of generality, we consider only the macro region $\mathcal{FR}_D$. In Section 6.4.1, Figures 6.6(a) and 6.9(a), we built region $\mathscr{R}_1$ by taking states along the invariant segment $[\mathcal{U}, D]$ and obtained two regions: an upper region $\mathscr{R}_1$ with boundaries $[O,\mathcal{U}]$, $[\mathcal{U}, V_0]$

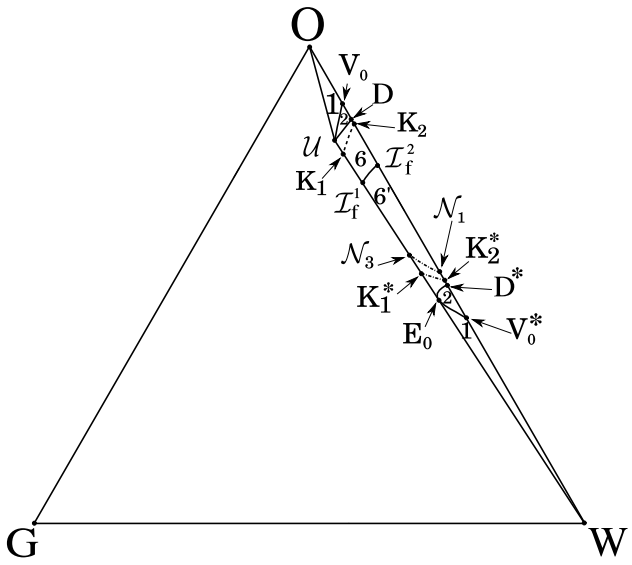

Figure 6.33: Subdivisions of $\mathcal{FR}_D$ in $\mathscr{R}$-regions for $(\nu_G^-)^2/\nu_G > 8$ and $\mathcal{U} \in II_O$. Notice that remain the regions $\mathscr{R}_i$ for $i \in \{1, 2, 6, 6'\}$.

and $[V_0, O]$, and a lower region $\mathscr{R}_1$ with boundaries $[W, E_0]$, $[E_0, V_0^*]$ and $[V_0^*, W]$. When $\mathcal{U}$ approaches the edge $[O, W]$, the region $\mathscr{R}_1$ vanishes. This occurs in the limit cases of $\mu_g \to 0$ or $\mu_o \to \infty$, which corresponds respectively to $\mathcal{U} \to D$ or $\mathcal{U} \to O$. Moreover, these limits also cause region $\mathcal{FR}_D$ to disappear. In other words, the existence of regions $\mathscr{R}_1$ is strongly connected to the existence of $\mathcal{FR}_D$, so $\mathscr{R}_1$ exists whenever $\mathcal{FR}_D$ exists.

In Sections 6.4.2 and 6.4.3, we saw that the existence of regions $\mathscr{R}_3$ (upper and lower), $\mathscr{R}_4$ and $\mathscr{R}_{4'}$ inside of $\mathcal{FR}_D$ depends on the fast double contact states Y_2 and $\mathcal{Y}_2$ (see Figure 6.32). We conclude from Lemma 5.3.2 that these regions do not exist when $\nu_G \geq 8$. As seen in Remark 5.2.2, even if Y_2 leaves the saturation triangle, it is still possible that regions $\mathscr{R}_5$ and $\mathscr{R}_{5'}$ exist. For these regions to disappear, it is necessary that state $\widehat{Y_2}$ be outside of the saturation triangle, see Figure 6.33(b). Another interesting scenario occurs when $\nu_G \leq 1$, and it is associated with the disappearance of the admissible branch of the fast double contact $[Y_2, \widehat{Y_2}]$ (or $[Y_2, H_4]$). Indeed, as ν_G tends to one, $\mathcal{Y}_2$ tends to Y_2 and $\mathcal{U}$ tends to the boundary of $\mathcal{T}_{\mathcal{U}}$ (straight line $s_w + s_o = 1/2$); these three states collapse to $\mathcal{U}$ at $\nu_G = 1$ (see Definition 3.3.6 and Lemma 5.3.2). Hence, regions $\mathscr{R}_i$ for $i \in \{5, 5', 6, 6'\}$ become smaller as ν_G tends to one, and collapse to the invariant line $[W, E]$ when $\nu_G = 1$. The case $\nu_G < 1$ will be studied in Sections 6.4.5.

Notice that, when two viscosities are equal, the fast inflection $\mathcal{I}_2$ coincides with segment $[\mathcal{U}, D]$. Therefore regions $\mathscr{R}_i$ with $i \in \{4, 5, 6, 4', 5,' 6'\}$ disappear and, by symmetry, the upper and lower parts of fast macro region $\mathcal{FR}_D$ are equal. These situations correspond to cases when $\nu_G < 1$ or when $\mathcal{U}$ is of type I.

6.4.5 Behavior of subregions $\mathscr{R}$ for $\nu_G \leq 1$ and $\mathcal{U} \in II_G$

As seen in Corollary 5.3.1, $\nu_\Gamma < 1$ if and only if $\mathcal{U}$ is type II_Γ. In this work, we study the fast macro region $\mathcal{FR}_D$ with $\mathcal{U}$ of type II_G. In this regime, there are regions where the backward fast wave curves behave in the same way as those in case $\nu_G > 1$. Therefore, these wave curves $\mathcal{W}_f^-(R)$ and their associated $\mathscr{R}$-regions are constructed in the same way as in Sections 6.4.2 and 6.4.3 with small modifications to some boundaries. Specifically, this is done for regions $\mathscr{R}_1, \mathscr{R}_2$ and $\mathscr{R}_3$, and also for regions $\mathscr{R}_4$ and $\mathscr{R}_{4'}$ when $\mu_w \neq \mu_o$. The main differences with respect to the case $\nu_G > 1$ are:

1. The fast inflection locus has two components (branches) inside this macro region ($\mathcal{FR}_D$) (three in the case of $\mu_w = \mu_o$), causing the analysis of f-rarefactions to grow in complexity. One of the components of the fast inflection is an oval section that passes through the umbilic point and intersects the segment $[\mathcal{U}, O]$ (see Section 4.5 and Figure 6.34(b)).

2. We know from [20] that the hysteresis locus, the inflection locus and an eigendirection field are all tangent to each other at certain points. The fast inflection has two separate branches: the oval part $[\mathcal{U}, \mathcal{I}_f^3]$ and the curve $[\mathcal{I}_f^1, \mathcal{I}_f^2]$, where $\mathcal{I}_f^3$ is the intersection between segment $[\mathcal{U}, O]$ and the fast inflection locus. The f-eigendirection field is tangent to $\mathcal{I}_2$ at $\mathcal{I}_T$, which belongs to the fast inflection $[\mathcal{U}, \mathcal{I}_f^3]$ (see Figure 6.34(b)).

3. The f-hysteresis locus (or f-left-extension of $[\mathcal{U}, \mathcal{I}_f^3]$) plays an important role in the division of segments of Lax f-shocks. But it may also lead to complex combinations of shock, rarefaction and composite segments in the local branch of $\mathcal{W}_f^-$ at some regions.

4. As seen in Lemma 5.3.2, states $\mathcal{Y}_2$ and Y_2 no longer exist along the invariant line $[G, D]$, hence regions $\mathscr{R}_i$ with $i \in \{5, 5'6, 6'\}$ disappear. But other parts of the fast double contact locus are involved in this region. Moreover, for some combinations of μ_w, μ_o and μ_g, it is possible to have more than one branch (and its corresponding branch) of the fast double contact locus in this region.

5. The state $\mathcal{I}_T$ belongs to the fast double contact locus (corresponding to itself).

There are other special points that define some boundaries in this regime. Consider the fast integral curve that passes through $\mathcal{I}_T \in [\mathcal{U}, \mathcal{I}_3^f]$ and intersects the invariant line $[G, D]$, we call this intersection K_0. The backward f-rarefaction segment $[K_0, \mathcal{I}_T]$ and the forward f-rarefaction segment $[K_0, K_0']$, with K_0' in fast inflection $[\mathcal{I}_f^1, \mathcal{I}_f^2]$, are the boundaries that limit backward f-rarefaction segment for states upon the fast inflection $[\mathcal{I}_f^1, \mathcal{I}_f^2]$ (see Figure 6.34(b)).

From Theorem 5.4.3 and Remark 5.4.1 of Section 5.4, we conclude that transitional shocks connecting states M_1 and M_2 are only possible in this regime when $M_1 \in [G, \mathcal{U}]$ and $M_2 \in [D_0, D]$. The state D_0 was defined in (5.26), and it always lies on the boundary of $\mathcal{T}_\mathcal{U}$ that separates regions of type I and II. Moreover, when $\nu_G = 1$, we see that $\mathcal{U} = D_0 = 1/2$. Figure 6.34(a) shows the Hugoniot curve from D_0; the importance of this state is that D_0 defines the boundary that separates regions that use transitional shocks from those that use transitional rarefactions. This boundary is the forward f-wave curve from D_0, ($\mathcal{W}_f^+(D_0)$) which is the last wave curve that we can use after a transitional wave.

The difficulty in describing $\mathcal{W}_f^+(D_0)$ is that it can change due to the relative position of K_0 and D_0 with respect to $\mathcal{U}$. When ν_G is close but less than one, $\mathcal{U}$ is close to D_0 and $D_0 \in (\mathcal{U}, K_0) \subset (\mathcal{U}, D)$; but

as we decrease ν_G, $\mathcal{U}$ moves away from D_0 (which is fixed on $[G, D]$), until D_0 and K_0 change position, with $K_0 \in (\mathcal{U}, D_0) \subset (\mathcal{U}, D)$. In this work we consider only the case when K_0 is not close to D_0 and we describe only the $\mathscr{R}$-regions that use transitional waves. In next section we describe these regions.

6.4.5.1 Subregions $\mathscr{R}_i$ with $i \in \{1, 2, 3, 4, 4'\}$

The construction of the boundary for the region $\mathscr{R}_1$ in this case ($\nu_G < 1$) is similar to the case $\nu_G > 1$. These cases differ in where the curve which separates $\mathscr{R}_1$ from $\mathscr{R}_2$ end: for $\nu_G > 1$ it ends at $\mathcal{U}$, whereas when $\nu_G \leq 1$ it ends at B_0. In both cases, this boundary begins at $V_0 \in [W, O]$. This follows from the fact that in the construction of this boundary (see Section 6.3.1), the last state along $[\mathcal{U}, D]$ to which we can apply the triple shock rule 2.4.3 with a state on $[G, \mathcal{U}]$ is the state D_0.

Recall that states $D_0 \in [G, D]$ and $\mathcal{U}$ satisfy $\sigma(\mathcal{U}; D_0) = \lambda_s(\mathcal{U}) = \lambda_f(\mathcal{U})$ and that the Hugoniot curve $\mathcal{H}(D_0)$ (found explicitly) intersects segments $[O, \mathcal{U}]$ and $[W, \mathcal{U}]$ at states B_0 and E_0 (see Figure 6.34(a)). Then, by the triple shock rule 2.4.3 we have $\sigma(D_0; \mathcal{U}) = \sigma(E_0; \mathcal{U}) = \sigma(B_0; \mathcal{U})$ and conclude that the boundary which separates the upper regions $\mathscr{R}_1$ and $\mathscr{R}_2$ is the curve $[V_0, B_0]$ (for lower regions, the boundary is $[V_0^*, E_0]$). Using the same argument, we see that the upper boundary that separate the regions $\mathscr{R}_2$ and $\mathscr{R}_3$ is the curve $[V_2, B_0]$ (for lower region, the boundary is $[V_2^*, B_0]$) and that the upper boundary for loss of admissibility of nonlocal shocks inside of $\mathscr{R}_2$ is the curve $[V_1, E_0]$ (for lower regions, it is $[V_1^*, B_0]$)(see Figure 6.34(b)).

For the upper region $\mathscr{R}_3$ the left and bottom boundaries are the f-shock segment $[D_0, B_0]$ of $\mathcal{H}(D_0)$ and the segment $[D_0, D]$. For the lower region $\mathscr{R}_3$ the left boundary is the f-shock segment $[Y_0, E_0]$ of $\mathcal{H}(D_0)$ and the top boundary is the same boundary as in case $\nu_G > 1$, namely the right f-extension of $[D_0, D](E_f^+([D_0, D]))$ given by the curve $[Y_0', D^*]$ (see Figure 6.34(b)).

The construction of the regions $\mathscr{R}_4$ and $\mathscr{R}_{4'}$ is similar to when $\nu_G > 1$. They lie below segment $[\mathcal{U}, D]$ and exist when one of the fast inflection loci does not coincide with this segment. As seen in Sections 6.4.2 and 6.4.3, the top and bottom boundaries for these regions are: segment $[\mathcal{U}, D]$ and the fast inflection $\mathcal{I}_2$ for $\mathscr{R}_4$; the fast inflection $\mathcal{I}_2$ and $E_f^+([\mathcal{U}, D])$ for $\mathscr{R}_{4'}$. Since D_0 is the last state in $[\mathcal{U}, D]$ that can join a transitional wave to a fast shock, the left boundaries for $\mathscr{R}_4$ and $\mathscr{R}_4'$ must be the f-rarefaction curve $[D_0, Y_0]$ and f-composite curve from $[Y_0, Y_0']$, see Figure 6.34(b).

Remark 6.4.10. In conclusion, backward fast wave curves $\mathcal{W}_f^-(R)$, for right states R in regions $\mathscr{R}_i$ with $i \in \{1, 2, 3, 4, 4'\}$ of $\mathcal{FR}_D$, with umbilic point being of type II_G and $\nu_G < 1$ satisfy Claims 6.4.2, 6.4.4, 6.4.7 6.4.9 and 6.4.14.

Remark 6.4.11. As in the case when $\nu_G > 1$ and $\mathcal{U}$ is of type II, for $0 < \nu_G < 1$, there is a curve of s-hysteresis inside regions $\mathscr{R}_2$ that defines the region $\mathscr{R}_2^H$ as in Claim 6.4.5, but in this case the curve ends at E_0 and it is given by the segment $[E_0, \mathcal{N}_1]$ (see Figure 6.34). This is because the slow inflection locus ends in $\mathcal{U}$ (see Section 4.5).

Remark 6.4.12. In the case of two equal viscosities, Matos *et al.* show in [31] Riemann solutions for left states in a neighborhood of the umbilic point and right states in almost the whole saturation triangle.

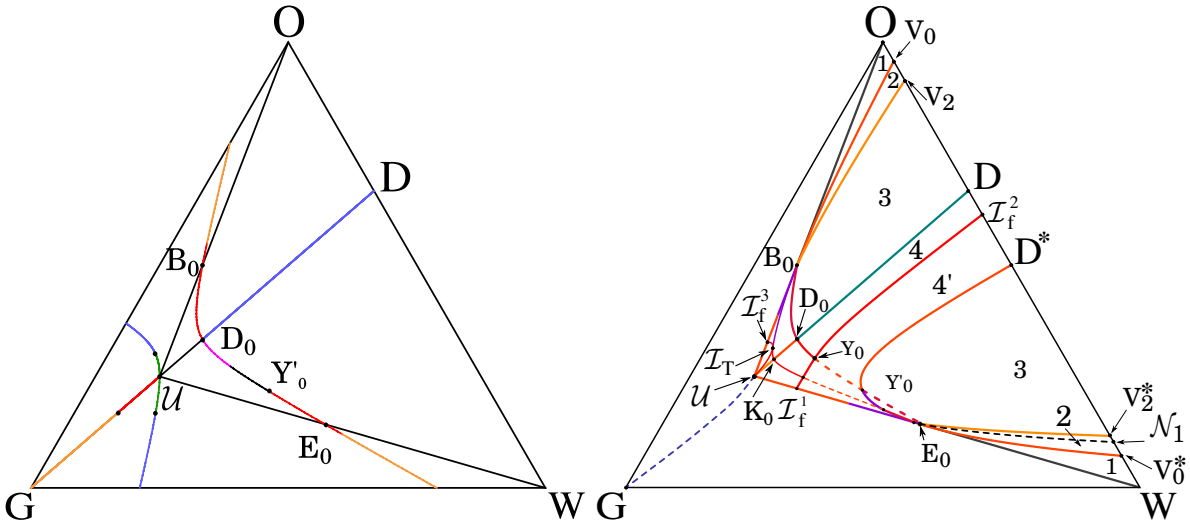

(a) Hugoniot curve for $D_0 \in [G, D]$. The states B_0 and E_0 also are extension of $\mathcal{U}$, see Remark 5.2.3.

(b) Subdivisions of $\mathcal{FR}_D$ into lower and upper regions $\mathscr{R}_1, \mathscr{R}_2$, $\mathscr{R}_3$, $\mathscr{R}_4$ and $\mathscr{R}'_4$. The curve (blue) is part of the slow inflection locus and the curve (violet) $[\mathcal{I}_T, B_0]$ is the $E_f^-([\mathcal{U}, \mathcal{I}_T])$, with $[\mathcal{U}, \mathcal{I}_T]$ is part of the fast inflection locus.

Figure 6.34: Subdivision of $\mathcal{FR}_D$ for $\nu_G < 1$ and $\mathcal{U} \in II_G$. Delta wing region limited by $[\mathcal{U}, E_0], [E_0, D_0], [D_0, B_0]$ and $[B_0, \mathcal{U}]$. The dashed curve $[G, \mathcal{U}]$ is part of the slow inflection loci.

6.4.5.2 Delta wing region

We name "delta wing" the region enclosed by $(B_0, D_0, E_0, \mathcal{U})$ in Figure 6.34. When K_0 (defined in Section 6.4.5) and D_0 are not close, $[D_0, B_0]$ is a Lax f-shock segment, $[D_0, Y_0]$ is a forward f-rarefaction segment, $[Y_0, Y_0']$ is a forward f-composite segment associated to $[D_0, Y_0]$ and $[Y_0', E_0]$ is a Lax f-shock segment along $\mathcal{H}(D_0)$, see Section 6.4.5.1. Notice that in the presence of the f-inflection segment $[\mathcal{U}, I_f^3]$, new bifurcation appears that were not present when $\nu_G > 1$. The interaction between the two f-inflection curves, the fast double contact and the f-hysteresis loci was studied in [31] in the case of two equal viscosities and umbilic point varying between $\mathcal{T}_{\mathcal{U}}$ and II_O. Since our present focus is on $\mathcal{U}$ of type II and this interaction between bifurcation manifolds also appears in cases where $\mathcal{U}$ is of type I, we leave the study of these delta $\mathscr{R}$-regions to future work.

6.4.6 Influence of mixed double contact in subregions $\mathscr{R}_i$ of macro regions $\mathcal{FR}_D$ for $\mathcal{U}$ of type II

As seen in Section 4.4 the mixed double contact only exists when the umbilic point is of type II. Though in this model we do not have admissible discontinuities between pairs of states belonging to the mixed double contact locus, this bifurcation locus plays a relevant role when we want to describe solutions of the Riemann problem; specifically, when characterizing the $\mathscr{L}_{\mathscr{R}}$-regions that depend on the $\mathscr{R}$-regions. This procedure will be explained in Chapter 8.

Inside $\mathscr{R}_i$, with $i \in \{6, 6'\}$, the mixed double contact locus subdivides some regions where the backward fast wave curves do not change but the way to reach the state R by slow or transitional wave curves changes (see Figure 6.35). This subdivision is based on the presence of a portion of mixed double contact locus and the state Y_1 that lies on invariant line $[G, D]$. In Lemma 5.3.3 of Section 5.3 it was shown that Y_1 remains inside the saturation triangle when $\frac{(\nu_G^-)^2}{\nu_G} \leq 8$. In case of Remark 6.4.5, the regions $\mathscr{R}_5$ and $\mathscr{R}_{5'}$ are also influenced by this mixed double contact locus. From state Y_1 we generate the following boundaries (see Figure 6.35):

a) the segment $[Y_1, K_1]$ that is part of the mixed double contact locus;

b) the forward f-rarefaction $[Y_1, Y_1']$ and its associated f-composite segment $[Y_1', Y_1^*]$;

c) the left f-extension of $[Y_1, K_1]$, $E_f^-([Y_1, K_1]) = [Y_1^*, K_1^*]$

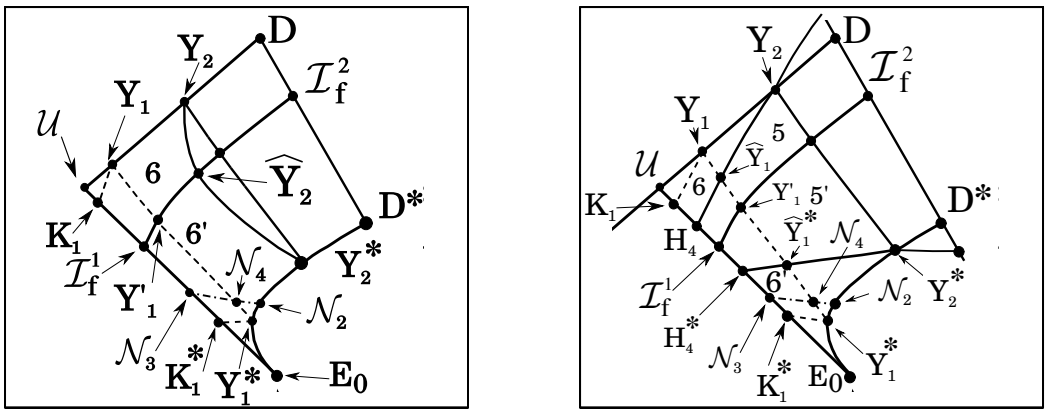

(a) Highlight of regions $\mathscr{R}_i$ for $i \in \{6, 6'\}$ affected by the presence of the mixed double contact locus.

(b) Highlight of regions $\mathscr{R}_i$ for $i \in \{5, 5', 6, 6'\}$ affected by the presence of the mixed double contact locus, in the case of Remark 6.4.5.

Figure 6.35: Subdivisions of regions $\mathscr{R}_6$ and $\mathscr{R}_{6'}$ in presence of the mixed double contact locus. Notice that in (b) the f-rarefaction segment $[Y_1, Y_1']$ and the f-composite segment $[Y_1', Y_1^*]$ also cross the regions $\mathscr{R}_5$ and $\mathscr{R}_{5'}$ then they are affected by the mixed double contact, see Remark 8.4.10.

Notice that the left s-extension of the slow inflection locus $[\mathcal{N}_2, \mathcal{N}_3]$ that defined the region $\mathscr{R}_{6'}^H$ (see Remark 6.4.9) intersects the f-composite curve $[Y_1', Y_1^*]$ at state $\mathcal{N}_4$, producing an area of $\mathscr{R}_{6'}^H$ that is not affected by the mixed double contact locus.

6.5 Final considerations

Following the discussion in this chapter, we present some conclusions about the backward f-wave curves for R in $\mathcal{FR}_D$ and umbilic point of type II. We verified numerically that the local branch of $\mathcal{W}_f^-(R)$

for $R \in \mathcal{FR}_D$ crosses the invariant segment $[\mathcal{U}, D]$ at a single point and satisfies the following result:

Claim 6.5.1. *The local branch of any fast backward wave curve $\mathcal{W}_f^-(R)$ for states R inside region $\mathcal{FR}_i$ with $i \in \{E, B, D\}$ remains totally contained within the same region.*

We conclude that for any R in regions $\mathscr{R}_i$ for $i \in \{1, 2, 3\}$ the intersection between the invariant segment $[\mathcal{U}, D]$ and the local branch of $\mathcal{W}_f^-(R)$ happens at a state corresponding to a fast shock with R. However, for any R in regions $\mathscr{R}_i$ for $i \in \{4, 4', 5, 5'6, 6'\}$, the intersection between the invariant segment $[\mathcal{U}, D]$ and the local branch of $\mathcal{W}_f^-(R)$ occurs on a rarefaction segment.

On the other hand, notice that $\mathcal{W}_f^-(R)$ has the same structure for R in region $\mathscr{R}_3$ and $\mathscr{R}_4$, even though regions $\mathscr{R}_3$ and $\mathscr{R}_4$ (or lower region $\mathscr{R}_3$ and $\mathscr{R}_{4'}$) are separated by the invariant segment $[\mathcal{U}, D]$ (or by the segment $[Y_2^*, D^*]$). However, considering the solution of Riemann problems it is better to consider them as distinct regions (see Chapter 8). Finally, we have an analogous result for the local branch of forward s-wave curves:

Claim 6.5.2. *The local branch of any slow forward wave curve $\mathcal{W}_s^+(L)$ for states L inside region $\mathcal{SR}_i$ with $i \in \{G, W, O\}$ remains totally contained within the same region.*

Chapter 7

The surface of transitional shocks: case $\mathcal{B}(U) = I$

In this chapter, we present the solutions of Riemann problems which involve transitional shocks constructed in a three dimensional phase space: besides two coordinates in the saturation triangle, we add as a third coordinate the shock speed (or characteristic speed, depending on the elementary wave). In this setting, we define the surface of transitional shocks when $\mathcal{B}(U)$ is a multiple of the identity matrix and study its construction. For each invariant line, we have a pair of planes (domain and codomain) orthogonal to the saturation triangle, which contain all transitional shocks that involve this secondary bifurcation. In this three dimensional phase space, we also construct the wave curves associated to each family and show solutions to Riemann problems for umbilic points of type II and arbitrary left and right states.

7.1 Transitional boundaries

We begin by presenting the nomenclature for our study of wave curves in the three dimensional phase space. We write a point in the three dimensional phase space as $(s_w, s_o, v) \in T \times \mathbb{R}^+$, with (s_w, s_o) in the saturation triangle T (see Definition 3.39) and v a speed; see Figure 7.1(a). In principle, a state $M \in T$ ($M = (M_w, M_o)$) has two associated characteristic speeds $\lambda_s(M)$ and $\lambda_f(M)$ which are equal only at $\mathcal{U}$, but when a state M belongs to an i-rarefaction, v represents the characteristic speed associated to the i-th family and the coordinates in the new phase space are $(M_w, M_o, \lambda_i(M))$, or simply $(M, \lambda_i(M))$. When there is a discontinuity between two states M and N, the speed associated to both states is the shock speed $\sigma = \sigma(M; N)$; then their coordinates are (M_w, M_o, σ) and (N_w, N_o, σ). In the case of a Hugoniot locus $\mathcal{H}(R)$, the center state R does not have an associated shock speed. We denote $\{(M_1, \sigma_1), (M_2, \sigma_2)\} \subset T \times \mathbb{R}^+$ the segment of curve that joins the points (M_1, σ_1) and (M_2, σ_2) belonging to $T \times \mathbb{R}^+$.

Recall that a shock wave between states U_l and U_r with $\sigma_T = \sigma(U_l; U_r)$ is classified as being transitional (for the assumed viscosity matrix $\mathcal{B}(U)$) provided that:

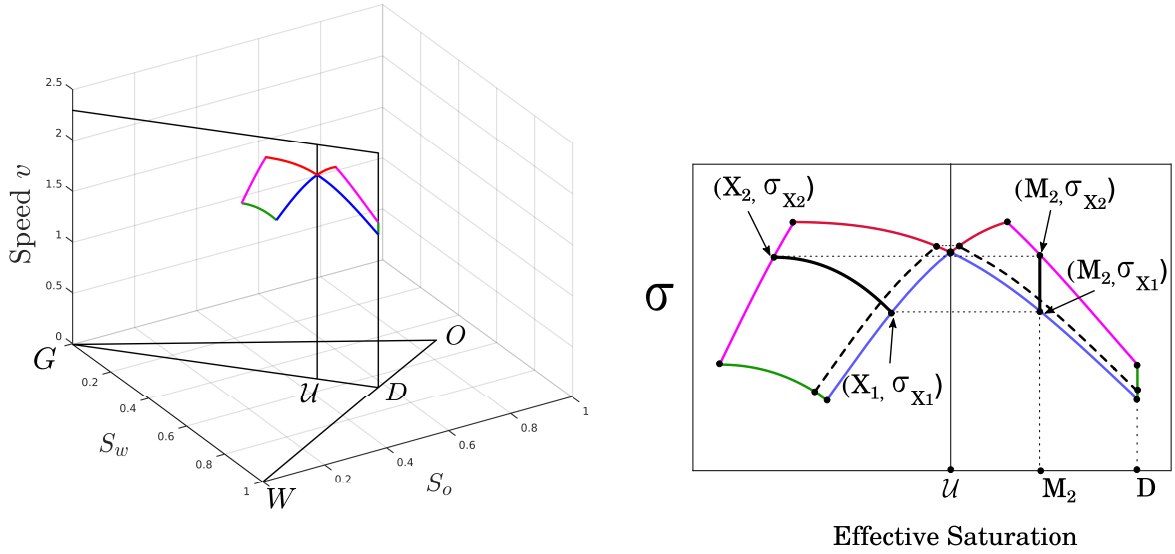

(a) Three dimensional phase space $T \times \mathbb{R}^+$ and orthonormal plane associated to invariant line $[G, D]$.

(b) Boundaries of the transitional plane (surface of transitional shocks) for the case $1 < \nu_G \leq 8$.

Figure 7.1: The surface of transitional shocks for the case $\mathcal{B}(U) = I$. (a) Representation of the invariant planes $[G, \mathcal{U}] \times \mathbb{R}^+$ and $[\mathcal{U}, D] \times \mathbb{R}^+$, see Definition 7.1.2. (b) Representation of the inverse transitional map for $M_2 \in [\mathcal{U}, D]$ and transitional segment $[X_2(M_2), X_1(M_2)]$ as objects in the three dimensional phase space. The horizontal axis corresponds to a parametrization of $[G, D]$ in terms of the effective saturation s and the vertical axis is the shock speed, see Remark 5.1.1.

(a) both U_l and U_r are saddle points for the associated traveling wave solution of the ODE system (2.24);

(b) there is an orbit connecting U_l to U_r (see Definition 2.2.4).

In Section 5.4, we presented the construction of a transitional map in terms of the effective saturation on each invariant line. Given a state M_2 along an invariant line associated to vertex $\Gamma \in \{G, D, W\}$, we compute the transitional segment $(X_2(M_2), X_1(M_2))$ which contains all states M_1 that have a transitional shock with M_2 such that $\sigma(X_1(M_2); M_2) \leq \sigma_T(M_1; M_2) \leq \sigma(X_2(M_2); M_2)$ (see X_1 and X_2 constructed in Theorem 5.4.1). Notice that, in the context of our three dimensional phase space, the transitional map constructs two pairs of curves in $T \times \mathbb{R}^+$: one given by $\{(M_2, \sigma(X_1; M_2)), (M_2, \sigma(X_2; M_2))\}$, and the other by $\{(X_1, \sigma(X_1; M_2)), (X_2, \sigma(X_2; M_2))\}$, see Figure 7.1(b).

Actually, these segments associated to M_2 can be understood as an image/pre-image pair of the transitional map $T^{-1}(M_2)$. The pre-image and image are each contained in a plane (domain and codomain) on which, by varying M_2 and successively computing these images and pre-images using Theorems 5.4.1, 5.4.2 and 5.4.3, we construct the *surface of transitional shocks* for each invariant line. Moreover, due to the triple shock rule 2.4.3, we construct the boundaries of the surface of transitional shocks, using the same procedure as the one used to construct the boundaries of admissibility and compatibility in

Sections 6.3.1-6.3.3. Because of this, we can use the surface of transitional shocks as an organization center to construct solutions of Riemann problems, verifying which left and right states are compatible with transitional shocks.

Now, we define the different types of boundaries for a surface of transitional shocks (*transitional boundaries*), associated to the boundaries of admissibility and compatibility constructed in Sections 6.3.1-6.3.3. Notice that each boundary is associated to one of the end points of the transitional segment $[X_2, X_1]$ constructed from a state M_2 in an invariant segment $[\mathcal{U}, \mathbb{B}]$ with $\mathbb{B} \in \{E, D, B\}$ (see Section 5.4). Then, while varying $M_2 \in [\mathcal{U}, \mathbb{B}]$, we compute the points (M_2, σ_{X_2}) and (M_2, σ_{X_1}) on the domain of transitional boundary, and the points (X_2, σ_{X_2}) and (X_1, σ_{X_1}) on the codomain where $\sigma_{X_i} = \sigma(M_2; X_i),\ i \in \{1, 2\}$ (see Figure 7.1).

Definition 7.1.1. Consider the surface of transitional shocks associated to the invariant line $[\Gamma, \mathbb{B}]$ with $\Gamma \in \{G, W, O\}$ and $\mathbb{B} \in \{D, E, B\}$ respectively. We define

1. the *slow sonic boundary* (SSB) as the set of pairs $(X_1(M_2), \sigma_{X_1})$, (M_2, σ_{X_1}) in $T \times \mathbb{R}^+$ such that there is a slow sonic shock between X_1 and M_2 with $\sigma_{X_1} = \lambda_s(X_1)$, where $X_1 \in (\Gamma,\ \mathcal{U})$, $M_2 \in (\mathcal{U}, \mathbb{B}]$ and $\sigma_{X_1} = \sigma(X_1; M_2)$.

2. the *fast sonic boundary* (FSB) as the set of pairs $(X_2(M_2), \sigma_{X_2})$, (M_2, σ_{X_2}) in $T \times \mathbb{R}^+$ such that there is a fast sonic shock between X_2 and M_2, where $\sigma_{X_2} = \lambda_f(M_2)$ with $X_2 \in (\Gamma,\ \mathcal{U})$, $M_2 \in (\mathcal{U}, \mathbb{B}]$ and $\sigma_{X_2} = \sigma(X_2; M_2)$.

3. the *transitional sonic boundary* (TSB) as the set of pairs $(X_2(M_2), \sigma_{X_2})$, (M_2, σ_{X_2}) in $T \times \mathbb{R}^+$ such that there is a transitional sonic shock between X_2 and M_2, where $\sigma_{X_2} = \lambda_f(X_2)$with $X_2 \in (\Gamma,\ \mathcal{U})$, $M_2 \in (\mathcal{U}, \mathbb{B})$ and $\sigma_{X_2} = \sigma(X_2; M_2)$.

4. the *genuine transitional boundary* (GTB) as the set of points $(M_1, \sigma(M_1; \mathbb{B}))$ and $(\mathbb{B}, \sigma(M_1; \mathbb{B}))$ in $T \times \mathbb{R}^+$ such that there is a transitional shock between M_1 and $\mathbb{B}$, where $M_1 \in (X_2(\mathbb{B}), X_1(\mathbb{B}))$.

Definition 7.1.2. The transitional map takes a state $M \in [G, \mathcal{U}]$ and maps it to another state $T(M) \in [\mathcal{U}, D]$, such that there is a transitional shock between them with $\sigma_T = \sigma(M; T(M))$. We define the *invariant plane* $[G, \mathcal{U}] \times \mathbb{R}^+$ as the domain and $[\mathcal{U}, D] \times \mathbb{R}^+$ as the codomain of the surface of transitional shocks. These invariant planes contain the transitional boundaries defined in Definition 7.1.1.

Remark 7.1.3. Notice that SSB is associated to the boundary for loss of compatibility between transitional and fast shocks given in Section 6.3.1, while TSB is associated to the boundary for loss of admissibility of nonlocal shocks given in Section 6.3.3.

In the next lemmas we show the different types of transitional boundaries, which depend on the values of the viscosity ratio ν_G defined in (5.11). We describe the procedure for the invariant line $[G, D]$, since the procedure for the other invariant lines is analogous.

Lemma 7.1.1. *Consider the invariant line $[G, D]$ with viscosity ratio satisfying $1 < \nu_G \leq 8$. Then, the surface of transitional shocks (domain and codomain) associated to the invariant plane corresponding to $[G, D]$ comprises the region bounded by the following curves (refer to Figure 7.2(a)):*

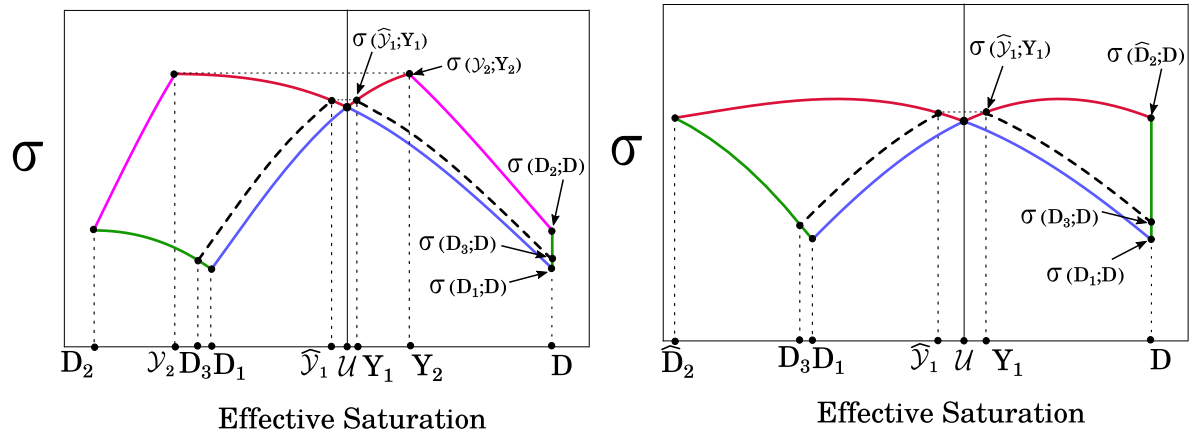

(a) Surface of transitional shocks (domain and codomain) for $[G, D]$, when $1 < \nu_G < 8$.

(b) Surface of transitional shocks (domain and codomain) for $[G, D]$, when $\nu_G > 8$ and $(\nu_G^-)^2/\nu_G \leq 8$.

Figure 7.2: Transitional boundaries given in Definition 7.1.1: The blue curves are SSB, red curves are FSB, magenta curves are TSB and green curves are GTB. The horizontal axis corresponds to a parametrization of $[G, D]$ in terms of the effective saturation s and the vertical axis is the shock speed, see Remark 5.1.1. The dashed curve is associated to the boundary for loss of compatibility of sonic shocks, see Section 6.3 and Remark 7.1.5.

1. *Slow sonic boundary* (SSB)*: with domain defined by the curve* $\{(D_1, \sigma(D; D_1)), (\mathcal{U}, 2)\}$*, and codomain defined by the curve* $\{(D, \sigma(D; D_1)), (\mathcal{U}, 2)\}$.

2. *Fast sonic boundary* (FSB)*: with domain defined by the curve* $\{(\mathcal{Y}_2, \sigma(\mathcal{Y}_2; Y_2)), (\mathcal{U}, 2)\}$*, and codomain defined by the curve* $\{(Y_2, \sigma(\mathcal{Y}_2; Y_2)), (\mathcal{U}, 2)\}$.

3. *Transitional sonic boundary* (TSB)*: with domain defined by the curve* $\{(\mathcal{Y}_2, \sigma(\mathcal{Y}_2; Y_2)), (D_2, \sigma(D; D_2))\}$ *and codomain defined by the curve* $\{(Y_2, \sigma(\mathcal{Y}_2; Y_2)), (D, \sigma(D; D_2))\}$.

4. *Genuine transitional boundary* (GTB)*: with domain defined by the curve* $\{(D_2, \sigma(D; D_2)), (D_1, \sigma(D; D_1))\}$*, and codomain define the curve* $\{(D, \sigma(D; D_2)), (D, \sigma(D; D_1))\}$.

Proof. This characterization of the transitional boundaries follows directly from Definition 7.1.1 and from Theorem 5.4.1. When M_2 varies along segment $(\mathcal{U}, D]$, we compute explicitly the transitional segment $[X_2(M_2), X_1(M_2)]$ that depends on M_2, such that $\sigma(X_1(M_2; M_2)) \leq \sigma_T \leq \sigma(X_1(M_2; M_2))$, which defines the four types of boundaries. ∎

Lemma 7.1.2. *For* $\nu_G > 8$*, let* $\widehat{D_2}$ *be the right* f*-extension of* D *on* $[G, D]$ *such that* $\sigma(\widehat{D_2}, D) = \lambda_f(D)$*, see Corollary 5.4.2. Then the surface of transitional shocks (domain and codomain) associated to the invariant plane corresponding to* $[G, D]$ *comprises the region bounded by the following curves (refer to Figure 7.2(b)):*

1. *SSB, as in Lemma 7.1.1 (1).*

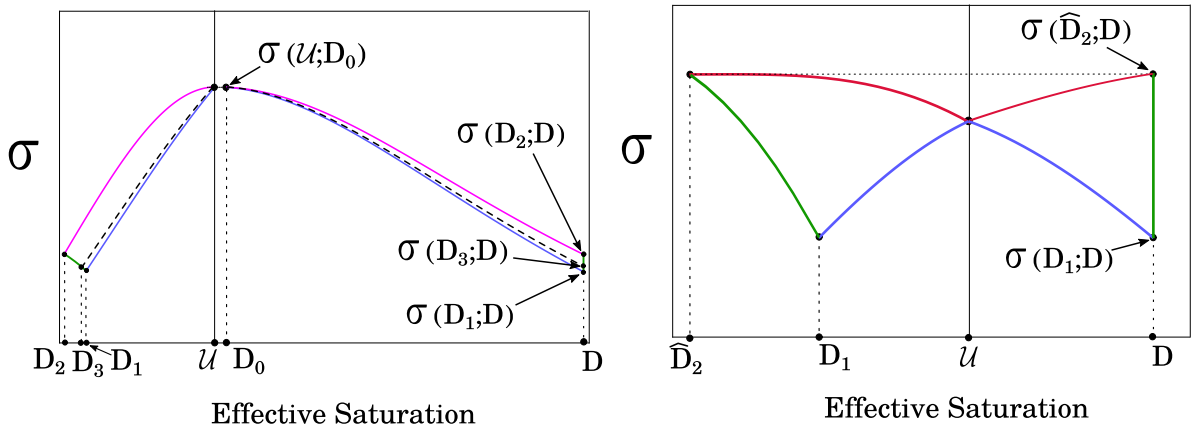

(a) Surface of transitional shocks (domain and codomain) for $[G, D]$, when $0 < \nu_G \leq 1$.

(b) Surface of transitional shocks (domain and codomain) for $[G, D]$, when $(\nu_\Gamma^-)^2/\nu_\Gamma > 8$.

Figure 7.3: Transitional boundaries given in Definition 7.1.1: The blue curves are SSB, red curves are FSB, magenta curves are TSB and green curves are GTB. The horizontal axis corresponds to a parametrization of $[G, D]$ in terms of the effective saturation s and the vertical axis is the shock speed, see Remark 5.1.1. The dashed curve is associated to the boundary for loss of compatibility of sonic shocks, see Section 6.3 and Remark 7.1.5.

2. *FSB with domain defined by the curve $\{(\widehat{D_2}, \sigma(\widehat{D_2}; D)), (\mathcal{U}, 2)\}$, and codomain defined by the curve $\{(D, \sigma(\widehat{D_2}; D)), (\mathcal{U}, 2)\}$.*

3. *GTB with domain defined by the curve $\{(\widehat{D_2}, \sigma(D; \widehat{D_2})), (D_1, \sigma(D; D_1))\}$, and codomain defined by the curve $\{(D, \sigma(D; \widehat{D_2})), (D, \sigma(D; D_1))\}$.*

Proof. The justification follows directly from Definition 7.1.1 and from Corollary 5.4.2. Notice that there is no boundary of type TSB. ∎

Lemma 7.1.3. *For $0 < \nu_G \leq 1$, let D_0 be the left f-extension of $\mathcal{U}$ as in the Theorem 5.4.3. Then the surface of transitional shocks (domain and codomain) associated to the invariant plane corresponding to $[G, D]$ comprises the region bounded by the following curves (refer to Figure 7.3(a)):*

1. *SSB with domain defined by the curve $\{(D_1, \sigma(D; D_1)), (\mathcal{U}, 2)\}$, and codomain defined by the curve $\{(D, \sigma(D; D_1)), (D_0, 2)\}$ (blue curves in Figure 7.3(a)).*

2. *TSB with domain defined by the curve $\{(D_2, \sigma(D; D_2)), (\mathcal{U}, 2)\}$, and codomain defined by the curve $\{(D, \sigma(D; D_2)), (D_0, 2)\}$ (magenta curves in Figure 7.3(a)).*

3. *GTB as in Lemma 7.1.1 (4).*

Proof. The justification follows directly from Definition 7.1.1 and from Theorem 5.4.3. Notice that there is no boundary of type FSB. ∎

Remark 7.1.4. Notice in Lemma 7.1.3, that there is a gap between states $\mathcal{U}$ and D_0; see Figure 7.3(a). This mean that, in this case, the amplitude of transitional shocks is bounded away from zero. This fact had been noted before, see [28]. The solutions that involve the segment between states $\mathcal{U}$ and D_0 use transitional rarefactions, see Sections 5.5 and 6.4.5.

Claim 7.1.1. *For $0 < \nu_G \leq 1$, let D_0 be the left f-extension of $\mathcal{U}$ as in Theorem 5.4.3. Then, for any right state R in the segment $(\mathcal{U}, D_0]$ there is no left state L along the invariant line $[G, D)$ such that L and R can be joined by a transitional shock (see Figure 7.4).*

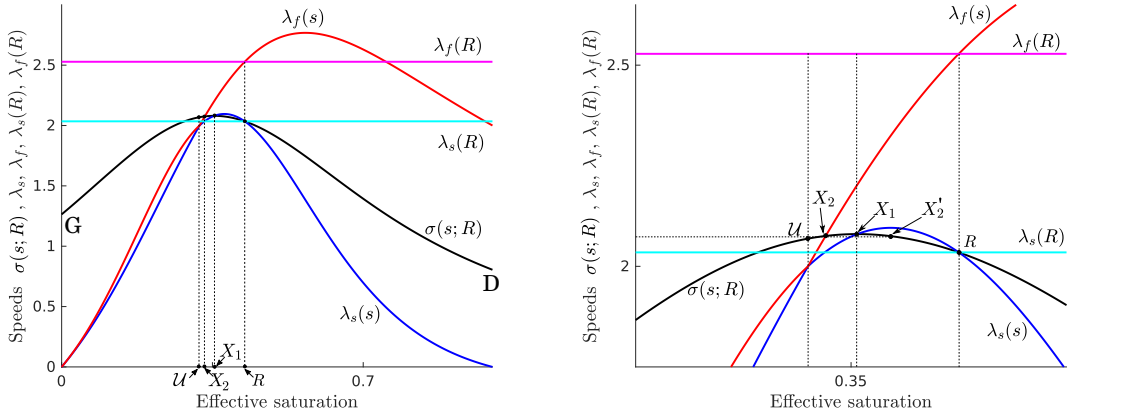

(a) Speed diagram: Primary branch $[G, D]$, for $\mathcal{H}(R)$ with $R \in (\mathcal{U}, D_0]$, when $0 < \nu_G < 1$.

(b) Speed diagram: Zoomed segment $[X_2, X_1]$ for $\mathcal{H}(R)$ with $R \in (\mathcal{U}, D_0]$.

Figure 7.4: Speed diagram for $\mathcal{H}(R)$, $R \in (\mathcal{U}, D_0]$. The horizontal axis corresponds to a parametrization given in terms effective saturation, and the vertical axis shows speeds. The blue (resp. red) line is the characteristic speed λ_s (resp. λ_f) while the black line is the shock speed σ. Horizontal cyan and magenta lines correspond to the constant values $\lambda_s(R)$ and $\lambda_f(R)$, respectively. States in the same dashed black line satisfy the tripe shock rule. Notice that X_1 is a Bethe-Wendroff state and for each state $M \in [X_2, X_1]$ there is a state in $M' \in [X_1, X_2']$ that satisfy $\sigma(M; R) = \sigma(M'; R)$.

Proof. Consider the Hugoniot curve $\mathcal{H}(R)$ for a right state R in the segment $(\mathcal{U}, D_0) \subset [G, D]$. The Hugoniot curve for states along invariant line is computed explicitly in [3]. Since the only possibility for the existence of a transitional shock between states L and R is that both lie in $[G, D]$, we only need to consider the primary branch $[G, D]$ of $\mathcal{H}(R)$. In Figure 7.4, we compare the characteristic speeds $\lambda_s(R)$,$\lambda_f(R)$, $\lambda_s(s)$, $\lambda_f(s)$ with the shock speed $\sigma(R; s)$, as s varies along the Hugoniot branch $[G, D]$, and identify the Bethe-Wendroff point X_1 and the transitional segment $[X_2, X_1]$. According to Figure 7.4 there is a state $X_2' \in [X_1, R]$ such that $\sigma(X_2; R) = \sigma(X_2'; R)$ and X_2' is a repeller. Notice that for any state $M \in [X_2, X_1]$ there is a state $M_1 \in [X_1, X_2']$ such that $\sigma(M; R) = \sigma(M_1; R)$. Since M_1 is between M and R there is no orbit connecting M to R along the invariant line $[G, D]$. Therefore, there is no admissible transitional shock from M to R when $R \in (\mathcal{U}, D_0]$. ∎

Remark 7.1.5. The transitional boundary associated to the boundary for loss of compatibility of sonic shocks given in Section 6.3 (shown in Figures 7.2-7.3 as black dashed lines) is computed by varying $M_2 \in [Y_1, D]$ and finding the states $X_3(M_2) \in [X_2(M_2), X_1(M_2)]$ with $\sigma(X_1(M_2); M_2) \leq \sigma(X_3(M_2); M_2) \leq \sigma(X_2(M_2); M_2)$. In Figure 7.3(b), we show the surface of transitional shocks for the case $(\nu_G^-)^2/\nu_G > 8$ in which this boundary does not appear because the state Y_1 ceases to exist within the saturation triangle, see Lemma 5.3.3.

7.2 Relations between macro regions, $\mathscr{R}$-regions and transitional boundaries for umbilic points of type II

As seen in Definition 7.1.1 and Lemmas 7.1.1-7.1.3, there is a straightforward connection between the transitional boundaries, the $\mathscr{R}$-regions defined in Chapter 6 and the boundaries of compatibility and admissibility given in Sections 6.3. We can use these relationships to establish the compatibility between transitional waves and fast waves.

Claim 7.2.1. *For $1 < \nu_G \leq 8$ and umbilic point of type II, given any right state $R \in \mathcal{FR}_D$, the local branch of the backward f-wave curve $W_f^-(R)$ on space $\mathcal{FR}_D \times \mathbb{R}^+$ intersects the invariant plane $[\mathcal{U}, D] \times \mathbb{R}^+$ in one of the following regions (see Figure 7.5(b)):*

1. *Region T_1, bounded by the curves $\{(\mathcal{U}, 2), (D, \sigma_{D_1})\}$, $\{(D, \sigma_{D_1}), (D, 1)\}$ and $\{(D, 1), (\mathcal{U}, 2)\}$;*
2. *Region T_2, bounded by the curves $\{(\mathcal{U}, 2), (Y_2, \sigma_{Y_2})\}$, $\{(Y_2, \sigma_{Y_2}), (D, \sigma_{D_2})\}$, $\{(D, \sigma_{D_2}), (D, \sigma_{D_1})\}$ and $\{(D, \sigma_{D_1}), (\mathcal{U}, 2)\}$;*
3. *Region T_3, bounded by the curves $\{(Y_2, \sigma_{Y_2}), (D, \lambda_f(D))\}$, $\{(D, \lambda_f(D)), (D, \sigma_{D_2})\}$ and $\{(D, \sigma_{D_2}), (Y_2, \sigma_{Y_2})\}$;*
4. *Curve A (cyan) given by $\{(Y_2, \sigma_{Y_2}), (D, \lambda_f(D))\}$;*
5. *Curve B (red) given by $\{(\mathcal{U}, 2), (Y_2, \sigma_{Y_2})\}$.*

Moreover, for the upper and lower regions $\mathscr{R}_i$, with $i \in \{1, 2, 3\}$, the correspondence with the regions T_1, T_2 and T_3 in the invariant plane is one-to-one. (Regions A, B in the saturation triangle are mapped to curves A, B on the invariant plane).

Proof. The justification of this Claim follows directly from the procedure to construct the boundaries for regions $\mathscr{R}_i$, $i = \{1, ..., 6\} \cup \{4', 5', 6'\}$, given in Sections 6.4.1-6.4.3. The local branch of $\mathcal{W}_f^-(R)$ for any state R in (lower or upper) $\mathscr{R}_i$, $i = \{1, 2, 3\}$, intersects the invariant segment $[\mathcal{U}, D]$ at a state M_2, such that there is a Lax f-shock with $\sigma = \sigma(M_2; R)$. For $R \in A \cup B$, the state M_2 belongs to a fast rarefaction segment. Then, we have that (M_2, σ) is in the invariant plane $[\mathcal{U}, D] \times \mathbb{R}^+$, see Figure 7.5(b). Conversely, if we consider the Hugoniot curves from states M_2 along $[\mathcal{U}, D]$, the segments of Lax f-shocks in the local branches (distinct from $[G, D]$) of $\mathcal{H}(M_2)$ foliate regions $\mathscr{R}_i$, $i = \{1, 2, 3\}$. Moreover, shock speeds are monotonic along these segments and their extrema occur outside these regions. Therefore, we

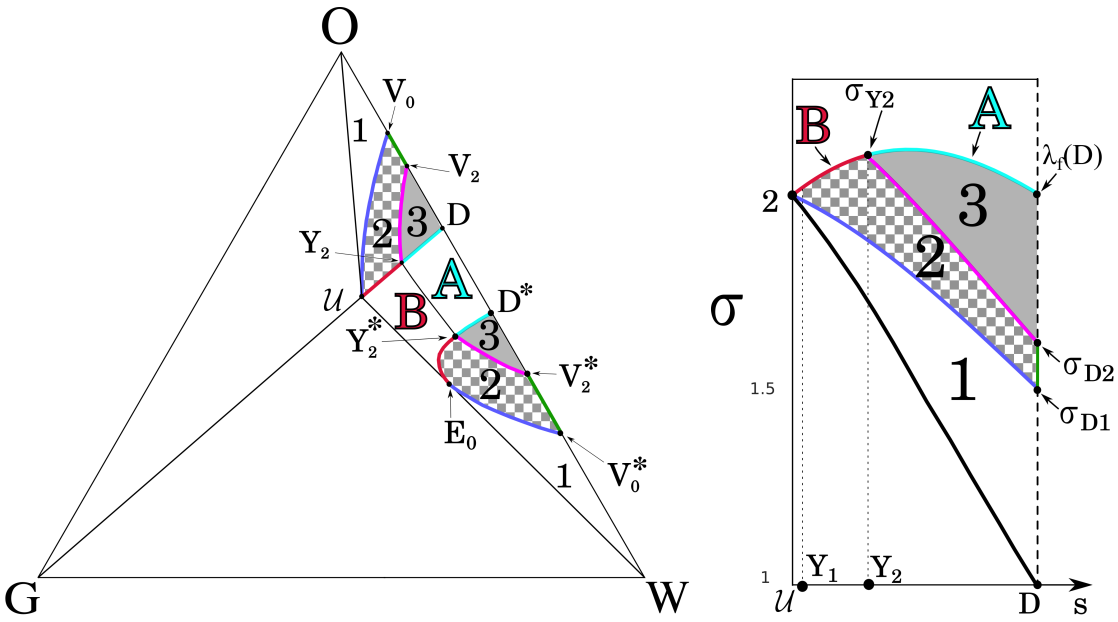

(a) $\mathscr{R}$-regions for the fast macro region $\mathcal{FR}_D$.

(b) Subdivision of the invariant plane $[\mathcal{U}, D] \times \mathbb{R}^+$ into regions T_1, T_2 and T_3 associated to $\mathscr{R}$-regions.

Figure 7.5: Relations among $\mathscr{R}$-regions, the invariant plane $[\mathcal{U}, D] \times \mathbb{R}^+$ and the transitional boundaries. (a) Subdivision of the fast macro region $\mathcal{FR}_D$ in $\mathscr{R}$-regions, see Chapter 6. Notice that region $A = \mathscr{R}_4 \cup \mathscr{R}_{4'}$ and region $B = \mathscr{R}_5 \cup \mathscr{R}_{5'} \cup \mathscr{R}_6 \cup \mathscr{R}_{6'}$. (b) The horizontal axis corresponds to a parametrization of $[G, D]$ in terms of the effective saturation s and the vertical axis indicates values of shock speeds, see Remark 5.1.1.

can define a one-to-one correspondence between the points (M_2, σ) in the invariant plane $[\mathcal{U}, D] \times \mathbb{R}^+$ and states R in these $\mathscr{R}$-regions via the shock speed between them. Now we study the boundaries of regions $\mathscr{R}_i$ with $i \in \{1, 2, 3\}$ in this context of invariant plane.

First, we consider the Hugoniot curve for M_2 varying along the segment $[\mathcal{U}, D]$ and compute the states $X_1(M_2)$ and $X_2(M_2)$ associated to it (see Theorem 5.4.1). Recall that the curves $[E_0, V_0^*]$ and $[\mathcal{U}, V_0]$ are the boundaries for the lower and upper regions $\mathscr{R}_1$, which separate $\mathscr{R}_1$ from region $\mathscr{R}_2$. Their construction is associated to shock speeds $\sigma(X_1(M_2); M_2)$ for $X_1(M_2) \in [G, D]$ which satisfy $\lambda_s(X_1(M_2)) = \sigma(X_1(M_2); M_2) = \sigma(V_0(M_2); M_2) = \sigma(V_0^*(M_2); M_2)$, where $V_0(M_2) \in [\mathcal{U}, V_0]$ and $V_0^*(M_2) \in [E_0, V_0^*]$ (see Remark 6.3.1 and Section 6.3.1).

Second, for M_2 varying along the segment $[Y_2, D]$ the curves $[Y_2^*, V_2^*]$ and $[Y_2, V_2]$ are the boundaries for the lower and upper regions $\mathscr{R}_3$, which separate $\mathscr{R}_3$ from region $\mathscr{R}_2$. Their construction is associated to shock speeds $\sigma(X_2(M_2); M_2)$ for $X_2(M_2) \in [G, D]$ and satisfy $\lambda_f(X_2) = \sigma(X_2(M_2); M_2) = \sigma(V_2(M_2); M_2) = \sigma(V_2^*(M_2); M_2)$, where $V_2(M_2) \in [Y_2, V_2]$ and $V_2^*(M_2) \in [Y_2^*, V_2^*]$ (see Remark 6.3.2 and Section 6.3.2). Similarly, for M_2 varying along the segment $[\mathcal{U}, Y_2]$, the curve $[E_0, Y_2^*]$ is a boundary for the lower region $\mathscr{R}_2$, which separate $\mathscr{R}_2$ from region $\mathscr{R}_{6'}$, see Figure 7.5(a). Its construction is associated to shock speed $\sigma(X_2(M_2); M_2)$ with $X_2(M_2) \in [G, D]$ satisfying $\lambda_f(M_2) =$

$\sigma(X_2(M_2); M_2) = \sigma(V_3(M_2); M_2)$, where $V_3(M_2) \in [E_0, Y_2^*]$ (see Section 6.4.3 for the construction of $\mathscr{R}_{6'}$). Moreover, for all $M_2 \in [\mathcal{U}, D]$, the states $V_0(M_2), V_0^*(M_2), V_2(M_2), V_2^*(M_2)$ and $V_3(M_2)$ are left states of Lax f-shocks with M_2. Additionally, $M_2 \in (Y_2, D)$, these points satisfy $\sigma(V_0(M_2); M_2) < \sigma(V_2(M_2); M_2) < \lambda_f(M_2)$ or $\sigma(V_0^*(M_2); M_2) < \sigma(V_2^*(M_2); M_2) < \sigma(V_3(M_2); M_2) = \lambda_f(M_2)$. From these considerations, we draw the following conclusions:

1. For $R \in [E_0, V_0^*] \cup [\mathcal{U}, V_0]$, there exists $M_2 \in [\mathcal{U}, D]$ such that $\lambda_s(X_1) = \sigma(X_1(M_2); M_2) = \sigma(R; M_2)$. Then, from Definition 7.1.1(1), the local branch of $\mathcal{W}_f^-(R) \times \mathbb{R}^+$ intersects the invariant plane $[\mathcal{U}, D] \times \mathbb{R}^+$ at $(M_2, \sigma(R; M_2))$, which belongs to the SSB (blue curve in Figure 7.5 (b)).

2. For $R \in [Y_2^*, V_2^*] \cup [Y_2, V_2]$, there exists $M_2 \in [\mathcal{U}, D]$ such that $\lambda_f(X_2) = \sigma(X_2(M_2); M_2) = \sigma(R; M_2)$. Then, from Definition 7.1.1(3), the local branch of $\mathcal{W}_f^-(R) \times \mathbb{R}^+$ intersects the invariant plane $[\mathcal{U}, D] \times \mathbb{R}^+$ at $(M_2, \sigma(R; M_2))$, which belongs to the TSB (magenta curve in Figure 7.5 (b)).

3. From the speed monotonicity along the segments of Lax f-shocks, we have that for any state $R \in \mathscr{R}_1$, $\sigma(R; M_2) < \lambda_s(X_1(M_2))$ (see Figure 7.5(a)) and that the local branch of $\mathcal{W}_f^-(R) \times \mathbb{R}^+$ intersects the invariant plane $[\mathcal{U}, D] \times \mathbb{R}^+$ at $(M_2, \sigma(R; M_2))$, which is below the curve $\{(\mathcal{U}, 2), (D, \sigma_{D_1})\}$ and is bounded by the curves $\{(\mathcal{U}, 2), (D, 1)\}$ and $\{(D, \sigma_{D_1}), (D, 1)\}$ (region T_1 in Figure 7.5(b)).

4. From the speed monotonicity along the segments of the Lax f-shocks, we have that for any state $R \in \mathscr{R}_2$, $\sigma(R; M_2) < \lambda_f(X_2(M_2))$ (see Figure 7.5(a)) and that the local branch of $\mathcal{W}_f^-(R) \times \mathbb{R}^+$ intersects the invariant plane $[\mathcal{U}, D] \times \mathbb{R}^+$ at $(M_2, \sigma(R; M_2))$, which is above the curve $\{(\mathcal{U}, 2), (D, \sigma_{D_1})\}$ and is bounded by the curves $\{(\mathcal{U}, 2), (Y_2, \sigma_{Y_2})\}$, $\{(Y_2, \sigma_{Y_2}), (D, \sigma_{D_2})\}$ and $\{(D, \sigma_{D_2}), (D, \sigma_{D_1})\}$ (region T_2 in Figure 7.5(b)).

5. For $R \in [E_0, Y_2^*]$, there exists $M_2 \in [\mathcal{U}, D]$ such that $\lambda_f(M_2) = \sigma(R; M_2)$. Then from Definition 7.1.1(2), the intersection between the local branch of $\mathcal{W}_f^-(R) \times \mathbb{R}^+$ and the invariant plane $[\mathcal{U}, D] \times \mathbb{R}^+$ happens at $(M_2, \sigma(R; M_2))$, which belongs to the FSB (red curve in Figure 7.5 (b)).

6. The curve $[Y_2^*, D^*]$ is the left f-extension of $[Y_2, D]$. From the construction of region $\mathscr{R}_{4'}$ (Section 6.4.3), this curve separates regions $\mathscr{R}_3$ and $\mathscr{R}_{4'}$. Then, for any $R \in [Y_2^*, D^*]$, there exists $M_2 \in [Y_2, D]$ such that $\lambda_f(M_2) = \sigma(R; M_2)$ and the intersection between the local branch of $\mathcal{W}_f^-(R) \times \mathbb{R}^+$ and the invariant plane $[\mathcal{U}, D] \times \mathbb{R}^+$ happens at $(M_2, \sigma(R; M_2))$, which belongs to the curve $\{(Y_2, \sigma_{Y_2}), (D, \lambda_f(D))\}$ (cyan curve A in Figure 7.5 (b)). Since for any $R \in \mathscr{R}_3$ the intersection between the local branch of $\mathcal{W}_f^-(R)$ and the invariant segment $[\mathcal{U}, D]$ corresponds to a Lax f-shock, we have $\sigma(R; M_2) < \lambda_f(M_2)$. Therefore, from the speed monotonicity along the segments of Lax f-shocks, we have that for any state $R \in \mathscr{R}_3$, the local branch of $\mathcal{W}_f^-(R) \times \mathbb{R}^+$ intersects the invariant plane $[\mathcal{U}, D] \times \mathbb{R}^+$ at $(M_2, \sigma(R; M_2))$, which is below the curve $\{(Y_2, \sigma_{Y_2}), (D, \lambda_f(D))\}$ and is bounded by the curves $\{(Y_2, \sigma_{Y_2}), (D, \sigma_{D_2})\}$ and $\{(D, \lambda_f(D)), (D, \sigma_{D_2})\}$ (shaded region Figure 7.5 (b)).

On the other hand, let us consider the regions $\mathscr{R}_i$, for $i \in \{4, 4', 5, 5', 6, 6'\}$, defined in Sections 6.4.2, 6.4.3 and Figures 6.32(b)-(c). We have seen that for any state $R \in \mathscr{R}_4 \cup \mathscr{R}_{4'}$, the local branch of $\mathcal{W}_f^-(R) \times \mathbb{R}^+$ intersects the invariant segment with a f-rarefaction. Then, for any $R \in A$, $A = \mathscr{R}_4 \cup \mathscr{R}_{4'} \subset \mathcal{FR}_D$, the intersection of the local branch of $\mathcal{W}_f^-(R)$ with the invariant plane $[\mathcal{U}, D] \times \mathbb{R}^+$ happens at $(M_2, \lambda_f(M_2))$, which lies on the curve $\{(Y_2, \sigma_{Y_2}), (D, \lambda_f(D))\}$ (cyan curve A Figure 7.5 (b)). Similarly, for $R \in B = \mathscr{R}_5 \cup \mathscr{R}_{5'} \cup \mathscr{R}_6 \cup \mathscr{R}_{6'}$, the local branch of $\mathcal{W}_f^-(R)$ intersects the invariant segment along a f-rarefaction segment. Then, for any $R \in B$ the intersection between the local branch of $\mathcal{W}_f^-(R) \times \mathbb{R}^+$ and the invariant plane $[\mathcal{U}, D] \times \mathbb{R}^+$ happens at $(M_2, \lambda_f(M_2))$, which belongs to the curve $\{(\mathcal{U}, 2), (Y_2, \sigma_{Y_2})\}$ (red curve B in Figure 7.5 (b)). Notice that for regions A and B, we do not have a bijective relationship with the invariant plane because the f-rarefaction reaches this plane with the same characteristic speed for distinct states R. ■

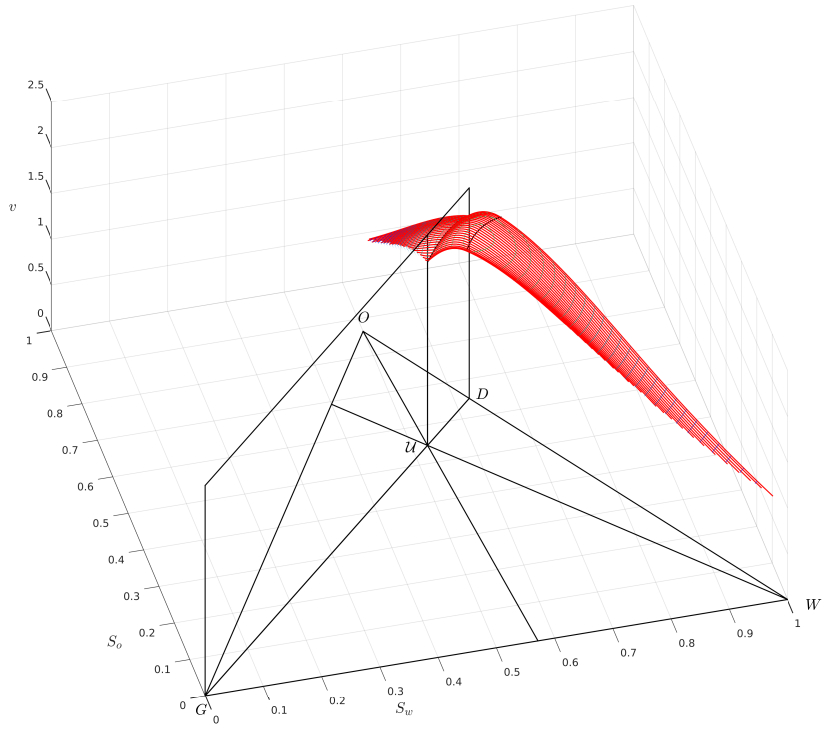

Figure 7.6: *Foliation surface* of forward f-wave curves associated to the macro region $\mathcal{FR}_D \times \mathbb{R}^+$, see Remark 7.2.1. Properties of foliation surface on plane $[\mathcal{U}, D] \times \mathbb{R}^+$ can be viewed in Figure 7.5(b).

Claim 7.2.2. *For $\nu_G > 8$ and umbilic point of type II, given any right state $R \in \mathcal{FR}_D$ the backward f-wave curve $W_f^-(R) \times \mathbb{R}^+$ intersects the invariant plane $[\mathcal{U}, D] \times \mathbb{R}^+$ in one of the following regions:*

1. *Region T_1, bounded by the curves $\{(\mathcal{U}, 2), (D, \sigma_{D_1})\}$, $\{(D, \sigma_{D_1}), (D, 1)\}$ and $\{(D, 1), (\mathcal{U}, 2)\}$.*
2. *Region T_2, bounded by the curves $\{(\mathcal{U}, 2), (D, \sigma_{\widehat{D_2}})\}$, $\{(D, \sigma_{\widehat{D_2}}), (D, \sigma_{D_1})\}$ and $\{(D, \sigma_{D_1}), (\mathcal{U}, 2)\}$.*
3. *Curve B (red) given by $\{(\mathcal{U}, 2), (D, \sigma_{\widehat{D_2}})\}$.*

Moreover, the correspondence between the upper or lower regions $\mathscr{R}_1$ and $\mathscr{R}_2$ with T_1 and T_2 is one-to-one.

Proof. Similar to the proof of Claim 7.2.1 and considering Section 6.4.4. The Figure is equivalent to Figure 7.5 without regions $\mathscr{R}_3, T_3$ and without the curve A. ∎

Remark 7.2.1. Following the results of Claim 7.2.1, we construct the *foliation surface* of forward f-wave curves associated to the macro region $\mathcal{FR}_D \times \mathbb{R}^+$, see Figure 7.6. This surface is constructed by gluing together local branches of forward f-wave curves for states $M_2 \in [\mathcal{U}, D]$. Each point in this surface is of the form (R, v), where $R \in \mathcal{FR}_D$ and v is the fastest speed associated to the wave group connecting M_2 to R. Moreover, points of the foliation surface can be associated with points in the invariant plane $[\mathcal{U}, D] \times \mathbb{R}^+$ defined in terms of the slowest speed of the wave group connecting M_2 to R: this association is one-to-one, if the wave group is a Lax f-shock; if the wave group is either a f-rarefaction or a f-composite the association is with a point in the curve $\{(\mathcal{U}, 2), (D, \lambda_f(D))\}$ that represents the set $\{(M_2, v) \in [\mathcal{U}, D] \times \mathbb{R}^+ | \ v = \lambda_f(M_2)\}$ (see Figure 7.5(b)).

Analogous to the case of fast macro region $\mathcal{FR}_D$, there is a relation between the slow macro region $\mathcal{SR}_G$ and the invariant plane $[G,\mathcal{U}] \times \mathbb{R}^+$.

Claim 7.2.3. *For $1 < \nu_G \leq 8$ and umbilic point of type II, given any left state $L \in \mathcal{SR}_G$, the local branch of the forward s-wave curve $\mathcal{W}_s^+(L) \times \mathbb{R}^+$ intersects the invariant plane $[G,\mathcal{U}] \times \mathbb{R}^+$ in one of the following regions (see Figure 7.7(b)):*

1. *Curve T_{S_1} (blue) given by $\{(G, 0), (\mathcal{U}, 2)\}$, which represents the set $\{(M_1, v) \in [G,\mathcal{U}] \times \mathbb{R}^+ | \ v = \lambda_s(M_1)\}$;*
2. *Region T_{S_2} (checkered) bounded by curve $\{(G, 0), (\widehat{\mathcal{Y}_1}, \sigma_{\widehat{\mathcal{Y}_1}})\}$, the red curve $\{(\widehat{\mathcal{Y}_1}, \sigma_{\widehat{\mathcal{Y}_1}})\}, (\mathcal{U}, 2)\}$ and $\{(\mathcal{U}, 2), (G, 0)\}$;*
3. *Curve T_{S_3} (orange) given by $\{(G, 0), (\widehat{\mathcal{Y}_1}, \sigma_{\widehat{\mathcal{Y}_1}})\}$;*
4. *Curve T_{S_4} (violet) given by $\{(\widehat{\mathcal{Y}_1}, \sigma_{\widehat{\mathcal{Y}_1}})\}, (\mathcal{U}, 2)\}$, just above the surface of transitional shocks.*

Proof. Assume that the viscosities μ_i, $i = w, o, g$, are different. From Section 4.5, we see that the slow inflection manifold $\mathcal{I}_s$ inside $\mathcal{SR}_G$ does not coincide with the segment $[G,\mathcal{U}]$; moreover, it belongs to either the triangle $\widehat{G\,\mathcal{U}E}$ or $\widehat{G\,\mathcal{U}B}$ (see Figure 7.7(a)). Without loss of generality, we assume that

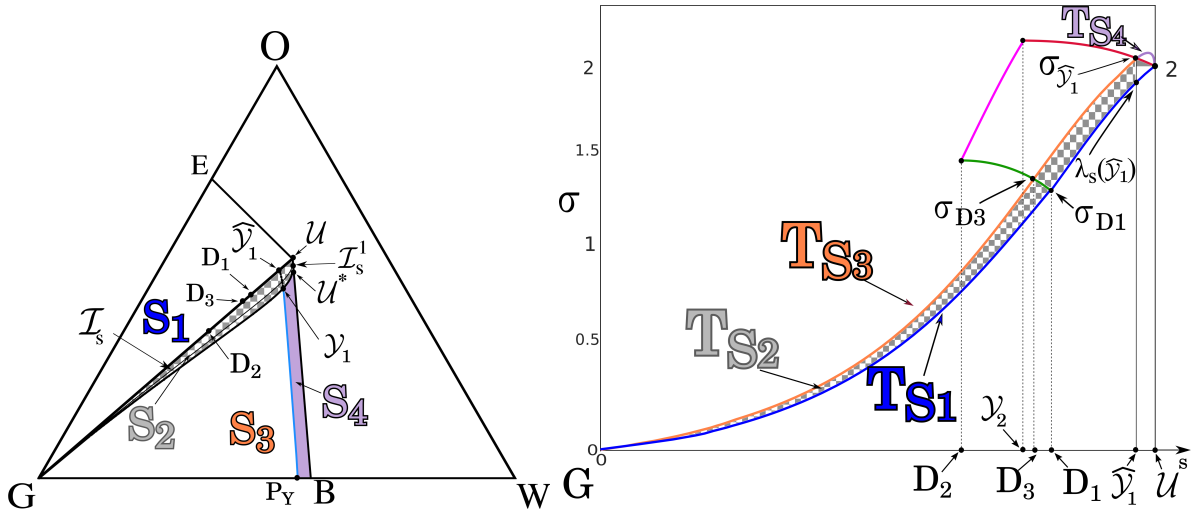

(a) Subdivision of the slow macro region $\mathcal{SR}_G$.

(b) Subdivision of the invariant plane $[G,\mathcal{U}] \times \mathbb{R}^+$ associated to subdivisions given in (a)

Figure 7.7: Correspondence between the invariant plane $[G,\mathcal{U}] \times \mathbb{R}^+$ and the transitional boundaries in $\mathcal{SR}_G$. (a) Subdivision of $\mathcal{SR}_G$ according to the type of wave group at the intersection between the local branch of $\mathcal{W}_s^+(L)$ and the invariant plane $[G,\mathcal{U}] \times \mathbb{R}^+$. For any L in region S_4, there are no transitional shocks compatible with the slow wave group from L. (b) The horizontal axis corresponds to a parametrization of $[G, D]$ in terms of the effective saturation s and the vertical axis is the shock speed, see Remark 5.1.1. Notice that the violet curve $\{(\widehat{\mathcal{Y}_1}, \sigma_{\mathcal{Y}_1}), (\mathcal{U}, 2)\}$ (T_{S_4}) is above the red curve $\{(\widehat{\mathcal{Y}_1}, \sigma_{\mathcal{Y}_1}), (\mathcal{U}, 2)\}$ which is associated to the transitional boundary FSB.

$\mathcal{I}_s \subset \widehat{G\,\mathcal{U}B}$. It follows from Section 4.1 that the s-rarefaction field foliates the slow macro region $\mathcal{SR}_G$. Then, for any state L in $\widehat{G\,\mathcal{U}E}$, *i.e.,* region S_1 in Figure 7.7(a), the forward s-rarefaction from L intersects the invariant segment $[G,\mathcal{U}]$ at a state $M_1(L)$ before it reaches the slow inflection $\mathcal{I}_s$, where it must end by Definition 2.1.3. Hence, the intersection between the local branch of $\mathcal{W}_s^+(L) \times \mathbb{R}^+$ and the invariant plane $[G,\mathcal{U}] \times \mathbb{R}^+$ is along the curve T_{S_1} (blue curve), given by $\{(G,0),(\mathcal{U},2)\}$ (see Figure 7.7(b)) and which represents the set $\{(M_1, v) \in [G,\mathcal{U}] \times \mathbb{R}^+ |\ v = \lambda_s(M_1)\}$.

Since the slow inflection is contained in $\widehat{G\,\mathcal{U}B}$, the right s-extension of $[G,\mathcal{U}]$ $(E_s^+([G,\mathcal{U}]))$, which is given by the orange curve $[G,\mathcal{Y}_1,\mathcal{U}^*]$, also lies in the triangle $\widehat{G\,\mathcal{U}B}$. Then, for all $M_1' \in E_s^+([G,\mathcal{U}])$, there is a state $M_1 \in [G,\mathcal{U}]$ with $M_1' \in \mathcal{H}(M_1)$ such that we have an admissible Lax s-shock between M_1 and M_1' with $\sigma(M_1; M_1') = \lambda_s(M_1')$. Recall from Section 6.3.3 that (refer to Figure 6.4(a)): (i) the segment $[D_3, \widehat{\mathcal{Y}_1}] \subset [G,\mathcal{U}]$ defines the boundary for loss of compatibility of sonic shocks which is associated to segment $[X_3^*(D), \mathcal{Y}_1] \subset [G,\mathcal{Y}_1,\mathcal{U}^*]$ where $\sigma(D_3; D) = \sigma(X_3(D); D) = \lambda_s(X_3^*(D))$; (ii) $\mathcal{Y}_1$ and Y_1 with $Y_1 \in [\mathcal{U}, D]$ is a mixed double contact pair; and (iii) $\sigma(\mathcal{Y}_1; Y_1) = \sigma(\widehat{\mathcal{Y}_1}; \mathcal{Y}_1) = \lambda_s(\mathcal{Y}_1) = \lambda_f(Y_1)$, with $\widehat{\mathcal{Y}_1} \in [G,\mathcal{U}]$ (see Figures 6.4(a) and 7.7). Then, if we consider a state $M_2 \in [\mathcal{U}, Y_1]$, the corresponding states $X_3(M_2) \in [\widehat{\mathcal{Y}_1},\mathcal{U}]$ and $X_3^*(M_2) \in [\mathcal{Y}_1,\mathcal{U}^*] \subset [G,\mathcal{Y}_1,\mathcal{U}^*]$ satisfy $\lambda_s(X_3^*(M_2)) = \sigma(X_3^*(M_2); M_2) = \sigma(X_3(M_2); X_3^*(M_2)) > \sigma(M_2; X_2(M_2)) > \sigma(M_2; X_1(M_2))$. Therefore, the slow

sonic shock joining $X_3(M_2)$ to $X_3^*(M_2)$ is incompatible with any transitional shock leading to M_2.

Taking these facts into account, we define the region $S_3 \in \mathcal{SR}_G$ bounded by the segment $[G, \mathcal{Y}_1] \subset E_s^+([G,\mathcal{U}])$, the backward s-rarefaction from $\mathcal{Y}_1$, $[\mathcal{Y}_1, P_Y]$, and the segment $[G, P_Y] \subset [G, W]$. For any state $L \in S_3$, the local branch of $\mathcal{W}_s^+(L)$ intersects the invariant segment $[G,\mathcal{U}]$ at state M_1 such that there is a s-composite wave group satisfying $L \xrightarrow{R_s} M_1' \xrightarrow{'S_s} M_1$ with $\sigma(M_1; M_1') = \lambda_s(M_1')$. Then, $(M_1, \sigma(M_1; M_1'))$ is in $\{(G,0), (\widehat{\mathcal{Y}_1}, \sigma_{\mathcal{Y}_1})\}$, which represents the set $\{(M_1, v) \in [G, \widehat{\mathcal{Y}_1}] \times \mathbb{R}^+ |\ v = \lambda_s(M_1') = \sigma(M_1; M_1'),$ with $M_1' \in [G, \mathcal{Y}_1] \in \mathcal{SR}_G\}$.

On the other hand, we define the region S_4 as the one bounded by the s-rarefaction $[\mathcal{Y}_1, P_Y]$, the segments $[P_Y, B]$ and $[B,\mathcal{U}]$, and the curve $[\mathcal{Y}_1,\mathcal{U}^*] \subset E_s^+([G,\mathcal{U}])$. For any state $L \in S_4$, the local branch of $\mathcal{W}_s^+(L)$ intersects the invariant segment $[G,\mathcal{U}]$ with a s-composite wave curve at $M_1 \in [\widehat{\mathcal{Y}_1},\mathcal{U}]$ which has a corresponding state $M_1' \in [\mathcal{Y}_1,\mathcal{U}^*]$ such that $\sigma(M_1; M_1') = \lambda_s(M_1')$. Notice that by the triple shock rule 2.4.3, there is a state $M_2 \in \mathcal{H}(M_1')$ such that $M_2 \in [\mathcal{U}, Y_1]$ with $\sigma(M_1; M_1') > \sigma(M_2; X_2(M_2))$, where $X_2(M_2)$ is an endpoint of the transitional segment ffor M_2. Hence, $(M_1, \sigma(M_1; M_1'))$ intersects the violet curve given by $\{(\widehat{\mathcal{Y}_1}, \sigma_{\mathcal{Y}_1}), (\mathcal{U}, 2)\}$ above the red transitional boundary $\{(\widehat{\mathcal{Y}_1}, \sigma_{\mathcal{Y}_1}), (\mathcal{U}, 2)\}$ (see Figure 7.7(b)).

Finally, we define the region $S_2 \in \mathcal{SR}_G$ (checkered region in Figure 7.7(a)) as the one bounded by the segments $[G,\mathcal{U}]$, $[\mathcal{U},\mathcal{U}^*]$ and the curve $[G, \mathcal{Y}_1,\mathcal{U}^*]$. Notice that since the slow inflection $\mathcal{I}_s$ is inside this region, we have two cases for a given L: either it lie between the curves $E_s^+([G,\mathcal{U}])$ and $\mathcal{I}_s$, or between $\mathcal{I}_s$ and the invariant segment $[G,\mathcal{U}]$. In the first case, the forward s-rarefaction from L has increasing velocity in the direction toward $[G,\mathcal{U}]$ and ends at a state $L' \in \mathcal{I}_s$, such that there is a s-composite segment $[L', L'']$ with $\sigma(L; L'') = \lambda_s(L)$ which L'' does not cross the invariant segment $[G,\mathcal{U}]$. This implies that the local branch of $\mathcal{W}_s^+(L)$ intersects $[G,\mathcal{U}]$ along a segment of admissible Lax s-shock at a state M_1 and $\sigma(M_1; L) > \lambda(M_1)$. In the second case, the forward s-rarefaction from L increases in the direction toward $\mathcal{I}_s$, while in the opposite direction we have an admissible Lax s-shock segment. Moreover, the local branch of $\mathcal{W}_s^+(L)$ intersects $[G,\mathcal{U}]$ along a segment of admissible Lax s-shock at a state M_1 and $\sigma(M_1; L) > \lambda(M_1)$. Moreover, for all $M_1 \in [G,\mathcal{U}]$, the Hugoniot locus $\mathcal{H}(M_1)$ has an admissible Lax s-shock segment $[M_1, L]$ with $L \in E_s^+([G,\mathcal{U}])$ and $\sigma(M_1; L) = \lambda_s(L)$, *i.e.*, L is a Bethe-Wendroff state with the speed $\sigma(M_1; L)$ as a maximum. For each M in the segment $[M_1, L]$ of Lax s-shocks $\lambda_s(M_1) < \sigma(M; M_1) < \sigma(M_1; L)$ holds. Therefore, for any $L \in S_2$, curve $(M_1, \sigma(L, M_1))$ intersects the invariant plane $[G,\mathcal{U}]\times\mathbb{R}^+$ in the checkered region bounded by the orange curve $\{(G,0), (\widehat{\mathcal{Y}_1}, \sigma_{\widehat{\mathcal{Y}_1}})\}$, the red curve $\{(\widehat{\mathcal{Y}_1}, \sigma_{\widehat{\mathcal{Y}_1}})\}, (\mathcal{U}, 2)\}$ and the blue curve $\{(\mathcal{U}, 2), (G, 0)\}$; see Figure 7.7(b). ∎

Remark 7.2.2. As in Remark 7.2.1, we use Claim 7.2.3 to construct the *foliation surface* of backward s-wave curves associated to the macro region $\mathcal{SR}_G$, see Figure 7.7(a). This surface is constructed by gluing together the local branches of backward s-wave curves for states $M_1 \in [G,\mathcal{U}]$. Each point in this surface is of the form (L, v), where $L \in \mathcal{SR}_G$ and v is the slowest speed associated to each wave group. Moreover, points of the foliation surface can be associated with points in the invariant plane $[G,\mathcal{U}] \times \mathbb{R}^+$ defined in terms of the fastest speed of the wave group connecting L to M_1: this association is one-to-one, if the wave group is a Lax s-shock; if the wave group is either a s-rarefaction or a s-composite the association is with a point in the curves T_{S1} and T_{S_3} given by Claim 7.2.3, see Figure 7.7(b).

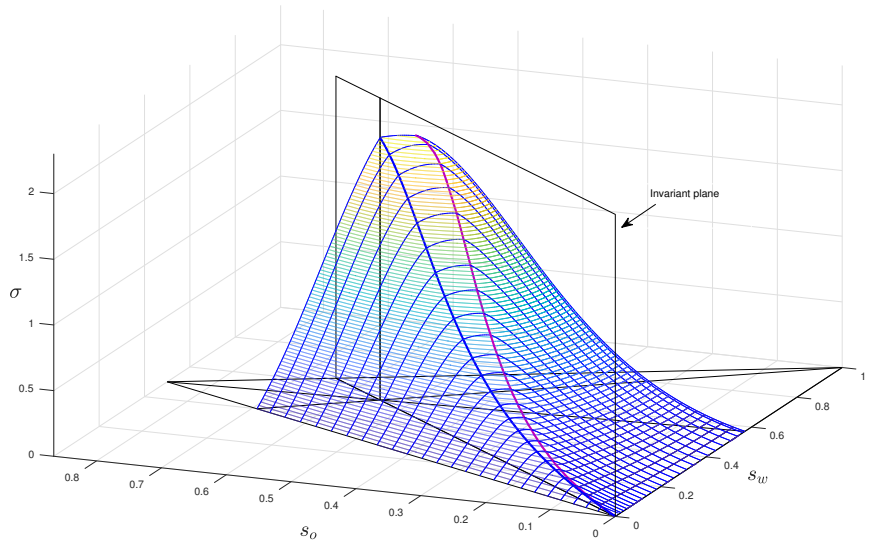

Figure 7.8: *Foliation surface* of backward s-wave curve in slow macro region $\mathcal{SR}_G$, see Remark 7.2.2

7.3 Description of transitional Waves

In this section we describe the procedure to identify which transitional shocks are compatible with slow or fast wave curves. To this end, we use the surface of transitional shocks which contains all pairs of points of $T \times \mathbb{R}^+$ that can be used to solve Riemann problems together with the Claims 7.2.1 and 7.2.3, where the surface of transitional shocks and the saturation triangle T are related. Without loss of generality we consider the surface associated to the invariant plane $[G, D] \times \mathbb{R}^+$ in this description; the procedure in the other invariant planes follows in a similar manner.

Since there are four transitional boundaries when $1 < \nu_G \leq 8$, we describe the procedure for this range of ν_G using Lemma 7.1.1 and Claim 7.2.1. In this work, we construct solutions for the Riemann problem by first building $\mathscr{R}$-regions and then the associated $\mathscr{L}_{\mathscr{R}}$-regions. This way, we begin with the intersection point (M_2, v) of the local branch of $\mathcal{W}_f^-(R)$ for $R \in \mathcal{FR}_D$ and the invariant plane $[\mathcal{U}, D] \times \mathbb{R}^+$, characterized in Claim 7.2.1 (see Figure 7.5); then, we use the inverse transitional map $T^{-1}(M_2)$ (defined in Section 5.4) and the surface of transitional shocks to find the curve of states that can be joined to M_2 by a transitional shock. Finally, we identify which states M_1 along the straight line $[G,\mathcal{U}]$ can be used to solve the Riemann problem. For this, we use Claim 7.2.3 to identify the points (M_1, v), which belong to the intersection of invariant plane $[G,\mathcal{U}] \times \mathbb{R}^+$ and the local branch of the forward s-wave curve $\mathcal{W}_s^+(L)$; see Figure 7.7(a) and (b).

Now we introduce some notation used in this section. Let $\sigma_{int}^f(M_2)$ be the fast "speed of intersection" associated to the state M_2, which is the speed corresponding to state M_2 where $\mathcal{W}_f^-(R) \times \mathbb{R}^+$ intersects the invariant plane $[\mathcal{U}, D] \times \mathbb{R}^+$. Therefore, if there is a Lax f-shock between R and M_2, $\sigma(R; M_2) =$

$\sigma^f_{int}(M_2)$ (or if M_2 is on a f-composite, $\sigma(M_2; M_2') = \sigma^f_{int}(M_2)$ with $M_2 \in \mathcal{W}^-_f(R)$); however, if M_2 lies on a f-rarefaction, $\sigma^f_{int}(M_2) = \lambda_f(M_2)$. Hence, we use the notation $(M_2, \sigma^f_{int}(M_2))$ (or simply (M_2, σ^f_{int})) to indicate the intersection point between the local branch of $\mathcal{W}^-_f(R)$ and the invariant plane $[\mathcal{U}, D] \times \mathbb{R}^+$.

Since $M_2 \in [\mathcal{U}, D]$, from Theorem 5.4.1 we conclude that it is always possible to compute the curves representing the transitional map $T^-(M_2)$ ($\{(M_2, \sigma_{X_2}), (M_2, \sigma_{X_1})\}$ in $[\mathcal{U}, D] \times \mathbb{R}^+$ and $\{(X_2, \sigma_{X_2}), (X_1, \sigma_{X_1})\}$ in $[G, \mathcal{U}] \times \mathbb{R}^+$), and the *curve of compatibility* among slow, transitional and fast wave groups $\{(M_2, \sigma^f_{int}), (M_2, \sigma_{X_1})\}$ in $[\mathcal{U}, D] \times \mathbb{R}^+$. In terms of shock speeds, $[\sigma_{X_1}, \sigma^f_{int}]$ is the *compatibility interval of speeds* and $[\sigma_{X_1}, \sigma_{X_2}]$ is the *transitional interval of speeds*. Notice that, as seen in Claim 7.2.1, if $R \in \mathscr{R}_3$ then $\sigma^f_{int} \geq \sigma_{X_2}$ and $[\sigma_{X_1}, \sigma_{X_2}] \subseteq [\sigma_{X_1}, \sigma^f_{int}]$; however if $R \in \mathscr{R}_2$ then $\sigma^f_{int} < \sigma_{X_2}$ and $[\sigma_{X_1}, \sigma^f_{int}] \subset [\sigma_{X_1}, \sigma_{X_2}]$.

Likewise, let M_1 be the intersection state between the invariant segment $[G, \mathcal{U}]$ and the local branch of forward s-wave curve $\mathcal{W}^+_s(L)$ for $L \in \mathcal{SR}_G$. We call $\sigma^s_{int}(M_1)$ the slow "speed of intersection", which would be equal to either the s-characteristic speed $\lambda_s(M_1)$ or the Lax s-shock speed $\sigma(L; M_1)$ (or $\sigma(M_1, M_1')$ if M_1 is s-composite, see Claim 7.2.3), depending on which wave group of $\mathcal{W}^+_s(L)$ intersects the invariant plane. Hence, we use the notation $(M_1, \sigma^s_{int}(M_1))$ (or simply (M_1, σ^s_{int})) to indicate the intersection point between the local branch of $\mathcal{W}^+_s(L) \times \mathbb{R}^+$ and the invariant plane $[G, \mathcal{U}] \times \mathbb{R}^+$.

From Theorem 5.4.1, when $M_2 \in [Y_2, D]$ (or $[D_0, D]$) we have that $X_2(M_2) \in [G, \mathcal{U}]$ satisfies $\sigma(X_2(M_2); M_2) = \lambda_f(X_2(M_2))$. Then, it is possible to concatenate a backward f-rarefaction wave from X_2 such that for all M_1 in this f-rarefaction there is a transitional composite wave given by $M_1 \xrightarrow{R_f} X_2 \xrightarrow{'S_T} M_2$ (see Section 2.5).

Definition 7.3.1. Refer to Figure 7.9(a)-(b). Consider a state $M_2 \in [\mathcal{U}, D]$ and its corresponding states $X_2(M_2)$ and $X_1(M_2)$ in $[G, \mathcal{U}]$ computed as in Theorem 5.4.1, such that $\sigma^f_{int} \geq \sigma_{X_2}$. On one hand, we construct the backward s-wave curve from X_2, $\mathcal{W}^-_s(X_2)$ given by the s-rarefaction curves $[X_2, E_2]$ and $[M(X_2), B_2]$, and the Lax s-shock segment $(X_2, M(X_2)]$, where $M(X_2)$ is the state associated to X_2 such that there is a sonic shock between $M(X_2)$ and X_2 with $\sigma(M(X_2); X_2) = \lambda_s(M(X_2))$ (see Figure 7.9 (a)); on the other hand, we construct the backward s-rarefaction curves $[X_1, E_1]$ and $[X_3^*, B_1]$, and the Lax s-shock segment $[X_1, X_3^*] \subset \mathcal{H}(M_2)$. We define the following sets in the slow macro region $\mathcal{SR}_G$ depending on the location of (M_2, σ^f_{int}):

a) The region $S_{1C}(X_2)$ bounded by the line segment $[G, X_2]$, the s-rarefaction $[X_2, E_2]$ and the segment $[E_2, G]$. From Claim 7.2.3, for any $L \in S_{1C}(X_2)$ the intersection between $\mathcal{W}^+_s(L) \times \mathbb{R}^+$ and $[G, \mathcal{U}] \times \mathbb{R}^+$ is in the curve $T_{S_{1C}} = \{(G, 0), (X_2, \lambda_s(X_2))\} \subset T_{S_1}$ and $S_{1C}(X_2) \subset S_1$.

b) The region $S_{2C}(X_2)$ bounded by the line segment $[G, X_2]$, the Lax s-shock $(X_2, M(X_2)]$ and the right s-extension $E^+_s[G, X_2]$ given by $[G, M(X_2)]$. From Claim 7.2.3, for any $L \in S_{2C}(X_2)$ the intersection between $\mathcal{W}^+_s(L) \times \mathbb{R}^+$ and $[G, \mathcal{U}] \times \mathbb{R}^+$ is in region $T_{S_{2C}} \subset T_{S_2}$ bounded by $\{(G, 0), (X_2, \lambda_s(X_2))\}$, $\{(X_2, \sigma_{M(X_2)}), (X_2, \lambda_s(X_2))\}$ and $\{(X_2, \lambda_s(X_2)), (G, 0)\}$, and we have that $S_{2C}(X_2) \subset S_2$.

c) The region $S_{3C}(X_2)$ bounded by the segment $[G, B_2]$, the s-rarefaction $[M(X_2), B_2]$ and the right

s-extension $E_s^+[G, X_2]$ given by $[G, M(X_2)]$. From Claim 7.2.3, for any $L \in S_{3C}(X_2)$ the intersection between $\mathcal{W}_s^+(L) \times \mathbb{R}^+$ and $[G,\mathcal{U}] \times \mathbb{R}^+$ is in the curve $T_{S_{3C}} = \{(G, 0), (X_2, \sigma_{M(X_2)})\} \subset T_{S_3}$ and $S_{3C}(X_2) \subset S_3$.

d) The region $S_{1T}(X_1)$ bounded by the line segment $[E_1, E_2]$, the s-rarefactions $[X_2, E_2]$ and $[X_1, E_1]$, and the segment $[X_2, X_1]$. From Claim 7.2.3, for any $L \in S_{1T}(X_1)$ the intersection between $\mathcal{W}_s^+(L) \times \mathbb{R}^+$ and $[G,\mathcal{U}] \times \mathbb{R}^+$ is in the curve $T_{S_{1T}} = \{(X_2, \lambda_s(X_2)), (X_1, \lambda_s(X_1))\} \subset T_{S_1}$ and $S_{1T}(X_1) \subset S_1$.

e) The region $S_{2T}(X_1)$ bounded by the line segment $[X_2, X_1]$, the Lax s-shock segments $(X_2, M(X_2)]$ and $(X_1, X_3^*]$ and the right s-extension $E_s^+[X_2, X_3]$ given by $[M(X_2), X_3^*]$. From Claim 7.2.3, for any $L \in S_{2T}(X_1)$ the intersection between $\mathcal{W}_s^+(L) \times \mathbb{R}^+$ and $[G,\mathcal{U}] \times \mathbb{R}^+$ is in region $T_{S_{2T}} \subset T_{S_2}$ bounded by $\{(X_2, \lambda_s(X_2)), (X_2, \sigma_{M(X_2)})\}$, $\{(X_2, \sigma_{M(X_2)}), (X_3, \sigma_{X_3})\}$, $\{(X_3, \sigma_{X_3}), (X_1, \sigma_{X_1})\}$ and $\{(X_1, \sigma_{X_1}), (X_2, \lambda_s(X_2))\}$, and we have that $S_{2T}(X_1) \subset S_2$.

f) The region $S_{3T}(X_1)$ bounded by the segment $[B_2, B_1]$, the s-rarefactions $[M(X_2), B_2]$ and $[X_3^*, B_1]$, and the right s-extension $E_s^+[X_2, X_3]$ given by $[M(X_2), X_3^*]$. From Claim 7.2.3, for any $L \in S_{3T}(X_1)$ the intersection between $\mathcal{W}_s^+(L) \times \mathbb{R}^+$ and $[G,\mathcal{U}] \times \mathbb{R}^+$ is in the curve $T_{S_{3T}} = \{(X_2, \sigma_{M(X_2)}), (X_3, \sigma_{X_3})\} \subset T_{S_3}$ and $S_{3T}(X_1) \subset S_3$.

Remark 7.3.2. Assume that $\sigma_{int}^f = \sigma_{X_2}$. When $M_2 \in (Y_1, Y_2)$ we only have the sets S_{1T}, S_{2T} and S_{3T} given in Definition 7.3.1 d), e) and f). On the other hand, when $M_2 \in (\mathcal{U}, Y_1)$ we only have the sets S_{1T} and S_{2T} given in Definition 7.3.1 d) and e).

Definition 7.3.3. In the setting of Definition 7.3.1 with $\sigma_{X_2} > \sigma_{int}^f$, let M_2' be the state in $[X_2, X_1] \subset [G,\mathcal{U}]$ such that $\sigma_{int}^f = \sigma(M_2, M_2')$. This case differs from the case given in Definition 7.3.1 only in that the boundaries of regions depend on M_2', instead of X_2. We have two sub-cases for the construction of the regions S_{iT} for $i \in \{1, 2, 3\}$ (there are no regions S_{iC} for $i \in \{1, 2, 3\}$).

(1) Case $\sigma_{int}^f \geq \sigma_{X_3}$:

Refer to Figure 7.10(a)-(b). We construct the backward s-wave curve from M_2'; $\mathcal{W}_s^-(M_2')$ is given by the s-rarefaction curves $[M_2', E_2]$ and $[N(M_2'), B_2]$, and the Lax s-shock segment $(M_2', N(M_2')]$, where $N(M_2')$ is the state associated to M_2' such that there is a sonic shock between $N(M_2')$ and M_2' with $\sigma_{N(M_2')} = \sigma(N(M_2'); M_2') = \lambda_s(N(M_2'))$ (see Figure 7.10 (a)); the boundaries that depend on X_1 are construct in the same way. We define the following sets depending on M_2 in the slow macro region $\mathcal{SR}_G$:

a) The region $S_{1T}(X_1)$ bounded by the line segment $[E_1, E_2]$, the s-rarefactions $[M_2', E_2]$ and $[X_1, E_1]$, and the segment $[M_2', X_1]$. From Claim 7.2.3, for any $L \in S_{1T}(X_1)$ the intersection between $\mathcal{W}_s^+(L) \times \mathbb{R}^+$ and $[G,\mathcal{U}] \times \mathbb{R}^+$ is in the curve $T_{S_{1T}} = \{(M_2', \lambda_s(M_2')), (X_1, \lambda_s(X_1))\} \subset T_{S_1}$ and $S_{1T}(X_1) \subset S_1$.

b) The region $S_{2T}(X_1)$ bounded by the line segment $[M_2', X_1]$, the Lax s-shock segments $(M_2', N(M_2')]$ and $(X_1, X_3^*]$ and the right s-extension $E_s^+[M_2', X_3]$ given by $[N(M_2'), X_3^*]$. From

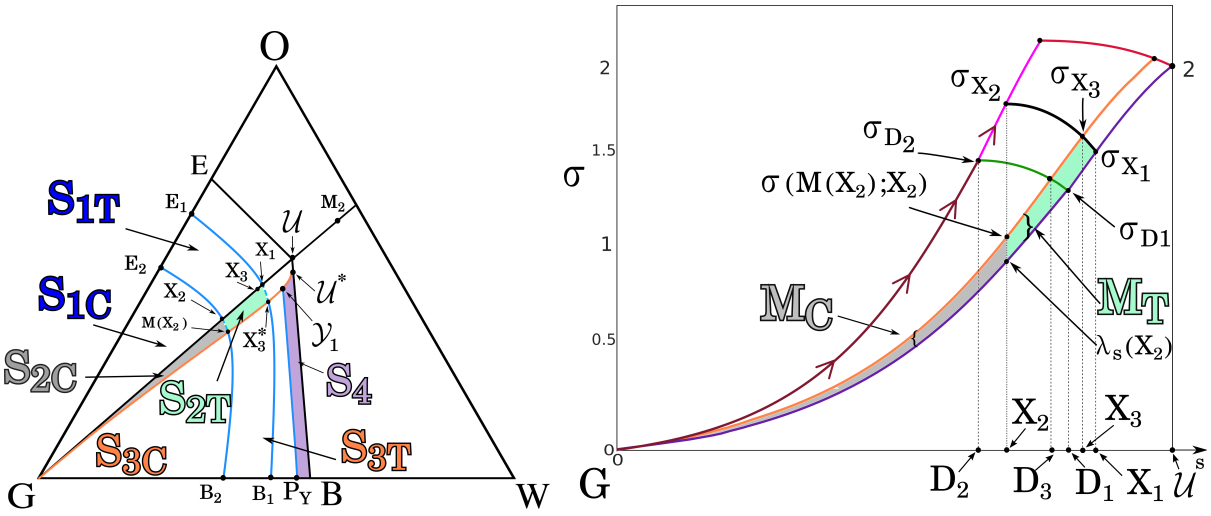

Figure 7.9: Regions associated to states $M_2 \in (\mathcal{U}, D]$ with $\sigma^f_{int} \geq \sigma_{X_2}$. a) Subdivision of $\mathcal{SR}_G$ in regions associated to M_2 where there is compatibility with transitional waves, see Definition 7.3.1. From Claim 7.2.3, regions S_{1T} and S_{1C} are subsets of S_1 and intersect the curve T_{S_1}, regions S_{2T} and S_{2C} are subsets of S_2 and intersect the region T_{S_2} and regions S_{3T} and S_{3C} are subsets of S_3 and intersect the curve T_{S_3}. b) Areas of intersection between the invariant plane $[G, D] \times \mathbb{R}^+$ and $\mathcal{W}^+_s(L) \times \mathbb{R}^+$ for $L \in \mathcal{SR}_G$. Regions M_C (gray) and M_T (green) defined in Definition 7.3.4 which admit transitional composite waves or single transitional shocks, respectively. The curve $\{(G, 0), (X_2, \sigma_{X_2})\}$ is a backward f-rarefaction from state X_2, the horizontal axis corresponds to a parametrization of the $[G, D]$ in terms of the effective saturation s and the vertical axis indicates the values of shock speeds.

Claim 7.2.3, for any $L \in S_{2T}(X_1)$ the intersection between $\mathcal{W}^+_s(L) \times \mathbb{R}^+$ and $[G,\mathcal{U}] \times \mathbb{R}^+$ is in region $T_{S_{2T}} \subset T_{S_2}$ bounded by $\{(M'_2, \lambda_s(M'_2)), (M'_2, \sigma_{N(M'_2)})\}$, $\{(M'_2, \sigma_{N(M'_2)}), (X_3, \sigma_{X_3})\}$, $\{(X_3, \sigma_{X_3}), (X_1, \sigma_{X_1})\}$ and $\{(X_1, \sigma_{X_1}), (M'_2, \lambda_s(M'_2))\}$, and we have that $S_{2T}(X_1) \subset S_2$.

c) The region $S_{3T}(X_1)$ bounded by the segment $[B_2, B_1]$, the s-rarefactions $[N(M'_2), B_2]$ and $[X^*_3, B_1]$, and the right s-extension $E^+_s[M'_2, X_3]$ given by $[N(M'_2), X^*_3]$. From Claim 7.2.3, for any $L \in S_{3T}(X_1)$ the intersection between $\mathcal{W}^+_s(L) \times \mathbb{R}^+$ and $[G,\mathcal{U}] \times \mathbb{R}^+$ is in the curve $T_{S_{3T}} = \{(M'_2, \sigma_{N(M'_2)}), (X_3, \sigma_{X_3})\} \subset T_{S_3}$ and $S_{3T}(X_1) \subset S_3$.

(2) Case $\sigma_{X_3} > \sigma^f_{int} \geq \sigma_{X_1}$:

Refer to Figure 7.11(a)-(b). We construct the backward s-rarefaction curve $[M'_2, E_2]$ and the Lax s-shock segment $(M'_2\ , N(M'_2)]$, where $N(M'_2)$ is the state associated to M'_2 such that $N(M'_2)$ is in the shock segment $[X_1, X_3] \subset \mathcal{H}(M_2)$ and $\sigma_{N(M'_2)} = \sigma(M_2; M'_2) = \sigma(M'_2; N(M'_2))$ (see Figure 7.11 (a)); the boundaries that depend on X_1 are constructed in the same way. We define the following sets depending on M_2 in the slow macro region $\mathcal{SR}_G$:

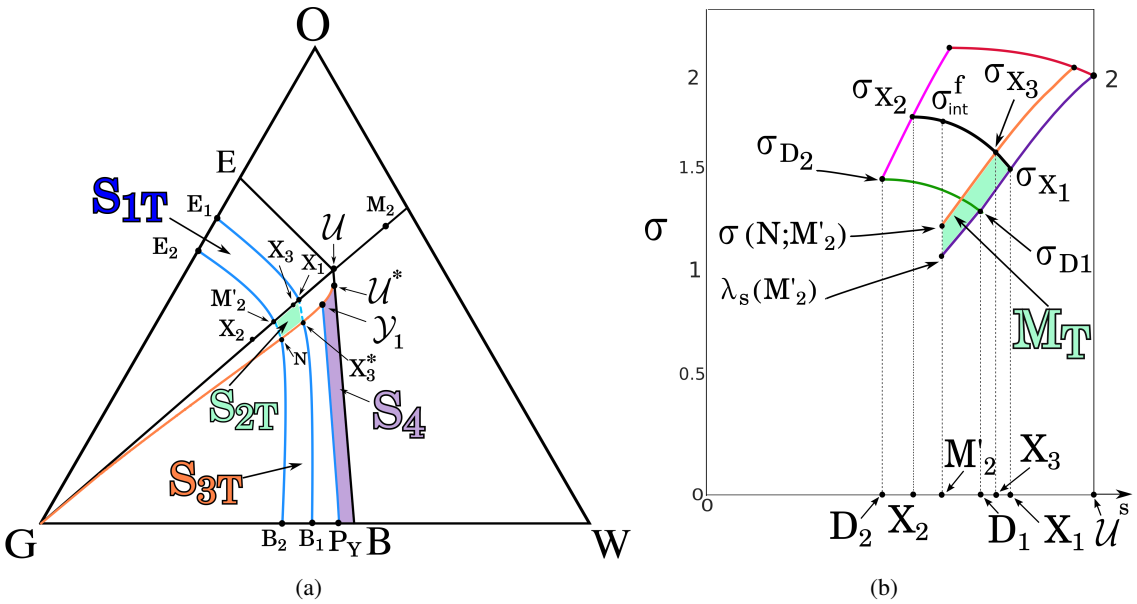

Figure 7.10: Regions associated to states $M_2 \in (\mathcal{U}, D]$ with $\sigma_{X_2} > \sigma^f_{int}$. The state $M_2' \in [G,\mathcal{U}]$ satisfy $\sigma(M_2; M_2') = \lambda_f(M_2)$, see Claim 6.4.4 with $M_2' = Z_2$. a) Subdivision of $\mathcal{SR}_G$ in regions associated to M_2 which there is compatibility with transitional waves, see Definition 7.3.3. From Claim 7.2.3, $S_{1T} \subset S_1$ and intersect the curve T_{S_1}, region $S_{2T} \subset S_2$ and intersect the region T_{S_2} and region $S_{3T} \subset S_3$ intersect the curve T_{S_3}. b) Area of intersection between the invariant plane $[G, D] \times \mathbb{R}^+$ and $\mathcal{W}_s^+(L) \times \mathbb{R}^+$ for $L \in \mathcal{SR}_G$. Region M_T (green) defined in Definition 7.3.4 which admit single transitional shocks. The horizontal axis corresponds to a parametrization of the $[G, D]$ in terms of the effective saturation s and the vertical axis indicates the values of shock speeds

a) The region $S_{1T}(X_1)$ is defined as in the previous case 1.a).

b) The region $S_{2T}(X_1)$ bounded by the line segment $[M_2', X_1]$, the Lax s-shock segments $(M_2', N(M_2')]$ and $(X_1, N(M_2')]$. From Claim 7.2.3, for any $L \in S_{2T}(X_1)$ the intersection between $\mathcal{W}_s^+(L) \times \mathbb{R}^+$ and $[G,\mathcal{U}] \times \mathbb{R}^+$ is in region $T_{S_{2T}} \subset T_{S_2}$ bounded by $\{(M_2', \lambda_s(M_2'))$, $(M_2', \sigma^f_{int})\}$, $\{(M_2', \sigma^f_{int})$, $(X_1, \sigma_{X_1})\}$ and $\{(X_1, \sigma_{X_1})$, $(M_2', \lambda_s(M_2'))\}$, and we have that $S_{2T}(X_1) \subset S_2$.

Definition 7.3.4. We name $M_C(M_2)$ the region of the invariant plane $[G,\mathcal{U}] \times \mathbb{R}^+$ associated to $M_2 \in [\mathcal{U}, D]$ that admits transitional composite waves between states $M_1 \in [G,\mathcal{U}]$ and M_2; see Figure 7.9(b). This region corresponds to $M_C = T_{S_{1C}} \cup T_{S_{2C}} \cup T_{S_{3C}}$, with $T_{S_{iC}}$, for $i \in \{1, 2, 3\}$ given in Definition 7.3.1 (see gray area in Figure 7.9(b)).

Analogously, we name $M_T(M_2)$ the region of $[G,\mathcal{U}] \times \mathbb{R}^+$ associated to M_2 that admits single transitional shock waves between states $M_1 \in [G,\mathcal{U}]$ and M_2, which corresponds to $M_T = T_{S_{1T}} \cup T_{S_{2T}} \cup T_{S_{3T}}$, with $T_{S_{iT}}$ for $i \in \{1, 2, 3\}$ given in Definition 7.3.1 (either Remark 7.3.2 or in Definition 7.3.3 where $M_T = T_{S_{1T}} \cup T_{S_{2T}}$); see green area in Figures 7.9(b), 7.10(b) and 7.11(b).

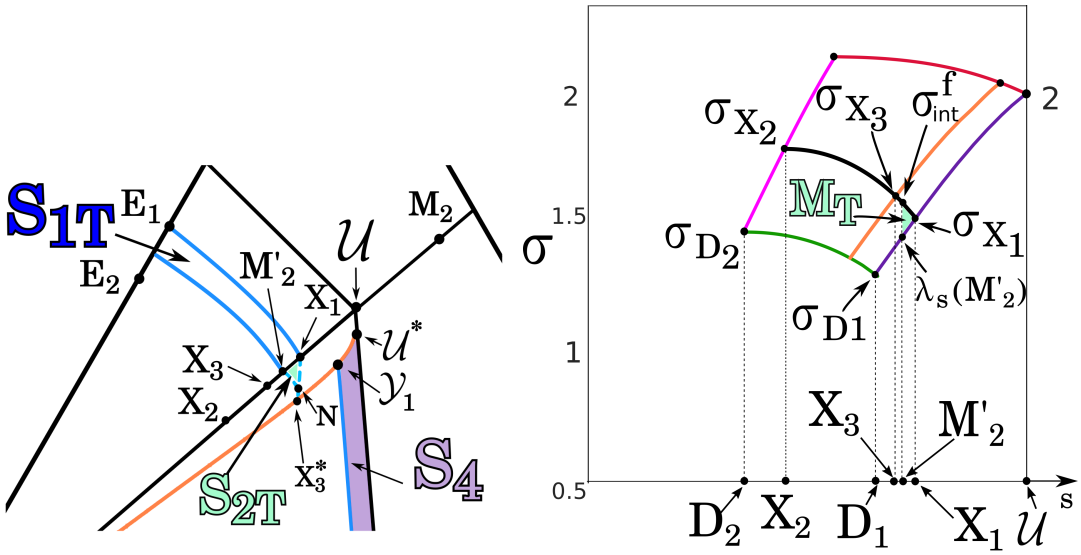

(a) (b)

Figure 7.11: Regions associated to states $M_2 \in (\mathcal{U}, D]$ with $\sigma_{X_3} > \sigma^f_{int}$. The state $M_2' \in [G, \mathcal{U}]$ satisfy $\sigma(M_2; M_2') = \lambda_f(M_2)$, see Claim 6.4.4 with $M_2' = Z_2$. a) Subdivision of $\mathcal{SR}_G$ in regions associated to M_2 which there is compatibility with transitional waves, see Definition 7.3.3. From Claim 7.2.3, $S_{1T} \subset S_1$ and intersect the curve T_{S_1} and region $S_{2T} \subset S_2$ intersect the curve T_{S_2}. b) Area of intersection between the invariant plane $[G, D] \times \mathbb{R}^+$ and $\mathcal{W}^+_s(L) \times \mathbb{R}^+$ for $L \in \mathcal{SR}_G$. Region M_T (green) defined in Definition 7.3.4 which admit single transitional shocks. The horizontal axis corresponds to a parametrization of the $[G, D]$ in terms of the effective saturation s and the vertical axis indicates the values of shock speeds.

Remark 7.3.5. In Definition 7.3.1 we assumed that for given M_2 we have sets $M_C(M_2)$ and $M_T(M_2)$, but it is possible that only the set $M_T(M_2)$ exists (*e.g.,* when $\nu_G > 8$) or that none exist (*e.g.,* when $\nu_G < 1$ and $M_2 \in [\mathcal{U}, D_0]$).

We define the following methodology for the use of surface of transitional shocks: given a state $R \in \mathcal{FR}_D$, we find $(M_2, \sigma^f_{int}) \in [\,\mathcal{U}, D] \times \mathbb{R}^+$ and compute the curves associated to the transitional map and the curve of compatibility. Then, we identify the regions of the surface of transitional shocks that can be reached by a forward s-wave curve. Given a point (M_1, σ^s_{int}), we draw a vertical line in a direction of increasing velocity until it intersects the curve $\{(X_2, \sigma_{X_2}), (X_1, \sigma_{X_1})\}$ defined from M_2, thus obtaining the speed $\sigma_T = \sigma(M_1; M_2)$ which allows a transitional shock. Finally, we verify if this transitional shock is compatible with the slow and fast wave groups.

7.3.1 (M_2, σ^f_{int}) intersecting the region T_3 or the curve A

As seen in Claim 7.2.1, given a state $R \in \mathcal{FR}_D$, the point $(M_2, \sigma^f_{int}) \in [\mathcal{U}, D] \times \mathbb{R}^+$ belongs to the region T_3 if the right state R lies to the (upper or lower) region $\mathscr{R}_3$; otherwise, the point $(M_2, \sigma^f_{int}) \in [\mathcal{U}, D] \times \mathbb{R}^+$ belongs to the curve A, when R lies on the region $A = \mathscr{R}_4 \cup \mathscr{R}_{4'} \subset \mathcal{FR}_D$ (see Sections

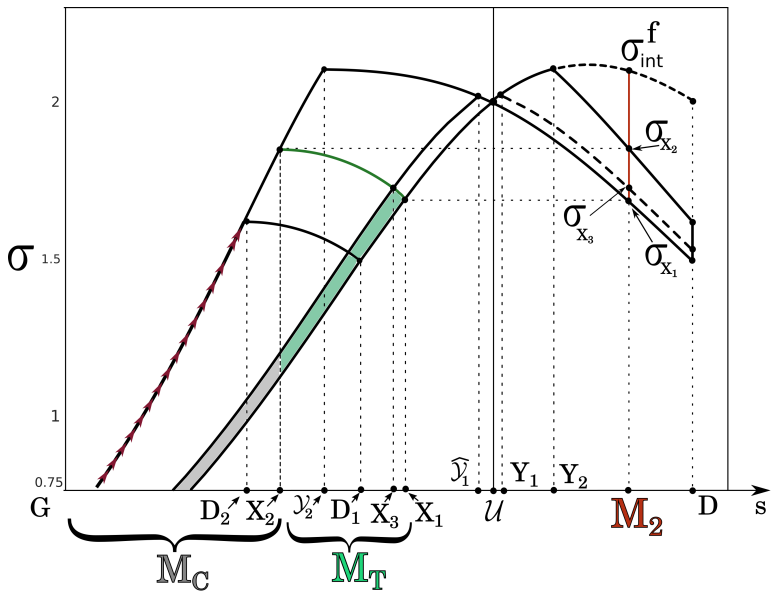

Figure 7.12: Regions $M_C(M_2)$ and $M_T(M_2)$ given in Definition 7.3.4 when (M_2, σ^f_{int}) intersects curve A, see Claim 7.2.1. The horizontal axis corresponds to a parametrization of the $[G, D]$ in terms of the effective saturation s and the vertical axis indicates the values of shock speeds. Notice that in this case $\sigma^f_{int} > \sigma_{X_2} > \sigma_{X_1}$ (see Definition 7.3.1). The curve $\{(G, 0), (X_2, \sigma_{X_2})\}$ (arrows) is a backward f-rarefaction from state X_2.

6.4.2 and 6.4.3). In both cases we have $\sigma^f_{int} \geq \sigma_{X_2}$ ($\sigma^f_{int} = \sigma_{X_2}$ when $R \in [V_2, Y_2] \cup [V_2^*, Y_2^*]$, see Figure 7.5(a)). This mean that for any R in the region $\mathscr{R}_3 \cup A$, depending on the left state L the transitional wave is either a single shock (*i.e.,* $W_s^+(L)$ intersecting $M_T(M_2)$) or a composite wave consisting of a f-rarefaction wave adjacent to a transitional shock (*i.e,* $W_s^+(L) \times \mathbb{R}^+$ intersecting $M_C(M_2)$). In Figure 7.12, we plot the curves representing the transitional map $T^-(M_2)$ and the curve of compatibility for the case when (M_2, σ^f_{int}) belongs to curve A. Then, we describe these two possibilities as follow:

(1) Case $W_s^+(L) \times \mathbb{R}^+$ intersects $M_C(M_2)$:

As we seen in the Claim 7.2.3, and from Definitions 7.3.1 and 7.3.4, for any (M_1, σ^s_{int}) we can reach the curve of f-rarefactions $\{(G, 0), (X_2, \sigma_{X_2})\}$ with a vertical line from (M_1, σ^s_{int}), intersecting this curve at $(M_1, \lambda_f(M_1))$ with $\sigma^s_{int} < \lambda_f(M_1) \leq \sigma_{X_2}$, see Figure 7.12. Notice that this "vertical speed jump" implies that M_1 represent a constant state in the solutions of the Riemann problem. Then, the construction continues it by following the f-rarefaction from $(M_1, \lambda_f(M_1))$ until the point (X_2, σ_{X_2}), where there is a transitional shock between X_2 and M_2 with $\sigma(X_2; M_2) = \lambda_f(X_2) = \sigma_{X_2} < \sigma^f_{int}$ satisfying the compatibility criterion of speeds. Therefore, we have the sequence of transitional wave $M_1 \xrightarrow{R_f} X_2 \xrightarrow{'S_T} M_2$.

(2) Case $W_s^+(L) \times \mathbb{R}^+$ intersects $M_T(M_2)$:

As we seen in the Claim 7.2.3 and from Definitions 7.3.1 and 7.3.4, for any (M_1, σ^s_{int}) we can reach the curve $\{(X_1, \sigma_{X_1}), (X_2, \sigma_{X_2})\}$ that represents the transitional map $T^-(M_2)$ with a vertical line from (M_1, σ^s_{int}), intersecting this curve at $(M_1, \sigma(M_1; M_2))$ with $\sigma^s_{int} \leq \sigma(M_1; M_2) \leq \sigma_{X_2}$, see Figure 7.12. Notice that this "vertical speed jump" implies that M_1 represents a constant state in the solutions of the Riemann problem. Then, there is a transitional shock between M_1 and M_2 with $\sigma(M_1; M_2) \leq \sigma^f_{int}$ satisfying the compatibility criterion of speeds. Therefore, we have the transitional wave $M_1 \xrightarrow{S_T} M_2$.

Remark 7.3.6. Notice that given a state $M_2 \in [Y_2, D]$ (or $M_2 \in [D_0, D]$, when $0 < \nu_G < 1$), for any $L \in \mathcal{SR}_G$ such that $\mathcal{W}^+_s(L) \times \mathbb{R}^+$intersects the invariant plane $[G,\mathcal{U}] \times \mathbb{R}^+$, at $(M_1, \sigma^s_{int}) \notin M_C(M_2)$ or at $(M_1, \sigma^s_{int}) \notin M_T(M_2)$, then there is no transitional wave joining M_1 and M_2 after the slow wave group from L to M_1 (see Figure 7.9).

7.3.2 (M_2, σ^f_{int}) intersecting the curve B

As seen in Claim 7.2.1 given a state $R \in \mathcal{FR}_D$, the point $(M_2, \sigma^f_{int}) \in [\mathcal{U}, D] \times \mathbb{R}^+$ belongs to the curve B when R lies on the region $B = \mathscr{R}_5 \cup \mathscr{R}_{5'} \cup \mathscr{R}_6 \cup \mathscr{R}_{6'} \subset \mathcal{FR}_D$ (see Sections 6.4.2, 6.4.3 and Figure 7.5(a)). In this case, we have $\sigma^f_{int} = \sigma_{X_2}$ and $\sigma_{X_2} = \sigma(M_2; X_2) = \lambda_f(M_2)$. This means that for any R in the region B, the transitional wave can only be a single shock, *i.e.,* $W^+_s(L) \times \mathbb{R}^+$ intersects $M_T(M_2)$. In Figure 7.13 we plot the curves representing the transitional map $T^-(M_2)$ and the curve of compatibility for the case of (M_2, σ^f_{int}) on curve B (in this case these curves coincide). This case is similar to the case (2) described in Section 7.3.1. Therefore, we have the transitional wave $M_1 \xrightarrow{S_T} M_2$.

Remark 7.3.7. Follows Remark 7.3.2, given a state $M_2 \in (Y_1, Y_2)$ (or $M_2 \in (Y_1, D]$, when $\nu_G > 8$), for any $L \in \mathcal{SR}_G$ such the intersection point (M_1, σ^s_{int}) between $\mathcal{W}^+_s(L) \times \mathbb{R}^+$ and the invariant plane $[G,\mathcal{U}] \times \mathbb{R}^+$ does not belong to $M_T(M_2) = T_{S_{1T}} \cup T_{S_{2T}} \cup T_{S_{3T}}$, there is no transitional wave joining M_1 and M_2 after the slow wave group from L to M_1. On the other hand, given a state $M_2 \in [\mathcal{U}, Y_1)$ (or $M_2 \in [\mathcal{U}, D]$, when $(\nu^-_G)^2/(\nu_G) > 8$), for any $L \in \mathcal{SR}_G$ such the intersection point (M_1, σ^s_{int}) does not belong to $M_T(M_2) = T_{S_{1T}} \cup T_{S_{2T}}$, there is no transitional wave joining M_1 and M_2 after the slow wave group from L to M_1.

7.3.3 (M_2, σ^f_{int}) intersecting the Region T_2

As seen in Claim 7.2.1, given a state $R \in \mathcal{FR}_D$, the point $(M_2, \sigma^f_{int}) \in [\mathcal{U}, D] \times \mathbb{R}^+$ belongs to the region T_2 when R lies on the (lower or upper) region $\mathscr{R}_2 \subset \mathcal{FR}_D$ (see Section 6.4.1 and Figure 7.5(a)). In this case, we have $\sigma_{X_2} > \sigma^f_{int}$ and there is a state $M_2' \in [G,\mathcal{U}]$ such that M_2 and M_2' can be joined by a transitional shock with $\sigma(M_2; M_2') = \sigma(M_2; R) = \sigma^f_{int}$. Therefore, there are points of the transitional map $T^-(M_2)$ that are incompatible with the Lax f-shock between M_2 and $R \in \mathscr{R}_2$ because the speed of the transitional shocks is larger that the intersection speed σ^f_{int}. In Definition 7.3.3, it is stated that the set $M_T(M_2)$ is formed by compatible states when $\sigma_{X_2} > \sigma^f_{int}$. Therefore, for any R in the region T_2, the transitional wave can only be a single shock, *i.e.,* $W^+_s(L) \times \mathbb{R}^+$ intersects $M_T(M_2)$. We have two possibilities for (M_2, σ^f_{int}) depending on σ^f_{int}: (i) $\sigma^f_{int} \geq \sigma_{X_3}$, shown in Figure 7.14; or (ii)

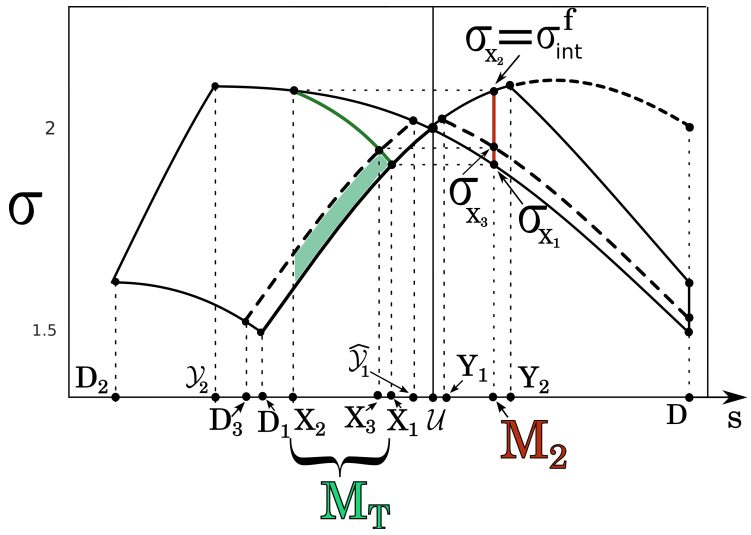

Figure 7.13: Region $M_T(M_2)$ given in Definition 7.3.4 when (M_2, σ_{int}^f) intersects curve B, see Claim 7.2.1. The horizontal axis corresponds to a parametrization of the $[G, D]$ in terms of the effective saturation s and the vertical axis indicates the values of shock speeds. Notice that in this case $\sigma_{int}^f = \sigma_{X_2} > \sigma_{X_1}$ (see Definition 7.3.1).

$\sigma_{X_3} > \sigma_{int}^f \geq \sigma_{X_1}$, show in Figure 7.15. In both cases the description of transitional shock is similar to the case (2) described in Section 7.3.1. Therefore, we have the transitional wave $M_1 \xrightarrow{S_T} M_2$.

7.4 Solving Riemann problems that involve transitional shocks

In this section we describe the use of the geometric construction developed in the previous sections to find the solutions that require a transitional shock to solve the Riemann problem. Without loss of generality, we describe the procedure for the surface of transitional shocks associated to invariant line $[G, D]$.

Consider a state $R \in \mathcal{FR}_D \backslash \mathscr{R}_1$ and construct $\mathcal{W}_f^-(R)$ following the procedure developed in Chapter 6. Using Claim 7.2.1, we can identify the intermediate state (M_2, σ_{int}^f), and we use Section 7.3 to identify sets $M_C(M_2)$ or $M_T(M_2)$. Then, we take L in some region of $\mathcal{SR}_G$ associate to $M_C(M_2)$ or $M_T(M_2)$ in order to construct the forward s-wave curve $\mathcal{W}_s^+(L)$. The Riemann solutions found using this procedure are compatible and the L^1_{Loc}-stability is verified for perturbations under change of problem parameters and variation of data. Moreover, the stability of transitional shocks is guaranteed in [28], which has shown the procedure for a general system of n equations and for more general sets of shocks that include transitional shocks. In Figure 7.16, we show the solution of a Riemann problem for right state R in the upper $\mathscr{R}_3$-region and left state L in $S_3 \subset \mathcal{SR}_G$.

Finally, in Figure 7.17 we look at the case of $1 < \nu_G \leq 8$ with umbilic point of type II_O and compare the foliation surfaces of backward s- and forward f-wave curves, and show the surface of transitional

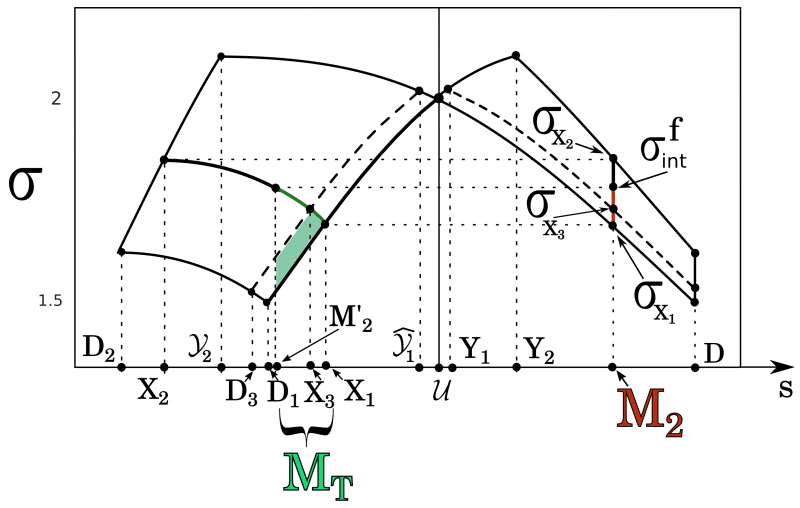

Figure 7.14: Region $M_T(M_2)$ given in Definition 7.3.4 when (M_2, σ^f_{int}) intersects the region T_2 with $\sigma_{X_2} > \sigma^f_{int} > \sigma_{X_1}$ (see Claim 7.2.1 and Definition 7.3.3). The horizontal axis corresponds to a parametrization of $[G, D]$ in terms of the effective saturation s and the vertical axis indicates the values of shock speeds. The state $M_2' \in [G, \mathcal{U}]$ satisfies $\sigma(M_2; M_2') = \lambda_f(M_2)$, see Claim 6.4.4 with $M_2' = Z_2$.

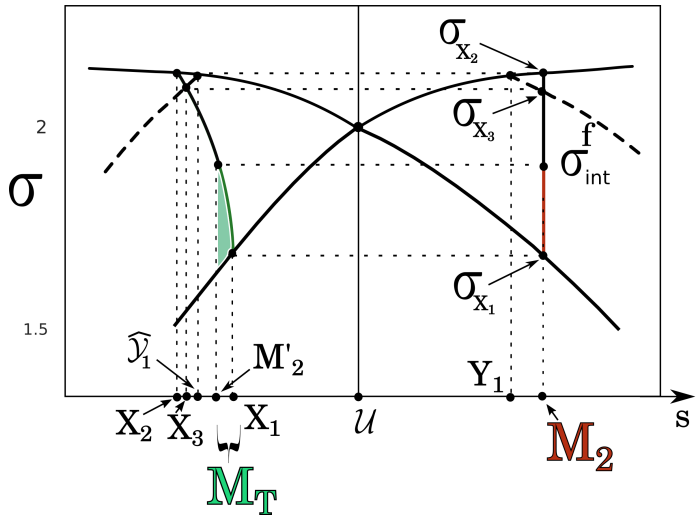

Figure 7.15: Region $M_T(M_2)$ given in Definition 7.3.4 when (M_2, σ^f_{int}) intersects the region T_2 with $\sigma_{X_3} > \sigma^f_{int} > \sigma_{X_1}$ (see Claim 7.2.1 and Definition 7.3.3 case (2)). The horizontal axis corresponds to a parametrization of $[G, D]$ in terms of the effective saturation s and the vertical axis indicates the values of shock speeds. The state $M_2' \in [G, \mathcal{U}]$ satisfies $\sigma(M_2; M_2') = \lambda_f(M_2)$, see Claim 6.4.4 with $M_2' = Z_2$.

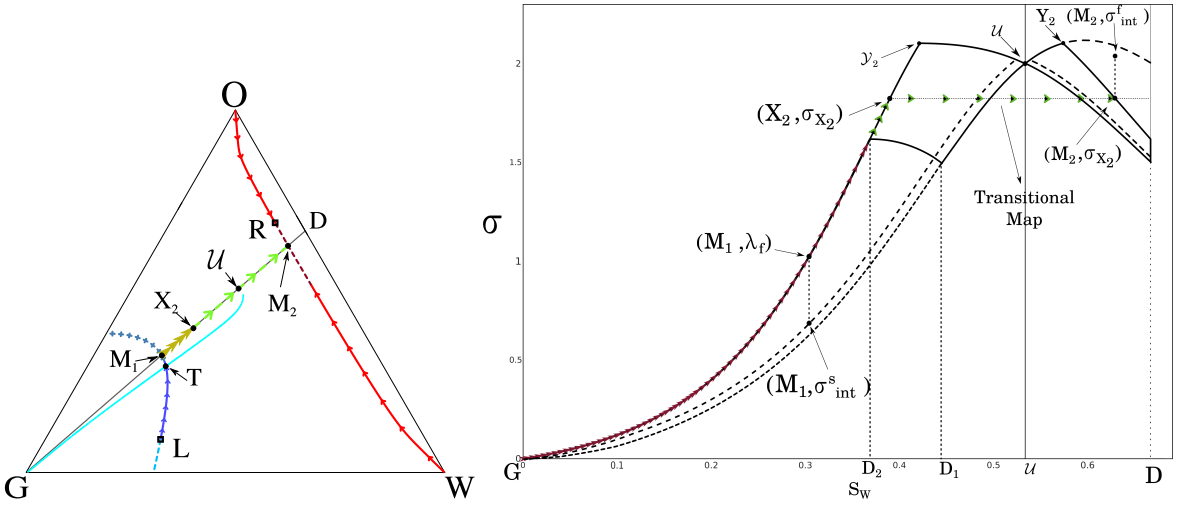

(a) Projection of Riemann problem in the saturation triangle.

(b) Transtional wave involve in the solution of Riemann problem in plane $[G, D] \times \mathbb{R}^+$.

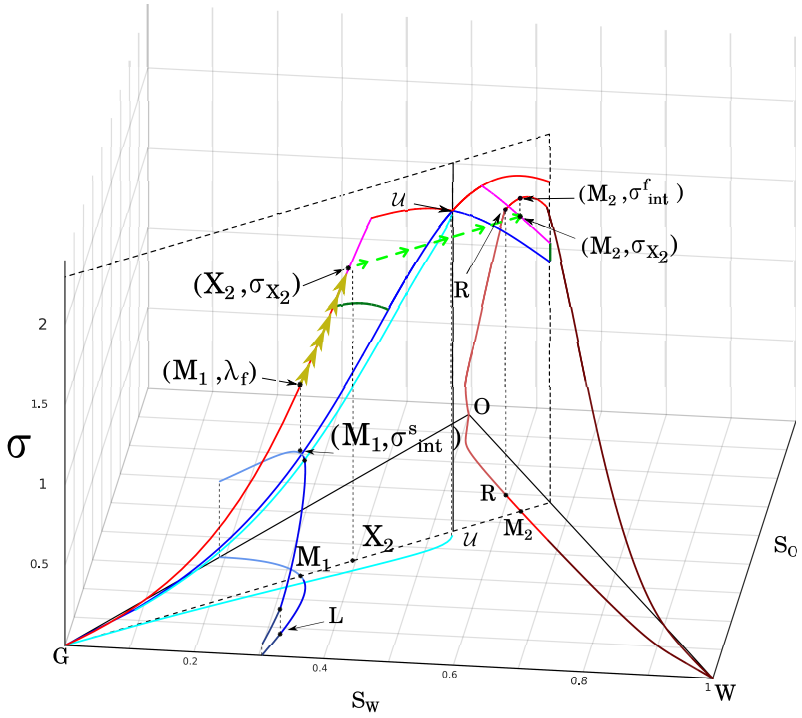

(c) Slow and fast wave curves in the three dimensional phase space.

Figure 7.16: Solution of Riemann problem using the surface of transitional shocks.

shocks associated to the invariant line $[G, D]$. Notice that any Riemann solution that involves transitional waves is contained in this Figure and it is possible to verify the compatibility of shock speeds between the slow, transitional and fast wave groups.

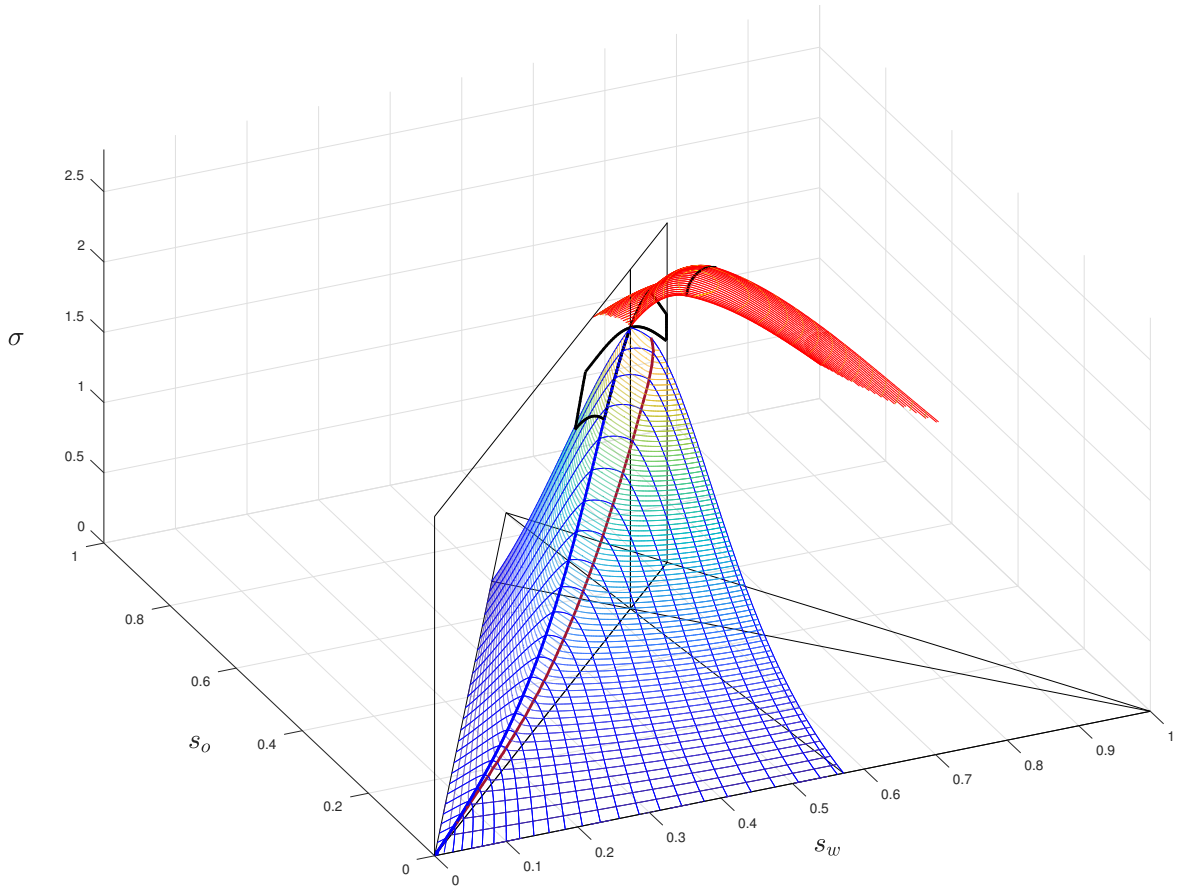

Figure 7.17: Surfaces describing solutions of Riemann problems with transitional waves. The fast and slow surfaces were defined in Remark 7.2.1 and 7.2.2, and Figures 7.6 and 7.8 respectively.

Chapter 8

Riemann solutions and $\mathscr{L}_{\mathscr{R}}$-regions

In this chapter, we construct the solution of the Riemann problem and find the backward $\mathscr{L}_{\mathscr{R}}$-regions that depend on the backward $\mathscr{R}$-regions defined in Chapter 6. For this purpose, we construct the right s-extension of the backward f-wave curve from R in each $\mathscr{R}$-region, which acts as a boundary for loss of speed compatibility; also from each state where the local or nonlocal branches of $\mathcal{W}_f^-(R)$ have a change of wave group type, we construct a backward s-wave curve, obtaining the boundaries of regions with the same structure for their Riemann solutions. Finally, we combine this analysis with the regions of transitional waves M_C and M_T studied in Chapter 7 to complete the subdivision of the saturation triangle in $\mathscr{L}_{\mathscr{R}}$-regions and find the Riemann solutions for any left state L and $R \in \mathscr{R}$.

8.1 Backward slow wave curve

To construct the $\mathscr{L}_{\mathscr{R}}$-regions for a given $\mathscr{R}$-region, it is necessary to build backward s-wave curves from certain points on $\mathcal{W}_f^-(R)$ and from a few other special points. These points are:

- The state R which by definition connects a shock segment and a rarefaction segment (unless R lies on fast-inflection locus).
- States $A_i \in \mathcal{W}_f^-(R)$ that are Bethe-Wendroff points. These points represent states at which different segments of wave groups start or end.
- States T_i which are intersection points between the s-inflection locus and $\mathcal{W}_f^-(R)$. At these points the $\mathcal{W}_s^-(T_i)$ changes structure.
- States associated to regions M_C and M_T described in Definition 7.3.4.
- States on shock segments of $\mathcal{W}_f^-$ that satisfy the triple shock rule.

In some situations we only require some components of $\mathcal{W}_s^-$ because it is possible that other components do not represent a true boundary of a $\mathscr{L}$-region. In this situation we clarify which components are constructed.

8.2 Right s-extension curves of $\mathcal{W}_f^-$

Given a state R in a $\mathscr{R}$-region, the backward f-wave curve from R parametrizes states in saturation triangle that can be connected to R, on the left, by a f-wave group. Since waves along the local and nonlocal branches of $\mathcal{W}_f^-(R)$ belong to the fast family, they can be preceded by a slow-family wave. Such concatenation of waves obey respect the speed compatibility criterion 2.5.1. The methodology to verify the speed compatibility of wave sequences in solutions consists of constructing the right s-extension curves (or simply s-extension curve) of the pertinent fast-family wave curves [9, 4, 3].

Since the discontinuities defining the extension curves are local shocks, by Claim 2.7.1 they have viscous profile. Moreover, states along these right s-extension curves are Bethe-Wendroff points.

8.3 Compatibility boundaries for $\mathscr{L}_{\mathscr{R}}$-regions

We have three types of curves associated to loss of speed compatibility that depend on the $\mathscr{R}$-regions, namely, segments of Lax s-shocks, over-compressive shocks and over-compressive composite waves. The first one occurs when Lax s-shocks and transitional shocks appearing in Riemann solutions have equal speeds; the second, when Lax s-shocks and Lax f-shocks have equal speeds and the last one when sonic s-shocks and Lax f-shocks have equal speeds. For more details, we refer the reader to [32].

8.4 Construction of $\mathscr{L}_{\mathscr{R}}$-regions

In this section we present the construction of $\mathscr{L}_{\mathscr{R}}$-regions for the $\mathscr{R}$-regions defined in Chapter 6. The procedure for their calculation as follows:

1. Compute the s-extension of $\mathcal{W}_f^-(R)$;
2. Construct the backward s-wave curve (or slow family waves) from the exceptional points of $\mathcal{W}_f^-(R)$ given in Section 8.1;
3. Construct the boundaries of compatibility defined in Section 8.3.

Remark 8.4.1. Consider a right state R in the saturation triangle. If a local or nonlocal f-rarefaction segment of $\mathcal{W}_f^-(R)$ is reached by a Lax s-shock wave, then this shock wave is slower than the fast-family rarefaction wave connecting to R. An analogous statement holds when $\mathcal{W}_f^-(R)$ is reached by a s-rarefaction wave.

Let us introduce some more notation. We use $\{A, B, C, D\}$ to denote the interior area of the saturation triangle bounded by the curves (or segments) $[A, B]$, $[B, C]$, $[C, D]$ and $[D, A]$. If some segment bounding $\{A, B, C, D\}$ belongs to the boundary of the saturation triangle, then we consider this segment as part of $\{A, B, C, D\}$.

Remark 8.4.2. If we consider a left state L in some boundary defined by backward s-wave curve (or a slow-family wave), the Riemann solution corresponds to the wave sequences defined by $\mathcal{W}_s^-(L)$. In

the case of L belonging to a s-extension curve, the Riemann solution starts with a s-shock between L and a point M in the wave curve to which this extension corresponds, and then follows the same wave structure as the solution for points in the interior of the region it defines.

8.4.1 $\mathscr{L}_{\mathscr{R}}$-regions for $R \in \mathscr{R}_1$

Consider a state R in the lower or upper region $\mathscr{R}_1$, see Section 6.4.1. We want to construct the $\mathscr{L}_{\mathscr{R}_1}$-regions that divide the saturation triangle in subregions where the solution of the Riemann problem has the same structure for any left state L . In Figure 8.1(a) we show the right s-extension of $\mathcal{W}_f^-(R)$ that was obtained numerically. The segments $[T_1, W]$, $[T_2, G]$ and $[T_R, O]$ are s-extensions of f-rarefaction segments $[A_1, W]$, $[A_2, G]$ and $[R, O]$ of $\mathcal{W}_f^-(R)$, respectively. The Lax f-shock segments of $\mathcal{W}_f^-(R)$ (R, A_4^*), (A_1^*, A_1) and (A_2^*, A_2) have respectively s-extension segments (T_R, A_4), (T^*, T_1) and (T^*, T_2).

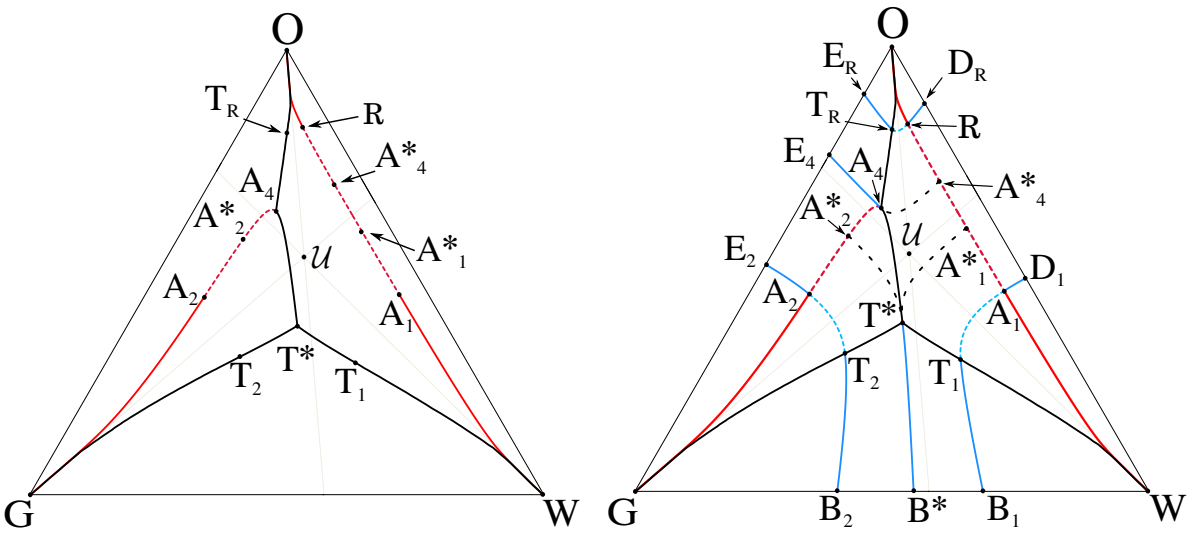

(a) Right s-extension of $\mathcal{W}_f^-(R)$ for R in region $\mathscr{R}_1$. The segment $[A_4, T^*]$ is an over-compressive shock segment of $\mathcal{H}(R)$.

(b) $\mathscr{L}$-regions for R in region $\mathscr{R}_1$. Black dashed curves are segments of Lax s-shocks, see Claim 8.4.1.

Figure 8.1: Subdivision of saturation triangle according to the structure of Riemann solutions for $R \in \mathscr{R}_1$.

From Claim 6.4.1 we have that $[A_4, T^*]$ is an over-compressive shock segment of $\mathcal{H}(R)$ and we have that $\sigma(T^*; A_1^*) = \sigma(A_1^*; R) = \sigma(T^*; A_2^*) = \sigma(A_2^*; R)$ as well as $\sigma(A_4; A_4^*) = \sigma(A_4^*; R)$. Then, we conclude that for any state $M \in [A_4, T^*]$, there are states $N_1 \in (A_4, A_2^*]$ and $N_2 \in (A_4^*, A_1^*]$ such that the discontinuity joining M with N_1 and N_2 is a Lax s-shock and $\sigma(M; N_1) = \sigma(N_1; R)$, and $\sigma(M; N_2) = \sigma(N_2; R)$ (see Figure 8.3).

Now, we construct the boundaries of $\mathscr{L}_{\mathscr{R}_1}$-regions taking into account the Claims 6.4.1 and 6.4.2. We construct the backward s-wave curve for states R, A_1 and A_2 of $\mathcal{W}_f^-(R)$ that are shown in Figure 8.1(b). From A_4 and T^* we trace the backward s-rarefaction segments $[A_4, E_4]$ and $[T^*, B^*]$. Notice

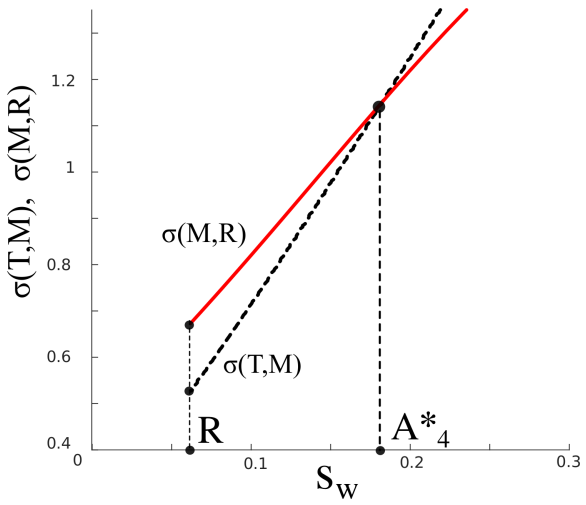

Figure 8.2: Speed diagram comparing shocks speeds $\sigma(T;M)$ and $\sigma(M;R)$ as M and T vary along the Lax f-shock segment $[R, A_4^*] \subset \mathcal{W}_f^-(R)$ and its s-extension curve $[T_R, A_4]$, respectively (see Claim 8.4.1 and Figure 8.1).

that $[A_4, E_4]$ separates regions where the structure of Riemann solutions change; $[T^*, B^*]$ represents a bifurcation where there is a coincidence of shocks speeds. In Figure 8.2, we present the shock/shock compatibility between the Lax s-shock wave from T to M with the Lax f-shock wave from M to R with $T \in [T_R, A_4]$ and $M \in [R, A_4^*]$.

Claim 8.4.1. *Refer to Figure 8.1(b). Let R be a fixed state in $\mathscr{R}_1$ and $\mathcal{W}_f^-(R)$ its backward fast wave curve. Let L be a state in the saturation triangle. Then:*

(i) if $L \in \{G, A_2, E_2\}$, the Riemann solution corresponds to the sequence $L \overset{R_s}{\longmapsto} M \overset{R_f}{\longmapsto} A_2 \overset{'S_f}{\longrightarrow} R$. Here M is in the f-rarefaction segment $[G, A_2] \subset \mathcal{W}_f^-(R)$. We have the same wave sequences for $L \in \{W, A_1, D_1\}$ by changing A_2 to A_1 with M in the f-rarefaction segment $[W, A_1] \subset \mathcal{W}_f^-(R)$.

(ii) if $L \in \{E_2, A_2, A_4, E_4\}$, the Riemann solution corresponds to the sequence $L \overset{R_s}{\longmapsto} M \overset{S_f}{\longmapsto} R$. Here M is in the Lax f-shock segment $(A_2, A_4] \subset \mathcal{W}_f^-(R)$. Again, we have the same wave sequences for $L \in \{D_1, A_1, R, D_R\}$ with M in the Lax f-shock segment $(A_1, R) \subset \mathcal{W}_f^-(R)$.

(iii) if $L \in \{D_R, R, O\}$, the Riemann solution corresponds to the sequence $L \overset{R_s}{\longmapsto} M \overset{R_f}{\longmapsto} R$. Here M is in the f-rarefaction segment $[O, R] \subset \mathcal{W}_f^-(R)$.

(iv) if $L \in \{G, B_2, T_2\}$, the Riemann solution corresponds to the sequence $L \overset{R_s}{\longmapsto} T \overset{'S_s}{\longrightarrow} M \overset{R_f}{\longmapsto} A_2 \overset{'S_f}{\longrightarrow} R$. Here T is in the s-extension curve $[G, T_2]$ and M in the f-rarefaction segment

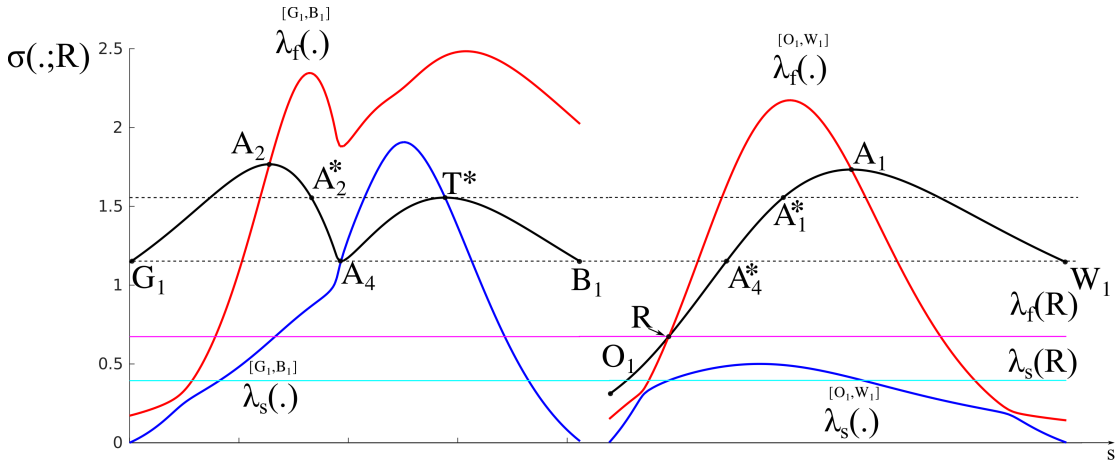

Figure 8.3: Schematic speed diagrams comparing speeds along the branches $[G_1, B_1]$ and $[O_1, W_1]$ of $\mathcal{H}(R)$ for $R \in \mathscr{R}_1$; see Figure 6.7(a). Black curves are the shock speed $\sigma(M, R)$ with M varying along the Hugoniot branches. States on the same horizontal dashed line satisfy the triple shock rule. The blue curves (resp. red curves) are the slow characteristic speed, λ_s (resp. fast characteristic speed λ_f). Horizontal cyan and magenta lines correspond to the constant values $\lambda_s(R)$ and $\lambda_f(R)$, respectively (see Claim 8.4.1).

$[G, A_2] \subset \mathcal{W}_f^-(R)$. *We have the same wave sequences for* $L \in \{W, B_1, T_1\}$ *by changing* A_2 *to* A_1 *with* T *in the* s*-extension curve* $[W, T_1]$ *and* M *in the* f*-rarefaction segment* $[W, A_1] \subset \mathcal{W}_f^-(R)$.

(v) if $L \in \{B_2, B^*, T^*, T_2\}$, *the Riemann solution corresponds to the sequence* $L \overset{R_s}{\longmapsto} T \overset{'S_s}{\longrightarrow} M \overset{S_f}{\longmapsto} R$. *Here* T *is in the* s*-extension curve* (T_2, T^*) *and* M *is in the Lax* f*-shock segment* $(A_2, A_2^*) \subset \mathcal{W}_f^-(R)$. *We have the same wave sequences for* $L \in \{B_1, T_1, T^*, B^*\} \cup \{E_R, T_R, A_4, E_4\}$ *with* T *in the* s*-extension curves* $(T_1, T^*) \cup (T_R, A_4)$ *and* M *in the Lax* f*-shock segments* $(A_1, A_1^*) \cup (R, A_4^*) \subset \mathcal{W}_f^-(R)$.

(vi) if $L \in \{G, T_2, A_2\}$, *the Riemann solution corresponds to the sequence* $L \overset{S_s}{\longmapsto} M \overset{R_f}{\longmapsto} A_2 \overset{'S_f}{\longrightarrow} R$. *Here* M *is in the* f*-rarefaction segment* $[G, A_2] \subset \mathcal{W}_f^-(R)$. *We have the same wave sequences for* $L \in \{W, T_1, A_1\}$ *by changing* A_2 *to* A_1 *with* M *in the* f*-rarefaction segments* $[W, A_1] \subset \mathcal{W}_f^-(R)$.

(vii) if $L \in \{R, T_R, O\}$, *the Riemann solution corresponds to the sequence* $L \overset{S_s}{\longmapsto} M \overset{R_f}{\longmapsto} R$. *Here* M *is in the* f*-rarefaction segment* $[O, R] \subset \mathcal{W}_f^-(R)$.

(viii) if $L \in \{T_R, E_R, O\}$, *the Riemann solution corresponds to the sequence* $L \overset{R_s}{\longmapsto} T \overset{'S_s}{\longrightarrow} M \overset{R_f}{\longmapsto} R$. *Here* T *is in the* s*-extension curve* $[O, T_R]$ *and* M *is in the* f*-rarefaction segment* $[O, R] \subset \mathcal{W}_f^-(R)$.

(ix) *if* $L \in \{A_2, A_4, T^*, T_2\}$, *the Riemann solution corresponds to the sequence* $L \overset{S_s}{\longmapsto} M \overset{S_f}{\longmapsto} R$. *Here* M *is in the Lax* f*-shock segment* $(A_2, A_4] \subset \mathcal{W}_f^-(R)$. *We have the same wave sequences for* $L \in \{A_1, R, T_R, A_4, T^*, T_1\}$ *with* M *in the Lax* f*-shock segment* $(A_1, R) \subset \mathcal{W}_f^-(R)$.

(x) *if* L *is in the* s*-rarefaction segment* $[B^*, T^*]$, *then we have three possible wave sequences in the state space corresponding to a unique solution in the* xt*-space, see [3, 9]. The Riemann solutions are:*

(a) $L \overset{R_s}{\longmapsto} T^* \overset{'S_s}{\longrightarrow} A_1^* \overset{S_f}{\longrightarrow} R$;

(b) $L \overset{R_s}{\longmapsto} T^* \overset{'S_s}{\longrightarrow} A_2^* \overset{S_f}{\longrightarrow} R$;

(c) $L \overset{R_s}{\longmapsto} T^* \overset{'S_O}{\longrightarrow} R$.

(xi) *if* L *is in the over-compressive shock segment* (A_4, T^*), *then we have three possible wave sequences in the state space corresponding to a unique solution in the* xt*-space, see [3, 9]. The Riemann solutions are:*

(a) $L \overset{S_s}{\longmapsto} N_1 \overset{S_f}{\longrightarrow} R$, *with* $N_1 \in (A_4, A_2^*)$;

(b) $L \overset{S_s}{\longmapsto} N_2 \overset{S_f}{\longrightarrow} R$, *with* $N_2 \in (A_4^*, A_1^*)$;

(c) $L \overset{S_O}{\longmapsto} R$.

Proof. Refer to Figure 8.1. The compatibility of speeds is justified by Remark 8.4.1, Figure 8.2 and [3]. In [3], it was shown the compatibility between the s-extension curves $[T_1, T^*]$ and $[T_2, T^*]$ with the Lax f-shock segments $[A_1, A_1^*]$ and $[A_2, A_2^*]$. The statements (*x*) and (*xi*) are justified by the triple shock rule. ∎

Remark 8.4.3. The solutions of the Riemann problem presented in Claim 8.4.1 with $L \in [G, W]$ coincide with those given in [3].

Remark 8.4.4. In the case that the right state $R \in \mathscr{R}_1$ is in between the s-inflection and a invariant line, $\mathcal{W}_f^-(R)$ intersects the s-inflection at state T_i generating a bifurcation in the form which the slow-family waves reach $\mathcal{W}_f^-(R)$. In Figure 8.6(b) is shown a example of this bifurcation at state T_3.

8.4.2 $\mathscr{L}_{\mathscr{R}}$-regions for $R \in \mathscr{R}_2$

As seen in Remark 6.4.3 of Section 6.4.1, the lower $\mathscr{R}_2$ region can be subdivided into two regions; a part similar to upper region $\mathscr{R}_2$, and the region $\mathscr{R}_2^H$ which appears because $\mathcal{W}_f^-(R)$ for $R \in \mathscr{R}_2^H$ has a nonlocal f-shock breaking into two components separated by an over-compressive shock. We first construct the $\mathscr{L}_{\mathscr{R}_2}$-regions for R in upper region $\mathscr{R}_2$, then we study the new $\mathscr{L}_{\mathscr{R}_2}$-regions that appear for $R \in \mathscr{R}_2^H$.

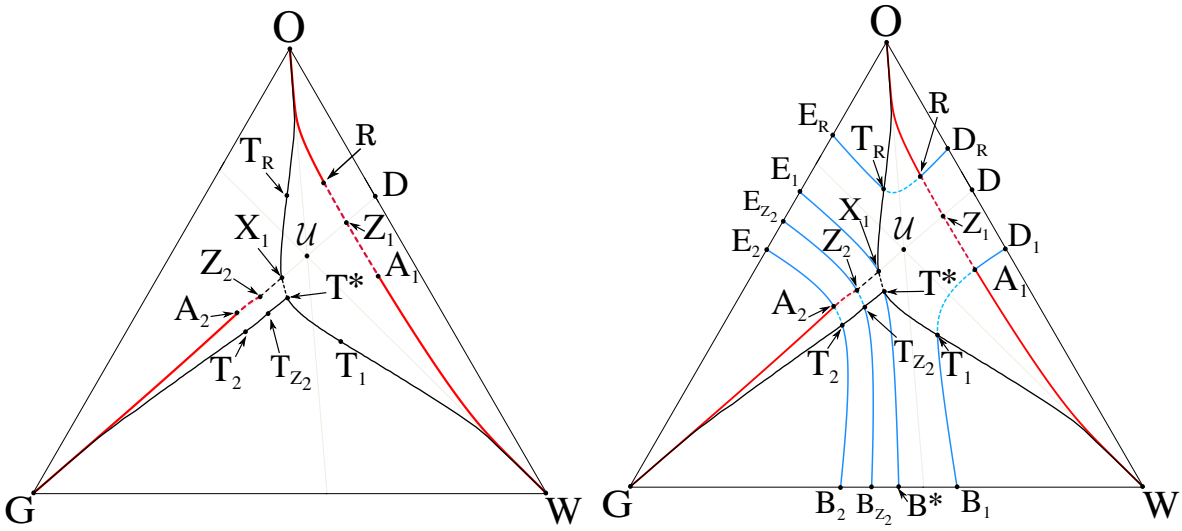

(a) Right s-extension of $[Z_2, X_1]$ and $\mathcal{W}_f^-(R)$ for R in region $\mathscr{R}_2$. The segment $[X_1, T^*]$ is a segment of Lax s-shocks of $\mathcal{H}(Z_1)$.

(b) $\mathscr{L}$-regions for R in region $\mathscr{R}_2$, see Claim 8.4.2.

Figure 8.4: Subdivision of saturation triangle according to the structure of Riemann solutions for $R \in \mathscr{R}_2$. In this case is consider $R \in \mathscr{R}_2$ such that $\mathcal{W}_f^-(R)$ has a single nonlocal component of fast shocks.

8.4.2.1 $\mathcal{W}_f^-(R)$ with a single nonlocal component of fast shocks

Consider a state R in the upper region $\mathscr{R}_2$. We want to construct the $\mathscr{L}_{\mathscr{R}_2}$-regions that divide the saturation triangle in subregions where the solution of the Riemann problem have the same structure for any left state L. Notice that in this case we have transitional waves associated to the intersection between $\mathcal{W}_f^-(R)$ and $[\mathcal{U}, D]$ at state Z_1 (see Section 7.3.3) with $Z_1 = M_2$ and $Z_2 = M_2'$. In Figure 8.4(a) we show the s-extensions of $\mathcal{W}_f^-(R)$ and the invariant segment $[Z_2, X_1]$, obtained numerically. The segments $[T_1, W]$, $[T_2, G]$ and $[T_R, O]$ are s-extensions of f-rarefaction segments $[A_1, W]$, $[A_2, G]$ and $[R, O]$ of $\mathcal{W}_f^-(R)$, respectively. The Lax f-shock segments of $\mathcal{W}_f^-(R)$, $(R, Z_1]$, $[Z_1, A_1)$ and $[Z_2, A_2)$ have respectively s-extension segments (T_R, X_1), (T^*, T_1) and (T_{Z_2}, T_2). The segment $[T_{Z_2}, T^*]$ is the s-extension curve of the invariant segment $[Z_2, X_1]$.

Now, we construct the boundaries of $\mathscr{L}_{\mathscr{R}_2}$-regions taking into account Claims 6.4.3 and 6.4.4, and Section 7.3.3. We construct the backward s-wave curve for the states R, A_1, A_2 and Z_2 of $\mathcal{W}_f^-(R)$ that are shown in Figure 8.4(b). Following Definition 7.3.3, we construct regions S_{1T}, S_{2T} and S_{3T} which are given by the areas $\{E_1, X_1, Z_2, E_{Z_2}\}$, $\{X_1, Z_2, T_{Z_2}, T^*\}$ and $\{T^*, T_{Z_2}, B_{Z_2}, B^*\}$, respectively. Recall that it is possible that region S_{3T} does not exist, which happens when R lies in the region between curves $[\mathcal{U}, V_0]$ and $[Y_1, V_1]$ inside of region $\mathscr{R}_2$ (see Definition 7.3.3(ii) and Figure 7.11).

In Figure 8.5, we present the shock/shock compatibility between the Lax s-shock wave from T to M with the Lax f-shock wave from M to R with $T \in [T_R, X_1]$ and $M \in [R, Z_1]$.

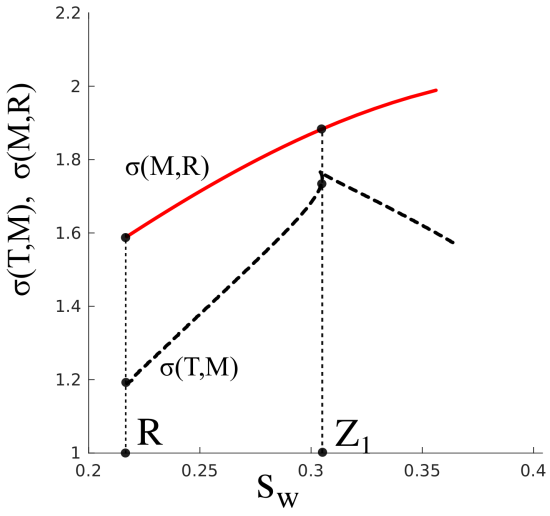

Figure 8.5: Speed diagram comparing shocks speeds $\sigma(T;M)$ and $\sigma(M;R)$ as M and T vary along the Lax f-shock segment $[R, Z_1] \subset \mathcal{W}_f^-(R)$ and its s-extension curve $[T_R, X_1]$, respectively (see Claim 8.4.2 and Figure 8.4).

Claim 8.4.2. *Refer to Figure 8.4(b). Take a fixed state R in $\mathscr{R}_2$ and $\mathcal{W}_f^-(R)$ its backward fast wave curve. Let L be a state in the saturation triangle. Then:*

(i) if $L \in \{G, A_2, E_2\}$, the Riemann solution corresponds to the sequence $L \overset{R_s}{\longmapsto} M \overset{R_f}{\longmapsto} A_2 \overset{'S_f}{\longrightarrow} R$. Here M is in the f-rarefaction segment $[G, A_2] \subset \mathcal{W}_f^-(R)$. We have the same wave sequences for $L \in \{W, A_1, D_1\}$ by changing A_2 to A_1 with M in the f-rarefaction segment $[W, A_1] \subset \mathcal{W}_f^-(R)$.

(ii) if $L \in \{E_2, A_2, Z_2, E_{Z_2}\}$, the Riemann solution corresponds to the sequence $L \overset{R_s}{\longmapsto} M \overset{S_f}{\longmapsto} R$. Here M is in the Lax f-shock segment $(A_2, Z_2) \subset \mathcal{W}_f^-(R)$. Again, we have the same wave sequences for $L \in \{D_1, A_1, R, D_R\}$ with M in the Lax f-shock segment $(A_1, R) \subset \mathcal{W}_f^-(R)$.

(iii) if $L \in \{D_R, R, O\}$, the Riemann solution corresponds to the sequence $L \overset{R_s}{\longmapsto} M \overset{R_f}{\longmapsto} R$. Here M is in the f-rarefaction segment $[O, R] \subset \mathcal{W}_f^-(R)$.

(iv) if $L \in \{G, B_2, T_2\}$, the Riemann solution corresponds to the sequence $L \overset{R_s}{\longmapsto} T \overset{'S_s}{\longrightarrow} M \overset{R_f}{\longmapsto} A_2 \overset{'S_f}{\longrightarrow} R$. Here T is in the s-extension curve $[G, T_2]$ and M in the f-rarefaction segment $[G, A_2] \subset \mathcal{W}_f^-(R)$. We have the same wave sequences for $L \in \{W, B_1, T_1\}$ by changing A_2 to A_1 with T in the s-extension curve $[W, T_1]$ and M in the f-rarefaction segment $[W, A_1] \subset \mathcal{W}_f^-(R)$.

(v) if $L \in \{B_2, B_{Z_2}, T_{Z_2}, T_2\}$, the Riemann solution corresponds to the sequence $L \overset{R_s}{\longmapsto} T \overset{'S_s}{\longrightarrow} M \overset{S_f}{\longmapsto} R$. Here T is in the s-extension curve (T_2, T_{Z_2}) and M is in the Lax f-shock seg-

ment $(A_2, Z_2) \subset \mathcal{W}_f^-(R)$. *We have the same wave sequences for* $L \in \{B_1, T_1, T^*, B^*\} \cup \{E_R, T_R, X_1, E_1\}$ *with* T *in the* s*-extension curves* $(T_1, T^*] \cup (T_R, X_1)$ *and* M *in the Lax* f*-shock segments* $(A_1, Z_1] \cup (R, Z_1) \subset \mathcal{W}_f^-(R)$.

(vi) if $L \in \{G, T_2, A_2\}$, *the Riemann solution corresponds to the sequence* $L \overset{S_s}{\longmapsto} M \overset{R_f}{\longmapsto} A_2 \overset{'S_f}{\longrightarrow} R$. *Here* M *is in the* f*-rarefaction segment* $[G, A_2] \subset \mathcal{W}_f^-(R)$. *We have the same wave sequences for* $L \in \{W, T_1, A_1\}$ *by changing* A_2 *to* A_1 *with* M *in the* f*-rarefaction segments* $[W, A_1] \subset \mathcal{W}_f^-(R)$.

(vii) if $L \in \{R, T_R, O\}$, *the Riemann solution corresponds to the sequence* $L \overset{S_s}{\longmapsto} M \overset{R_f}{\longmapsto} R$. *Here* M *is in the* f*-rarefaction segment* $[O, R] \subset \mathcal{W}_f^-(R)$.

(viii) if $L \in \{T_R, E_R, O\}$, *the Riemann solution corresponds to the sequence* $L \overset{R_s}{\longmapsto} T \overset{'S_s}{\longrightarrow} M \overset{R_f}{\longmapsto} R$. *Here* T *is in the* s*-extension curve* $[O, T_R]$ *and* M *is in the* f*-rarefaction segment* $[O, R] \subset \mathcal{W}_f^-(R)$.

(ix) if $L \in \{A_2, Z_2, T_{Z_2}, T_2\}$, *the Riemann solution corresponds to the sequence* $L \overset{S_s}{\longmapsto} M \overset{S_f}{\longmapsto} R$. *Here* M *is in the Lax* f*-shock segment* $(A_2, Z_2] \subset \mathcal{W}_f^-(R)$. *We have the same wave sequences for* $L \in \{A_1, R, T_R, X_1, T^*, T_1\}$ *with* M *in the Lax* f*-shock segment* $(A_1, R) \subset \mathcal{W}_f^-(R)$.

(x) if $L \in S_{1T} = \{E_1, X_1, Z_2, E_{Z_2}\}$, *the Riemann solution corresponds to the sequence* $L \overset{R_s}{\longmapsto} M \overset{S_T}{\longmapsto} Z_1 \overset{S_f}{\longmapsto} R$. *Here* M *is in the transitional segment* (Z_2, X_1) *associated to* Z_1.

(xi) if $L \in S_{2T} = \{X_1, Z_2, T_{Z_2}, T^*\}$, *the Riemann solution corresponds to the sequence* $L \overset{S_s}{\longmapsto} M \overset{S_T}{\longmapsto} Z_1 \overset{S_f}{\longmapsto} R$. *Here* M *is in the transitional segment* (Z_2, X_1) *associated to* Z_1.

(xii) if $L \in S_{3T} = \{T^*, T_{Z_2}, B_{Z_2}, B^*\}$, *the Riemann solution corresponds to the sequence* $L \overset{R_s}{\longmapsto} T \overset{'S_s}{\longrightarrow} M \overset{S_T}{\longmapsto} Z_1 \overset{S_f}{\longmapsto} R$. *Here* M *is in the transitional segment* (Z_2, X_3) *associated to* Z_1.

(xiii) if L *is in the* s*-rarefaction segment* $[B^*, T^*]$, *then the Riemann solution corresponds to the sequence* $L \overset{R_s}{\longmapsto} T^* \overset{'S_s}{\longrightarrow} X_3 \overset{S_T}{\longrightarrow} Z_1 \overset{S_f}{\longmapsto} R$. *Here* $X_3 \in (Z_2, X_1)$ *and satisfy* $\sigma(T^*; X_3) = \sigma(X_3; Z_1) = \sigma(T^*; X_3)$.

(xiv) if L *is in the Lax* s*-shock segment* $[X_1, T^*) \subset \mathcal{H}(Z_1)$ *then the Riemann solution corresponds to the sequence* $L \overset{S_s}{\longmapsto} M \overset{S_T}{\longrightarrow} Z_1 \overset{S_f}{\longmapsto} R$. *Here* $M \in (X_3, X_1)$ *and satisfy* $\sigma(L; M) = \sigma(M; Z_1) = \sigma(L; Z_1)$.

Proof. Refer to Figure 8.4. The compatibility of speeds is justified by Remark 8.4.1, Figure 8.5 and [4]. In [4], it was shown the compatibility between the s-extension curve $[T_1, T^*]$ with the Lax f-shock segment $[A_1, Z_1]$. The compatibility with the transitional waves were shown in Section 7.3.3. ∎

Remark 8.4.5. Refer to Figure 8.4(b). For statements (*xiii*) and (*xiv*) of Claim 8.4.2 there are other solutions given by the triple shock rule in which the Lax s-shock and the transitional shock collapse:

1. if L is in the s-rarefaction segment $[B^*, T^*]$, we have the sequence $L \overset{R_s}{\longmapsto} T^* \overset{'S_s}{\longrightarrow} Z_1 \overset{S_f}{\longmapsto} R$;

2. if L is in the Lax s-shock segment $[X_1, T^*) \subset \mathcal{H}(Z_1)$, we have the sequence $L \overset{S_s}{\longmapsto} Z_1 \overset{S_f}{\longmapsto} R$.

But these solutions are inadmissible because the Lax s-shocks do not have viscous profile.

Remark 8.4.6. The solutions of the Riemann problem presented in Claim 8.4.2 with $L \in [G, W]$ coincide with those given in [4].

8.4.2.2 $\mathcal{W}_f^-(R)$ with two nonlocal components of fast shocks

Consider a state R in the lower region $\mathscr{R}_2$ which is shows in Figure 8.6(a). If $\mathscr{R}$ belongs to $\{\mathcal{N}_1, V_2^*, Y_2^*, \mathcal{N}_2\}$ we have the same subdivision of $\mathscr{L}_{\mathscr{R}_2}$-regions than Claim 8.4.2; if $\mathscr{R}$ belongs to $\mathscr{R}_2^H = \{\mathcal{N}_1, V_0^*, E_0, \mathcal{N}_2\}$ it appears two nonlocal components of fast shocks in $\mathcal{W}_f^-(R)$. Notice that the curve $[V_1^*, Y_1^*]$ (defined in Section 6.3.3) crosses the region $\mathscr{R}_2^H$ dividing it into two subregions: $\{\mathcal{N}_1, V_1^*, Y_1^*, \mathcal{N}_2\}$ and $\{V_1^*, V_0^*\ E_0, Y_1^*\}$. If R belongs $\{\mathcal{N}_1, V_1^*, Y_1^*, \mathcal{N}_2\}$ the S_{3T} is one of the $\mathscr{L}_{\mathscr{R}_2^H}$-regions, otherwise it is not, see Definition 7.3.3.

We construct the $\mathscr{L}_{\mathscr{R}_2^H}$-regions for R inside $\{V_1^*, V_0^*\ E_0, Y_1^*\}$, the other case is similar. In Figure 8.6(b) we show the s-extensions of $\mathcal{W}_f^-(R)$, obtained numerically. The segments $[T_1, O]$ and $[T_R, W]$ are s-extensions of f-rarefaction segments $[A_1, O]$, $[R, W]$ of $\mathcal{W}_f^-(R)$, respectively. The f-rarefaction segment $[A_2, G]$ intersects the s-inflection locus at state T_3. This produces a change in the slow-family waves that is used to reach this segment. Then, the segments $[T_2, T_3]$ and $[T_3, G]$ are s-extensions of f-rarefaction segments $[A_2, T_3]$, $[T_3, G]$ of $\mathcal{W}_f^-(R)$, respectively.

The Lax f-shock segments of $\mathcal{W}_f^-(R)$ $(R, A_4^*]$, $[Z_1, A_1)$ and $(A_2, \widehat{T^*}]$ have respectively s-extension segments $(T_R, A_4]$, $[X_1, T_1)$ and $(T_2, T^*]$. From Remark 6.4.3 and Claim 6.4.5 we have that $[T^*, A_4]$ is an admissible over-compressive shock segment of $\mathcal{H}(R)$ and satisfy $\sigma(T^*; \widehat{T^*}) = \sigma(T^*; R)$ and $\sigma(A_4; A_4^*) = \sigma(A_4; R)$. Moreover, there are states Z_2, Z_2' and Z_2^* associated to $Z_1 \in [\mathcal{U}, D] \cap \mathcal{W}_f^-(R)$ such that $\sigma(Z_1; Z_2) = \sigma(Z_2; Z_2') = \sigma(Z_1; R)$ and $\sigma(Z_1; Z_2') = \sigma(Z_2^*; Z_2') = \sigma(Z_2'; R)$, where Z_2 is the initial point of the nonlocal branch of $\mathcal{W}_f^-(R)$, Z_2' lies on the over-compressive shock segment $[T^*, A_4]$ and $Z_2^* \in [\widehat{T^*}, A_4]$. Then, by the triple shock rule the shock speeds of these states with R are equal and $Z_2' \in \mathcal{H}(Z_1)$ such that $[X_1, Z_2'] \subset \mathcal{H}(Z_1)$ is a Lax s-shock segment. Therefore, we conclude that (refer to Figure 8.7):

(1) for any state M on the over-compressive shock segment $(T^*, Z_2'] \subset \mathcal{H}(R)$, there are states $N_1 \in (T^*, Z_2] \subset \mathcal{H}(R)$ and $N_2 \in (\widehat{T^*}, Z_2^*] \subset \mathcal{H}(R)$ such that the discontinuity joining M to N_1 and N_2 is a Lax s-shock and $\sigma(M; N_1) = \sigma(N_1; R)$, and $\sigma(M; N_2) = \sigma(N_2; R)$;

(2) for any state M on the over-compressive shock segment $[Z_2', A_4) \subset \mathcal{H}(R)$, there are states $N_1 \in [Z_1, A_4^*) \subset \mathcal{H}(R)$ and $N_2 \in (Z_2^*, A_4) \subset \mathcal{H}(R)$ such that the discontinuity joining M to N_1 and N_2 is a Lax s-shock and $\sigma(M; N_1) = \sigma(N_1; R)$, and $\sigma(M; N_2) = \sigma(N_2; R)$.

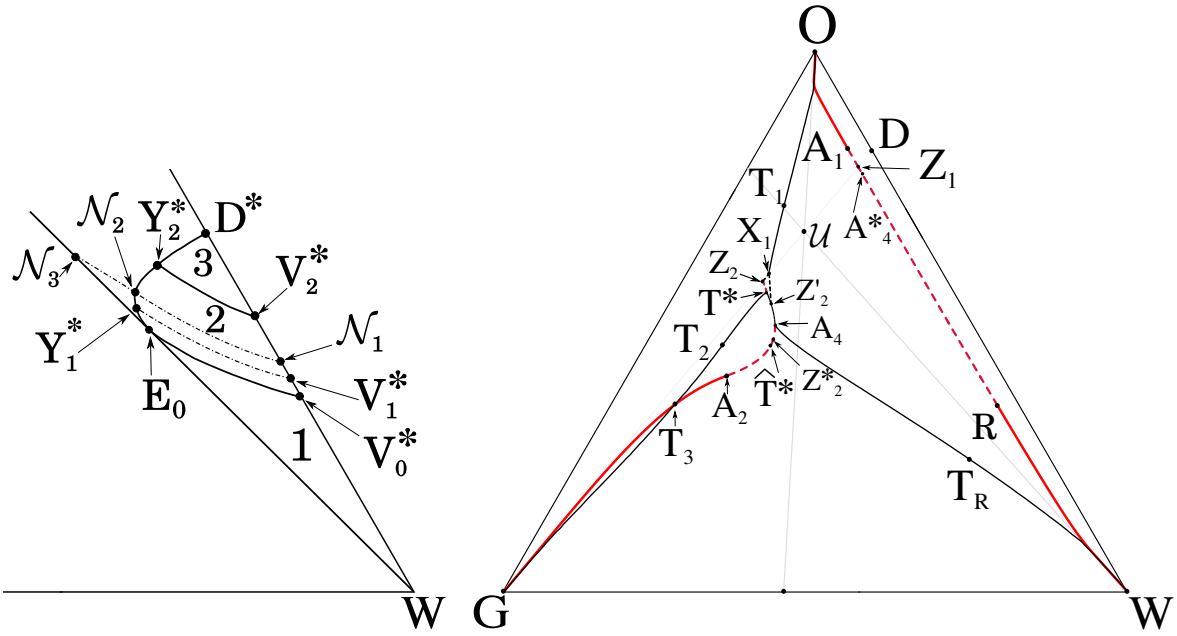

(a) Lower regions $\mathscr{R}_i$, $i \in \{1,2,3\}$ for fast macro region $\mathcal{FR}_D$.

(b) Right s-extension of $\mathcal{W}_f^-(R)$ for R in region $\mathscr{R}_2^H$.

Figure 8.6: (a) Boundaries that define the lower regions $\mathscr{R}_i$, $i \in \{1,2,3\}$. Curve $[V_1^*, Y_1^*]$ is the boundary for loss of compatibility of sonic shocks (see Remark 6.3.3) and $[\mathcal{N}_1, \mathcal{N}_2, \mathcal{N}_3]$ is the left s-hysteresis, see Definition 2.4.2. (b) Backward f-wave curve for R inside of $\mathscr{R}_2^H \subset \mathscr{R}_2$. The over-compressive admissible shock segment $[T^*, A_4]$ separates two admissible segments of Lax f-shocks, $[Z_2, T^*)$ and $(A_4, A_2]$. The segment $[X_1, T^*]$ is a segment of Lax s-shocks of $\mathcal{H}(Z_1)$ and T_3 is the intersection between the f-rarefaction segment $[A_2, G]$ and the s-inflection locus.

Now, we construct the boundaries of $\mathscr{L}_{\mathscr{R}_2^H}$-regions taking into account Remark 6.4.3, Claim 6.4.5 and Section 7.3.3. We construct the backward s-wave curve for the states R, A_1 and A_2 of $\mathcal{W}_f^-(R)$ that are shown in Figure 8.7(a). Following Definition 7.3.3, we construct regions S_{1T} and S_{2T} which are given by the areas $\{E_1, X_1, Z_2, E_{Z_2}\}$ and $\{X_1, Z_2, Z_2'\}$. From T^* and A_4 we trace the backward s-rarefaction curves and form T_3 we trace the s-integral curve.

Claim 8.4.3. *Let R be a fixed state in $\mathscr{R}_2^H$ and construct $\mathcal{W}_f^-(R)$ (see Figure 8.7). Let L be a state in the saturation triangle. Then:*

(i) if $L \in \{W, D_R, R\}$, the Riemann solution corresponds to the sequence $L \overset{R_s}{\longmapsto} M \overset{R_f}{\longmapsto} R$. Here M is in the f-rarefaction segment $[W, R] \subset \mathcal{W}_f^-(R)$.

(ii) if $L \in \{W, T_R, R\}$, the Riemann solution corresponds to the sequence $L \overset{S_s}{\longmapsto} M \overset{R_f}{\longmapsto} R$, with M in $[W, R] \subset \mathcal{W}_f^-(R)$.

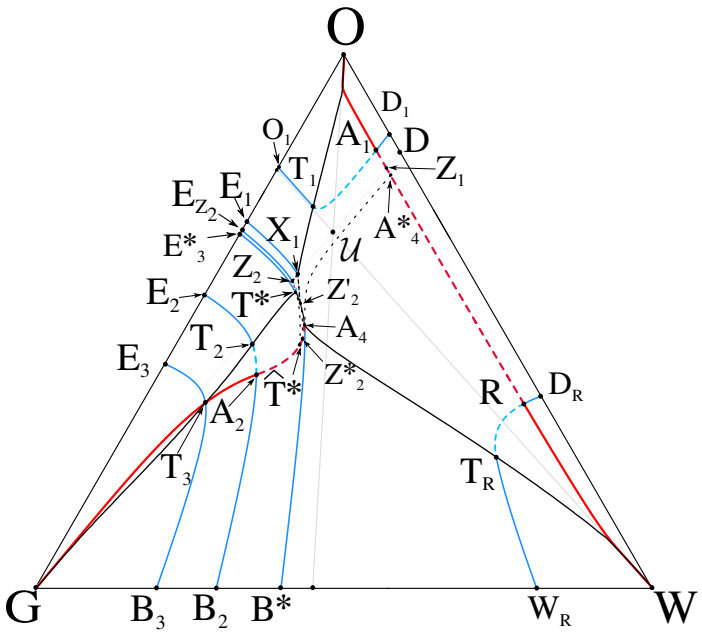

(a) $\mathscr{L}$-regions for R in lower region $\mathscr{R}_2$, see Claim 8.4.3.

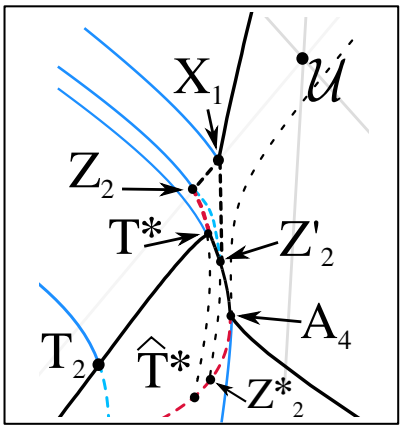

(b) Zoom of area close to segment of over-compressive shocks $[T^*, A_4]$. Black dashed curves are segments of Lax s-shocks

Figure 8.7: Subdivision of saturation triangle according to the structure of Riemann solutions for $R \in \mathscr{R}_2$. In this case is consider $R \in \mathscr{R}_2^H$ which $\mathcal{W}_f^-(R)$ has two nonlocal components of fast shocks. T_3 is the intersection between the f-rarefaction segment $[A_2, G]$ and the s-inflection locus.

(iii) *if $L \in \{W, W_R, T_R\}$, the Riemann solution corresponds to the sequence $L \overset{R_s}{\longmapsto} T \overset{'S_s}{\longrightarrow} M \overset{R_f}{\longmapsto} R$, with M in $[W, R] \subset \mathcal{W}_f^-(R)$.*

(iv) *if $L \in \{D_R, D_1, A_1, R\}$, the Riemann solution corresponds to the sequence $L \overset{R_s}{\longmapsto} M \overset{S_f}{\longmapsto} R$. Here M is in the Lax f-shock segment $(R, A_1) \subset \mathcal{W}_f^-(R)$. We have the same wave sequences for $L \in \{Z_2, T^*, E_3^*, E_{Z_2}\} \cup \{B_2, B^*, A_4, A_2\}$ with M in the Lax f-shock segments $[Z_2, T^*) \cup (A_2, A_4) \subset \mathcal{W}_f^-(R)$.*

(v) *if $L \in \{W_R, T_R, A_4, B^*\}$, the Riemann solution corresponds to the sequence $L \overset{R_s}{\longmapsto} T \overset{'S_s}{\longrightarrow} M \overset{S_f}{\longmapsto} R$. Here T is in the s-extension curve $[T_R, A_4]$ and M is in the Lax f-shock segment $(R, A_4^*] \subset \mathcal{W}_f^-(R)$. We have the same wave sequences for $L \in \{E_2, T_2, T^*, E_3^*\} \cup \{E_1, X_1, T_1, O_1\}$ with T in the s-extension curves $(T_2, T^*) \cup (X_1, T_1)$, and M in the Lax f-shock segments $(A_2, A_4] \cup [Z_1, A_1) \subset \mathcal{W}_f^-(R)$.*

(vi) *if $L \in \{A_2, T_2, T^*, A_4\}$, the Riemann solution corresponds to the sequence $L \overset{S_s}{\longmapsto} M \overset{S_f}{\longmapsto} R$. Here M is in the Lax f-shock segment $(A_2, A_4] \subset \mathcal{W}_f^-(R)$. We have the same wave sequences for*

$L \in \{T^*, Z_2, Z_2'\} \cup \{A_1, T_1, X_1, Z_2', A_4, T_R, R\}$ *with* M *in the Lax* f*-shock segments* $[Z_2, T^*] \cup (A_1, R) \subset \mathcal{W}_f^-(R)$.

(vii) if $L \in \{O, D_1, A_1\}$*, the Riemann solution corresponds to the sequence* $L \overset{R_s}{\longmapsto} M \overset{R_f}{\longmapsto} A_1 \overset{'S_f}{\longrightarrow} R$*. Here* M *is in the* f*-rarefaction segment* $[O, A_1] \subset \mathcal{W}_f^-(R)$*. We have the same wave sequences for* $L \in \{B_2, A_2, T_3, B_3\} \cup \{E_3, T_3, G\}$ *by changing* A_1 *to* A_2 *with* M *in the* f*-rarefaction segment* $[G, A_2] \subset \mathcal{W}_f^-(R)$.

(viii) if $L \in \{O, A_1, T_1\}$*, the Riemann solution corresponds to the sequence* $L \overset{S_s}{\longmapsto} M \overset{R_f}{\longmapsto} A_1 \overset{'S_f}{\longrightarrow} R$*. Here* M *is in the* f*-rarefaction segment* $[O, A_1] \subset \mathcal{W}_f^-(R)$*. We have the same wave sequences for* $L \in \{T_2, A_2, T_3\} \cup \{T_3, G\}$ *by changing* A_1 *to* A_2 *with* M *in the* f*-rarefaction segment* $[G, A_2] \subset \mathcal{W}_f^-(R)$.

(ix) if $L \in \{O, T_1, O_1\}$*, the Riemann solution corresponds to the sequence* $L \overset{R_s}{\longmapsto} T \overset{'S_s}{\longrightarrow} M \overset{R_f}{\longmapsto} A_1 \overset{'S_f}{\longrightarrow} R$*. Here* T *is in the* s*-extension curve* $[T_1, O]$ *and* M *is in the* f*-rarefaction segment* $[A_1, O] \subset \mathcal{W}_f^-(R)$*. We have the same wave sequences for* $L \in \{T_2, E_2, E_3, T_3\} \cup \{B_3, T_3, G\}$ *by changing* A_1 *to* A_2 *with* T *in the* s*-extension curves* $[T_2, T_3] \cup [T_3, G]$ *and* M *in the* f*-rarefaction segment* $[G, A_2] \subset \mathcal{W}_f^-(R)$.

(x) if $L \in S_{1T} = \{E_1, X_1, Z_2, E_{Z_2}\}$*, the Riemann solution corresponds to the sequence* $L \overset{R_s}{\longmapsto} M \overset{S_T}{\longmapsto} Z_1 \overset{S_f}{\longmapsto} R$*. Here* M *is in the transitional segment* (Z_2, X_1) *associated to* Z_1.

(xi) if $L \in S_{2T} = \{X_1, Z_2, Z_2'\}$*, the Riemann solution corresponds to the sequence* $L \overset{S_s}{\longmapsto} M \overset{S_T}{\longmapsto} Z_1 \overset{S_f}{\longmapsto} R$*. Here* M *is in the transitional segment* (Z_2, X_1) *associated to* Z_1.

(xii) if L *is in the Lax* s*-shock segment* $[X_1, Z_2') \subset \mathcal{H}(Z_1)$ *then the Riemann solution corresponds to the sequence* $L \overset{S_s}{\longmapsto} M \overset{S_T}{\longrightarrow} Z_1 \overset{S_f}{\longmapsto} R$*. Here* $M \in [X_1, Z_2]$ *such that satisfy* $\sigma(L; M) = \sigma(M; Z_1)$.

(xiii) if L *is in the over-compressive shock segment* $(T^*, Z_2']$*, then we have three possible wave sequences in the state space corresponding to a unique solution in the* xt*-space, see [3, 9]. The Riemann solutions are:*

(a) $L \overset{S_s}{\longmapsto} N_1 \overset{S_f}{\longrightarrow} R$*, with* $N_1 \in (T^*, Z_2]$ *in the local branch of* $\mathcal{H}(R)$*;*

(b) $L \overset{S_s}{\longmapsto} N_2 \overset{S_f}{\longrightarrow} R$*, with* $N_2 \in (\widehat{T^*}, Z_2^*]$ *in the detached branch of* $\mathcal{H}(R)$*;*

(c) $L \overset{S_O}{\longmapsto} R$.

(xiv) if L *is in the over-compressive shock segment* (Z_2', A_4)*, then we have three possible wave sequences in the state space corresponding to a unique solution in the* xt*-space, see [3, 9]. The Riemann solutions are:*

(a) $L \overset{S_s}{\longmapsto} N_1 \overset{S_f}{\longrightarrow} R$, *with* $N_1 \in (Z_1, A_4^*)$;

(b) $L \overset{S_s}{\longmapsto} N_2 \overset{S_f}{\longrightarrow} R$, *with* $N_2 \in (Z_2^*, A_4)$;

(c) $L \overset{S_O}{\longmapsto} R$.

Proof. Similar to the proof of Claim 8.4.2 (see Figure 8.7). ∎

Remark 8.4.7. Remark 8.4.5 also holds for statement (*xii*) of Claim 8.4.3.

8.4.3 $\mathscr{L}_{\mathscr{R}}$-regions for $R \in \mathscr{R}_3$

Consider a state R in the region $\mathscr{R}_3$. Recall that $\mathcal{W}_f^-(R)$ has only a local branch and there are two types of transitional waves associated to the intersection state between $\mathcal{W}_f^-(R)$ and $[\mathcal{U}, D]$ at Z_1 (see Section 7.3.1 with $Z_1 = M_2$). In Figure 8.8(a) we show the s-extensions of $\mathcal{W}_f^-(R)$ and of the invariant segment $[G, X_1]$, obtained numerically. The segments $[T_1, W]$ and $[T_R, O]$ are s-extensions of the f-rarefaction segments $[A_1, W]$ and $[R, O]$ of $\mathcal{W}_f^-(R)$, respectively. The Lax f-shock segments of $\mathcal{W}_f^-(R)$, $(R, Z_1]$ and $[Z_1, A_1)$, and the invariant segment $[G, X_1]$ have respectively s-extension segments (T_R, X_1), (T^*, T_1) and $[T^*, T_2, G]$.

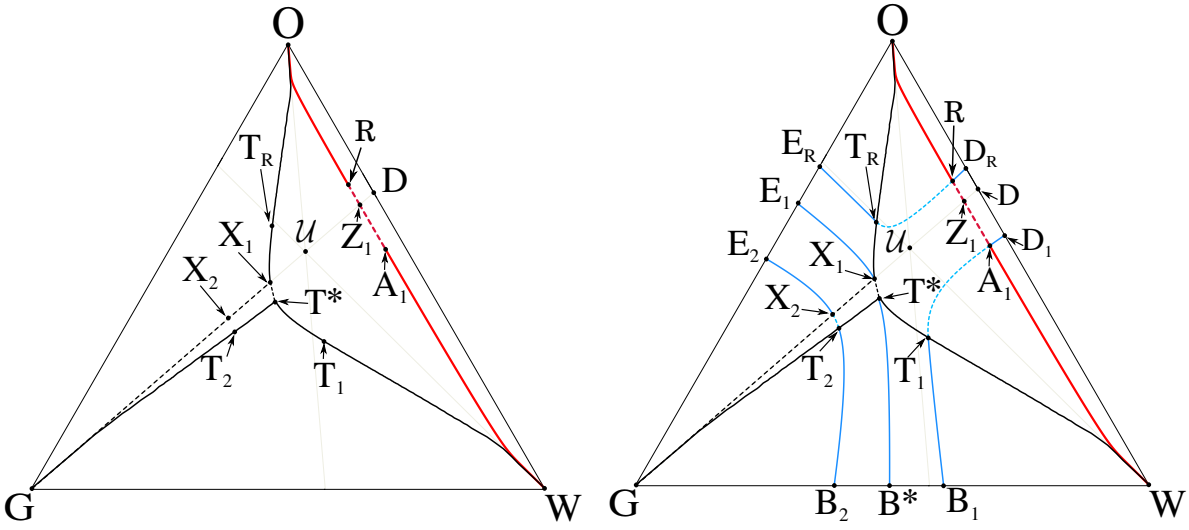

(a) Right s-extension of $[G, X_1]$ and $\mathcal{W}_f^-(R)$ for R in region $\mathscr{R}_3$.

(b) $\mathscr{L}$-regions for R in region $\mathscr{R}_3$, see Claim 8.4.4.

Figure 8.8: Subdivision of saturation triangle according to the structure of Riemann solutions for $R \in \mathscr{R}_3$.

Now, we construct the boundaries of $\mathscr{L}_{\mathscr{R}_3}$-regions taking into account the Claims 6.4.6 and 6.4.7 and Section 7.3.1. We construct the backward s-wave curve for the states R and A_1 of $\mathcal{W}_f^-(R)$ and from X_2 that are shown in Figure 8.8(b). Following Definition 7.3.1 we construct the regions S_{1C}, S_{2C} and S_{3C}

which are given by the areas $\{G, X_2, E_2\}$, $\{G, X_2, T_2\}$ and $\{G, T_2, B_2\}$, respectively. We also construct the regions S_{1T}, S_{2T} and S_{3T} which are given by the areas $\{X_2, X_1, E_1, E_2\}$, $\{X_2, X_1, T^*, T_2\}$ and $\{T_2, B_2, B^*, T^*\}$, respectively.

The shock/shock compatibility between the Lax s-shock wave from T to M with the Lax f-shock wave from M to R with $T \in [T_R, X_1]$ and $M \in [R, Z_1]$ for this case is shown in Figure 8.5 which is similar than the case for $R \in \mathscr{R}_2$.

Claim 8.4.4. *Take a fixed state R in $\mathscr{R}_3$ and construct $\mathcal{W}_f^-(R)$ (see Figure 8.8(b)). Let L be a state in the saturation triangle. Then:*

(i) if $L \in S_{1C} = \{G, X_2, E_2\}$, the Riemann solution corresponds to the sequence $L \overset{R_s}{\longmapsto} M \overset{R_f}{\longmapsto} X_2 \overset{'S_T}{\longrightarrow} Z_1 \overset{S_f}{\longmapsto} R$. Here M is in the invariant segment $[G, X_2]$.

(ii) if $L \in S_{2C} = \{G, X_2, T_2\}$, the Riemann solution corresponds to the sequence $L \overset{S_s}{\longmapsto} M \overset{R_f}{\longmapsto} X_2 \overset{'S_T}{\longrightarrow} Z_1 \overset{S_f}{\longmapsto} R$. Here M is in the invariant segment $[G, X_2]$.

(iii) if $L \in S_{3C} = \{G, T_2, B_2\}$, the Riemann solution corresponds to the sequence $L \overset{R_s}{\longmapsto} T \overset{'S_s}{\longrightarrow} M \overset{R_f}{\longmapsto} X_2 \overset{'S_T}{\longrightarrow} Z_1 \overset{S_f}{\longmapsto} R$. Here T is in the s-extension curve $[G, T_2]$ and M is in the invariant segment $[G, X_2]$.

(iv) if $L \in S_{1T} = \{X_2, X_1, E_1, E_2\}$, the Riemann solution corresponds to the sequence $L \overset{R_s}{\longmapsto} M \overset{S_T}{\longrightarrow} Z_1 \overset{S_f}{\longmapsto} R$. Here M is in the transitional segment (X_2, X_1).

(v) if $L \in S_{2T} = \{X_2, X_1, T^*, T_2\}$ the Riemann solution corresponds to the sequence $L \overset{S_s}{\longmapsto} M \overset{S_T}{\longmapsto} Z_1 \overset{S_f}{\longmapsto} R$. Here M is in the transitional segment (X_2, X_1).

(vi) if $L \in S_{3T} = \{T_2, B_2, B^*, T^*\}$, the Riemann solution corresponds to the sequence $L \overset{R_s}{\longmapsto} T \overset{'S_s}{\longrightarrow} M \overset{S_T}{\longmapsto} Z_1 \overset{S_f}{\longmapsto} R$. Here T is in the s-extension curve (T_2, T^*) and M is in the transitional segment (X_2, X_1).

The other cases are similar to Claim 8.4.2.

Proof. Refer to Figure 8.8. The compatibility of speeds is justified by Remark 8.4.1, Figure 8.5 and [4]. In [4] was shown the compatibility between the s-extension curve $[T_1, T^*]$ with the Lax f-shock segment $[A_1, Z_1]$. The compatibility with the transitional waves were shown in Section 7.3.1. ∎

Remark 8.4.8. The solutions of the Riemann problem presented in Claim 8.4.4 with $L \in [G, W]$ coincide with those given in [4].

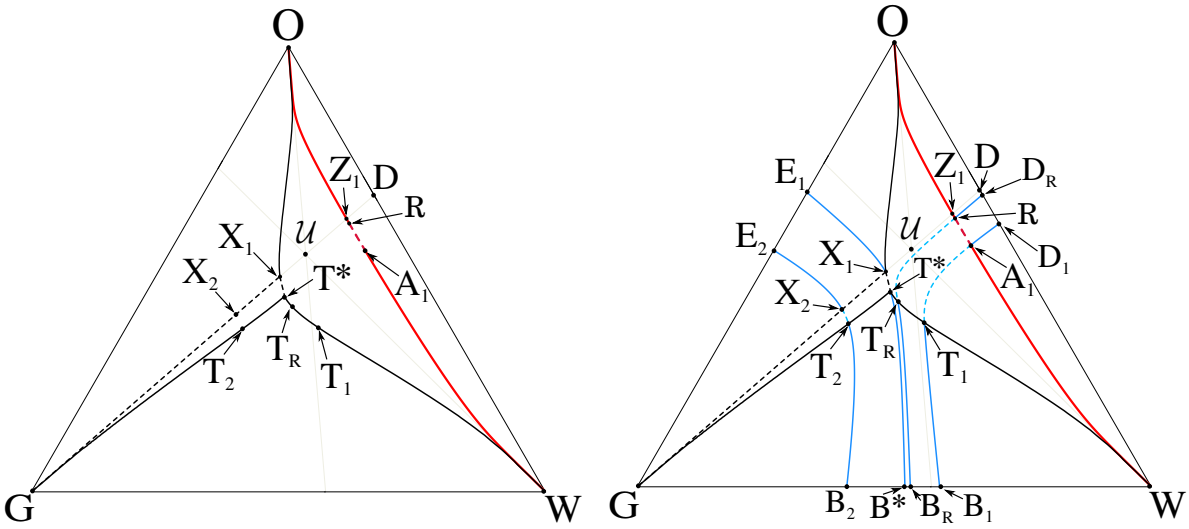

(a) Right s-extension of $[G, X_1]$ and $\mathcal{W}_f^-(R)$ for R in region $\mathscr{R}_4$.

(b) $\mathscr{L}$-regions for R in region $\mathscr{R}_4$, see Claim 8.4.5.

Figure 8.9: Subdivision of saturation triangle according to the structure of Riemann solutions for $R \in \mathscr{R}_4$.

8.4.4 $\mathscr{L}_{\mathscr{R}}$-regions for $R \in \mathscr{R}_4$

Consider a state R in the region $\mathscr{R}_4$, see Figure 8.9. Recall that $\mathcal{W}_f^-(R)$ has only a local branch and there are two types of transitional waves associated to the intersection state between $\mathcal{W}_f^-(R)$ and $[\mathcal{U}, D]$ at Z_1 (see Section 7.3.1 with $Z_1 = M_2$). From Section 6.5 and Claim 7.2.1, the state Z_1 lies in a f-rarefaction segment, then, the last wave group to used after a transitional wave is a f-rarefaction, indeed that the case $R \in \mathscr{R}_3$ that is a Lax f-shock. Because of this, the subdivision in $\mathscr{L}_{\mathscr{R}_4}$-regions is similar to case before.

In Figure 8.9(a) we show the s-extension of $\mathcal{W}_f^-(R)$ and of the invariant segment $[G, X_1]$ that was obtained numerically. The segments $[T_1, W]$, $[T_R, T^*]$ and $[X_1, O]$ are s-extensions of the f-rarefaction segments $[A_1, W]$, $[R, Z_1]$ and $[Z_1, O]$ of $\mathcal{W}_f^-(R)$, respectively. The Lax f-shock segment of $\mathcal{W}_f^-(R)$, (R, A_1), and the invariant segment $[G, X_1]$ have respectively s-extension segments (T_R, T_1) and $[T^*, T_2, G]$.

In Figure 8.10, we present the shock/shock compatibility between the Lax s-shock wave from T to M with the Lax f-shock wave from M to R with $T \in [T_R, T_1]$ and $M \in [R, A_1]$.

Now, we construct the boundaries of $\mathscr{L}_{\mathscr{R}_4}$-regions taking into account the Claims 6.4.8 and 6.4.9 and Section 7.3.1. We construct the backward s-wave curve for the states R and A_1 of $\mathcal{W}_f^-(R)$ and from X_2 that are shown in Figure 8.9(b). Following Definition 7.3.1 we construct the regions S_{1C}, S_{2C} and S_{3C} which are given by the areas $\{G, X_2, E_2\}$, $\{G, X_2, T_2\}$ and $\{G, T_2, B_2\}$, respectively. We also construct the regions S_{1T}, S_{2T} and S_{3T} which are given by the areas $\{X_2, X_1, E_1, E_2\}$, $\{X_2, X_1, T^*, T_2\}$ and $\{T_2, B_2, B^*, T^*\}$, respectively.

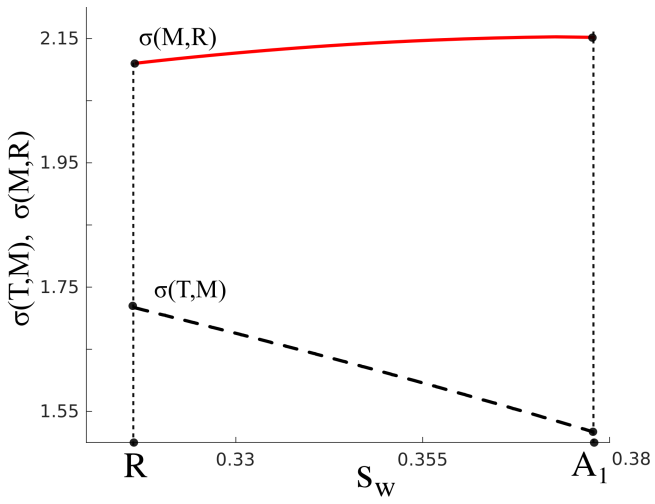

Figure 8.10: Speed diagram comparing shocks speeds $\sigma(T;M)$ and $\sigma(M;R)$ as M and T vary along the Lax f-shock segment $[R, A_1] \subset \mathcal{W}_f^-(R)$ and its s-extension curve $[T_R, T_1]$, respectively (see Claim 8.4.5 and Figure 8.9).

Claim 8.4.5. *Take a fixed state R in $\mathscr{R}_4$ and construct $\mathcal{W}_f^-(R)$ (see Figure 8.9(b)). Let L be a state in the saturation triangle.*

(i) if $L \in \bigcup S_{iC}$ the Riemann solution corresponds to the same sequence as in Claim 8.4.4 that uses a transitional composite, changing the last fast-family wave by a f-rarefaction, i.e.,

$$L \cdots \overset{R_f}{\longmapsto} X_2 \overset{'S_T}{\longrightarrow} Z_1 \overset{\boldsymbol{R_f}}{\longmapsto} R;$$

(ii) if $L \in \bigcup S_{iT}$ the Riemann solution corresponds to the same sequence as in Claim 8.4.4 that uses a transitional shock, changing the last fast-family wave by a f-rarefaction, i.e.,

$$L \cdots \overset{S_T}{\longrightarrow} Z_1 \overset{\boldsymbol{R_f}}{\longmapsto} R.$$

The other cases are similar to Claim 8.4.4.

Proof. Refer to Figure 8.9. The compatibility of speeds is justified by Remark 8.4.1 and Figure 8.10. The compatibility with the transitional waves were shown in Section 7.3.1. ∎

8.4.5 $\mathscr{L}_{\mathscr{R}}$-regions for $R \in \mathscr{R}_5$

Consider a state R in the upper region $\mathscr{R}_5$, see Figure 8.11. Notice that in this case we have transitional waves associated to the intersection between $\mathcal{W}_f^-(R)$ and $[\mathcal{U}, D]$ at state Z_1, see Section 7.3.2 with $Z_1 = M_2$ and $Z_2 = M_2'$. In Figure 8.11(a) we show the s-extension of $\mathcal{W}_f^-(R)$ and of the segment $[Z_2, X_1] \subset [G, \mathcal{U}]$ that was obtained numerically. The segments $[T_1, W]$, $[T_R, T^*]$, $[T_2, G]$ and

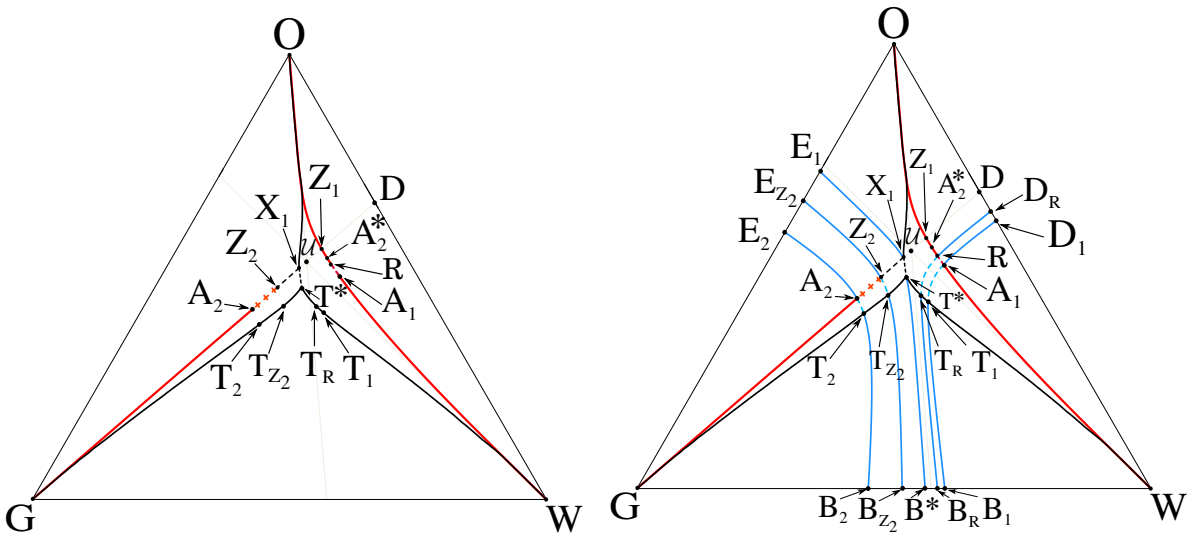

(a) Right s-extension of $[Z_2, X_1]$ and $\mathcal{W}_f^-(R)$ for R in region $\mathscr{R}_5$. The segment $[X_1, T^*]$ is a segment of Lax s-shocks of $\mathcal{H}(Z_1)$.

(b) $\mathscr{L}$-regions for R in region $\mathscr{R}_5$, see Claim 8.4.6.

Figure 8.11: Subdivision of saturation triangle according to the structure of Riemann solutions for $R \in \mathscr{R}_5$. Notice that A_2 and A_2^* are a pair of fast double contact states.

$[X_1, O]$ are s-extensions of f-rarefaction segments $[A_1, W]$, $[R, Z_1]$, $[A_2, G]$ and $(Z_1, O]$ of $\mathcal{W}_f^-(R)$, respectively. The Lax f-shock segment of $\mathcal{W}_f^-(R)$, $(R, A_1]$ and the f-composite segment $[Z_2, A_2)$ have respectively s-extension segments (T_R, T_1) and (T_{Z_2}, T_2), and $[T_{Z_2}, T^*]$ is the s-extension curve of the $[Z_2, X_1]$.

Now, we construct the boundaries of $\mathscr{L}_{\mathscr{R}_5}$-regions taking into account the Claims 6.4.10 and 6.4.11, and Section 7.3.2. We construct the backward s-wave curve for the states R, A_1, A_2 and Z_2 of $\mathcal{W}_f^-(R)$ that are shown in Figure 8.11(b). Following Definition 7.3.3 we construct regions S_{1T}, S_{2T} and S_{3T} which are given by the areas $\{E_1, X_1, Z_2, E_{Z_2}\}$, $\{X_1, Z_2, T_{Z_2}, T^*\}$ and $\{T^*, T_{Z_2}, B_{Z_2}, B^*\}$, respectively.

In Figure 8.12(a) and (b) are present the shock/shock and shock/composite compatibility. The first is between the Lax s-shock wave from T to M with the Lax f-shock wave from M to R with $T \in [T_R, T_1]$ and $M \in [R, A_1]$; the second is between the Lax s-shock wave from T to M with the sonic f-shock wave from M to N with $T \in [T_2, T_{Z_2}]$, $M \in [A_2, Z_2]$ and $N \in [A_2^*, R]$.

Claim 8.4.6. *Take a fixed state R in $\mathscr{R}_5$ and construct $\mathcal{W}_f^-(R)$ (see Figure 8.11(b)). Let L be a state in the saturation triangle. Then:*

(i) if $L \in \{G, A_2, E_2\}$, the Riemann solution corresponds to the sequence $L \overset{R_s}{\longmapsto} M \overset{R_f}{\longmapsto} A_2 \overset{'S_f'}{\longrightarrow} A_2^* \overset{R_f}{\longrightarrow} R$. Here M is in the f-rarefaction segment $[G, A_2] \subset \mathcal{W}_f^-(R)$ and, A_2 and A_2^* are a pair of fast double contact states.

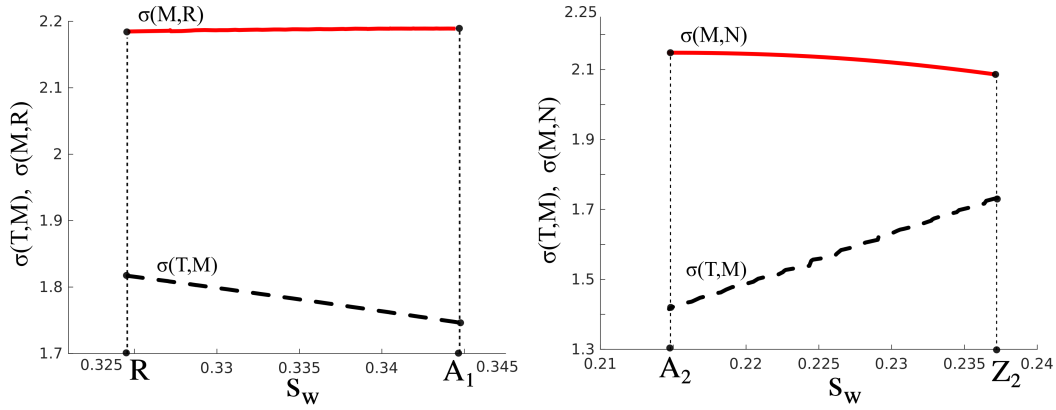

(a) Slow shock/fast shock.

(b) Slow shock/fast shock.

Figure 8.12: Speed diagrams along $\mathcal{W}_f^-(R)$ and its extension curve. (a) Shocks speeds $\sigma(T;M)$ and $\sigma(M;R)$ as M and T vary along the Lax f-shock segment $[R, Z_1] \subset \mathcal{W}_f^-(R)$ and its s-extension curve $[T_R, X_1]$, respectively. (b) Shocks speeds $\sigma(T;M)$ and $\sigma(M;N)$ as M,N and T vary along the f-composite segment $[A_2, Z_2] \subset \mathcal{W}_f^-(R)$, the f-rarefaction segment $[A_2^*, R] \subset \mathcal{W}_f^-(R)$ and its s-extension curve $[T_2, T_{Z_2}]$, respectively (see Claim 8.4.6 and Figure 8.11).

(ii) *if* $L \in \{G, A_2, T_2\}$ *the Riemann solution corresponds to the sequence* $L \overset{S_s}{\longmapsto} M \overset{R_f}{\longmapsto} A_2 \overset{'S_f'}{\longrightarrow} A_2^* \overset{R_f}{\longrightarrow} R$. *Here* M *is in the* f*-rarefaction segment* $[G, A_2] \subset \mathcal{W}_f^-(R)$ *and,* A_2 *and* A_2^* *are a pair of fast double contact states.*

(iii) *if* $L \in \{G, T_2, B_2\}$, *the Riemann solution corresponds to the sequence* $L \overset{R_s}{\longmapsto} T \overset{'S_s}{\longrightarrow} M \overset{R_f}{\longmapsto} A_2 \overset{'S_f'}{\longrightarrow} A_2^* \overset{R_f}{\longrightarrow} R$. *Here* T *is in the* s*-extension curve* $[G, T_2]$, M *is in the* f*-rarefaction segment* $[G, A_2] \subset \mathcal{W}_f^-(R)$ *and,* A_2 *and* A_2^* *are a pair of fast double contact states.*

(iv) *if* $L \in \{A_2, E_2, E_{Z_2}, Z_2\}$ *the Riemann solution corresponds to the sequence* $L \overset{R_s}{\longmapsto} M \overset{S_f'}{\longmapsto} N \overset{R_f}{\longrightarrow} R$. *Here* M *is in the* f*-composite curve* $(A_2, Z_2] \subset \mathcal{W}_f^-(R)$ *and* N *in the* f*-rarefaction segment* $(A_2^*, Z_1] \subset \mathcal{W}_f^-(R)$.

(v) *if* $L \in \{A_2, T_2, T_{Z_2}, Z_2\}$ *the Riemann solution corresponds to the sequence* $L \overset{S_s}{\longmapsto} M \overset{S_f'}{\longmapsto} N \overset{R_f}{\longrightarrow} R$. *Here* M *is in the* f*-composite curve* $(A_2, Z_2] \subset \mathcal{W}_f^-(R)$ *and* N *is in the* f*-rarefaction segment* $(A_2^*, Z_1] \subset \mathcal{W}_f^-(R)$.

(vi) *if* $L \in \{B_2, T_2, T_{Z_2}, B_{Z_2}\}$ *the Riemann solution corresponds to the sequence* $L \overset{R_s}{\longmapsto} T \overset{'S_s}{\longrightarrow} M \overset{S_f'}{\longmapsto} N \overset{R_f}{\longrightarrow} R$. *Here* T *is in the* s*-extension curve* (T_2, T_{Z_2}), M *is in the* f*-composite curve* $(A_2, Z_2] \subset \mathcal{W}_f^-(R)$ *and* N *is in the* f*-rarefaction segment* $(A_2^*, Z_1] \subset \mathcal{W}_f^-(R)$.

(vii) *if* $L \in S_{1T} = \{E_1, X_1, Z_2, E_{Z_2}\}$, *the Riemann solution corresponds to the sequence* $L \overset{R_s}{\longmapsto} M \overset{S_T}{\longmapsto} Z_1 \overset{R_f}{\longmapsto} R$. *Here* M *is in the invariant segment* (Z_2, X_1).

(viii) *if* $L \in S_{2T} = \{X_1, Z_2, T_{Z_2}, T^*\}$, *the Riemann solution corresponds to the sequence* $L \overset{S_s}{\longmapsto} M \overset{S_T}{\longmapsto} Z_1 \overset{R_f}{\longmapsto} R$. *Here* M *is in the transitional segment* (Z_2, X_1).

(ix) *if* $L \in S_{3T} = \{T^*, T_{Z_2}, B_{Z_2}, B^*\}$, *the Riemann solution corresponds to the sequence* $L \overset{R_s}{\longmapsto} T \overset{'S_s}{\longmapsto} M \overset{S_T}{\longmapsto} Z_1 \overset{R_f}{\longmapsto} R$. *Here* T *is in the* s*-extension curve* (T_{Z_2}, T^*) *and* M *is in the transitional segment* (Z_2, X_1).

(x) *if* $L \in \{O, E_1, X_1\}$, *the Riemann solution corresponds to the sequence* $L \overset{R_s}{\longmapsto} T \overset{'S_s}{\longmapsto} M \overset{R_f}{\longmapsto} R$. *Here* T *is in the* s*-extension curve* $[X_1, O]$ *and* M *is in the* f*-rarefaction segment* $[Z_1, O] \subset \mathcal{W}_f^-(R)$. *We have the same wave sequences for* $L \in \{B^*, T^*, T_R, B_R\}$ *with* T *in the* s*-extension curve* $(T^*, T_R]$ *and* M *in the* f*-rarefaction segment* $(Z_1, R] \subset \mathcal{W}_f^-(R)$.

(xi) *if* $L \in \{O, X_1, T^*, T_R, R\}$, *the Riemann solution corresponds to the sequence* $L \overset{S_s}{\longmapsto} M \overset{R_f}{\longmapsto} R$. *Here* M *is in the* f*-rarefaction segment* $[O, R] \subset \mathcal{W}_f^-(R)$.

(xii) *if* $L \in \{O, R, D_R\}$, *the Riemann solution corresponds to the sequence* $L \overset{R_s}{\longmapsto} M \overset{R_f}{\longmapsto} R$. *Here* M *is in the* f*-rarefaction segment* $[O, R] \subset \mathcal{W}_f^-(R)$.

(xiii) *if* $L \in \{D_R, R, A_1, D_1\}$, *the Riemann solution corresponds to the sequence* $L \overset{R_s}{\longmapsto} M \overset{S_f}{\longmapsto} R$. *Here* M *is in the Lax* f*-shock segment* $(R, A_1) \subset \mathcal{W}_f^-(R)$.

(xiv) *if* $L \in \{R, A_1, T_1, T_R\}$, *the Riemann solution corresponds to the sequence* $L \overset{S_s}{\longmapsto} M \overset{S_f}{\longmapsto} R$. *Here* M *is in the Lax* f*-shock segment* $(R, A_1) \subset \mathcal{W}_f^-(R)$.

(xv) *if* $L \in \{T_1, B_1, B_R, T_R\}$, *the Riemann solution corresponds to the sequence* $L \overset{S_s}{\longmapsto} T \overset{'S_s}{\longmapsto} M \overset{S_f}{\longmapsto} R$. *Here* T *is in the* s*-extension curve* (T_R, T_1) *and* M *is in the Lax* f*-shock segment* $(R, A_1) \subset \mathcal{W}_f^-(R)$.

(xvi) *if* $L \in \{W, A_1, D_1\}$, *the Riemann solution corresponds to the sequence* $L \overset{R_s}{\longmapsto} M \overset{R_f}{\longmapsto} A_1 \overset{'S_f}{\longrightarrow} R$. *Here* M *is in the* f*-rarefaction segment* $[W, A_1] \subset \mathcal{W}_f^-(R)$.

(xvii) *if* $L \in \{W, A_1, T_1\}$, *the Riemann solution corresponds to the sequence* $L \overset{S_s}{\longmapsto} M \overset{R_f}{\longmapsto} A_1 \overset{'S_f}{\longrightarrow} R$. *Here* M *is in the Lax* f*-shock segment* $(R, A_1) \subset \mathcal{W}_f^-(R)$.

(xviii) *if* $L \in \{W, T_1, B_1\}$, *the Riemann solution corresponds to the sequence* $L \overset{R_s}{\longmapsto} T \overset{'S_s}{\longrightarrow} M \overset{R_f}{\longmapsto} A_1 \overset{'S_f}{\longrightarrow} R$. *Here* T *is in the* s*-extension curve* $[W, T_1]$ *and* M *is in the* f*-rarefaction segment* $[W, A_1] \subset \mathcal{W}_f^-(R)$.

(xix) if L is in the s-rarefaction segment $[B^*, T^*]$, then the Riemann solution corresponds to the sequence $L \overset{R_s}{\longmapsto} T^* \overset{'S_s}{\longrightarrow} X_3 \overset{S_T}{\longrightarrow} Z_1 \overset{S_f}{\longmapsto} R$. Here $X_3 \in (Z_2, X_1)$ and satisfy $\sigma(T^*; X_3) = \sigma(X_3, Z_1)$.

(xx) if L is in the Lax s-shock segment $[X_1, T^*) \subset \mathcal{H}(Z_1)$ then the Riemann solution corresponds to the sequence $L \overset{S_s}{\longmapsto} M \overset{S_T}{\longrightarrow} Z_1 \overset{S_f}{\longmapsto} R$. Here M is in the segment $[Z_2, X_1]$. Notice that $\sigma(L; M) = \sigma(M, Z_1)$.

Proof. Refer to Figure 8.11. The compatibility of speeds is justified by Remark 8.4.1 and Figure 8.12(a)-(b). The compatibility of speeds with the transitional waves were established in Section 7.3.2. ∎

Remark 8.4.9. Remark 8.4.5 also holds for statements (*xix*) and (*xx*) of Claim 8.4.6.

Remark 8.4.10. In case of Remark 6.4.5 we have that for $R \in \mathscr{R}_5$, it is possible that the f-rarefaction segment $[R, O] \subset \mathcal{W}_f^-(R)$ intersects the segment $[K_1, Y_1]$ of the mixed double contact (see Figures 8.13 and 8.14(b). This actually happens when R crosses the f-rarefaction segment $[\widehat{Y_1}, Y_1']$ (see region $\{\widehat{Y_1}, Y_1', \mathcal{I}_f^1, H_4\}$ in Figure 8.14(b)). In this case the f-rarefaction segment of $\mathcal{W}_f^-(R)$ intersects first the segment $[H_4, \widehat{Y_1}]$ and then the segment $[K_1, Y_1]$ before crossing $[\mathcal{U}, Y_1]$. Figure 8.13(b) is a blow-up of the region close to the umbilic point in Figure 8.13(a), displaying the f-composite segment $[A_2, Z_2] \subset \mathcal{W}_f^-(R)$ for R inside $\{H_4, \widehat{Y_1}, Y_1', \mathcal{I}_f^1\}$ (see Figure 8.14(b)). The states A_2^* and A_2 belong to the fast double contact locus and the segment $[A_2, Z_2] \subset \mathcal{W}_f^-(R)$ is a f-composite segment associate to the f-rarefaction segment $[A_2^*, Z_1] \subset \mathcal{W}_f^-(R)$. The f-rarefaction segment $[P_1, Z_1] \subset [A_2^*, Z_1]$ also generates the over-compressive composite $[P_1, T^*]$ which is admissible and serves as a boundary for loss of compatibility of speeds. The states P_1 and P_1' belong to the mixed double contact locus and satisfies $\sigma(P_1; P_1') = \lambda_f(P_1) = \lambda_s(P_1')$ as well as $\sigma(P_1''; P_1') = \sigma(P_1''; P_1) = \lambda_f(P_1)$ with $P_1'' \in [A_2, Z_2] \subset \mathcal{W}_f^-(R)$.

Notice that in this case, Z_1 lies in $[\mathcal{U}, Y_1]$, then we do not have the region S_{3T} of transitional waves (see Remark 7.3.2). Therefore, the segments $[Z_2, T_{Z_2}]$ of Lax s-shocks and $[T_{Z_2}, B_{Z_2}]$ of f-rarefaction disappear, see Figures 8.11(b) and 8.13. The f-composite segment $[A_2, Z_2]$ has two distinct boundaries for loss of compatibility speeds: the s-extension $[T_2, P_1']$ associated to segment $[A_2, P_1'']$ and the over-compressive composite segment $[P_1', T^*]$ associated to segment $[P_1'', Z_2]$. Moreover, for each $M \in [P_1', T^*]$ there are states $N_1 \in [P_1'', Z_2]$ and $N_2 \in [P_1, Z_1]$ such that the discontinuity joining M with N_1 and N_2 is a Lax s-shock and $\sigma(M; N_1) = \sigma(M; N_2) = \lambda_f(N_2)$, see Figure 8.14. Therefore, we have the following result:

Claim 8.4.7. *Take a fixed state R in $\mathscr{R}_5$ inside of region $\{H_4, \widehat{Y_1}, Y_1', \mathcal{I}_f^1\}$ and construct $\mathcal{W}_f^-(R)$ (see Figures 8.13(a),(b) and 8.14(b)). Let L be a state in the saturation triangle. Then:*

(i) if $L \in \{A_2, Z_2, T^*, P_1', T_2\}$, the Riemann solution corresponds to the sequence $L \overset{S_s}{\longmapsto} M \overset{S_f'}{\longmapsto} N \overset{R_f}{\longrightarrow} R$. Here M is in the f-composite segment $[A_2, Z_2] \subset \mathcal{W}_f^-(R)$ and N is in the f-rarefaction segment $[A_2^*, Z_1] \subset \mathcal{W}_f^-(R)$.

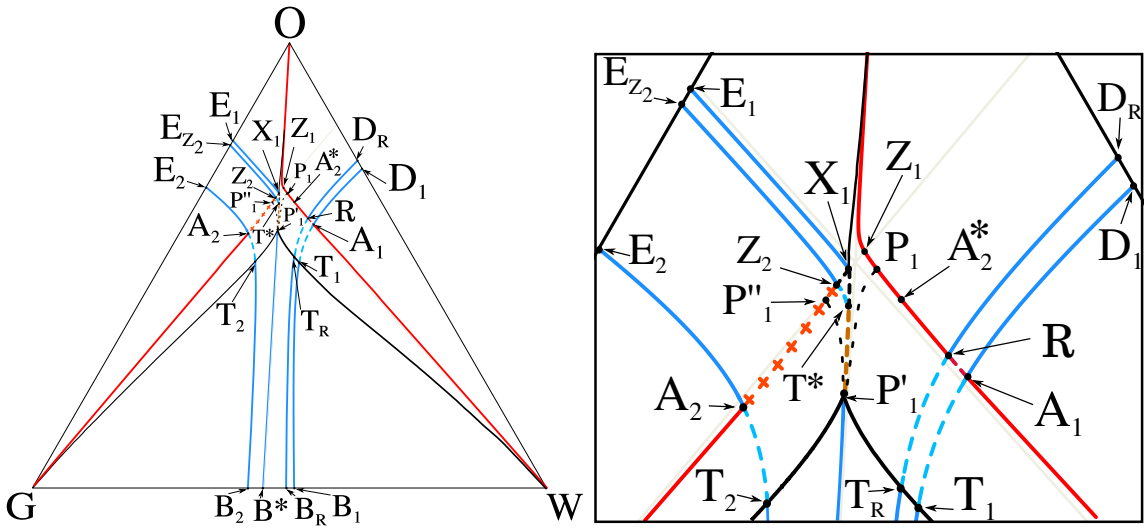

(a) $\mathscr{L}$-regions for R in region $\mathscr{R}_5$, see Claim 8.4.7.

(b) Zoom of area close to over-compressive shock segment $[T^*, P_1']$.

Figure 8.13: (a) Subdivision of saturation triangle according to the structure of Riemann solutions for $R \in \mathscr{R}_5$ in the case of Remark 6.4.5. Notice that A_2 and A_2^* are a pair of fast double contact states. (b) Zoom of region close to the over-compressive composite segment $[P_1', T^*]$ associated to f-rarefaction segment $[P_1', Z_1] \subset \mathcal{W}_f^-(R)$ for R inside $\{H_4, \widehat{Y_1}, Y_1', \mathcal{I}_f^1\}$. The region S_{3T} collapse in the segment of f-rarefaction $[P_1', B^*]$. Notice that this bifurcation in the $\mathscr{L}_{\mathscr{R}_5}$-regions occurs only for Remark 6.4.5. Black dashed curves are segments of Lax s-shocks.

(ii) *if* $L \in \{T_2, P_1', B^*, B_2\}$ *the Riemann solution corresponds to the sequence* $L \overset{R_s}{\longmapsto} T \overset{'S_s}{\longrightarrow} M \overset{S_f'}{\longmapsto} N \overset{R_f}{\longrightarrow} R$. *Here* T *is in the* s*-extension segment* $[T_2, P_1']$, M *is in the* f*-composite segment* $[A_2, Z_2] \subset \mathcal{W}_f^-(R)$ *and* N *is in the* f*-rarefaction segment* $[A_2^*, Z_1] \subset \mathcal{W}_f^-(R)$.

(iii) *if* $L \in \{T_R, B_R, B^*, P_1'\}$, *the Riemann solution corresponds to the sequence* $L \overset{R_s}{\longmapsto} T \overset{'S_s}{\longrightarrow} M \overset{R_f}{\longmapsto} R$. *Here* T *is in the* s*-extension curve* $[T_R, P_1']$ *and* M *is in the* f*-rarefaction segment* $[R, P_1] \subset \mathcal{W}_f^-(R)$.

(iv) *if* $L \in \{O, X_1, T^*, P_1', T_R, R\}$, *the Riemann solution corresponds to the sequence* $L \overset{S_s}{\longmapsto} M \overset{R_f}{\longmapsto} R$. *Here* M *is in the* f*-rarefaction segment* $[O, R] \subset \mathcal{W}_f^-(R)$.

(v) *if* $L \in S_{2T} = \{X_1, T^*, Z_2\}$ *the Riemann solution corresponds to the sequence* $L \overset{S_s}{\longmapsto} M \overset{S_T}{\longmapsto} Z_1 \overset{R_f}{\longmapsto} R$. *Here* M *is in the transitional segment* (Z_2, X_1).

(vi) *if* L *is in the* s*-rarefaction segment* $[B^*, P_1']$, *then the Riemann solution corresponds to the sequence* $L \overset{R_s}{\longmapsto} P_1' \overset{'S_s}{\longrightarrow} P_1'' \overset{S_f'}{\longrightarrow} P_1 \overset{R_f}{\longrightarrow} R$. *Here* P_1 *and* P_1' *are a pair of mixed double contact states and* $P_1'' \in [A_2, Z_2] \subset \mathcal{W}_f^-(R)$.

(vii) *if L is in the Lax s-shock segment $[X_1, T^*) \subset \mathcal{H}(Z_1)$ then the Riemann solution corresponds to the sequence $L \overset{S_s}{\longmapsto} M \overset{S_T}{\longrightarrow} Z_1 \overset{S_f}{\longmapsto} R$. Notice that $\sigma(L;M) = \sigma(M;Z_1)$.*

(viii) *if L is in the over-compressive composite segment (P_1', T^*), then we have two possible wave sequences in the state space corresponding to a unique solution in the xt-space. The Riemann solutions are:*

(a) $L \overset{S_s}{\longmapsto} N_1 \overset{S_f'}{\longrightarrow} M \overset{R_f}{\longrightarrow} R$, *with* $N_1 \in (P_1'', Z_2)$;

(b) $L \overset{S_O'}{\longmapsto} N_2 \overset{R_f}{\longrightarrow} R$, *with* $N_2 \in (P_1, Z_1)$.

The other cases are similar to Claim 8.4.6.

Proof. Similar to the proof of Claim 8.4.6 (see Figure 8.13). ∎

Remark 8.4.11. Remark 8.4.5 also holds for statement (*vii*) of Claim 8.4.7. Notice that for the statement (*vi*) of Claim 8.4.7, there is other solution given by the triple shock rule in which the Lax s-shock and f-shock collapse : $L \overset{R_s}{\longmapsto} P_1' \overset{'S_O'}{\longrightarrow} P_1 \overset{R_f}{\longrightarrow} R$. But the discontinuity joining P_1 and P_1' do not have viscous profile.

8.4.6 $\mathscr{L}_{\mathscr{R}}$-regions for $R \in \mathscr{R}_6$

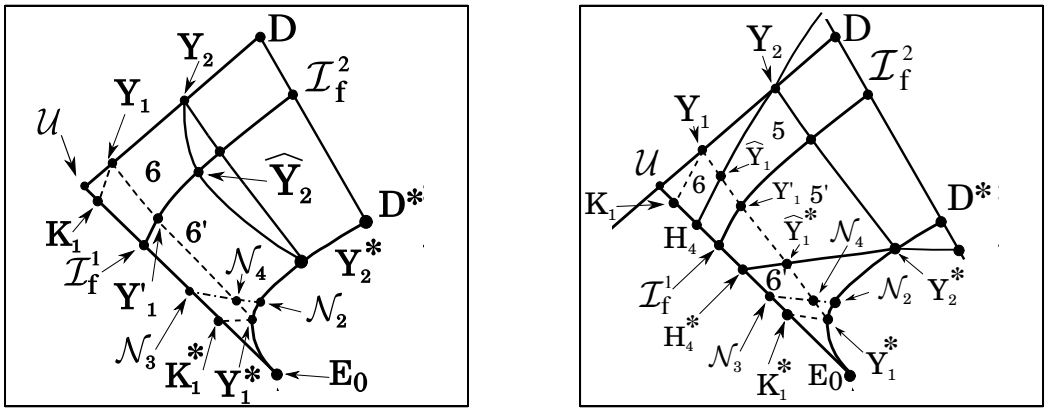

(a) Highlight of regions $\mathscr{R}_i$ for $i \in \{6, 6'\}$ affected by the presence of the mixed double contact locus.

(b) Highlight of regions $\mathscr{R}_i$ for $i \in \{5, 5', 6, 6'\}$ affected by the presence of the mixed double contact locus, in the case of Remark 6.4.5.

Figure 8.14: Subdivisions of regions $\mathscr{R}_5, \mathscr{R}_{5'}, \mathscr{R}_6$ and $\mathscr{R}_{6'}$ in presence of the mixed double contact locus.

The subdivision of the saturation triangle in terms of $\mathscr{L}_{\mathscr{R}}$-regions for $R \in \mathscr{R}_6$ is more complex that others regions because the presence of mixed double contact locus makes that the $\mathscr{L}_{\mathscr{R}}$-regions must be

subdivide into three different regions: $\{Y_2, Y_1, Y_1', \widehat{Y_2}\}$, $\{Y_1, Y_1', \mathcal{I}_f^1, K_1\}$ and $\{Y_1, K_1, \mathcal{U}\}$, see Figure 8.14(a) (in the case of Remark 6.4.5 changing $\mathcal{I}_f^1$ by H_4 and Figure 8.14(b)).

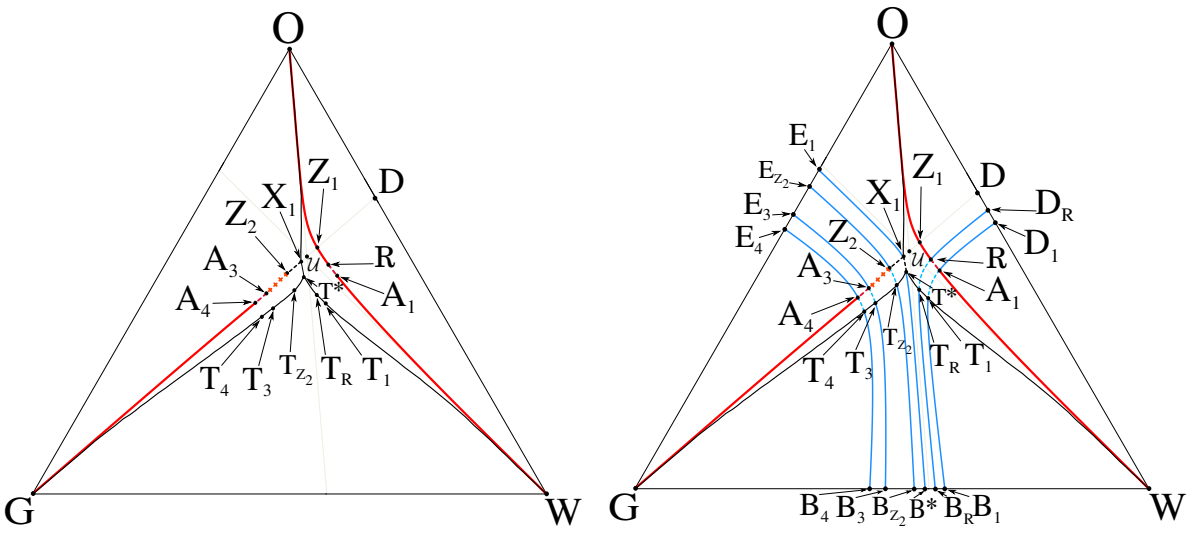

(a) Right s-extension of $[Z_2, X_1]$ and $\mathcal{W}_f^-(R)$ for R in region $\mathscr{R}_6$. The segment $[X_1, T^*]$ is a segment of Lax s-shocks of $\mathcal{H}(Z_1)$.

(b) $\mathscr{L}$-regions for R in region $\mathscr{R}_6$, see Claim 8.4.8.

Figure 8.15: Subdivision of saturation triangle according to the structure of Riemann solutions for $R \in \mathscr{R}_6$.

From Remark 8.4.10 we seen that the changes in $\mathscr{L}_{\mathscr{R}}$-regions is due to the intersection of the local branch of $\mathcal{W}_f^-(R)$ and the segment $[K_1, Y_1]$. This causes that the boundaries for loss of compatibility of speeds associate to components of the nonlocal branch of $\mathcal{W}_f^-(R)$ change. According to Figure 8.15(a), the nonlocal branch of $\mathcal{W}_f^-(R)$ for $R \in \mathscr{R}_6$ has three components: a f-composite segment $[A_3, Z_2]$, a Lax f-shock segment (A_4, A_3) and a f-rarefaction segment $[A_4, G]$. Because of this, we describe first the case where the local branch of $\mathcal{W}_f^-(R)$ does not cross the segment $[K_1, Y_1]$, then we describe the case where R is inside $\{Y_1, K_1, \mathcal{U}\}$. The wave sequences for R inside $\{Y_1, Y_1', \mathcal{I}_f^1, K_1\}$ is similar to the one given in Claim 8.4.7 for $R \in \mathscr{R}_5$.

Consider a state R in region $\mathscr{R}_6$, see Figure 8.15(a). Notice that in this case we have transitional waves associated to the intersection between $\mathcal{W}_f^-(R)$ and $[\mathcal{U}, D]$ at state Z_1, see Section 7.3.2 with $Z_1 = M_2$ and $Z_2 = M_2'$. In Figure 8.15(a) we show the s-extension of $\mathcal{W}_f^-(R)$ and of the invariant segment $[Z_2, X_1]$ that was obtained numerically. The segments $[T_1, W]$, $[T_R, T^*]$, $[T_4, G]$ and $[X_1, O]$ are s-extensions of f-rarefaction segments $[A_1, W]$, $[R, Z_1]$, $[A_4, G]$ and $(Z_1, O]$ of $\mathcal{W}_f^-(R)$, respectively. The Lax f-shock segments of $\mathcal{W}_f^-(R)$, $(R, A_1]$ and (A_4, A_3) and, the f-composite segment $[A_3, Z_2]$ have respectively s-extension segments (T_R, T_1), (T_4, T_3) and $[T_3, T_{Z_2}]$; the segment $[T_{Z_2}, T^*]$ is the s-extension curve of the $[Z_2, X_1]$.

Now, we construct the boundaries of $\mathscr{L}_{\mathscr{R}_6}$-regions taking into account the Claims 6.4.12 and 6.4.13, and Section 7.3.2 (see Figure 8.15(b)). First construct the backward s-wave curve for the states R, A_1, A_3, A_4

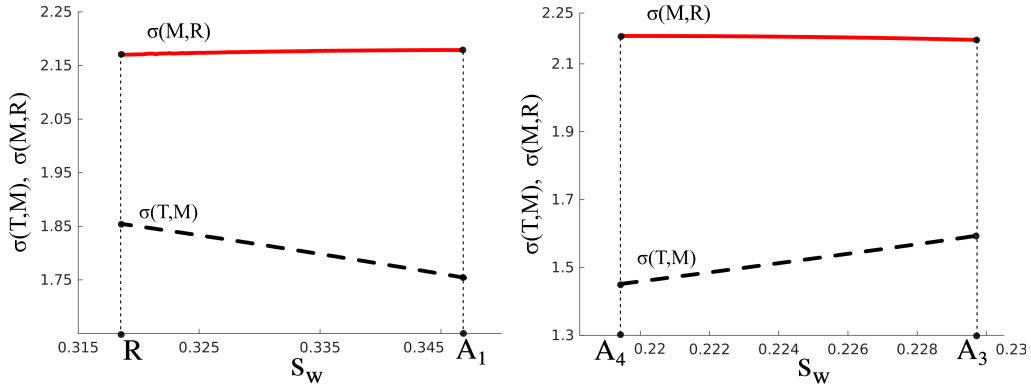

(a) Slow shock/fast shock. Local Lax f-shock segment $(R, A_1) \subset \mathcal{W}_f^-(R)$.

(b) Slow shock/fast shock. Nonlocal f-shock segment $(A_4, A_3) \subset \mathcal{W}_f^-(R)$.

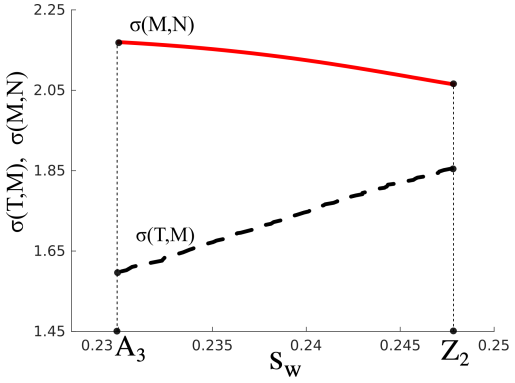

(c) Slow shock/fast shock. f-composite segment $(A_3, Z_2) \subset \mathcal{W}_f^-(R)$.

Figure 8.16: Speed diagrams along $\mathcal{W}_f^-(R)$ and its extension curve. (a) Shocks speeds $\sigma(T; M)$ and $\sigma(M; R)$ as M and T vary along the Lax f-shock segment $[R, A_1] \subset \mathcal{W}_f^-(R)$ and its s-extension curve $[T_R, T_1]$, respectively. (b) Shocks speeds $\sigma(T; M)$ and $\sigma(M; R)$ as M and T vary along the Lax f-shock segment $[A_4, A_3] \subset \mathcal{W}_f^-(R)$ and its s-extension curve $[T_4, T_3]$, respectively. (c) Shocks speeds $\sigma(T; M)$ and $\sigma(M; N)$ as M,N and T vary along the f-composite segment $[A_3, Z_2] \subset \mathcal{W}_f^-(R)$, the f-rarefaction segment $[R, Z_1] \subset \mathcal{W}_f^-(R)$ and its s-extension curve $[T^*, T_R]$, respectively (see Claim 8.4.8 and Figure 8.15).

and Z_2 of $\mathcal{W}_f^-(R)$ that are shown in Figure 8.15(b). Following Definition 7.3.3 we construct regions S_{1T}, S_{2T} and S_{3T} which are given by the areas $\{E_1, X_1, Z_2, E_{Z_2}\}$, $\{X_1, Z_2, T_{Z_2}, T^*\}$ and $\{T^*, T_{Z_2}, B_{Z_2}, B^*\}$, respectively.

In Figure 8.16(a), (b) and (c) are present the speed diagrams that show shock/shock and shock/composite compatibility. In (a) and (b) are presented the compatibility with local and nonlocal Lax f-shock segments is between the Lax s-shock wave from T to M with the Lax f-shock wave from M to R with $T \in [T_R, T_1]$ and $M \in [R, A_1]$; the second between the Lax s-shock wave from T to M with the sonic

f-shock wave from M to N with $T \in [T_2, T_{Z_2}]$, $M \in [A_2, Z_2]$ and $N \in [A_2^*, R]$.

Claim 8.4.8. *Take a fixed state R in $\mathscr{R}_6$ and construct $\mathcal{W}_f^-(R)$ (see Figure 8.15(b)). Let L be a state in the saturation triangle. Then:*

(i) if $L \in \{G, A_4, E_4\}$, the Riemann solution corresponds to the sequence $L \overset{R_s}{\longmapsto} M \overset{R_f}{\longmapsto} A_4 \overset{'S_f}{\longrightarrow} R$. Here M is in the f-rarefaction segment $[G, A_4] \subset \mathcal{W}_f^-(R)$. We have the same wave sequences for $L \in \{W, A_1, D_1\}$ by changing A_4 to A_1 with M in the f-rarefaction segment $[W, A_1] \subset \mathcal{W}_f^-(R)$.

(ii) if $L \in \{E_4, A_4, A_3, E_3\}$, the Riemann solution corresponds to the sequence $L \overset{R_s}{\longmapsto} M \overset{S_f}{\longmapsto} R$. Here M is in the Lax f-shock segment $(A_4, A_3) \subset \mathcal{W}_f^-(R)$. Again, we have the same wave sequences for $L \in \{D_1, A_1, R, D_R\}$ with M in the Lax f-shock segment $(A_1, R) \subset \mathcal{W}_f^-(R)$.

(iii) if $L \in \{D_R, R, O\}$, the Riemann solution corresponds to the sequence $L \overset{R_s}{\longmapsto} M \overset{R_f}{\longmapsto} R$. Here M is in the f-rarefaction segment $[O, R] \subset \mathcal{W}_f^-(R)$.

(iv) if $L \in \{G, B_4, T_4\}$, the Riemann solution corresponds to the sequence $L \overset{R_s}{\longmapsto} T \overset{'S_s}{\longrightarrow} M \overset{R_f}{\longmapsto} A_4 \overset{'S_f}{\longrightarrow} R$. Here T is in the s-extension curve $[G, T_4]$ and M in the f-rarefaction segment $[G, A_4] \subset \mathcal{W}_f^-(R)$. We have the same wave sequences for $L \in \{W, B_1, T_1\}$ by changing A_4 to A_1 with T in the s-extension curve $[W, T_1]$ and M in the f-rarefaction segment $[W, A_1] \subset \mathcal{W}_f^-(R)$.

(v) if $L \in \{B_4, B_3, T_3, T_4\}$, the Riemann solution corresponds to the sequence $L \overset{R_s}{\longmapsto} T \overset{'S_s}{\longrightarrow} M \overset{S_f}{\longmapsto} R$. Here T is in the s-extension curve (T_4, T_3) and M is in the Lax f-shock segment $(A_4, A_3) \subset \mathcal{W}_f^-(R)$. We have the same wave sequences for $L \in \{B_1, B_R, T_R, T_1\}$ with T in the s-extension curve (T_1, T_R) and M in the Lax f-shock segment $(A_1, R) \subset \mathcal{W}_f^-(R)$.

(vi) if $L \in \{G, T_4, A_4\}$, the Riemann solution corresponds to the sequence $L \overset{S_s}{\longmapsto} M \overset{R_f}{\longmapsto} A_4 \overset{'S_f}{\longrightarrow} R$. Here M is in the f-rarefaction segment $[G, A_4] \subset \mathcal{W}_f^-(R)$. We have the same wave sequences for $L \in \{W, T_1, A_1\}$ by changing A_4 to A_1 with M in the f-rarefaction segments $[W, A_1] \subset \mathcal{W}_f^-(R)$.

(vii) if $L \in \{A_4, A_3, T_3, T_4\}$, the Riemann solution corresponds to the sequence $L \overset{S_s}{\longmapsto} M \overset{S_f}{\longmapsto} R$. Here M is in the Lax f-shock segment $(A_4, A_3) \subset \mathcal{W}_f^-(R)$. We have the same wave sequences for $L \in \{A_1, R, T_R, T_1\}$ with M in the Lax f-shock segment $(A_1, R) \subset \mathcal{W}_f^-(R)$.

The other cases are similar to Claim 8.4.6.

Proof. Refer to Figure 8.15. The compatibility of speeds is justified by Remark 8.4.1 and Figure 8.16. The compatibility of speeds with the transitional waves were established in Section 7.3.2 ∎

Now we consider $R \in \{Y_1, K_1, \mathcal{U}\}$ in Figure 8.14. Figure 8.17(b) is a blow-up of the region close to the umbilic point in Figure 8.17(a), displaying the f-composite segment $[A_3, Z_2] \subset \mathcal{W}_f^-(R)$ for $R \in \{Y_1, K_1, \mathcal{U}\}$ (see Figure 8.14(a)). Notice that in this case, Z_1 lies in $[\mathcal{U}, Y_1]$ and the f-shock segment $[R, A_1]$ intersects $[Y_1, K_1]$. We have two boundaries for loss of compatibility of speeds: the over-compressive shock segment $[A_5, T^*]$ and the over-compressive composite segment $[T_R, A_5]$. When these two boundaries appear, we loss two $\mathscr{L}_{\mathscr{R}}$-regions: the region $S_{3T} = \{T_{Z_2}, T^*, B^*, B_{Z_2}\}$ (see Remark 7.3.2) and $\{T_3, T_{Z_2}, B_{Z_2}, B_3\}$, see Figures 8.15(b) and 8.17. The Lax f-shock segments $[A_4, A_3]$ and $[R, A_1]$ have distinct boundaries for loss of compatibility speeds: the s-extension segments $[T_4, T^*]$ and $[T_1, T^*]$ associated to the segment $[A_4, A_3^*]$ and $[A_1, A_1^*]$, respectively, and the over-compressive shock segment $[A_5, T^*]$ associated to the Lax f-shock segments $[A_3^*, A_3]$ and $[A_1^*, R]$. The over-compressive composite segment $[T_R, A_5]$ is associated with the f-composite segment $[A_3, Z_2]$ and the f-rarefaction segment $[R, Z_1]$. Notice that by the triple shock rule we conclude that (refer to Figure 8.17):

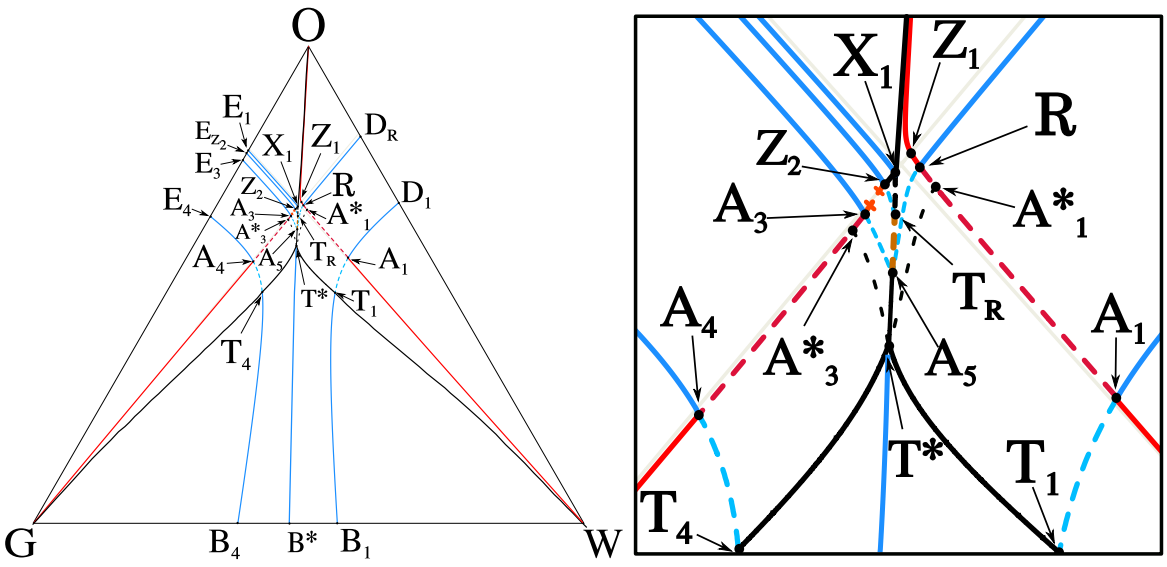

(a) $\mathscr{L}$-regions for R in region $\mathscr{R}_6$ inside $\{Y_1, K_1, \mathcal{U}\}$, see Claim 8.4.9.

(b) Zoom of area close to f-composte segment $[A_3, Z_2]$.

Figure 8.17: (a) Subdivision of saturation triangle according to the structure of Riemann solutions for $R \in \mathscr{R}_6$. Notice that regions $\{T_3, T_{Z_2}, B_{Z_2}, B_3\}$, $S_{3T} = \{T_{Z_2}, T^*, B^*, B_{Z_2}\}$ and $\{B_R, B^*, T^*, T_R\}$of the one shown in Figure 8.15(b) collapsed on the segment $[B^*, T^*]$. (b) Zoom of region close to the f-composite segment $[A_3, Z_2]$ associated to f-rarefaction segment $[R, Z_1] \subset \mathcal{W}_f^-(R)$ for R inside $\{Y_1, K_1, \mathcal{U}\}$. There are two boundaries for loss of compatibility of speeds: the over-compressive composite segment $[A_5, T_R]$ and the over-compressive shock segment $[A_5, T^*]$. Black dashed curves are segments of Lax s-shocks

(1) for any state $M \in (T^*, A_5]$, there are states $N_1 \in (A_3^*, A_3)$ and $N_2 \in (A_1^*, R)$ such that the discontinuity joining M with N_1 and N_2 is a Lax s-shock and $\sigma(M; N_1) = \sigma(N_1; R)$ as well as $\sigma(M; N_2) = \sigma(N_2; R)$;

(2) for any state $M \in [A_5, T_R]$ there are states $N_1 \in [A_3, Z_2]$ and $N_2 \in [R, Z_1]$ such that the discontinuity joining M with N_1 and N_2 is a Lax s-shock and $\sigma(M; N_1) = \sigma(M; N_2) = \lambda_f(N_2)$.

Therefore, we have the following result

Claim 8.4.9. *Take a fixed state R in $\mathscr{R}_6$ inside of region $\{Y_1, K_1, \mathcal{U}\}$ and construct $\mathcal{W}_f^-(R)$ (see Figures 8.14(b) and 8.17). Let L be a state in the saturation triangle. Then:*

(i) if $L \in \{A_1, R, A_5, T^*, T_1\}$, the Riemann solution corresponds to the sequence $L \overset{S_s}{\longmapsto} M \overset{S_f}{\longmapsto} R$. Here M is in the Lax f-shock segment $(A_1, R) \subset \mathcal{W}_f^-(R)$. We have the same wave sequences for $L \in \{A_4, T_4, T^*, A_5, A_3\}$ with M in the Lax f-shock segment $(A_4, A_3) \subset \mathcal{W}_f^-(R)$.

(ii) if $L \in \{T_4, B_4, B^*, T^*\}$ the Riemann solution corresponds to the sequence $L \overset{R_s}{\longmapsto} T \overset{'S_s}{\longrightarrow} M \overset{S_f}{\longmapsto} R$. Here T is in the s-extension curve (T_4, T^*) and M is in the Lax f-shock segment $(A_4, A_3^*) \subset \mathcal{W}_f^-(R)$. We have the same wave sequences for $L \in \{T_1, B_1, B^*, T^*\}$ with T in the s-extension curve (T_1, T^*) and M in the Lax f-shock segment $(A_1, A_1^*) \subset \mathcal{W}_f^-(R)$.

(iii) if $L \in \{A_3, A_5, T_R, Z_2\}$, the Riemann solution corresponds to the sequence $L \overset{S_s}{\longmapsto} M \overset{S'_f}{\longmapsto} N \overset{R_f}{\longrightarrow} R$. Here M is in the f-composite segment $[A_3, Z_2] \subset \mathcal{W}_f^-(R)$ and N is in the f-rarefaction segment $[R, Z_1] \subset \mathcal{W}_f^-(R)$.

(iv) if $L \in \{O, X_1, T_R, A_5, R\}$, the Riemann solution corresponds to the sequence $L \overset{S_s}{\longmapsto} M \overset{R_f}{\longmapsto} R$. Here M is in the f-rarefaction segment $[O, R] \subset \mathcal{W}_f^-(R)$.

(v) if $L \in S_{2T} = \{X_1, T_R, Z_2\}$ the Riemann solution corresponds to the sequence $L \overset{S_s}{\longmapsto} M \overset{S_T}{\longmapsto} Z_1 \overset{R_f}{\longmapsto} R$. Here M is in the transitional segment (Z_2, X_1).

(vi) if L is in the s-rarefaction segment $[B^*, T^*]$, then we have three possible wave sequences in the state space corresponding to a unique solution in the xt-space, see [3, 9]. The Riemann solutions are:

(a) $L \overset{R_s}{\longmapsto} T^* \overset{'S_s}{\longrightarrow} A_1^* \overset{S_f}{\longrightarrow} R$;

(b) $L \overset{R_s}{\longmapsto} T^* \overset{'S_s}{\longrightarrow} A_3^* \overset{S_f}{\longrightarrow} R$;

(c) $L \overset{R_s}{\longmapsto} T^* \overset{'S_O}{\longrightarrow} R$.

(vii) if L is in the Lax s-shock segment $[X_1, T_R) \subset \mathcal{H}(Z_1)$ then the Riemann solution corresponds to the sequence $L \overset{S_s}{\longmapsto} M \overset{S_T}{\longrightarrow} Z_1 \overset{S_f}{\longmapsto} R$. Here $M \in [Z_2, X_1]$ and satisfy $\sigma(L; M) = \sigma(M; Z_1)$.

(viii) if L is in the over-compressive shock segment (T^*, A_5), then we have three possible wave sequences in the state space corresponding to a unique solution in the xt-space, see [3, 9]. The Riemann solutions are:

(a) $L \overset{S_s}{\longmapsto} N_1 \overset{S_f}{\longrightarrow} R$, *with* $N_1 \in (A_3^*, A_3)$;

(b) $L \overset{S_s}{\longmapsto} N_2 \overset{S_f}{\longrightarrow} R$, *with* $N_2 \in (A_1^*, R)$;

(c) $L \overset{S_O}{\longmapsto} R$.

(ix) if L is in the over-compressive composite segment (A_5, T_R), then we have two possible wave sequences in the state space corresponding to a unique solution in the xt-space. The Riemann solutions are:

(a) $L \overset{S_s}{\longmapsto} N_1 \overset{S'_f}{\longrightarrow} M \overset{R_f}{\longrightarrow} R$, *with* $N_1 \in (A_3, Z_2)$;

(b) $L \overset{S'_O}{\longmapsto} N_2 \overset{R_f}{\longrightarrow} R$, *with* $N_2 \in (R, Z_1)$.

The other cases are similar to Claim 8.4.8.

Proof. Similar to the proof of Claim 8.4.8 (see Figure 8.17). ∎

Remark 8.4.12. Remark 8.4.5 also holds for statement (*vii*) of Claim 8.4.9.

8.4.7 $\mathscr{L}_{\mathscr{R}}$-regions for $R \in \mathscr{R}_i$ with $i \in \{4', 5', 6'\}$

The subdivision of the saturation triangle in terms of $\mathscr{L}_{\mathscr{R}}$-regions for $R \in \mathscr{R}_{4'}$ or $R \in \mathscr{R}_{5'}$ is similar to the one shown in Sections 8.4.4 and 8.4.5 for R in regions $\mathscr{R}_4$ and $\mathscr{R}_5$. The main difference, which is induced by the fast inflection locus, is that the last wave reaching R is not a f-rarefaction but rather a f-composite wave.

The $\mathscr{R}_{6'}$ has some additional particularities because both the s-hysteresis segment $[\mathcal{N}_2, \mathcal{N}_3]$ and the extension of the mixed double contact segment $[Y_1^*, K_1^*]$ cross this region (see Figure 8.14) and form the subregion $\mathscr{R}_{6'}^H$ defined in Remark 6.4.9. Then, for this region we apply a combination of the procedures performed for region $\mathscr{R}_2^H$ in Claim 8.4.3 and those performed for region $\mathscr{R}_6$ in Claim 8.4.9.

8.5 Diagrams of comparison between regions

In this section, we summarize the distinct Riemann solutions and study the behavior of these solutions in two types of data variation. In the first setting, we fix the right state R and see how solutions change continuously as L traverses the phase space continuously. Notice how the bifurcations and the compatibility boundaries take the role of transition bridges between regions. The triple shock rule is fundamental to understand how transitions with states in different positions of the saturation triangle representing the same solution in the xt-space. In the second variation scenario, by fixing L and varying R continuously, we can see how $\mathscr{L}$-regions arise or disappear continuously. There is a third possible variation study to analyze the behavior of Riemann solutions: when we vary the viscosities (while keeping the umbilic point of type II) the boundaries of the $\mathscr{R}$-regions move. So, even with the right state R fixed, it changes regions continuously in a similar manner to the first variation setting.

$\mathcal{A}:\ S_s\,S_f$	$\mathcal{B}:\ S_s\,R_f$	$\mathcal{C}:\ R_s\,S_f$
$\mathcal{D}:\ R_s\,R_f$	$\mathcal{E}:\ R_s\,'S_s\,S_f$	$\mathcal{F}:\ R_s\,'S_s\,R_f$
$\mathcal{G}:\ S_s\,R_f\,'S_f$	$\mathcal{H}:\ R_s\,R_f\,'S_f$	$\mathcal{I}:\ R_s\,'S_s\,R_f\,'S_f$
$\mathcal{J}_1:\ R_s\,'S_s\,S_T\,S_f$	$\mathcal{J}_2:\ S_s\,S_T\,S_f$	$\mathcal{J}_3:\ R_s\,S_T\,S_f$
$\mathcal{J}_4:\ R_s\,'S_s\,S_T\,R_f$	$\mathcal{J}_5:\ S_s\,S_T\,R_f$	$\mathcal{J}_6:\ R_s\,S_T\,R_f$
$\mathcal{J}_7:\ R_s\,'S_s\,S_T\,R_f\,'S_f$	$\mathcal{J}_8:\ S_s\,S_T\,R_f\,'S_f$	$\mathcal{J}_9:\ R_s\,S_T\,R_f\,'S_f$
$\mathcal{K}_1:\ R_s\,'S_s\,R_f\,'S_T\,S_f$	$\mathcal{K}_2:\ S_s\,R_f\,'S_T\,S_f$	$\mathcal{K}_3:\ R_s\,R_f\,'S_T\,S_f$
$\mathcal{K}_4:\ R_s\,'S_s\,R_f\,'S_T\,R_f$	$\mathcal{K}_4:\ S_s\,R_f\,'S_T\,R_f$	$\mathcal{K}_6:\ R_s\,R_f\,'S_T\,R_f$
$\mathcal{K}_7:\ R_s\,'S_s\,R_f\,'S_T\,R_f\,'S_f$	$\mathcal{K}_8:\ S_s\,R_f\,'S_T\,R_f\,'S_f$	$\mathcal{K}_9:\ R_s\,R_f\,'S_T\,R_f\,'S_f$
$\mathcal{L}_1:\ R_s\,S'_f\,R_f$	$\mathcal{M}_1:\ S_s\,S'_f\,R_f$	$\mathcal{N}_1:\ R_s\,'S_s\,S'_f\,R_f$
$\mathcal{L}_2:\ R_s\,S'_f\,R_f\,'S_f$	$\mathcal{M}_2:\ S_s\,S'_f\,R_f\,'S_f$	$\mathcal{N}_2:\ R_s\,'S_s\,S'_f\,R_f\,'S_f$
$\mathcal{O}_1:\ R_s\,'S_s\,R_f\,'S'_f R_f$	$\mathcal{P}_1:\ S_s\,R_f\,'S'_f R_f$	$\mathcal{Q}_1:\ R_s\,R_f\,'S'_f R_f$
$\mathcal{O}_2:\ R_s\,'S_s\,R_f\,'S'_f R_f\,'S_f$	$\mathcal{P}_2:\ S_s\,R_f\,'S'_f R_f\,'S_f$	$\mathcal{Q}_2:\ R_s\,R_f\,'S'_f R_f\,'S_f$

Table 8.1: Nomenclature of distinct waves structures in $\mathscr{L}$-regions.

In table 8.1 we summarizes the possible solutions that are involved in classical and transitional Riemann solutions, not considering the delta wing (see Section 6.4.5.2) and transitional rarefactions. Notice that the number of different structures varies as we change the $\mathscr{R}$-region. For example, if considering $R \in \mathscr{R}_1$, we have only nine distinct structures, see Figure 8.18(a). Notice that transitional waves are not used in this case.

In the case of R in the region $\mathscr{R}_2$ we have two possibilities: if R is inside of $\{V_0, \mathcal{U}, Y_1, V_1\} \cup \{V_0^*, E_0, Y_1^*, V_1^*\}$; we have 11 distinct structures; otherwise we have 12, see Figure 8.18(b). This is due to the loss of set S_{3T} represented in Table 8.1 for $\mathcal{J}_1$, see Remark 7.3.2. This happens because $\mathcal{J}_1$ collapses on a s-rarefaction segment, while $\mathcal{J}_2$ and $\mathcal{J}_3$ remain, see Figure 8.18(b). Notice that, for $R \in \mathscr{R}_2^H$, no new structures are added but, more of the same Riemann solutions appear in different positions on the saturation triangle.

In the case of R in the region $\mathscr{R}_3$ and $\mathscr{R}_4$ we always have 15 distinct structures. Notice in Figures 8.19 that when R crosses the invariant line $[G, D]$, we have two changes: a) the last fast-family used to reach R by transitional waves changes, *i.e.,* the structures $\mathcal{J}_i$ and $\mathcal{K}_i$ for $i \in \{1, 2, 3\}$ are changed to those for $i \in \{4, 5, 6\}$, see Table 8.1; b) one of the regions $\mathcal{E}$ collapses and a additional $\mathcal{F}$ region appear. In the same way, following Section 8.4.7, the number of distinct structures of Riemann solutions for $\mathscr{R}_{4'}$ is also 15. Using Table 8.1 and Figure 8.19(b), we can find the distinct structures of Riemann solutions for $\mathscr{R}_{4'}$: $\mathcal{A}, \mathcal{C}$ and $\mathcal{E}$, remain in the same location; $\mathcal{D}, \mathcal{B}$ and $\mathcal{F}$ change to $\mathcal{H}, \mathcal{G}$ and $\mathcal{I}$, respectively; and the structures $\mathcal{J}_i$ and $\mathcal{K}_i$ for $i \in \{4, 5, 6\}$ change to $i \in \{7, 8, 9\}$.

If R belongs to region $\mathscr{R}_5$, we have two possibilities depending on whether $\mathcal{W}_f^-(R)$ crosses the segment $[Y_1, K_1]$, see Remark 8.4.10. Then, we have 18 distinct structures of Riemann solutions or 17 when $\mathcal{J}_4$ collapse, see Figure 8.20(a). Since the nonlocal branch of $\mathcal{W}_f^-(R)$ has a f-composite segment that is associated to a pair of states from the fast double contact locus, we have new structures of Riemann

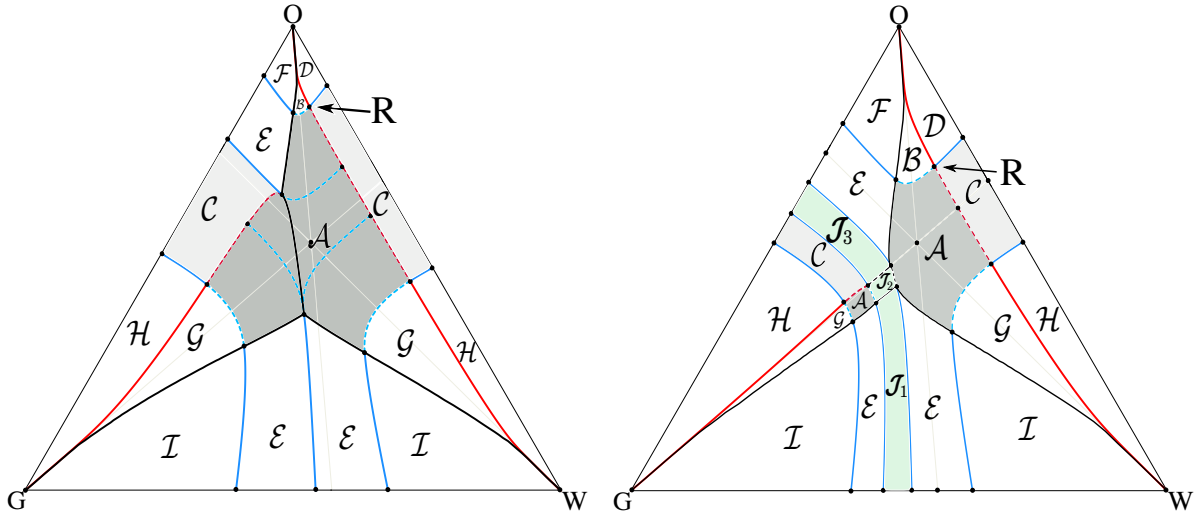

(a) $\mathscr{L}$-regions for R in region $\mathscr{R}_1$.

(b) $\mathscr{L}$-regions for R in region $\mathscr{R}_2$.

Figure 8.18: Diagrams of changes between $\mathscr{L}$-regions for R in region $\mathscr{R}_1$ and $\mathscr{R}_2$, see Figures 8.1(b) and 8.4(b). Green region represents the left states L that use single transitional shocks in the Riemann solution. The nomenclature for structures $\mathcal{A}, \mathcal{B}, \ldots, \mathcal{I}, \mathcal{J}_1, \mathcal{J}_2$ and $\mathcal{J}_3$ are in Table 8.1.

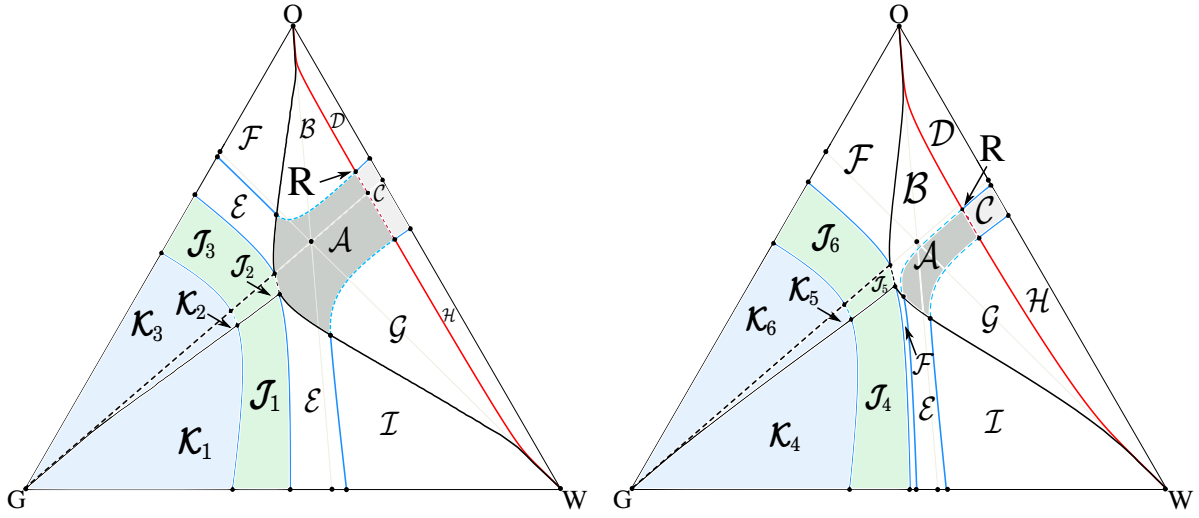

(a) $\mathscr{L}$-regions for R in region $\mathscr{R}_3$.

(b) $\mathscr{L}$-regions for R in region $\mathscr{R}_4$.

Figure 8.19: Diagrams of changes between $\mathscr{L}$-regions for R in region $\mathscr{R}_3$ and $\mathscr{R}_4$, see Figures 8.8(b) and 8.9(b). Blue and green regions represent the left states L that use composite or single transitional waves in the Riemann solution, respectively. The nomenclature for structures $\mathcal{A}, \mathcal{B}, \ldots, \mathcal{I}, \mathcal{J}_i$ and $\mathcal{K}_i$ for $i \in \{1, 2, \ldots, 6\}$ are in Table 8.1.

solutions that are used to reach R: $\mathcal{L}_1$, $\mathcal{M}_1$, $\mathcal{N}_1$, $\mathcal{O}_1$, $\mathcal{P}_1$ and $\mathcal{Q}_1$, see Claim 6.4.11 and Table 8.1. Notice that regions with structures $\mathcal{O}_1, \mathcal{P}_1$ and $\mathcal{Q}_1$ depend on the admissibility of the fast double contact locus. To identify the structures for $\mathscr{R}_{5'}$, we can apply the same procedure as in $\mathscr{R}_{4'}$. In Figures 8.20(a) and (b), we see the transition between regions $\mathscr{R}_5$ and $\mathscr{R}_6$. Notice that the regions $\mathcal{O}_1, \mathcal{P}_1$ and $\mathcal{Q}_1$ are replaced by $\mathcal{I}, \mathcal{G}$ and $\mathcal{H}$, respectively. Since these structures are already part of $\mathscr{R}_6$, we can conclude that the maximal number of different structures for $\mathscr{R}_6$ is 15.

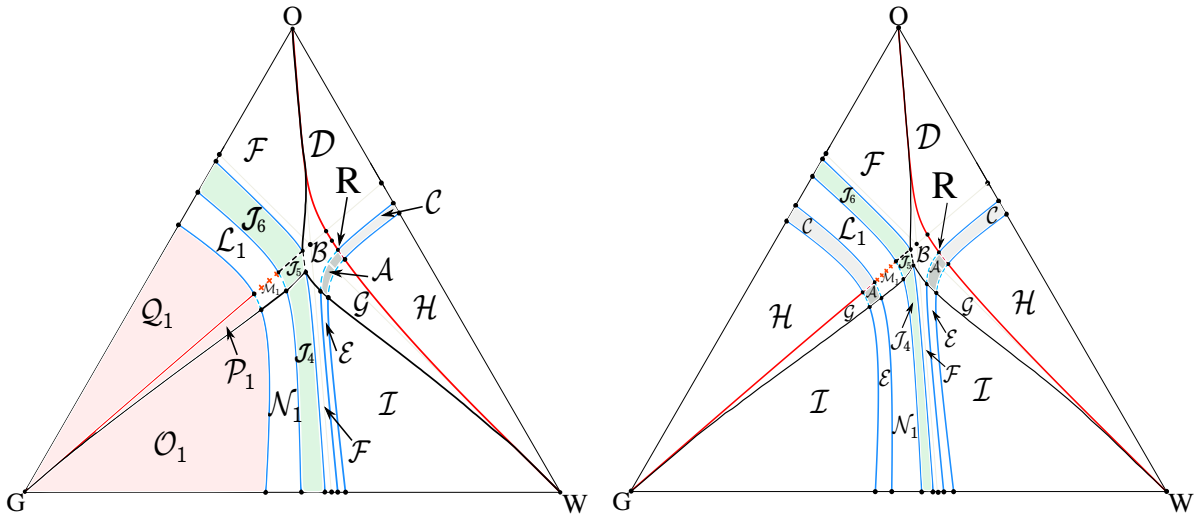

(a) $\mathscr{L}$-regions for R in region $\mathscr{R}_5$.

(b) $\mathscr{L}$-regions for R in region $\mathscr{R}_6$.

Figure 8.20: Diagrams of changes between $\mathscr{L}$-regions for R in region $\mathscr{R}_5$ and $\mathscr{R}_6$, see Figures 8.11(b) and 8.15(b). Green region represents the left states L that use single transitional shocks in the Riemann solution. Light red region is associated to solutions that depends of the admissible fast double contact locus. The nomenclature for structures $\mathcal{A}, \mathcal{B}, \ldots, \mathcal{I}, \mathcal{L}_1, \ldots, \mathcal{Q}_1$ and $\mathcal{J}_i$ for $i \in \{4, 5, 6\}$ are in Table 8.1

From Sections 6.4.6 and 8.4.6, when R enters regions influenced by the mixed double contact, the $\mathscr{L}_{\mathscr{R}}$-regions change. In the case of $\mathscr{R}_6$, we seen that some $\mathscr{L}_{\mathscr{R}_6}$-regions collapse. For example, when R is inside $\{Y_1, Y_1', \mathcal{I}_f^1, K_1\}$ the region $\mathcal{J}_4$ collapses, while if R is inside $\{Y_1, K_1, \mathcal{U}\}$ them both $\mathcal{J}_4$ and $\mathcal{N}_1$ collapse, see Figures 8.14(a) and 8.20(b). Therefore, depending on the location of R inside $\mathscr{R}_6$, we have 14, 15 or 16 distinct structures in the Riemann solutions.

Chapter 9

Nonlinear effects of capillarity induced diffusion in conservation laws

In this chapter we construct numerically the surface of transitional shocks for the case $\mathcal{B}(U) \neq I$. We consider the general case with $\mathcal{B}(U)$ defined in Section 3.4. This matrix is associated directly with the correct modelling of the physical diffusive effects caused by capillary pressures [1, 2, 7]. We show that the surface of transitional shocks for this case has the same topological structure found in the case of $\mathcal{B}(U) = I$. In the last section we perform some numerical simulations comparing the solutions for identity and non-identity matrices.

9.1 Saddle-saddle connections

When the viscosity matrix is not the identity, the secondary bifurcation manifold is no longer invariant lines of the parabolic system (3.25) and the admissible transitional shocks occur in regions away from these lines. The solutions described in Chapter 8 are not applicable to this regime. In [36] the approximation of Corey flux function in terms of a quadratic homogeneous system for a neighborhood of the umbilic point was studied. For this quadratic approximation, [19] exhibits transitional shocks away from the bifurcation lines with the particularity that the left and right states lie within cones with vertices at the umbilic point and that the orbits joining these states occur along straight lines. In [28], Marchesin and Mailybaev showed that the transitional shocks are structurally stable under perturbations of the viscosity matrix.

Recall that in this work we adopt the viscous profile criterion for shock admissibility. Then, admissibility of Riemann solutions that involve shocks are affected by perturbations of the viscosity matrix. As in the case of the identity matrix, we want to identify the surface of transitional shocks for a general matrix, to use them as an organizing structure, and to study the Riemann solutions. To determine the connections between saddles of X_σ (2.24), we follow the results mentioned above for quadratic systems and look for connections near the umbilic point. For each U_- fixed in a certain set, we computationally verify the existence of a bifurcation value σ_0, for which the dynamical system has a connection between saddles. This bifurcation value σ_0 is unique and allows for the construction of the surface of transitional

shocks and regions for loss of compatibility of shock speeds, see Figure 9.1.

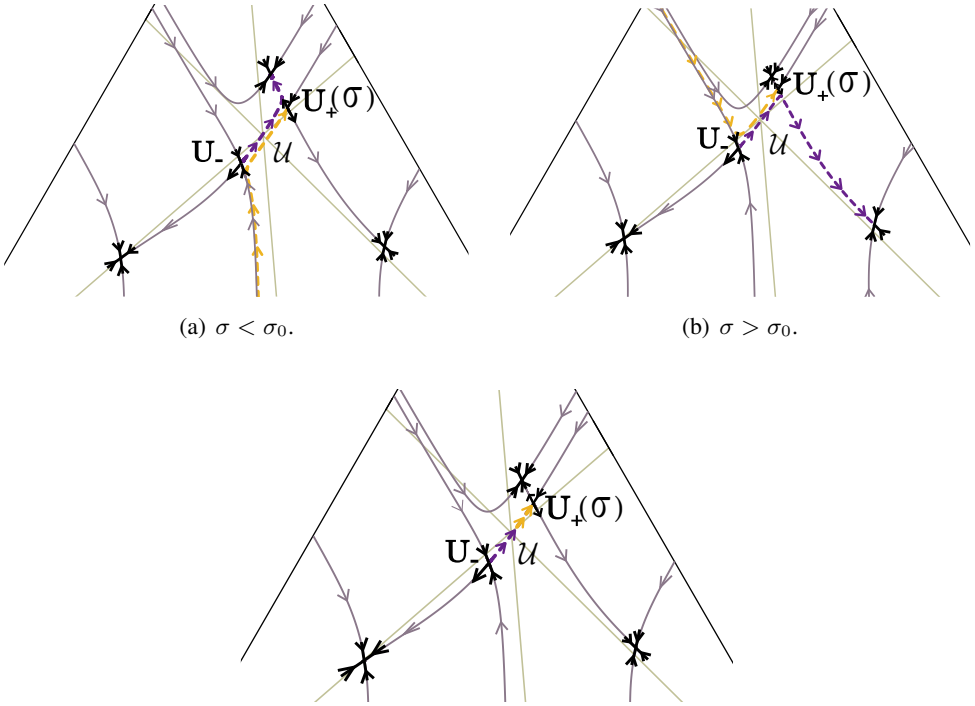

(a) $\sigma < \sigma_0$.

(b) $\sigma > \sigma_0$.

(c) $\sigma = \sigma_0$.

Figure 9.1: Procedure to find connections between saddles. U_- is a fixed state close to the umbilic point and $U_+(\sigma) \in \mathcal{H}(U_-)$. The violet orbit is the unstable manifold for U_- and the yellow orbit is the stable manifold for $U_+(\sigma)$ for the dynamical system associated to U_-, σ_0. Here, we consider $\mathcal{U} \in II_O$.

We verify numerically that the set of states U_- for which there is a connection between saddles comprises regions in the phase space. In Figure 9.1 we show the procedure to find the orbits between saddles: let U_- be a fixed state close to the umbilic point $\mathcal{U}$. The Hugoniot curve $\mathcal{H}(U_-)$ can be parametrized by the shock speed σ in a neighborhood of U_+. The method for locating heteroclinic orbits considers hyperbolic equilibria and two orbits, one with initial condition in an unstable manifold and the other one with initial condition in a stable manifold. Then it tries to annihilate the difference vector between the intersection points of these orbits with a transversal line that is conveniently chosen. When this procedure is successful, *i.e.,* when we find (U_-, σ_0, U_+) such that there is a connection between the saddles points U_- and U_+, we take the perturbation state U_-^* and repeat the procedure until we find the transitional regions in phase space.

9.2 Saddle node-saddle connection.

As seen in Chapter 7 in the case of an identity matrix, a saddle-node is a singularity (equilibrium) where the eigenvalues of the dynamical system (2.20) satisfy $\mu_s\,\mu_f = 0$ and $\mu_s + \mu_f \neq 0$. In this case the eigenvalues are characterized by a simple equation $\mu_i = -\sigma + \lambda_i$, where λ_i is the ith characteristic speed and σ is the shock speed, see Remark 2.2.7. When $\mathcal{B}(U) \neq I$ the eigenvalues are not characterized by this formula. Then, to construct the map of sonic shocks we need to find the shock speed σ_0 such that there is an orbit connecting U_- to a state $U_+ \in \mathcal{H}(U_-)$, such that U_- is a saddle-repeller and U_+ is a saddle (slow sonic shock) or U_- is a saddle and U_+ is a saddle-attractor (fast-sonic-shock), see Definition 2.3.2. The procedure to find these sonic shocks is similar to the one described in Section 9.1 to find transitional shocks, see Figure 9.2.

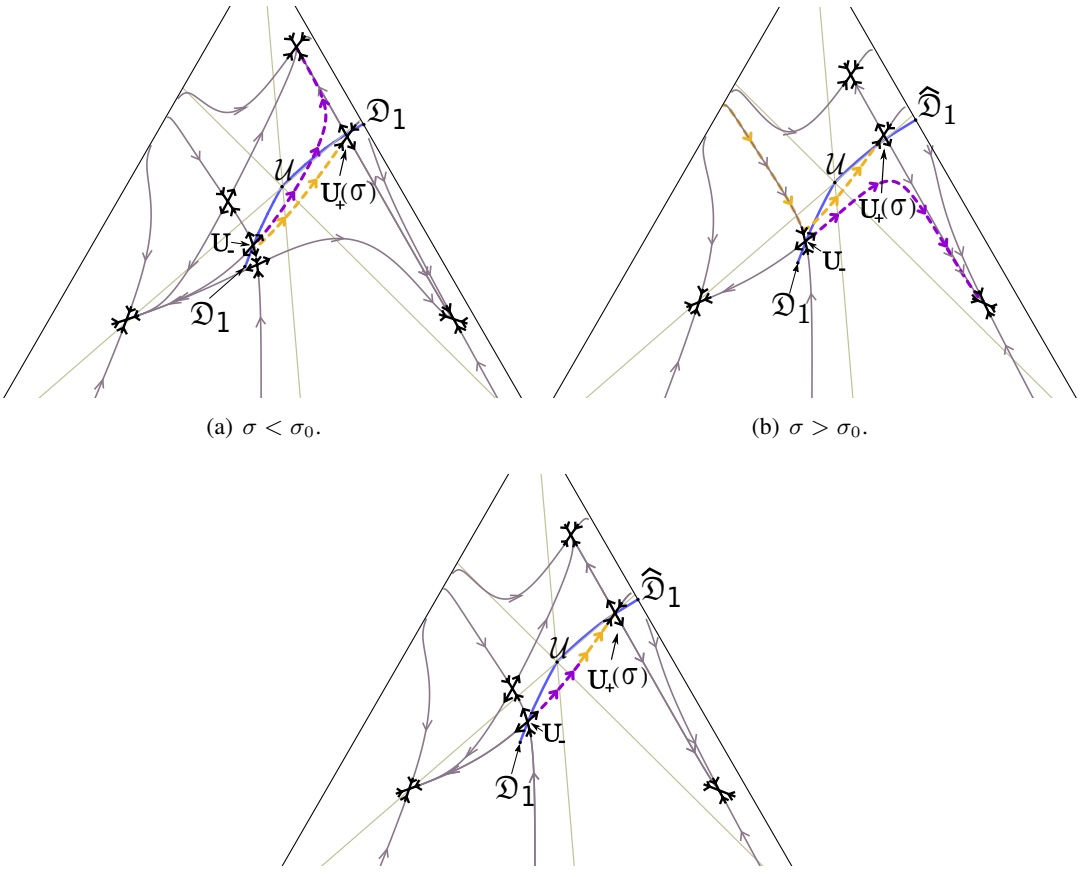

(a) $\sigma < \sigma_0$.

(b) $\sigma > \sigma_0$.

(c) $\sigma = \sigma_0$.

Figure 9.2: Procedure to find connections between saddle and saddle-node. U_- is a fixed state close to the umbilic point and $U_+ \in \mathcal{H}(U_-)$. The blue curves $[\mathcal{U}, \mathfrak{D}_1]$ and $[\mathcal{U}, \widehat{\mathfrak{D}_1}]$ are the slow sonic boundaries for $\mathcal{B}(\mathcal{U}) \neq I$. The violet orbit is the unstable manifold for U_- and the yellow orbit the stable manifold for U_+ for the dynamical system associated to U_-, σ_0.

9.3 Transitional boundaries

Recall that for the case of an identity viscosity matrix, the boundaries of the surface of transitional shocks are built by sonic shocks. These sonic shocks are connections between saddles and saddle-nodes, and are limits of connections between saddles. In the general case, finding these boundaries is complex (see Section 9.2). One way to find this boundary is to use a bisection method which starts with a saddle-saddle shock (U_-, σ_0, U_+) in the interior of the surface of transitional shocks. Then, we obtain the same type of borders as in the case of identity matrix, with the difference that the transitional shocks comprise an area of the saturation triangle. In Figure 9.3 we show the surface of transitional shocks for umbilic point of type II.

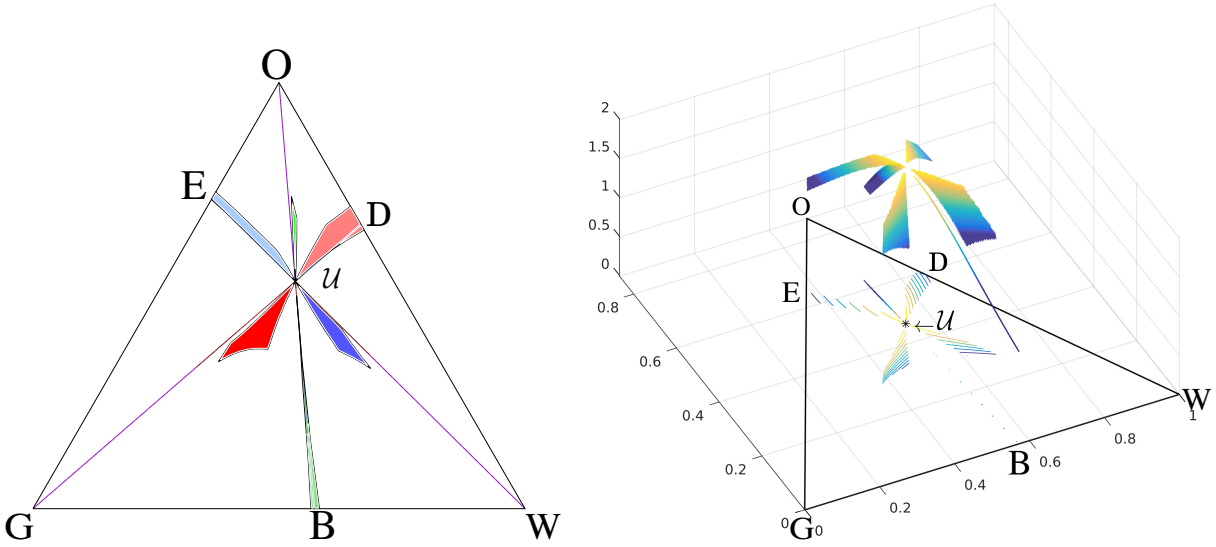

(a) Projection of the surface of transitional shocks in the saturation triangle.

(b) Surfaces of transitional shocks associated to segments $[G, D]$, $[W, E]$ and $[O, B]$ in the three dimensional phase space.

Figure 9.3: Surfaces of transitional shocks for umbilic point of type II_O and $\mathcal{B}(U) \neq I$.

Now, we define the boundaries of the surface of transitional shocks. As in the case $\mathcal{B}(U) = I$, we can associate a surface to straight lines $[G, D]$, $[W, E]$ and $[O, B]$. The type and the number of boundaries are the same as in the case of the identity matrix, but classifying them is more elaborated. We identify the following cases for $\mathcal{B}(U)$ defined in Section 3.4:

1. if the umbilic point is of type I, the three surfaces of transitional shocks have the four boundaries given in Definition 7.1.1;

2. if the umbilic point is in region II_Γ for $\Gamma \in \{G, W, O\}$, then the surface of transitional shocks associated to the segment $[\Gamma, \mathbb{B}]$ with $\mathbb{B} \in \{D, E, B\}$ has three boundaries and a gap between $\mathcal{U}$ and $\mathbb{B}_0 \in \{D_0, E_0, B_0\}$, similar to the case described in Lemma 7.1.3 (recall that in this case $\nu_\Gamma < 1$);

3. if the umbilic point is in region II_Γ with $\Gamma \in \{G, W, O\}$, the surface of transitional shocks associated to the segment from vertex $\mathcal{A}$ with $\mathcal{A} \in \{G, W, O\}$, $\mathcal{A} \neq \Gamma$ and $\nu_\mathcal{A} > 8$ has three boundaries, similar to the case described in Lemma 7.1.2.

4. if the umbilic point is in region II_Γ with $\Gamma \in \{G, W, O\}$, the surface of transitional shocks associated to the segment from vertex $\mathcal{A}$ with $\mathcal{A} \in \{G, W, O\}$, $\mathcal{A} \neq \Gamma$ and $\nu_\mathcal{A} \leq 8$ it can have three or four boundaries depending on whether points $\mathfrak{Y}_2$ and $\widehat{\mathfrak{Y}_2}$ exists, see Figure 9.4. Similar to cases described in Lemmas 7.1.1 and 7.1.2.

In Figure 9.3, we present the three surfaces for a case where $\mathcal{U} \in II_O$. In Figure 9.4 we show the projection of the surface of transitional shocks, the *transitional area* associated to $[G, D]$. This area has the following boundaries:

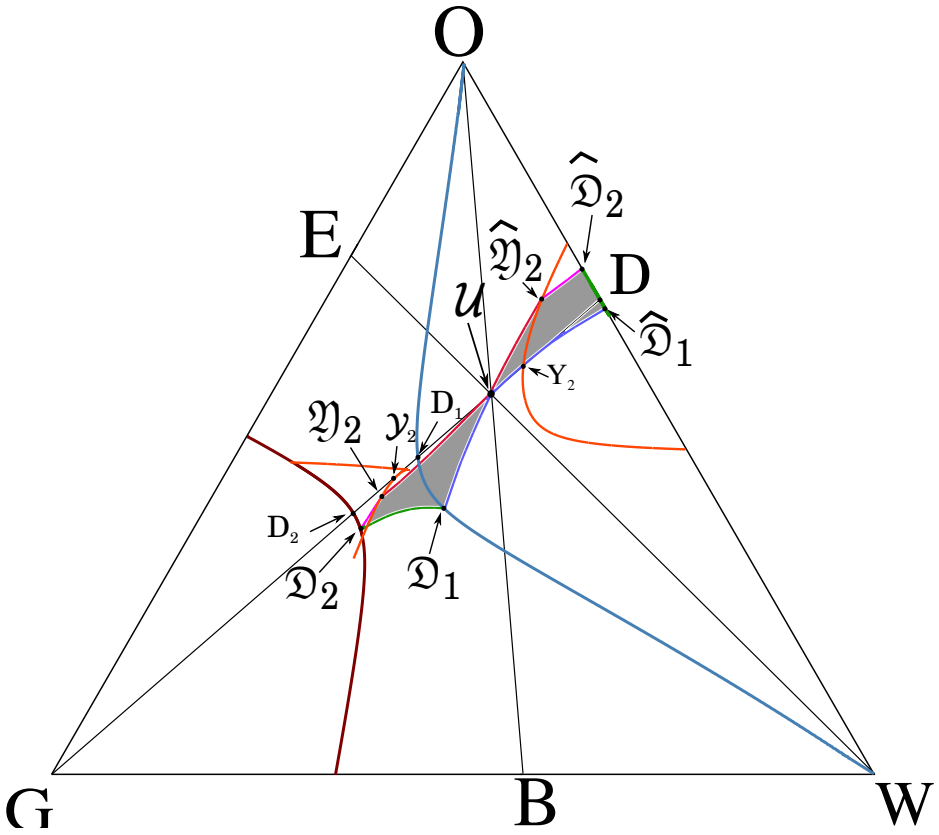

Figure 9.4: Projection of the surface of transitional shocks on the saturation triangle (shaded area). The states $D_1, D_2, \mathcal{Y}_2$ and Y_2 lie on $[G, D]$. These states define the surface of transitional shocks when $\mathcal{B}(U) = I$, see Chapter 7. The curve $[O, D_1, \mathfrak{D}_1, W]$ is the s-extension of $[O, W]$, the curve that crosses $[D_2, \mathfrak{D}_2]$ is the f-extension of $[O, W]$ and the curve segments $[\widehat{\mathfrak{Y}_2}, Y_2]$ and $[\mathfrak{Y}_2, \mathcal{Y}_2]$ are part of the fast double contact manifold (orange curves). The states $\widehat{\mathfrak{D}_1}$ and $\widehat{\mathfrak{D}_2}$ lie on $[O, W]$ and are associated to $\mathfrak{D}_1$ and $\mathfrak{D}_2$ such that $\sigma(\mathfrak{D}_1, \widehat{\mathfrak{D}_1}) = \lambda_s(\mathfrak{D}_1)$ and $\sigma(\mathfrak{D}_2, \widehat{\mathfrak{D}_2}) = \lambda_f(\mathfrak{D}_2)$.

- A *slow sonic boundary* (SSB), defined by the set of states $U_- \in [\mathfrak{D}_1, \mathcal{U}]$ for which there is a corresponding state $U_+ \in [\widehat{\mathfrak{D}_1}, \mathcal{U}]$, such that there is an admissible sonic s-shock between U_- and U_+, with $\sigma(U_-; U_+) = \lambda_s(U_-)$. The state $\widehat{\mathfrak{D}_1}$ lies in $[W, O]$ and its corresponding state $\mathfrak{D}_1$ lies in $E_s^+([W, O])$;

- A *fast sonic boundary* (FSB), defined by the set of states $U_- \in [\mathfrak{D}_2, \mathcal{U}]$ for which there is a corresponding state $U_+ \in [\widehat{\mathfrak{D}_2}, \mathcal{U}]$, such that there is an admissible sonic f-shock between U_- and U_+, with $\sigma(U_-; U_+) = \lambda_f(U_-)$. The state $\widehat{\mathfrak{D}_2}$ lies in $[W, O]$ and its corresponding state $\mathfrak{D}_2$ lies in $E_f^+([W, O])$;

- A *transitional sonic boundary* (TSB), defined by the set of states $U_- \in [\mathfrak{Y}_2, \mathfrak{D}_2)$ for which there is a corresponding state $U_+ \in [\widehat{\mathfrak{Y}_2}, \widehat{\mathfrak{D}_2})$, such that there is an admissible sonic transitional shock between U_- and U_+, with $\sigma(U_-; U_+) = \lambda_f(U_-)$. The pair of states $\mathfrak{Y}_2$ and $\widehat{\mathfrak{Y}_2}$ belong to the double fast contact manifold;

- A *genuine transitional boundary* (GTB) defined by the set of states $U_- \in (\mathfrak{D}_1, \mathfrak{D}_2)$ for which there is a corresponding state $U_+ \in (\widehat{\mathfrak{D}_1}, \widehat{\mathfrak{D}_2})$, such that there is an admissible transitional shock between U_- and U_+.

In Figure 9.5 we compare the projection of the surface of transitional shocks on the plane $[G, D] \times \mathbb{R}^+$ for the case $\mathbb{B}(U) \neq I$ with the case $\mathbb{B}(U) = I$. Notice that the structure of these boundaries is the same as of those boundaries defined for the identity matrix, see Definition 7.1.1.

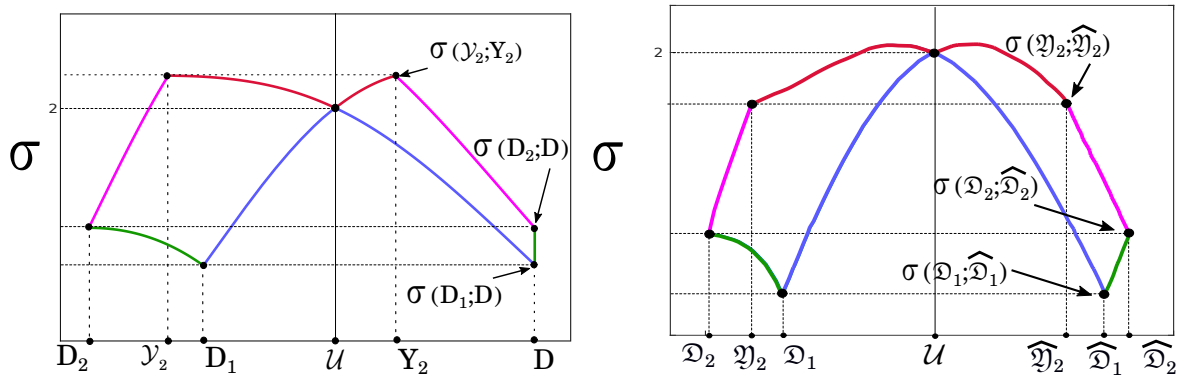

(a) Case $\mathcal{B}(U) = I$.

(b) Case $\mathcal{B}(U) \neq I$.

Figure 9.5: Projection of the surface of transitional shocks on the plane $[G, D] \times \mathbb{R}^+$ for identity and non-identity matrices. (a) The states $D_1, D_2, \mathcal{Y}_2$ and Y_2 lie on $[G, D]$. These states define the surface of transitional shocks when $\mathcal{B}(U) = I$, see Chapter 7. (b) The states $\mathfrak{D}_1, \mathfrak{D}_2, \widehat{\mathfrak{D}_1}, \widehat{\mathfrak{D}_2}, \mathfrak{Y}_2$ and $\widehat{\mathfrak{Y}_2}$ lie inside of the saturation triangle. The blue curves are slow sonic boundaries (SSB), red curves are fast sonic boundaries (FSB), pink curves are transitional sonic boundaries and green curves are genuine transitional boundaries (GTB).

9.4 Simulations

In this section, we present numerical simulations illustrating the effect in the solution when the matrix $\mathcal{B}(U) \neq I$ is used. We chose the nonlinear Crank-Nicolson implicit finite-difference scheme, using Newton's method to perform numerical simulations for system (3.30). This scheme is second-order accurate in space and time. We consider umbilic point type II_O with $\mu_w = 1.0, \mu_o = 2.0$ and $\mu_g = 0.75$, and consider the viscosity matrix defined in (3.34) and (3.59) with $c_{ow} = c_{og} = 1$.

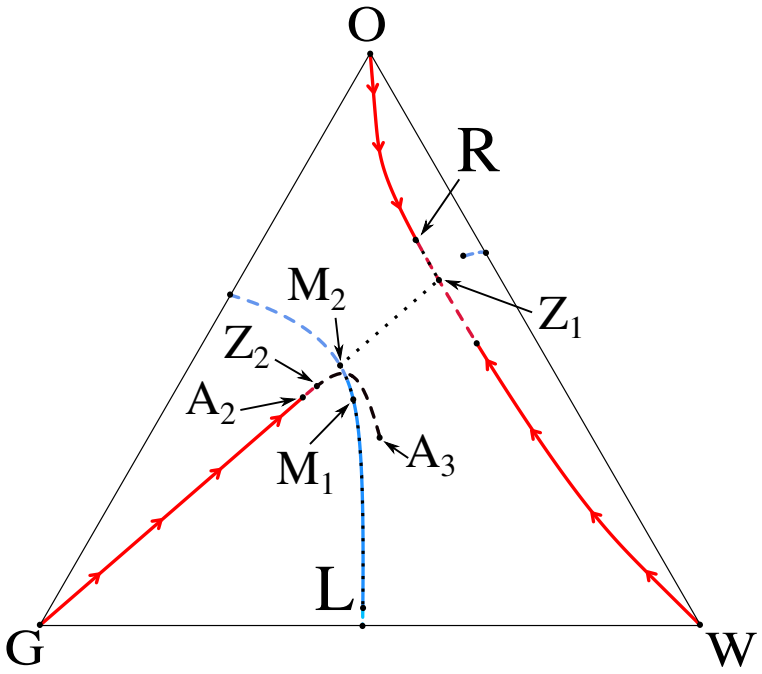

Figure 9.6: Solution of the Riemann problem for left state $L = (0.475708, 0.02608)^T$ and right state $R = (0.235578, 0.670876)^T$. For $\mathcal{B}(U) = I$, $R \in \mathscr{R}_2$ -region and $L \in \mathscr{L}_{\mathscr{R}_2}$-region named $\mathcal{J}_1$, see Claim 8.4.2 (*xii*) and Table 8.1. We present the solution using the wave curve method [8] (analytic solution) and the numerical solution (simulation using a finite-difference method). The red curves represent $\mathcal{W}_f^-(R)$ and the blue curves, $\mathcal{W}_s^+(L)$. The black dotted curve is the numerical simulation using the Crank-Nicholson scheme. Notice that the dashed curve $[A_2, A_3]$ is a nonlocal fast shock segment of $\mathcal{H}(R)$, but for $\mathcal{B}(U) = I$ only the segment $[A_2, Z_2]$ has viscous profile.

We consider first the case $\mathcal{B}(U) = I$ with $R \in \mathscr{R}_2$ -region and $L \in \mathscr{L}_{\mathscr{R}_2}$ -region, see Figure 9.6. From Claim 8.4.2 (*xii*) the solution for the Riemann problem consists in the sequence

$$L \overset{R_s}{\longmapsto} M_1 \overset{'S_s}{\longrightarrow} M_2 \overset{S_T}{\longmapsto} Z_1 \overset{S_f}{\longmapsto} R.$$

Notice that this solution has three elementary waves which have a transitional shock between the states M_2 and Z_1 that are on the invariant segment $[G, D]$. In Figure 9.6 the nonlocal shock segment $[A_2, A_3] \subset \mathcal{H}(R)$ is shown. This curve intersects the invariant segment $[G, D]$ at Z_2 such that the shock segment $[A_2, Z_2] \subset [A_2, A_3]$ is admissible, by Claim 2.7.2; which is not the case for segment $(Z_2, A_3]$.

In Figure 9.7 we show the profiles for saturation S_w and S_o obtained by the numerical simulation. We consider $\Delta x = 0.01$, $\Delta t = 0.01$, final time $T_f = 100$ and a small amount of artificial diffusion, $\epsilon = 0.005$. Note that the three wave groups and the two constant states of these solutions are clearly represented in this simulation.

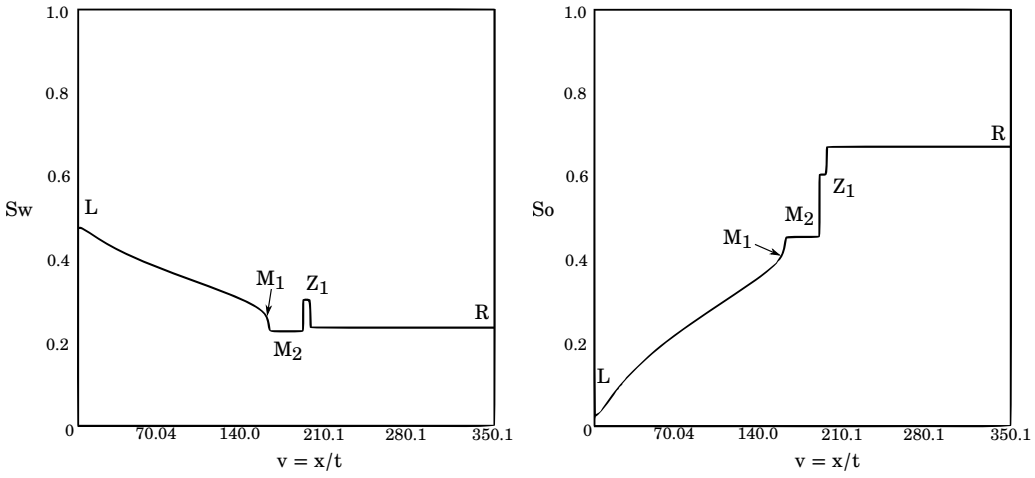

(a) Profile solution for S_w.

(b) Profile solution for S_o.

Figure 9.7: Solution of Riemann problem for left state $L = (0.475708, 0.02608)^T$ and right state $R = (0.235578, 0.670876)^T$. For $\mathcal{B}(U) = I$, $R \in \mathscr{R}_2$ -region and $L \in \mathscr{L}_{\mathscr{R}_2}$-region named $\mathcal{J}_1$, see Claim 8.4.2 (*xii*) and Table 8.1. The horizontal axis is given by $v = x/t$. The solution profiles are shown at $t = 100$.

Now we consider the viscosity matrix $\mathcal{B} \neq I$. In Figure 9.8 the backward fast and the forward slow wave curves from states R and L are shown. Notice that the admissible criterium given in Claim 2.7.2 does not apply in this case. Then the admissibility of the nonlocal fast shock segment $[A_2, A_3] \subset \mathcal{H}(R)$ changes, *i.e.*, the shock segment $[A_2, Z_2, A_4] \subset [A_2, A_3]$ is admissible in the case $\mathcal{B}(U) \neq I$. Therefore, there is an intersection between $\mathcal{W}_s^+(L)$ and $\mathcal{W}_f^-(R)$ at point M_2^*, which satisfies

- the state M_2^* belongs to s-composite segment of $\mathcal{W}_s^+(L)$, then there is a state M_1^* in the s-rarefaction segment of $\mathcal{W}_s^+(L)$ such that $\sigma_s = \sigma(M_1^*; M_2^*) = \lambda_s(M_1^*)$;
- the state M_2^* belongs to f-shock segment of $\mathcal{W}_f^-(R)$ with $\sigma_f = \sigma(M_2^*; R)$ such that this shock has viscous profile and $\sigma_s < \sigma_f$.

Then the solution for the Riemann problem consists in the sequence

$$L \overset{R_s}{\longmapsto} M_1^* \overset{'S_s}{\longrightarrow} M_2^* \overset{S_f}{\longmapsto} R.$$

Therefore, when we change the viscous matrix, the solution only uses an intermediate state M_2^* and the transitional shock that is used when $\mathcal{B}(U) = I$ disappears. In Figure 9.9 we show the profiles for saturations S_w and S_o obtained in the numerical simulation. We consider $\Delta x = 0.01$, $\Delta t = 0.01$, final time $T_f = 100$ and the real matrix of diffusion given by the capillary effects.

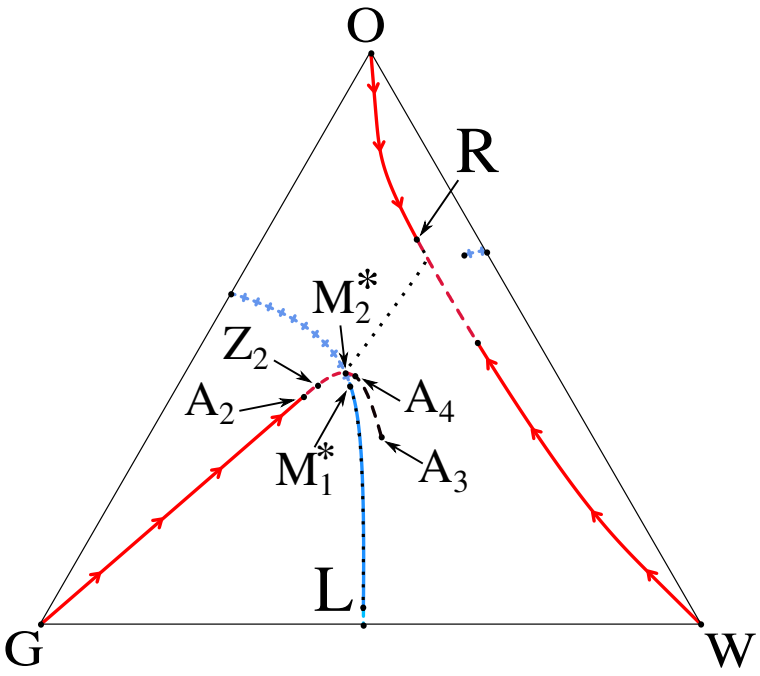

Figure 9.8: Solution of the Riemann problem for left state $L = (0.475708, 0.02608)^T$, right state $R = (0.235578, 0.670876)^T$ and $\mathcal{B}(U) \neq I$. We present the solution using the wave curve method [8] (analytic solution) and the numerical solution (simulation using a finite-difference method). The red curves represent $\mathcal{W}_f^-(R)$ and the blue curves, $\mathcal{W}_s^+(L)$. The black dotted curve is the numerical simulation using the Crank-Nicholson scheme. Notice that the dashed curve $[A_2, A_3]$ is a nonlocal fast shock segment of $\mathcal{H}(R)$, but for $\mathcal{B}(U) \neq I$ only the segment $[A_2, A_4]$ has viscous profile.

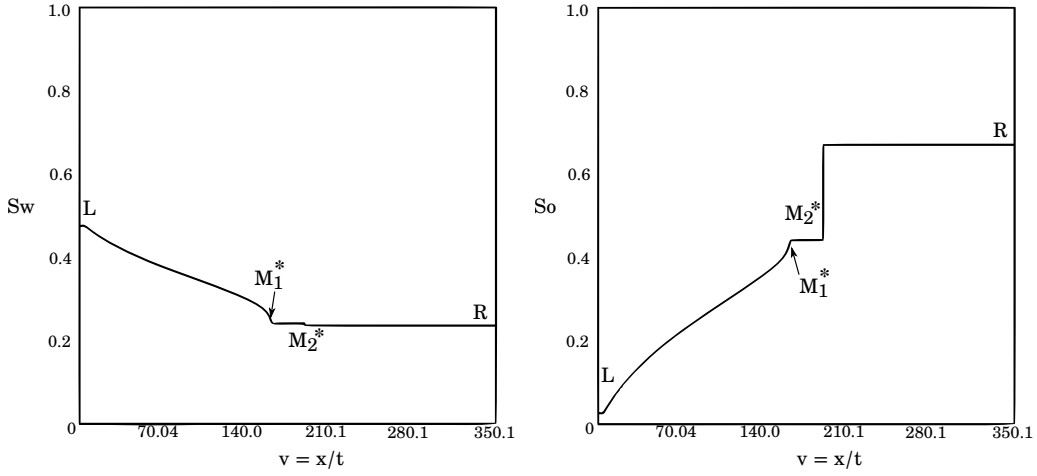

(a) Profile solution for S_w.

(b) Profile solution for S_o.

Figure 9.9: Solution of the Riemann problem for left state $L = (0.475708, 0.02608)^T$, right state $R = (0.235578, 0.670876)^T$ and $\mathcal{B}(U) \neq I$. The solution only comprises a slow wave group followed by a fast shock wave. The horizontal axis is given by $v = x/t$. The solution profiles are shown at $t = 100$.

Chapter 10

Conclusions

Here is a summary of our main contributions to the problem of three-phase flow in a porous medium. Taking the viscosity matrix to be a multiple of the identity, and for arbitrary fluid viscosities placing the umbilic point in case II of the Schaeffer-Shearer classification:

- We constructed the surface of transitional shocks in the enlarged three-dimensional phase space of saturations and speeds. Using this surface, we characterized the set of Riemann problems that display nonclassical transitional waves in their solutions. This characterization entails the understanding of how speed compatibility between transitional and classical waves is lost, which was facilated by our working in the enlarged phase space.

- We characterized the structurally stable Riemann solutions. Namely, we determined the sets of Riemann problems whose solutions have the same wave structure, in terms of number, type and sequence of elementary waves. In the process, we thoroughly studied the bifurcations of both the backward-fast and forward-slow wave curves. This study led to the understanding of how the saturation triangle is subdivided, depending on viscosity values, into $\mathscr{R}$-regions of right Riemann states for which the backward-fast wave curves are structurally stable. This subdivision, in turn, induces a subsequent subdivision of the saturation triangle, for each $\mathscr{R}$-region, into $\mathscr{L}$-regions of left Riemann states for which the corresponding Riemann solutions are structurally stable.

- We present the complete solution to the Riemann problem for the equations of three-phase flow. This includes formulating and demonstrating a successful entropy condition for choosing the stable family of solutions, and establishing the compelling result that such a family exists having the property of continuous dependence on left and right states.

We have also constructed the surface of transitional shocks for the general case of nonlinear viscosity matrices resulting from physically correct capillarity induced diffusive effects.

Bibliography

[1] E. Abreu. Numerical modelling of three-phase immiscible flow in heterogeneous porous media with gravitational effects. *Mathematics and Computers in Simulation*, 97:234–259, 2014.

[2] E. Abreu, J. Douglas, F. Furtado, D. Marchesin, and F. Pereira. Three-phase immiscible displacement in heterogeneous petroleum reservoirs. *Mathematics and Computers in Simulation*, 73:2–20, 2006.

[3] P. Andrade, A. de Souza, F. Furtado, and D. Marchesin. Oil displacement by water and gas in a porous medium: the Riemann problem. *Bull. Braz. Math. Soc. (N.S.)*, 47(1):1–14, 2016.

[4] P. Andrade, A. de Souza, F. Furtado, and D. Marchesin. Three-phase fluid displacement in a porous medium. *Journal of Hyperbolic Differential Equations*, 15(4):731–753, 2018.

[5] F. Asakura. Stone-Marchesin Model Equations of Three-Phase Flow in Oil Reservoir Simulation. pages 1–56.

[6] A. Azevedo. *Soluções fundamentais múltiplas em sistemas de leis de conservação hiperbólico–elíticos, D.Sc. thesis, in Portuguese* . PhD thesis, Pontifícia Universidade Católica do Rio de Janeiro, Rio de Janeiro, Brazil, 1991.

[7] A. Azevedo, D. Marchesin, B. Plohr, and K. Zumbrun. Capillary instability in models for three-phase flow. *Zeitschrift fur Angewandte Mathematik und Physik*, 53(5):713–746, 2002.

[8] A. Azevedo, A. de Souza, F. Furtado, D. Marchesin, and B. Plohr. The solution by the wave curve method of three-phase flow in virgin reservoirs. *Transport in Porous Media*, 83(1):99–125, 2010.

[9] A. Azevedo, A. de Souza, F. Furtado, and D. Marchesin. Uniqueness of the Riemann solution for three-phase flow in a porous medium. *SIAM J. Appl. Math.*, 74(6):1967–1997, 2014.

[10] K. Aziz and A. Settari. *Petroleum reservoir simulation*. Chapman & Hall, 1979.

[11] A. Bressan. Hyperbolic systems of conservation laws. *Oxford University Press*, (Oxford), 2000.

[12] S. E. Buckley and M. Leverett. Mechanism of fluid displacement in sands. *Trans, AIME*, (146): 1–7, 1942.

[13] P. Castañeda. A new computational method for locating the secondary bifurcation of a Rankine-Hugoniot curve. In *30º Colóquio Brasileiro de Matemática - 2015*, Rio de janerio, 2015.

[14] P. Castañeda and F. Furtado. The role of sonic shocks between two- and three-phase states in porous media. *Bull. Braz. Math. Soc.*, 47(1):227–240, 2016.

[15] T. Chang and H. Ling. *The Riemann problem and interaction of waves in gas dynamics*. John Wiley & Sons, Inc., New York, New York, 1989.

[16] Constantine M. Dafermos. *Hyperbolic Conservation Laws in Continuum Physics*. Springer, Heidelberg, Berlin, Heidelberg, 2005.

[17] A. de Souza. Stability of singular fundamental solutions under perturbations for flow in porous media. *Mat. Apl. Comput.*, 11(2):43, 1992.

[18] J. Glimm. Solutions in the large for nonlinear hyperbolic systems of equations. *Comm. Pure Appl. Math.*, pages 697–715, 1952.

[19] E. Isaacson, D. Marchesin, and B. Plohr. Transitional waves for conservation laws. *SIAM J. Math. Anal.*, 21(4):837–866, 1990.

[20] E. Isaacson, D Marchesin, F. Palmeira, and B. , Plohr. A global formalism for nonlinear waves in conservation laws. *Comm. Math. Phys.*, 146(3):505–552, 1992.

[21] E. Isaacson, D. Marchesin, B. Plohr, and B. Temple. Multiphase flow models with singular Riemann problems. *Comput. Appl. Math.*, 11(2):147–166, 1992.

[22] A. Kulikovskii. Surfaces of discontinuity separating two perfect media of different properties. Recombination waves in magnetohydrodynamics. *Journal of Applied Mathematics and Mechanics,*, 32(6):1125–1131, 1968.

[23] P. Lax. Hyperbolic systems of conservation laws II. *Comm. Pure Appl. Math.*, X, 1952.

[24] T. P. Liu. The Riemann problem for general 2X2 conservations laws. *Trans. Amer. Math. Soc.,*, 199:89–112, 1974.

[25] T. P. Liu. The Riemann problem for general systems of conservations laws. *J. Differential Equations,*, 18:218–234, 1975.

[26] A. Majda and R. L. Pego. Stable viscosity matrices for systems of conservation laws. *J. of Differential Equations*, 56(2):229–262, 1985.

[27] D. Marchesin and A. A. Mailybaev. Dual-family viscous shock waves in systems of conservation laws: a surprising example. In *Proc. Conf. on Analysis, Modeling and Computation of PDE and Multiphase Flow. Stony Brook NY*, 2004.

[28] D. Marchesin and A. A. Mailybaev. Dual-family viscous shock waves in n conservation laws with application to multi-phase flow in porous media. *Arch. Rational Mech. Anal.*, 182(1):1–24, 2006.

[29] D. Marchesin and B. Plohr. Wave Structure in WAG Recovery. *Society of Petroleum Engineers*, 6 (2):209–219, 2001.

[30] V. Matos, P. Castañeda, and D. Marchesin. Classification of the umbilic point in immiscible three-phase flow in porous media. In *Proceedings of HYP2012 - 14th International Conference on Hyperbolic Problems: Theory, Numerics, Applications*, 2014.

[31] V. Matos, A. Azevedo, J. Mota, and D. Marchesin. Bifurcation under parameter change of Riemann solutions for nonstrictly hyperbolic systems. *Z. Angew. Math. Phys.*, 66(4):1413–1452, 2015.

[32] V. Matos, J. D. Silva, and D. Marchesin. Loss of hyperbolicity changes the number of wave groups in Riemann problems. *Bulletin of the Brazilian Mathematical Society*, 47(2):545–559, 2016.

[33] O. A. Oleĭnik. On the uniqueness of generalized solution of Cauchy problem for non linear system of equations ocurring in mechanics. *Uspekhi Mat Nauk*, 12:169–176, 1957.

[34] D.W. Peaceman. *Fundamentals of Numerical Reservoir Simulation, Volume 6*. 1977.

[35] F. S. Rezende. *Ondas elementares no modelo de escoamento trifásico, D.Sc. thesis, in Portuguese* . PhD thesis, Pontifícia Universidade Católica do Rio de Janeiro, Rio de Janeiro, Brazil, 1998.

[36] D. Schaeffer and M. Shearer. The Classification of 2 X 2 Systems of Non-Strictly Hyperbolic Conservation Laws, with Application to Oil Recovery. *Comm. Pure Appl. Math.*, 40:141–178, 1987.

[37] S. Schecter, D. Marchesin, and B. Plohr. Structurally stable Riemann solutions. *J. Differential Equations*, 126(2):303–354, 1996.

[38] D. Serre. *Systems of Conservation Laws 1: Hyperbolicity, Entropies, Shock Waves*. Cambridge University Press, Cambridge, UK, 1999.

[39] M. Shearer and J. A. Trangenstein. Loss of real characteristics for models of three-phase flow in a porous medium. *Transport in Porous Media*, 4(5):499–525, 1989.

[40] J. Smoller. *Shock Waves and Reaction—Diffusion Equations*. Second ed. Springer New York, 1994.

[41] J. Smoller and L. johnson J. Global Solutions for an Extended Class of Hyperbolic Systems of Conservation Laws. *Arch. Rat. Mech. Anal.*, 32(x), 1968.

[42] B. Wendroff. The Riemann problem for materials with Non Convex Equations of state: I Isentropic flow; II General flow. *J. Math. Anal Appl.*, (38):454 – 466; 640 – 658, 1972.